RÉPUBLIQUE ALGÉRIENNE DÉMOCRATIQUE ET POPULAIRE
MINISTÈRE DE L'ENSEIGNEMENT SUPÉRIEUR ET DE LA RECHERCHE SCIENTIFIQUE
UNIVERSITE MOULOUD MAMMERI DE TIZI-OUZOU

FACULTÉ DES SCIENCES

DÉPARTEMENT DE CHIMIE

Thèse de Doctorat LMD en chimie

Option : physico-chimie des matériaux

Présentée par

M^{elle} Fatima MOUSLI

Thème

Composites polyaniline-oxydes mixtes : synthèse, contrôle des interfaces par les sels de diazonium, imprégnation sur tissus et activités catalytiques

Soutenue le / /

Devant le jury composé de :

Mme. BENBRAHIM Nassima	Professeur	UMMTO	**Présidente**
M. KADRI Abdelaziz	Professeur	UMMTO	**Directeur de thèse**
M. CHEHIMI M. Mohamed.	DR1	CNRS-Thiais- France	**Co-directeur de thèse**
M. ZITOUNI Safidine	MCA	EMP Bordj El Bahri, Alger	**Examinateur**
Mme HAMADOU Lamia ep MEZEGHRANE	Professeur	UMMTO	**Examinatrice**

Thèse réalisée au

Laboratoire de Physique et Chimie des Matériaux (LPCM)

Université Mouloud MAMMERI B.P.17 RP, 15000 Tizi-Ouzou (Algérie)

Web :http://labs.ummto.dz/lpcm/

Institut de Chimie et des Matériaux Paris Est

CNRS-UPEC-UMR7182

Laboratoire SystèmesPolymères Complexes

(SPC)

2-8, rue Henri Dunant

94320 Thiais, France

Tél : +33(0)1 49 78 11 73

Web : http://www.icmpe.cnrs.fr/

Interfaces, Traitements, Organisation et

Dynamique des Systèmes (ITODYS)

Université Paris Diderot - CNRS (UMR 7086)

15 ue Jean Antoine de Baïf, 75013 Paris, France

Tél : +33 (0)1 57 27 68 68

Web :www.itodys.univ-paris-diderot.fr/fr/

*"*We raise in degrees whom we will, but over every possessor of knowledge is one (more) knowing"

Sūrat yūsuf (Joseph). 12 vs 76

Avant-propos

Cette thèse a été rédigée sous forme d'un recueil de quatre publications, parues, soumise, en cours de soumission ou en cours de préparation dans des revues à comité de lecture et indexées dans Web of Science.

Acknowledgments

This work has been performed in Laboratoire de Physique et Chimie des Matériaux (LPCM), Mouloud Mammeri of Tizi-Ouzou University, Institut de Chimie et des Matériaux Paris Est, CNRS-UPEC-UMR7182 (ICMPE) and in Interfaces, Traitements, Organisation et Dynamique des Systèmes (ITODYS) of Paris Diderot University.

I would like to thank Mrs Benbrahim Nassima, professor at Mouloud Mammeri University for facilitating my mobility and for accepting to be president of the jury. I also thank all members of the jury, Mrs Hamadou-Mezeghrane Lamia professor at Mouloud Mammeri University and Mr Zitouni Safidine, Dr/lecturer at Ecole Millitaire Polytechnique (EMP) de Bordj El-Behri, Alger, for agreeing to read my thesis and to attend the presentation of my work.

Through this thesis, I would like to express my sincere gratitude to my supervisor in LPCM, Mr KADRI Abdelaziz for the trust he has given me, for these advices that allowed me to evolve in my vision of research and in the way of conducting it, for its assistance and follow-up throughout my training. I consider myself immensely lucky and privileged to work with him. I also thank him for his for the unconditional support in and out the laboratory to facilitate my scientific stay in France.

I sincerely thank my supervisor in ICMPE and ITODYS Mr CHEHIMI M. Mohamed for the continuous support of my PhD study and research, for his patience, motivation, enthusiasm, and immense knowledge. His guidance helped me in all the time of research and writing of this thesis. I could not have imagined having a better advisor and mentor for my PhD study.
I am grateful and thankful to Mr Maurel François, Director of ITODYS lab for welcoming me to his laboratory. Thank you for giving me the opportunity to work with high-level multidisciplinary teams.

I wish to express my gratitude and my appreciation to Mr Hocine Smain and Chaouchi Ahcène, professors at Mouloud Mammeri University who generously provided time, energy and valuable help in the discussion of my results.

Special thanks to Mr Lamouri Aazdine and Mr Jouini Mohamed for receiving me in your labs and for teaching me organic chemistry and electrochemistry, you were really helpful to me during my scientific stay. I do not forget to thank Mr Pinson Jean for his tips and his kindness.

I also thank the administrative staff specially Mr Quenin Pièrre-Francois from ITODYS for support and for facilitating my mobility.

Now, I dedicate this work to my parents, source of my joys, secrets of my strength. Thank you for all your sacrifices for me to grow and prosper, thank you to work tirelessly despite the vicissitudes of life to my well-being. Thank you for being just my parents; it is to you that I owe this success.

I also dedicate it to my brothers and sisters for their infinite support and their constant help, to whom I wish a better future.

To my soulmate, thank you for being with me, thank you for your lifelong support, for your generous love, and thank you for loving me.

Finally, I express my deep sense of gratitude to everyone contributed to this thesis from near or far.

Table of contents

General introduction

General introduction

Today, the textile industry is the second most polluting industry in the world after oil. It has a great deal of impact on the environment. The production techniques of certain fibers, especially cotton, are particularly costly in natural resources and highly polluting for the environment but also very harmful for the people who work in these sectors.

With the advancement of technologies used in this industry and the explosion of the production, the transport of finished products weighs heavily in the carbon footprint as it generates more than 1 billion tons of CO_2, in addition to the amount of water that this industry 'swallows' more than 4% of the world's drinking water resources. These are scary figures that give the scale of the damage caused by this sector.

In general, all cotton production areas are highly polluted because of dyeing which causes pollution of river water as well as dyes and fixers that contain heavy metals such as Cr and Pb. For example, in China, about 70% of the rivers, lakes and reservoirs are affected by the pollution caused by textile industry. Numerous studies that were devoted to water purification led to an improvement in the oxidative degradation processes of organic compounds. Particularly, heterogeneous photocatalysis is an attractive for pollution problem solving because it permits to degrade organic matter into elementary and less toxic products.

Currently, photocatalytic applications are very attractive; however, they are considerably limited because of the low probability of separation of photo-induced electron-hole pairs in the most stable semi-conductor photocatalysts. Therefore, the big challenge for researchers in this field is to develop stable photocatalytic materials that improve the charge carriers' separation providing better catalytic activity to preserve the environment.

The development of heterostructure photocatalysts by metal doping of the semiconductors and the corresponding nanocomposite materials by coupling with conducting polymer with a suitable band can reduce the recombination phenomena by vectorial transfer of charge carriers. It is in this context that our research has been conducted.

Several TiO_2/conductive polymer and TiO_2-based heterostructure/conductive polymer composite materials have been developed to improve the catalytic reactivity of catalysts in organic pollutant degradation processes. Polyaniline is one of the most widely used conductive polymers in the design of such photo/catalytic systems, thanks to its power to improve the separation of electron-hole pairs photogenerated by the inorganic material which makes the photocatalyst effective under visible light and sometimes in darkness.

The interest of the combination of TiO_2 with organic and inorganic materials and the benefit of coupling it with polyaniline in the improvement of the photo/catalytic performances of the nanocatalyst are the subject of the first Chapter of this Thesis.

The second part of this manuscript is devoted to the development of a nanocomposite based on TiO_2 and PANI involving an aryl diazonium salt as a coupling agent for the polymer on TiO_2 nanoparticles. The interface chemistry of the diazonium salt is highlighted and the grafting reaction is thoroughly described in this Chapter. The catalytic performances of the elaborated materials are evaluated and discussed.

The third Chapter outlines the strategy adopted to improve the catalytic performances of the nanocomposites materials conceived during the first part. It consists in the doping of TiO_2nanoparticles by the RuO_2 metal via sol gel rout. The heterostructure thus obtained is subjected to the treatment with the same diazonium salt in order to obtain the same nanocomposite as the first but with RuO_2-modified TiO_2 heterostructure. The effect of the doping, the advantage of the diazonium salt in the design of this kind of materials as well as the effect of PANI during the catalytic process studied were well discussed with mechanism, chemical reactions and schematic illustrations which are represented in this Chapter.

The fourth and last Chapter is based on the idea of preparing functional textiles such as cotton clothing that is active against all chemical attacks (chemical weapons, pesticides ...). The chapter presents the different methods of synthesis of hybrid textile materials containing an organic/inorganic nanostructured system composed of TiO_2-RuO_2/PANI nanocomposites immobilized on the surface of cellulose-based fabrics. The stability of the final sample has been studied in this section. The Chapter presents also a detailed study of the kinetics of Methyl Orange degradation reaction.

The Thesis dissertation finishes by a General Conclusion on the work and highlights the salient features of diazonium reactivity at the surface of TiO_2-based particles in view of designing outstanding composite (photo)catalysts that are employed as such or coated on cotton fabrics for the mineralization of model organic pollutants. Moreover, we clarify the subtle architecturing of composite catalysts for continuous day and night catalyzed degradation of pollutants. This Thesis paves thus the way for novel 24h use catalysts for environmental applications.

List of publications

Publications

1. **Diazonium-modified TiO_2/polyaniline core/shell nanoparticles. Structural characterization, interfacial aspects and photocatalytic performances**, Fatima Mousli, Ahcène Chaouchi, Smain Hocine, Abdelaziz Kadri, Aazdine Lamouri, Mohamed M. Chehimi. *Applied Surface Science*, 465 (2019) 1078-1095.

2. **Polyaniline-Grafted RuO_2-TiO_2 heterostructure for the catalyzed degradation of methyl orange in darkness.** Fatima Mousli, AhcèneChaouchi, Mohamed Jouini, François Maurel, AbdelazizKadri, Mohamed M. Chehimi. Catalysts (2019). 9(7), 578.

3. **Surface modification of polymers, methods and applications**, Mousli. F; Snoussi. Y; Khalil. Ahmed. M; Jlassi. K; Mekki. A; Chehimi. M. M. Book chapter (2019). (In press).

4. **Mixed oxide-polyaniline composite-coated woven cotton fabrics for the visible light catalyzed degradation of hazardous organic pollutants,** Fatima Mousli, Ahmed Khalil, François Maurel, AbdelazizKadri, Mohamed M. Chehimi, submitted to Cellulose.

5. **Synergetic effects of conductive polymers and doped TiO_2 in (photo)catalyzed degradation of organic pollutants,** Fatima Mousli, François Maurel, AbdelazizKadri, Mohamed M. Chehimi, under final editing to be submitted to Chemical Society Reviews.

Communications

- 2nd International Symposium on Materials and Sustainable Development9-10 November 2015, Boumerdes, Algeria.
- GDR 3661 Polynano, Polymères nanochargés, Paris, 9-10 juillet 2018.
- Journée scientifiques et pédagogiques de la faculté de chimie USTHB. Algérie. 2015.
- 7th African Conference on Non Destructive Testing (ACNDT) and 5th conference on Welding and Non Destructive Testing and Materials and Alloys Industry (IC-WNDT-MI), November 26-28, Oran, Algeria.
- 1ère Journée Nationale de l'Agro-alimentaire, Engineering et Environnement, 16 avril 2017, Boumerdès, Algérie.
- Congrès des doctorants de la FSTGAT-USTHB, Algérie, 24-25 avril 2017.
- Journées d'électrochimie (JE'2017) Bordeaux 26-29 juin 2017.
- Advanced Nano Materials Aveiro (ANM2017) Aveiro, Portugal July 19-21, 2017.
- 8th International Conference on Electrochemistry in Nanoscience, May 29-31, 2018, Nancy, France.

- Frontiers in Nanomaterials for Energy Harvesting and Storage, August 27-29, 2018, Tours, France.

Issue cover

Catalysts, Vol. 9, Iss. 7. July 2019

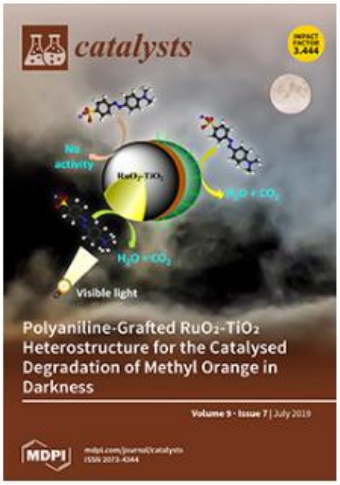

Cover Story: The cover illustrates a metal–semiconductor/polyaniline nanocomposite with spectacular catalytic properties. The nanocomposites catalyze the decomposition of methyl orange (MO) in darkness. Indeed, the RuO_2–TiO_2 mixed oxide is an excellent photocatalyst under visible light, while the nanocomposite RuO_2–TiO_2/aryl/polyaniline exhibits unique, fast catalytic performance in the dark. Total discoloration of MO was noted without any spectral evidence for organic products, thus suggesting complete mineralization of the dye. This activity does not only depend on the components that constitute these materials but also on the subtle interface chemical composition which is driven by diazonium modification of RuO_2–TiO_2.

Chapter 1: Synergetic effects of conductive polymers and doped TiO_2 in (photo)catalyzed degradation of organic pollutants

Synergetic effects of conductive polymers and doped TiO_2 in (photo)catalyzed degradation of organic pollutants

Fatima Mousli[1,2,3]*, François Maurel[2], Abdelaziz Kadri[1], Mohamed M. Chehimi[3]

Review to be submitted to Chemical Society Reviews

Graphical abstract

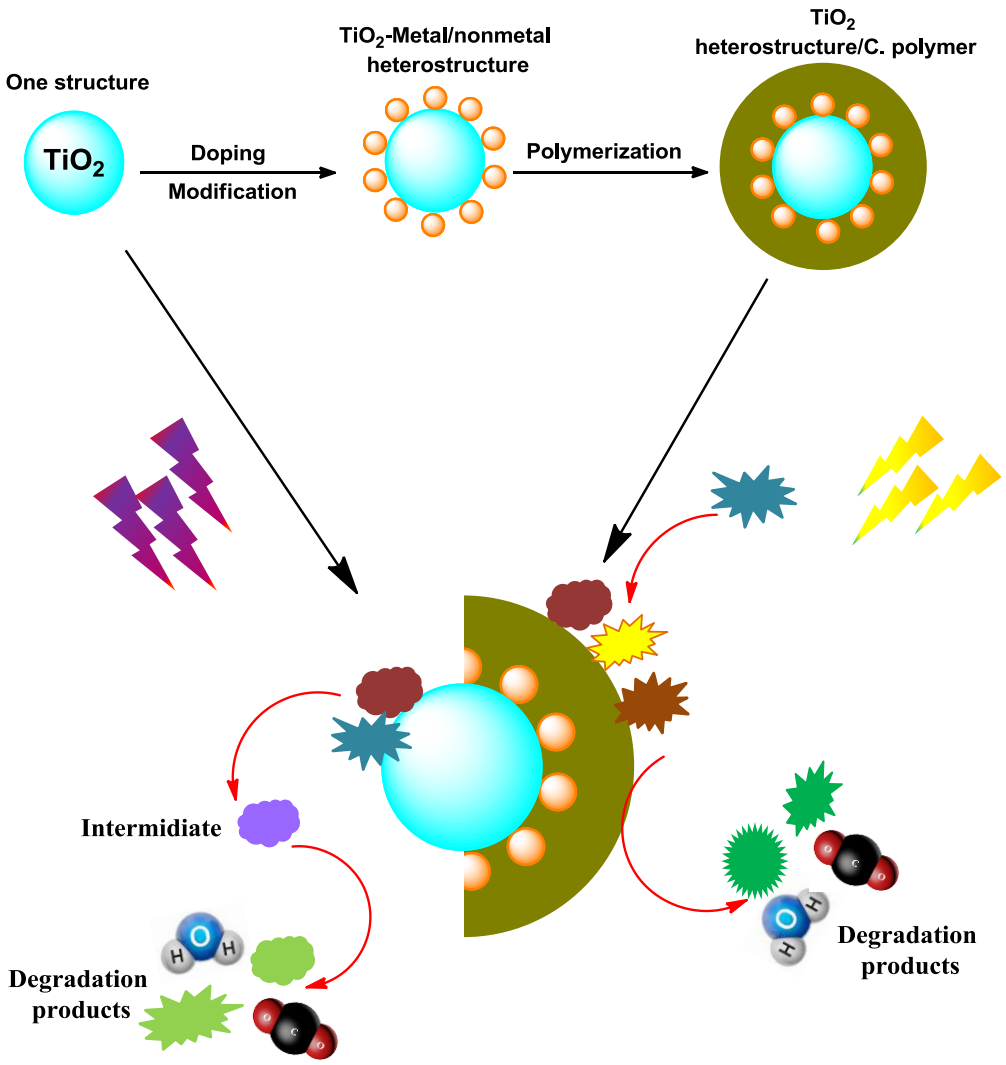

Objectives and scope of the review

The main objective of this critical review is to report the recent progress made on polyaniline-TiO_2 hybrid materials, designed for the catalyzed (photo)degradation of organic pollutants. One key issue is to bridge the gap between recent advances in the domain and present/future challenges in the science and technology of polyaniline-TiO_2 catalysts to address ever growing organic pollutant environmental concerns.

Significance

This review gives a general, brief overview of TiO_2 as a photocatalyst and tackles the results obtained using TiO_2/conductive polymer nanocomposite photocatalyst. Herein, we demonstrate the interest of doping TiO_2 with organic and inorganic materials and the benefit of the combination of TiO_2-based heterostructures with conductive polymers in particular polyaniline and its effect on the improvement of the (photo)catalytic performances owing to the synergistic effects of the different constituents of the nanocomposite (photo)catalyst.

Synergetic effects of conductive polymers and doped TiO_2 in (photo)catalyzed degradation of organic pollutants

Fatima Mousli[1,2,3]*, François Maurel[2], Abdelaziz Kadri[1], Mohamed M. Chehimi[3,]*

[1] Laboratoire de Physique et Chimie des Matériaux (LPCM), Faculté des Sciences, Université Mouloud Mammeri, Tizi-Ouzou 15000, Algeria.
[2] Sorbonne Paris Cité, Université Paris Diderot, CNRS, ITODYS (UMR 7086), 75013 Paris, France
[3] Université Paris Est, CNRS, ICMPE (UMR 7182), 94320 Thiais, France

Abstract

This critical review summarizes recent research dealing with development of titanium dioxide (TiO_2)-based heterostructure/conductive polymer nanocomposite photocatalysts used for environmental applications. TiO_2 plays a spectacular role in the protection of the environment; it is the most suitable catalyst for its high stability, physico-chemical properties and great capacity to degrade a wide range of organic pollutants. However, TiO_2 does not satisfy all practical requirements due to its wide band gap and the strong recombination of photogenerated charges on top of its usage under UV light whereas real world applications require operation under visible light or even in darkness. In this regard, efforts have been made to improve these physico-chemical and catalytic properties by modifying its electronic and optical properties. The recent literature witnessed problem solving arising from numerous smart combinations of several materials with TiO_2 to efficiently achieve catalyzed photodegradation of organics under visible or simulated sunlight, if not in darkness. Whilst TiO2 has been hybridized with other inorganic materials for visible light degradation of organics, in this review we stress the unique features of polyaniline as a component to impart the existing hybrid photocatalysts significant pollutant degradation performances which will be discussed in terms of composition, structure, kinetics and recovery.

This review is of interest to experts and new comers in the fields involved in the design of nanostructured materials in general, and conductive polymer composites as well as photocatylic TiO_2-based composites, in particular.

Keywords: TiO_2, TiO_2 heterostructure, conductive polymers, nanocomposite, catalysis, pollutants, dyes, heterojunction.

Contents

1. Introduction

The technological development as well as the growth of the industry throughout the world leads to the spread and accumulation of waste in the environment.[1] The textile industry is one of the first sectors that affect the ecosystem; it generates a very important pollution of the aquatic environment with toxic chemicals and dyes thus representing a serious risk not only for the aquatic organisms but also for humans. [2,3,4] The azo dyes are the most used (with a worldwide production of about 500000 tons/year.[5] and are consequently, the most discharged ones in the environment. Of environmental concern issue, over 50% of azo dyes are stable and non-biodegradable compounds.[6] Others are partially degradable but generate very stable and often more toxic intermediates molecules than the starting compound.

So far, various approaches have been adapted to reduce the rate of azo dyes by a complete decomposition, including physicochemical and biological methods.2 The latter are unable to effectively eliminate several refractory and toxic chemicals from industry, they minimize the level of toxicity but unable to neutralize it.2 In addition, the conventional treatments (membrane processes, sedimentation, filtration, electrochemical destruction, activated carbon

adsorption, chemical oxidation ...) involve only phase transfer of pollutants from the liquid phase to another new phase, with a large release of residues. [7,8] This has made it necessary to develop new efficient treatment systems. Recent progress in the depollution of the environment in particular water treatment has shown that Advanced Oxidation Processes (AOP) are very effective, including heterogeneous photocatalysis which has been recognized as an ideal and promising route for the decomposition and the mineralization of organic pollutants in aqueous medium by generating very active radical species.[9]

Titanium dioxide (TiO_2) is one of the most successful photocatalysts in the photodegradation processes of wade range of organic contaminants, due to its strong oxidizing power under UV light and its strong photocatalytic activity,[10,11,7] high chemical, biological and photochemical stability, [12] physical, optical and electrical properties,[13] low cost, natural abundance, non-toxicity and environment-friendly.[14,15,16] However, some limitations affect the photocatalytic efficiency of TiO_2, such as low electron transfer and high photoelectron-hole recombination rate, the narrow absorption spectral range and its photoactivity only under UV light due to its wide bandgap (3.2 eV for anatase and 3.02 eV for rutile). [7,17,18, 19,20]The modification of TiO_2 with another material which has a narrow band gap is necessary in order to shift the photocatalysis from UV to visible light and to improve the photocatalytic activity of TiO_2-based photocatalysts.[7,21,22] In this context, various doping, co-doping, composite, coupling techniques have been investigated in order to impart new performances to TiO_2. Metallic (Pt, Au, Cu…) or non-metallic dopants (N, S, B, P...) [22,23,24] and metallic oxides semiconductor visible photocatalyst were used to form TiO_2-based heterostructures, [25] In particular, noble metals (Au, Ag, Pt,…) which have shown high photocatalytic enhancing property by inhibiting charge carrier recombination within TiO_2 semi-conductor.[26]

The incorporation of conductive polymers such as polypyrrole (PPy), polythiophene (PTh), and polyaniline (PANI) has also been reported for the preparation of photocatalyst composites.[27,28,29] These polymers act as electron donors and good hole transporters in addition to their ability to prevent the oxidation and the reduction of the TiO_2 under irradiation.[28] PANI is the most used in photocatalysis due to its power to improve the separation of electron-hole pairs photogenerated by the inorganic material which makes the photocatalyst effective under visible light.[30] Actually, PANI is a good sensitizer for TiO_2 under visible light, due to its low band gap of 2.8 eV. In addition, it has a high absorption coefficient and a high mobility of charge carriers. [31] The level of the conductance band (CB) of PANI is lower than that of TiO_2, which facilitates the transfer of electrons at PANI//TiO_2

interface and leads to an improvement of the photocatalytic properties of the composite material under visible light.[32] The enhancement in the catalytic performances of the composite material is due to the synergistic effects of the different materials constituting the composite.[33] Based on the aforementioned considerations, the design of a hybrid multi-component material based on PANI and TiO_2 heterostructure is a unique strategy for enhancing (photo)-catalytic kinetics. In this challenging context, efforts have been focused on the design and the development of new catalysts for environment purification. Several studies have been reported on the association of PANI with doped/co-doped-TiO_2 or TiO_2-based heterostructure.[34,35,36] This combination imparts to the hybrid material the flexibility and controllability of the polymer, the physical and chemical properties of the inorganic components, unique and new photocatalytic performances, reusability and catalytic efficiency even in the darkness.[30,37,38]

The synthesis of the (photo)-catalytic hybrid materials and the characterization of their physico-chemical, optical and electrical properties are the subject of numerous advanced studies intended for better fundamental understanding of this type of (photo)catalysts.

Despite the spectacular photocatalytic effect of these materials, they are very little exploited in (photo)-catalysis. To the very best of our knowledge there are no reviews summarizing the knowledge on PANI-TiO2 based (photo)catalysts. As these hybrid materials have unique features and timely environmental applications, we reasoned to gather and discuss the recently and currently reported studies on the subject in a critical review and to provide some possible future directions.

Table 1. Reviews on TiO_2/polymer nanocomposites used in photocatalytic application.

Title of the review	**Polymer**	**Application**	**Review reference**
Surface modification and enhanced photocatalytic CO_2 reduction performance of TiO_2	Triblock copolymer Pluronic F127	Photocatalytic CO_2 reduction	[39]
Molecularly Imprinted Polymers Modified TiO_2 Nanomaterials	Molecularly Imprinted Polymers	Application in Photocatalytic Degradation	[40]
Polystyrene/Titanium Dioxide Nanocomposites for Photocatalytic Degradation Application	Polystyrene	Application in Photocatalytic Degradation	[41]
Polymeric membrane graphene oxide-TiO_2 for removal of azo dye	Polymeric membranes (Nafion, cellulose acetate, polycarbonate (PC), polysulfone fluoride (PSF), and polyvinylidene fluoride (PVDF)	Photocatalytic removal of Azo Dye	[42]
Polymeric catalytically active membranes for reaction-separation coupling	Polymeric catalytically active membrane (PVA, PVDF, PES, CA, PAN, PTFE, PSF, PEI,Nafion, Chitosan, Sodium alginate)	Reaction-separation coupling	[43]
Photocatalytic coatings via thermal spraying	Polymeric substrates	Application in Photocatalytic Degradation	[44]
TiO_2 based photocatalytic membranes	Polymers membranes (polyamide, polyvinylidenefluoride, polyethersulfone poly(vinylidene fluoride), sulfonated polyethersulfone,, poly(vinylidene fluoride), polyurethane, polyethylene terephthalate, polyester, polyacrylonitrile and polytetrafluoroethylene).	Wastewater treatment and water purification	[45]
Role of conducting polymers in enhancing TiO_2-based photocatalytic dye degradation	Conducting Polymers	Photocatalytic Dye Degradation	[46]

In Table 1, we report handpicked selection of related reviews discussing advances on TiO_2 heterostructure/polymer based catalysts which permits us to emphasize the unique features of the present paper. Indeed, the previously published reviews tackled insulating polymers as

supports for TiO_2 essentially with emphasis on reduction of CO_2 [39], waste water treatment [45] or selective molecular recognition for targeted photocatalyzed degradation of organics [40]. As far as conductive polymer/TiO_2 composites are concerned, much has been done in the past decades but they concern outdated designs and applications. [47,48,49] One can nevertheless cite the review by Riaz *et al* [46] which was devoted to the general role of conducting polymers in enhancing TiO_2-based photocatalytic dye degradation.

Despite the massive material reviewed on TiO_2-polymer catalytic composites, a review that summarizes the knowledge on TiO_2 heterostructre/conductive polymer is lacking. Such a review is important for the following reasons: the combination of other metals, metal oxides, semi-conductors or sp^2 carbon with conductive polymers, particularly polyaniline, permit to impart TiO_2 new features and unprecedented performances that cannot be achieved without such subtle architecting of the hybrid (photo)catalysts. As discussed above, the new salient features include optical properties and catalytic activity under visible light or (simulated) sunlight, if not in darkness.

This is what has motivated us and encouraged to summarize the knowledge on this timely topic.

The present review paper is organized in the following main sections:

- We will give a general insight into TiO_2 as photocatalyst and describe its essential features
- We will then summarize the findings on conductive polymer/TiO_2-based heterostructure nanocomposite photocatalysts
- Then we will concentrate on the design and catalytic performances of PANI/TiO_2-based heterostructures nanocomposites in the (photo)-degradation of organic pollutant applications.

We will finish by critical opinion and future prospects.

2. TiO_2 Photocatalyst

The photo-degradation of organic pollutants with n-type semiconductors, *i.e*, TiO_2 has been the subject of several studies.[50,51] The anatase phase is the most efficient in the photocatalytic degradation systems. The degradation of organic pollutants goes through several stages: (i) the absorption of the contaminating molecule on the surface of the catalyst, often in the dark. The absorption rate strongly depends on the size, the specific surface, the porosity, the morphology and the surface charge of the catalyst; (ii) the catalyst is excited under the effect

of the irradiation, generating active sites which are at the origin of the pollutant's absorption; (iii) the catalytic process ends with a series of radical and oxidation-reduction reactions leading to the decomposition of the pollutant and the formation of H_2O and CO_2. During the photocatalytic degradation of a pollutant, intermediary species are produced, it desorbs from the surface of the catalyst so that the active sites can be re-excited once again and repeats the same procedure until the total mineralization.[33] Figure 1 schematically displays the photo-degradation process of organic pollutant in water in the presence of photo-catalysts.

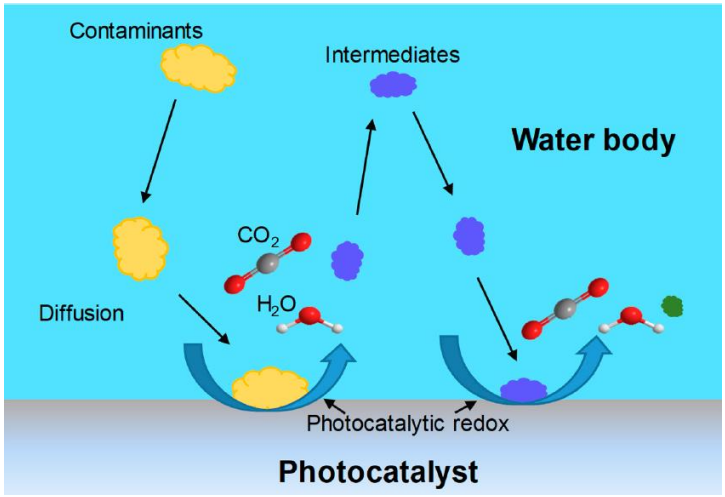

Figure 1. Schematic diagram demonstrating the removal of organic pollutant in water in the presence of photocatalysts.[33]

All photocatalytic oxidation processes are directly linked to the electron-hole pair photo-generated by the catalyst exposed to irradiation. Generally as in the case of TiO_2, the electrons that are present on the TiO_2 valence band (VB) are excited and move toward the conductance band (CB) leaving holes on the VB. The electrons and the holes thus photo-generated migrate towards the surface of the catalyst and participate in the formation of radical species such as $O_2^{-\bullet}$, $OH^\bullet$ from O_2 molecules adsorbed on the surface of the catalyst, H_2O and H_2O_2 which is a strong oxidant used in photocatalysis process in water, as well as hydroxyl radicals originated from the oxidation of water as explained by equations 1-4 (Figure 2, upper panel).[52,53,54] These species are very powerful and they are responsible for any photo-decomposition reaction of pollutants.

$$TiO_2 + h\nu \longrightarrow TiO_2(h_{VB}^{+} + e_{CB}^{-}) \quad (1)$$

$$TiO_2(h_{VB}^{+}) + H_2O \longrightarrow H^{+} + H\dot{O} \quad (2)$$

$$TiO_2(e_{CB}^{-}) + O_2 \longrightarrow TiO_2 + \dot{O}_2^{\ominus} \quad (3)$$

$$TiO_2(e_{CB}^{-}) + H_2O_2 \longrightarrow TiO_2 + OH^{-} + 2H\dot{O} \quad (4)$$

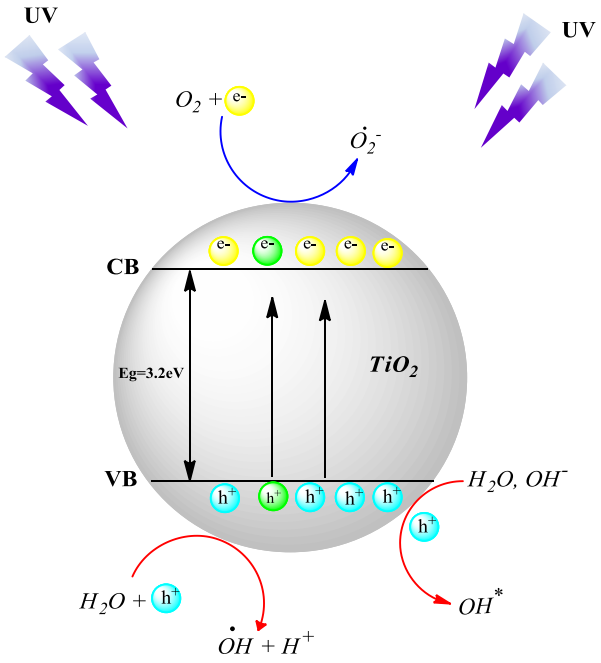

Figure 2. Schematic representation of electron-holes pair separation of TiO_2 under UV irradiation

The mechanism of photocatalyzed degradation of organic pollutants is very well documented and the process is very efficient justifying real life applications of TiO_2, however under UV irradiation only.

3. TiO_2-based heterostructure photocatalyst

The use of TiO_2 photocatalyst is limited because of the wide band gap that limits the absorption threshold of light under 400 nm, and the strong combination of the photogenerated charges, which cause a low photocatalytic yield (Figure 3).

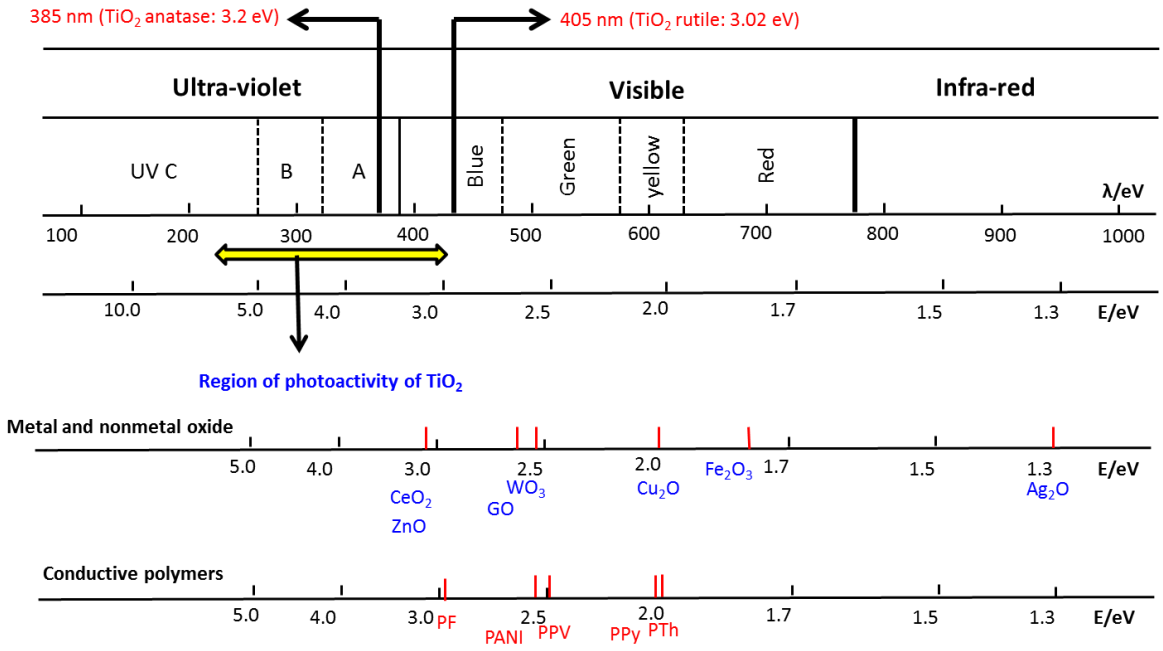

Figure 3. UV region for photoactivity of TiO_2, some metal oxides and conductive polymers most used in the preparation of TiO_2 heterostructures. PF: polyfluorene, PPV: poly(p-phenylene vinylene), Ppy: polypyrrole, PANI: polyaniline and PTh: polythiopphene.

As stated above, the modification of TiO_2 surface with noble metals, metal and non-metal doping, semi-conductors, dye sensitization and ion implantation are strategies for solving the above-mentioned problems, result in very catalytically active heterostructure/heterojunction materials with a broad absorption spectra.[55]

The photocatalytic performances of the heterostructure are often superior to those of single-phase photocatalysts. Therefore, photocatalysts based on TiO_2 heterostructure have been the subject of much study in the last decade. They have shown great potential for application in the degradation of a large variety of organic pollutants and the fractionation of water for the generation of hydrogen. [56]

Several metal-doped TiO_2 materials were fabricated in these last years in order to improve the photocatalytic properties of TiO_2 in the photodegradation of various contaminants under visible light. The doping of TiO_2 is often done by the sol-gel method, co-precipitation and the impregnation method and leads generally to the formation of core-shell structures or random aggregates of mixed particles during the process of preparing structures.[57] The photocatalytic activity of these materials depends strongly on the concentration of the dopant in the final material. This has been demonstrated by Ambrus et al. [58] and Tong et al. [59] who have

indicated in their studies that for an optimal concentration of Fe, the photocatalytic performances of the material is greater, beyond this concentration, the photocatalytic activity decreased. According to these authors, the dopant in optimal concentration participates in the separation of the electron-hole pairs, while in higher concentration; the dopant blocks the photo-catalytic activity of the material by recombinant electron-holes pairs. It is noted that the dopants may occupy the TiO_2 surface sites, affecting the surface properties as well as the zero charge point of TiO_2, and this, is a function of the type and the concentration of doping metal.[24]

Moreover, TiO_2 doped with metallic oxides semi-conductor have received great attention due to the new physico-chemical, electrical, and photocatalytic performances that these oxides confer to the heterojunction. [60] For example, the addition of CeO_2 brings new photocatalytic properties to TiO_2 nanotubes (NTs), this has been investigated by Quang et al.[61] by studying the photodegradation kinetics of methylene blue under visible light. The efficient of degradation of the dye was 100% after 120 min in the presence of CeO_2/TiO_2 NTs and 68% in the presence of TiO_2 P25, indicating the successfully improvements of the catalytic behavior of TiO_2 NTs. Similar results were obtained by Cano-Franco et al. [62], Fiorenza et al.[63] and and Henych et al.[64] in the case of Rhodamine B. ZnO coupled with TiO_2 is also widely used in the field of photocatalysis. Recently, Khaki et al.[65] developed TiO_2-ZnO heterojunction by sol-gel route for photo-remove of dyes. They found that the presence of ZnO significantly enhance the photodegradation of both methyl orange (MO) and methylene blue (MB) in water and under visible light. The photodegradation of MO is 7.75% higher than the MB, which is due to the negative charge of MO and thus its strong adsorption on the surface of the heterojunction catalyst. Mouradi et al.[66] reported TiO_2-coated ZnO nanocomposite fabricated via sol-gel method with ZnO: TiO_2 different molar ratio of 1:50, 3:50, 5:50, 10:50, and 15:50 in TiO_2/ZnO for the decomposition of MB dyes under UV light. According to the Authors, the catalytic activity of the TiO_2/ZnO heterojunction increased with the increase of ZnO molar ratio up to 10 in the heterostructure. Beyond 10, the nanocomposite dislocates its power to absorb UV light and reduces the catalytic efficiency of TiO_2/ZnO heterostructure. Kubiakt et al.[67] demonstrated that the TiO_2/ZnO heterojunction obtained with TiO_2:ZnO molar ratio of 9:1 is much more reactive under UV light in the decomposition of Basic Blue 9 (MB), Basic Red 1 (R6G), and Basic Violet 10 (RhB) dyes. This activity is attributed to the formation of $ZnTiO_3$ during the synthesis of the TiO_2/ZnO heterostructure and the presence TiO_2 anatase as the dominant phase in the photocatalyst. Other metal oxide semi-conductors were selected for

the development of new TiO_2-based heterostructure photocatalysts, namely SnO_2,[68] SiO_2,[69] WO_2,[70] Fe_2O_3,[71] Cu_2O, [72] and NiO. [73] among others.

The non-metallic dopants could also be effective to extend the light absorbance of TiO_2 into the visible region. Their impurity states are near the valence band, but they cannot carry charge and they weakly recombine the electron-hole pair. It was found that the co-doping of TiO_2 with three different non-metal dopants such as N, C and S improves significantly the photo-catalytic activity of TiO_2 under visible light comparing to single non-metallic dopant doped-TiO_2.[74,75,76]

El-Sheikh et al.[77] reported the co-doping of TiO_2 mesoporous anatase–brookite nano-heterojunction photocatalysts with Carbon, nitrogen and sulfur (C, N and S) via sol–gel route. The authors found that the co-doping of TiO_2 mesoporous allowed increasing the photodegradation rate of the cyanotoxin microcystin-LR (MC-LR) under visible light. This photocatalytic efficiency is attributed to the large adsorption capacity of MC-LR target molecule resulting from it faster and easier diffusion to the active sites via the porous TiO_2 system (Figure 4).

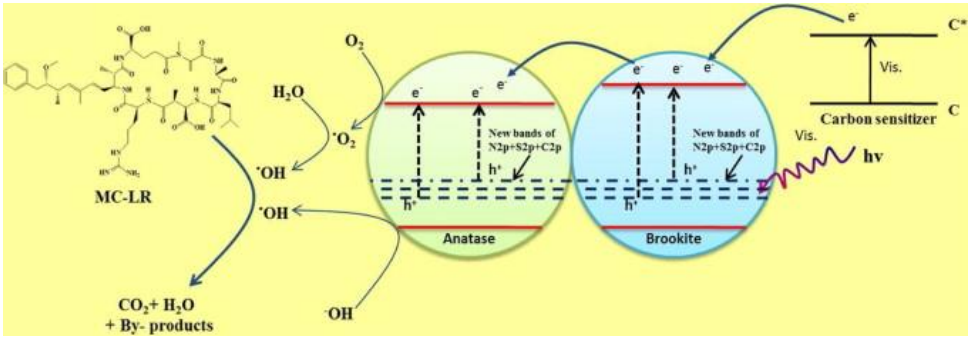

Figure 4. Proposed mechanism illustrating the action of the visible-light-induced C, N and S doped mesoporous anatase–brookite nano-heterojunction photocatalysts for the destruction of microcystin-LR (MC-LR).[77]

Natarajan et al. [78] have studied the effect of adding activated carbon (AC) on the photo-catalytic performance of TiO_2 by preparing CA-loaded anatase TiO_2 nanotube (ATNT) nanocomposite by the hydrothermal method and tested it in the degradation of rhodamine 6G (RhB-6G) under UV light. The results showed that 85% of RhB-6G was degraded in the presence of AC/ATNT, 78% in the presence of ATNT, 60% in the presence of Degussa-P25

TiO_2 and 56% in the presence of anatase TiO_2 NPs (ATNP). The enhancement of the catalytic effect of the nanocomposite is due to the AC that improved dye adsorption on the surface of the photocatalyst as well as the visible light response and reduced the recombination rate of the electron-hole pair within TiO_2 nanotube (Figure 5).

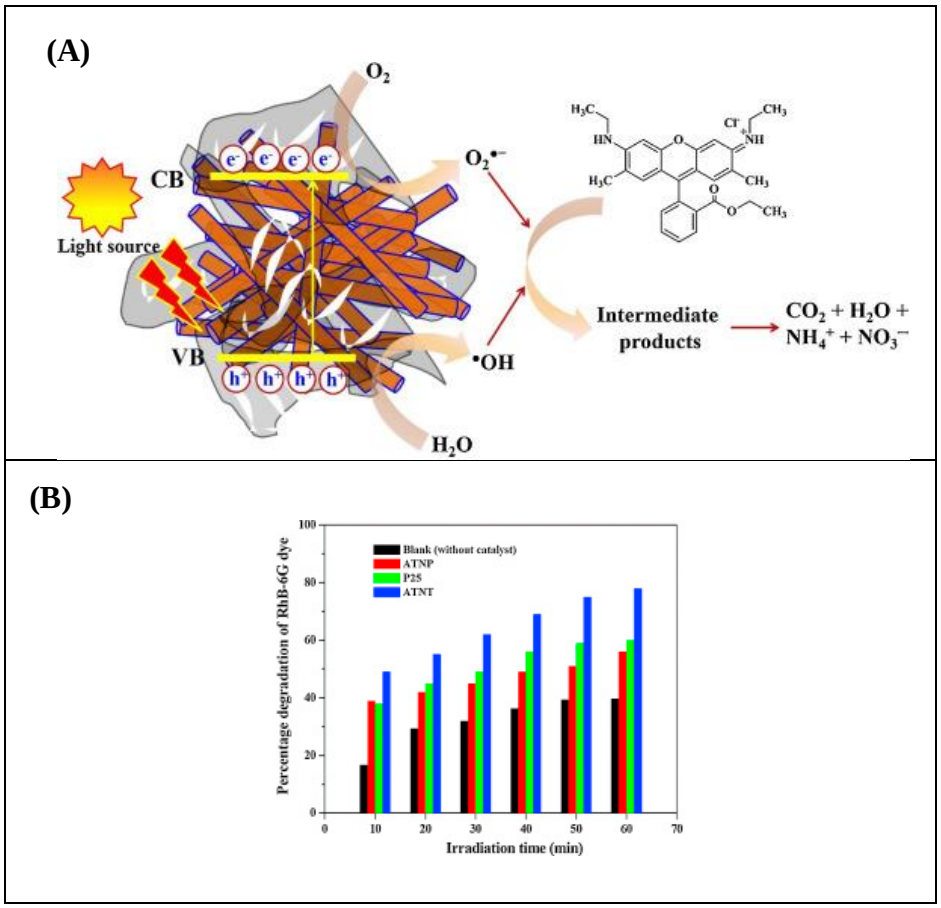

Figure. 5. (A) Schematic representation of RhB-6G dye degradation in the presence of AC/ATNT composite under UV light. (B) Percentage degradation of RhB-6G dye using (a) blank, ATNP, P25, ATNT, (b) and x%-AC/ATNT composites. [78]

Membrane composites modified with TiO_2 for photocatalytic applications were developed. Li et al. [79] prepared a poly(vinylidene fluoride) (PVDF)/TiO_2/Ag membrane for the degradation of MB under visible light. The study showed the increase of the hydrophilic character of the membrane in the presence of TiO_2/Ag nanoparticles (NPs) with a very considerable improvement in catalytic performances with respect to the degradation reaction of MB and the inactivation of bacteria.

Graphene oxide (GO) coupled with TiO_2 NPs are also widely used for the design of membrane composite based on an organic and inorganic blend.[80,81,82] Goa et al.[83] have investigated the degradation reaction of MB in the presence of the Polysulfone/TiO_2/GO membrane under UV light. According to the Authors, the photocatalytic decomposition rate of the dye under UV light is 4 times higher than that obtained under visible light. In addition, Zhang et al.[84] developed membranes of TiO_2 (core)/oleic acid (OA) (shell) modified PVDF supports under UV irradiation to create a new complex named NTiP composites as illustrated in Figure 6. The authors have recorded an excellent photocatalytic efficiency of the membrane in the process of the photo-decomposition of MO under UV light and this thanks to the release of the active sites of TiO_2 particles by the nanolayer located between a particle of TiO_2 and PVDF support, leading to improve mass transfer and photocatalytic activity.

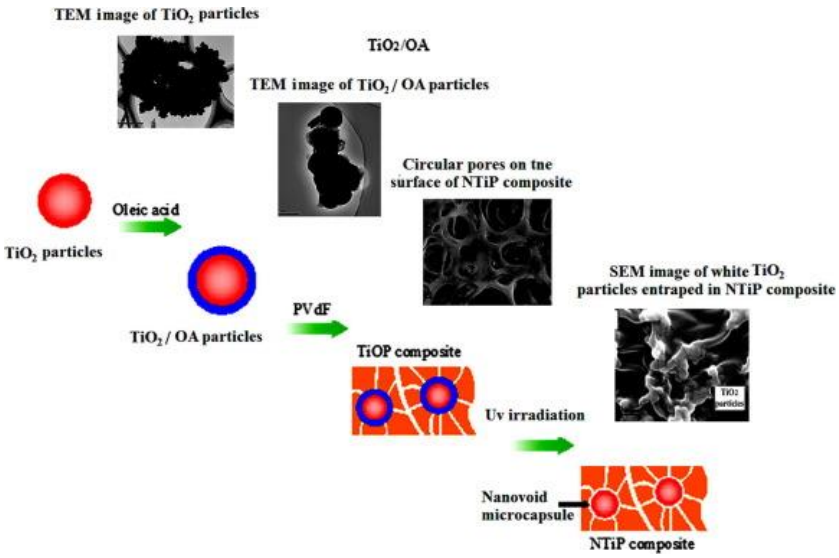

Figure. 6 The scheme for fabrication of NTiP composite and related TEM images (adopted from [84] and [85]).

Despite the catalytic efficiency of TiO_2-based heterostructure, it should be noted that most of the work on metal/nonmetal/semi-conductor-doped TiO_2 heterostructure developed for photocatalytic applications have been done under UV light, indicating that there is still progress to be made to improve the catalytic performances of these materials and so that they can be used effectively under visible light even in the dark.

4. TiO_2/Conductive polymer photocatalyst

The development of organic/inorganic photoactive materials has led to significant advances in heterogeneous photocatalysis under visible irradiation. Recently, the nanocomposites of TiO_2 and conducting polymers have been the subject of a lot of studies due to the advantages that this association offers.[86]

Conducting polymers are good additives able to improving the electrical conductivity, corrosion resistance, solar energy transfer and environmental stability [87,88]. They are also widely known to enhance the photocatalytic efficiency of TiO_2 and many other metallic oxide semi-conductors due to their high absorption coefficients in the visible light. They are good electron donors and transporters and very effective photosensitizers that improve the charge separation at the inorganic (TiO_2)/organic (Conducting polymers) interface. The electrons that are at the highest molecular orbital (HOMO) of the polymer are excited and move to the lowest unoccupied molecular orbital (LUMO). Then, excited electrons (e-) can be injected into TiO_2 conductance band, while the holes (h^+) remain in HOMO of the polymer. In the meantime, holes generated in the TiO_2 valence band. Hence, the improvement of the photocatalytic performances of TiO_2 under visible light. [89]

Several nano(photo)catalysts based on TiO_2/conducting polymer have been developed in different forms such as: 0D (zero-dimensional) nanospheres/particles, 1D nanofibers/wires, 2D nanosheets, and 3D hierarchical architectures. [10]

PANI remains the most widely used conducting polymer in the design of photocatalytic materials that is coupled with TiO_2 or with other inorganic materials.

Recently, we have confirmed the effectiveness of PANI by studying the MO degradation reaction in the presence of TiO_2/PANI and TiO_2/diphenylamine diazonium (DPA)/PANI core/sell nanocomposites under UV irradiation (Figure 7). [90]

The presence of PANI in the nanocomposite promotes the photodegradation of the dye, the latter was completely decomposed and mineralized after 20 min in the presence of the different nanocatalysts (TiO_2, TiO_2/PANI and TiO_2/DPA/PANI) but the degradation rate differs. The rate constant k (min^{-1}) of the photoreaction is 0.1333 min^{-1} in presence of TiO2/DPA/PANI, 0.085 min^{-1} in the presence of TiO_2/PANI and 0.059 min^{-1} in the presence of TiO_2. This difference is due to the amount of PANI in the nanocomposite, namely, TiO_2/DPA/PANI contains a large amount of PANI thanks to the diazonium layer which acts as a coupling agent of the polymer to TiO_2 surface.

This thick layer of PANI constitutes a protective layer of TiO_2; the nanocomposite TiO_2/DPA/PANI is very stable under irradiation and can be reused at least 6 times under the same conditions, 4 times for TiO_2/PANI and only 2 times for the TiO_2.

Table 2 brings together the main (photo)catalytic composite materials based on TiO2/conducting polymer used in the photo-degradation of organic pollutants.

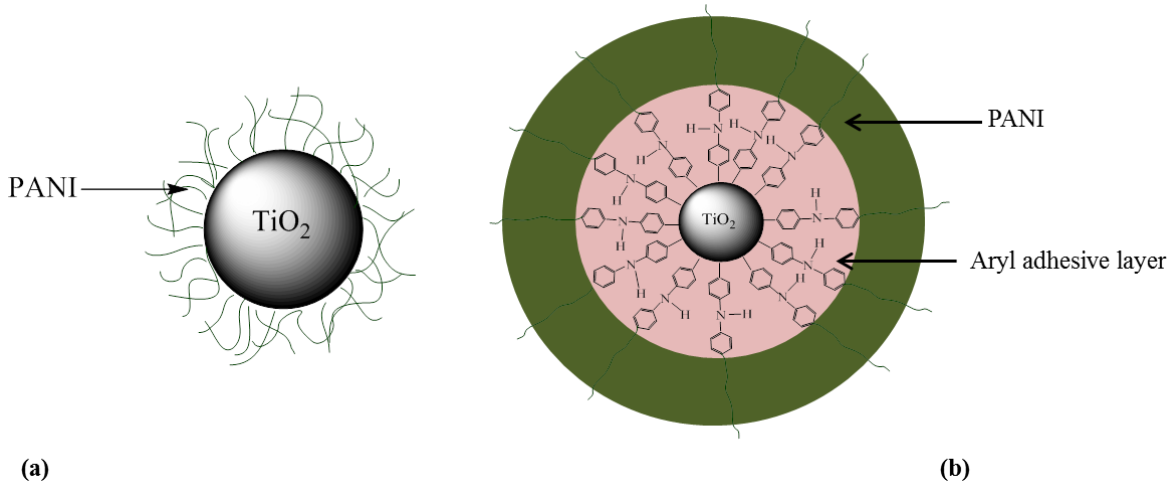

Figure 7. Schematic illustration of the core/shell structure of TiO_2/PANI nanoparticles: (a) TiO_2-PANI prepared without diazonium, and (b) TiO_2-DPA-PANI.[90]

Table 2.TiO_2/conducting polymer (photo)catalysts used in the degradation of organic pollutants.

TiO_2/Conductive polymer (photo)catalyst	**Pollutants**	**Experimental conditions**	**Degradation rate (%)**	**Rate constant (min^{-1})**	**Reference**
Polythiophene (PTh)/TiO_2 0.1g in 100 ml of MO	MO	RT t=120min Visible light [MO]=20 mg/L	85.6%	–	**91**
Poly(3-hexylthiophene) (P3HTh)/TiO_2 0.45g in 450 ml of MO	MO	RT t=10h Visible light [MO]=10 mg/L	88.5%		**92**
(P3HTh)/TiO_2 300mg in 300ml of MO	MO	RT t=60min Visible light [MO]= 10 ppm	96%	0.0408	93
(P3HTh)/TiO_2 10mg in 20ml of MO	MO	RT t=180min Visible light [MO]=2* 10^{-4} M	70%	–	**94**

Ppy/TiO_2 15mg in 100ml of MB	MB	RT t=90min Sunlight light [MB]=10mg/L	>90%	0.0253	**95**
Ppy/TiO_2 40 mg	MB	RT t=80min Visible light [MB]= 15 μM	99%	0.4	**96**
PANI/TiO_2 10mg in 50ml of MO	MO	RT t=20min UV light [MO]=50 mg/L	98.6%	0.0853	**90**
PANI/TiO_2 30mg in 30ml of of MB	MB	RT t=180min UV light [C]=40 mg/L	60%	0.0051	**97**
PANI/TiO_2 1 g/L in 75 mL of Reactive Red 45	Reactive Red 45	RT pH=4 t=180min UV light [C]=30 mg/L	77%	–	**98**
PANI/TiO_2 5 g/L	MO	RT t=60min visible light [MO]=60 mg/L	99%	–	**99**

5. Conductive polymer/TiO_2-based heterostructure photocatalyst

5.1. Polythiophene (PTh)/TiO_2-based heterostructure photocatalyst

PTh is rarely part of the components constituting the TiO_2-based heterojunction (photo)catalysts nanocomposite, only two publications reporting degradation of organic pollutants have been undertaken in the last decade. It is made up of the sulfur and is known by its chemical and thermal stability, charge mobility and its strong absorption in the range of the visible region.

Chandra and co-workers **[100]** have studied the degradation process of nitrobenzene (NB) and malachite green (MG) under visible light in the presence of Sn-doped TiO_2/PTh nanocomposite synthesized by sol gel route at low temperature and oxidative polymerization of thiophene monomer in acidic aqueous $(NH_4)_2S_2O_8$ solution. They reported that the presence of PTh gives the final material a better catalytic activity compared to Sn-doped TiO_2 and high stability under irradiation. Both pollutants are completely decomposed in the presence of PTh with a degradation rate of 99.4% and 98.6% for NB and MG respectively and 72.5% and 70.5% in the presence of Sn-doped TiO_2. Similar results are obtained by the same authors in the case of Cu-doped TiO_2/PTh nanorods used in the degradation of Rhodamine B (Rh B) and Orange G (OG). **[101]** The authors linked this activity to the strong adsorption of the

pollutant on the surface thanks to the large specific surface area of the catalyst and the presence of the PTh on the surface, which protected the photocatalyst and shifted the zone of the activation of TiO_2 towards the visible. In addition, the Cu and Sn metals favored the collection of visible light and charge transport between the different nanocomposite components.

5.2. Polypyrrole (PPy)/TiO_2-based heterostructure photocatalyst

Ppy is one of the most used conductive polymers in several fields such as: biology or medicine, electronics, mechanics, photovoltaic systems, energy-conversion and energy-storage devices…ect.

It is widely used as a component in supercapacitors and has been studied extensively in electrochemistry.[102] However, its low compatibility with aqueous electrolyte as well as its globular and agglomerated morphology affect its electrochemical performances but this does not prevent it from being a promoter candidate for improving the corrosion resistance. [103]

It is also studied in heterogeneous catalysis due to its high thermal, chemical and environmental stability whish make it a stable photosensitizer under irradiation, able to enhance the photo-activity of TiO_2 and other inorganic photo-catalysts.[28]

Ppy coated Ag-Ag_2O/TiO_2 heterojunction nanocomposite was developed by Kumar et al. [28] through the reduction of $AgNO_3$ and in situ oxidative polymerization of pyrrole on TiO_2 Rutile in aqueous medium. They achieved a narrow band gap for the multi-component Ag-Ag_2O/TiO_2/Ppy nanocomposite than Ag/TiO_2 and TiO_2/Ppy; therefore the enhancement of the catalytic efficient of the catalyst under both UV and visible light in the degradation process of MB. They found that the photo-catalytic behavior of the composite under UV is much higher than under visible light irradiation with a divergence of degradation rate of the following order: TiO_2<TiO_2@Ppy<Ag/TiO_2<Ag/TiO_2@Ppy. This order is due to the presence of Ag NPs and Ppy which contribute to the reduction of the electron-hole recombination rate and act as an interfacial electron carrier in the Ag-Ag_2O/TiO_2@Ppy nanocomposite (Figure 8).

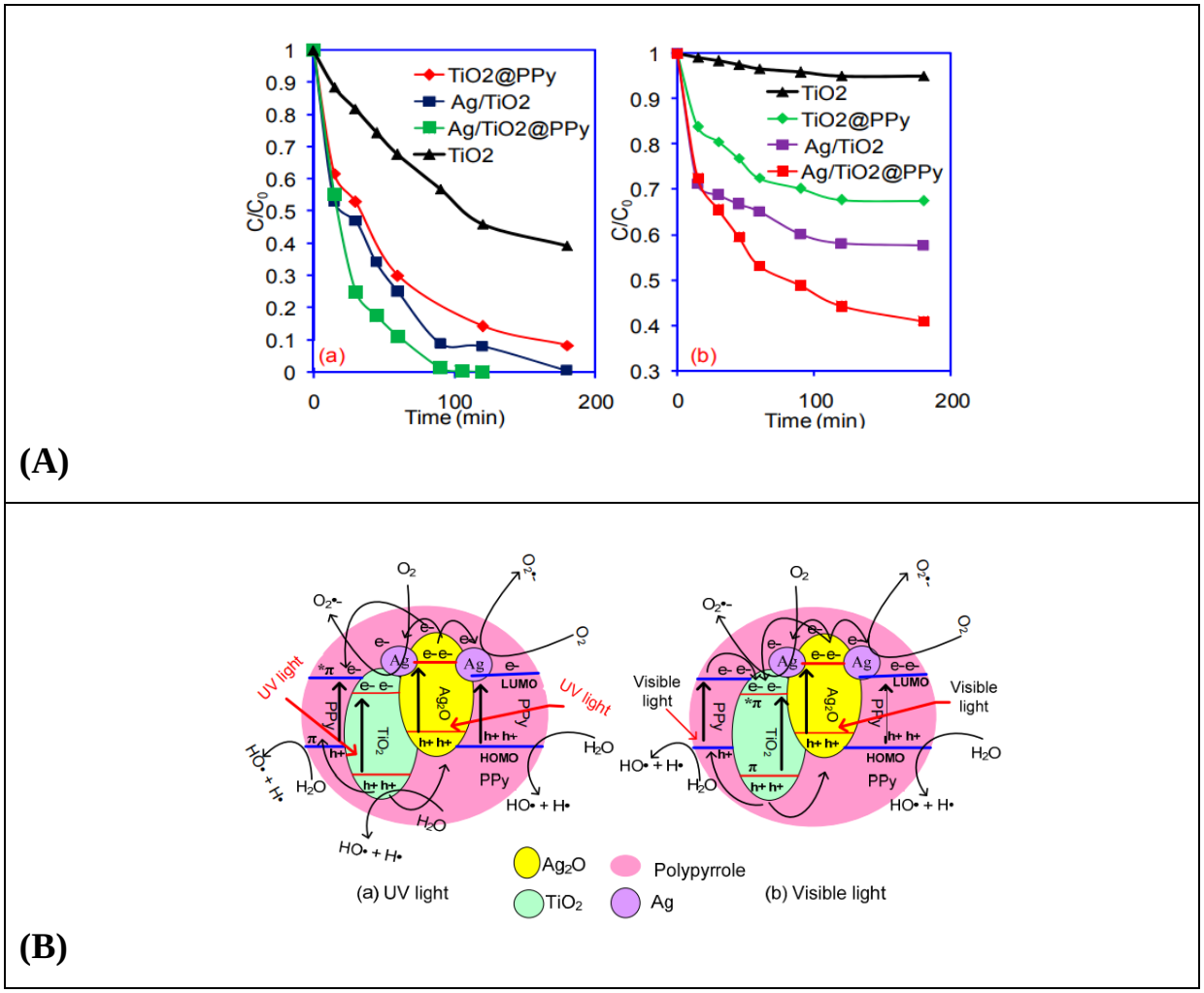

Figure 8. (A) Comparison of photocatalytic degradation efficiency of synthetized heterojunction (a) under UV and (b) under visible light and **(B)** schematic representation of possible electron/hole pair separation mechanism of the Ag-Ag_2O/TiO_2@PPy heterostructure under (a) under UV light (b) under visible light. Adapted from [28].

Yang et al. [104] prepared core-shell Ag-TiO_2-Ppy nanofibers by electrospinning followed by in situ polymerization of pyrrole on Ag-TiO_2 nanofibers in the presence of sodium dodecyl sulfonate, used to reduce the aggregation of Ag-TiO_2 nanofibers during the polymerization reaction. They found that the core-shell structure is very beneficial. The Ppy layer served as a protective layer of Ag NPs that are very reactive and easily oxidize.

They stated also that the band gap of Ag-TiO_2 decreased compared to pristine TiO_2 and this was the effect of the metallic clusters introduced which localized energy levels in the TiO_2 band gap. The presence of Ppy caused a significant increase in the absorption capacity of the UV light, the latter increases with the increase of the amount of the polymer in Ag-Ag_2O/TiO_2@PPy nanocomposite (Figure 9). Since Ppy is an e-donor, it distributes its excited electrons in the CB of TiO_2 for subsequent injection into Fermi levels of Ag, this leads

to improve the catalytic activity of the nanohybrid material. This photocatalytic efficiency has been demonstrated by the decomposition of the gaseous acetone under visible-light irradiation. The study confirmed that the decomposition of the gaseous acetone strongly depends on the content of the polymer in the material. The nanocomposites with an optimal content of 0.1% in Ppy are much more photoreactive than those with 0.2 and 0.5% of Ppy. This shift is due to the balance between the increase of the highest occupied orbital electron potential (HOMO) of Ppy and the decrease in the capacity of light adsorption, due to the balance between the HOMO on the highest atomic orbital of Ppy and the decrease in light adsorption capacity. The light adsorption of TiO_2 is affected by the high load of Ppy, resulting in a blockage of the photocatalytic activity under irradiation.

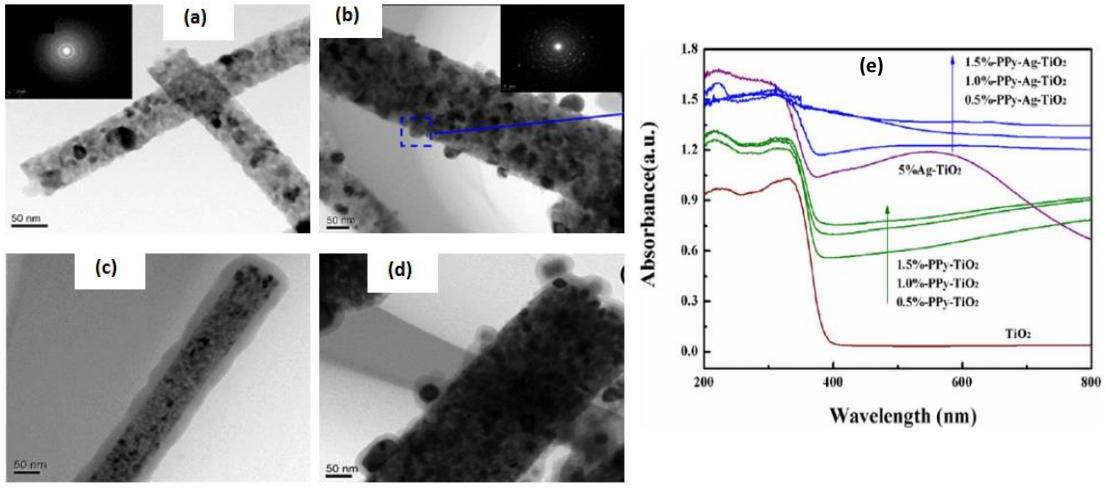

Figure 9. TEM image of (a) TiO_2 nanofibers, (b) Ag-TiO_2 nanofibers, (c) a magnified PPy-TiO_2 nanofiber image and (d) a magnified image of PPy-Ag-TiO_2 nanofiber. (e) UV−vis absorption spectra of different samples adapted from **[104]**.

Other hybrid materials of the type of metal oxides/polymer nanocomposites, namely TiO_2/(TiO_2–V_2O_5)/PPy were designed via sol-gel hydrolysis and in situ oxidative polymerization of pyrrole at different polymerization times (2, 4, 6 and 8 h) on TiO_2 and TiO_2-V_2O_5 particles in the presence of $FeCl_3$ initiator at 0°C.**[105]** The photocatalytic test carried out with the degradation of the MB under the UV light revealed that the incorporation of the V_2O_5 does not bring any improvement of the catalytic activity of the materials. TiO_2/TiO_2-V_2O_5 hybrid material presents photocatalytic activity lower than that of bare TiO_2, which is due to its low UV light absorption capacity. The authors have reported that the incorporation

of Ppy on TiO_2/TiO_2-V_2O_5 hybrid material surface, can significantly improve the separation of the photoexcited charge carriers and making the material active in darkness.

This activity is due also to the light of the energy storage ability of the hybrid metal oxide TiO_2/TiO_2-V_2O_5. The UV light generated photo-excited electrons, some of which were conserved by TiO_2-V_2O_5 mixed oxide; in the dark, these electrons were released to continue the dye decomposition reaction. This corresponds to the loading of TiO_2-V_2O_5 under UV irradiation and discharging in darkness.

Under visible light, the catalytic performances of TiO_2/Ppy composite were worse than that of pristine TiO_2 because of the low reactivity of the Ti metal in the presence of Ppy under irradiation, this was observed generally when the TiO_2 is modified with some metals such as Fe **[106]**, Cr **[107]** and V **[108]**. However, for the hybrid metal oxides TiO_2/TiO_2-V_2O_5, the presence of Ppy has strengthened material activity under visible light; this is attributed to the energy storage capacity of V_2O_5 and the power of Ppy to act as a binder for hybrid metal oxides.

Coconut shell activated carbon (CSC) covered with the Ppy-modified TiO_2 NPs was designed by Tiana and co-workers **[109]**. The conception of CSC-PPy-TiO_2 nanocomposite was made in two steps: the first consists in the in situ polymerization of pyrrole on TiO_2 surface in the presence of ammonium persulfates as initiator; and the second is the combination of the different materials CSC and Ppy/TiO_2 to form the nanocomposite CSC-PPy-TiO_2.

The Ppy-TiO_2 powder was mixed with a mass of CSC active carbon in the presence of Na_2SO_3. The CSC used was already ultrasonicated for 1h and then soaked in HNO_3 for 12h in order to increase the acidity of the surface and the oxygen content with the increase of functional groups containing O_2. The authors studied the effect of load ratio of CSD and Na_2SO_3 with respect to Ppy-modified TiO_2 on the catalytic activity of CSC-PPy-TiO_2 nanocomposite in the degradation of Methyl Orange (MO) under visible light.

They found that for 1:20 and 6:20 ratio of CSD:Ppy-TiO_2, the decomposition rate of MO increases progressively, indicating the increase of the photocatalytic efficiency of CSC-PPy-TiO_2 nanocatalyst. Whereas for a ratio superior than 6:20, the photocatalytic activity of the nanocomposite does not increase, which is due to the large amount of the catalyst which cannot be completely adherent on the surface of CSC and which blocks the pores of the CSC surface and thus reduces the adsorption properties of active carbon. The load ratio of the Na_2SO_3 also has an effect on the photocatalytic activity of the material, ie for a mass of between 0.2 and 1.2 g, the catalytic activity of the nanocomposite increases gradually with the increase of Na_2SO_3 mass but for a mass less than 1.2 g , the catalytic efficiency decreases and

the degradation of MO is slowed down. The reason is that Na_2SO_3 is stuck on the CSC and sealed the porosity of the active carbon which makes its adsorption capacity very low.

For optimal conditions, CSC-PPy-TiO_2 nanocomposite showed a good synergistic effect in the MO degradation process under visible light. Similar results were obtained by Nosrati *et al*. [110] in the degradation of Methylene Blue (MB) under visible light using polyacrylic coating modified with TiO_2/Ppy. The study was carried out by varying the TiO_2 to Ppy weight ratios (100:1, 100:5, and 100:10) on the one hand and the TiO_2/Ppy percentage on the other hand in the conception of the final nanocomposite. They noted that the photocatalytic activity increases with the increase of ppy mass in the material thanks to its contribution in the reduction of the recombination rate of electron-hole pairs in TiO_2. They also found that the nanocomposite containing 3% TiO_2/Ppy (100: 10) has the highest decolonization efficiency.

Same study was investigated by Murugan *et al.* [111] using chitosan-polypyrrole-TiO_2 (Chit-Ppy-TiO_2) hybrid material exploited in the degradation of Methylene Blue dye.

5.3. Polyaniline (PANI)/TiO_2-based heterostructure photocatalyst

5.3.1. PANI/metal-TiO_2

Gnaser et al. [112] had reported that the efficiency and selectivity of a photocatalytic process can be improved by doping the surface of the semi-conductor with metal ions. Various metal ions such as Zn, Fe, Co, Cu, Pt, Au and Ag are widely used as dopant ions of TiO_2 in order to tunes the electronic structure, shifts the light absorption region from UV to visible light and enhance the photocatalytic activity. [113] The activity of TiO_2/metal heterostructure type varies with the amount and the properties of dopant ion. The shift of the absorption zone to the visible region is generally caused by the charge transfer between the metal transition layer d and the TiO_2 conduction or valence band, which generates a new electronic state in the electronic structure of TiO_2. [114] The metal can capture the excited electrons of TiO_2 from the valence band and prevent recombination of the charge carriers. [115]

5.3.2. PANI@TiO_2/Ag

Ansari *et al*. [116] reported the synthesis of an eelectrically conducting Ag/TiO_2@PANI nanocomposites by biogenic−chemical route. At first, Ag-doped TiO_2 heterostructure was prepared using electrochemically active biofilm (EAB) which was suspended in a suspension of TiO_2 and $AgNO_3$. The formation of the heterostructure TiO_2/Ag was followed by its

incorporation into PANI by mixing emeraldine-based PANI/N-methyl-2-pyrrolidone (NMP) with TiO_2/Ag nanocomposite with a percentage of 3% of PANI, using solution casting technique to prepare thin free standing film of Ag/TiO_2@Pani nanocomposite. (Figure 10)

In addition to the thermal stability that the addition of TiO_2/Ag heterostructure confers on the nanocomposite Ag/TiO_2@PANI, it improves the electrical conductivity of the polymer, this has been revealed by the conductivity measurement performed by 4-in-line probe technique, ie, the electrical conductivity of the PANI jumps from 4.54 to 5.45 S/cm after adding TiO_2/Ag heterostructure. This is due to the combination TiO_2/Ag which led to a decrease in the conjugated lengths in the PANI chains and the high mobility of charge carrier, which leads to an increase in the electrical conductivity and thus improves the photocatalytic activity of the material.

The authors reported superior photocatalytic activity in the presence of TiO_2/AG by the degradation process of Methylene Blue (MB) under visible light. In addition, the nanocomposite Ag/TiO_2@PANI has a better stability and can be reused several times without much loss in visible light. The addition of TiO_2/Ag improved the absorption of visible light; the nanocomposite has a high photocurrent compared to that of PANI, resulting in a large separation of electron-hole pairs hence its photocatalytic activity under visible light. Similar results were obtained by Shi et al. [34] by studying the mechanism of degradation of MB under visible light using PANI/TiO_2/Ag membrane.

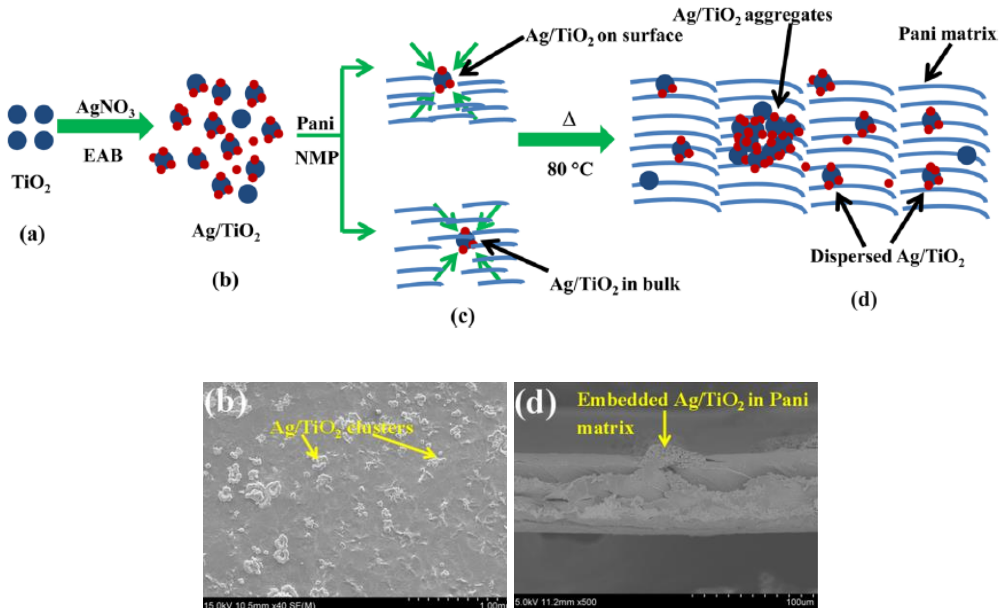

Figure 10. Schematic of the synthesis process of TiO_2/Ag@PANI nanocomposite and SEM images of (b) as-prepared Ag/TiO_2@Pani, and (d) fractured side view of Ag/TiO_2@Pani nanocomposite film. adapted from [116].

In other research studies, the photocatalytic degradation of the MB dye in the presence of PANI/Fe-doped TiO_2 (10, 20 and 30 wt.% of TiO_2) nanocomposites under ultraviolet light irradiation was studied. [113] The doping of TiO_2 NPs with iron (Fe) was carried out by the wet impregnation method, then, aniline monomer was synthetized via in situ polymerization on the surface of Fe-TiO_2 heterostructure.

The study of the optical properties allowed to determine the value of the band gap of TiO_2-Fe/PANI and the reference materials. 2.93, 3.18, 2.30, 2.43 and 2.71 eV for TiO_2, Fe–TiO_2, PANI, PANI/TiO_2 and PANI/Fe–TiO_2 respectively. The TiO_2 band gap expanded after doping with Fe ion and approaches to the UV light region (4.4-12.4 eV), making the material photocatalytically effective under UV light.

Fe-doped TiO_2-based nanocomposites (TiO_2-Fe/PANI and TiO_2-Fe) exhibit superior photocatalytic activity than pristine TiO_2, pure PANI and TiO_2/PANI nanocomposite reference materials. The TiO_2-Fe/PANI nanocomposite is more photo-efficient than TiO_2-Fe under UV irradiation and the best photocatalytic activity was observed using TiO_2-Fe/PANI with 30 wt.% of TiO_2 NPS in the reaction of the degradation of MB.

The participation of the Fe ion during the reaction of dye degradation under UV light lies in its ability to prevent the recombination of photo-induced charge carriers, thus improving the

photocatalytic activity of the nanocomposite.

Other nanocomposites of PANI/metal-TiO_2 type have been developed for applications in photo/catalysis under or without irradiation other than the degradation of organic pollutants are classified in the table 3. All of these studies point to the same conclusion: the doping of TiO_2 with a metal ion improves significantly the (photo)catalytic activity of the corresponding PANI/metal-TiO_2 nanocomposite.

Table 3. Metal/TiO_2/PANI nanocomposites used in (photo)catalysis

Metal/TiO_2/PANI photocatalysts	**Synthesis method**	**Application**	**Experimental conditions**	**results**	**Ref**
Au/TiO_2/PANI	Chemical and electrochemical methods	Photoelectrochemical Biosensing (detection of lactate)	-Substrate ITO -Visible light	- dynamic range of 0.5−210 μM - sensitivity of 0.0401 μA μM^{-1} - detection limit of 0.15 μM	[117]
TiO_2-PANI-Au	Chemical method	synthesis of propargylamines by A^3-coupling between aldehydes, terminal alkynes and amines	-Visible light -T_{room} -Polar/non-polar solvents	**Yield (%)** Toluene 72 $CHCl_3$ 68 DMF 78 CH_3CN 82 DMSO 82 DCM 88 H_2O 92	[118]
Pd/PANI/TiO_2	electrochemical method	methanol electro-oxidation	-Substrate glassy carbon -alkaline media [Methanol]= 0.05- 4.5 M -Without irradiation -scan speed: 50 mV S^{-1}	I=0.24mA cm^{-2} - onset potential= -0.53V	[119]
Pt−TiO2−PANI	Chemical method	methanol electro-oxidation	-UV light irradiation -Acidic medium (H_2SO_4) -scan speed: 50 mV S^{-1}	I=0.84 mA cm^{-2} in dark. I=1.15 mA cm^{-2} under irradiation	[120]
PANI-Pt@ TiO_2	Chemical method	H_2 generation	-visible light -0.10g of catalyst in 80 ml of thioglycolic acid	-visible light activity (61.8 μmol $h^{-1}g^{-1}$ -apparent quantum yield of 10.1%	[121]

5.3.3. PANI/semi-conductor-TiO_2

The construction of photocatalytic nanocomposite materials based on metallic oxide semi-conductor/TiO_2 heterostructure coupled with PANI has increased in the latter decade, designed for applications in photocatalysis thanks to the synergetic effect between the different materials constituting the nanocomposite.

PANI/semi-conductor-TiO_2 are very photo-catalytically active materials due to the ability to reduce the recombination rate of the photo-excessive charge carriers which constitutes a major problem directly associated with the activation of visible light by adding doping materials or defects in the TiO_2 gap band.[122]

The study conducted by Brooms et al. [123] Reports the doping of TiO_2 anatase nanoparticles with ZnO prepared in the first stage via co-precipitation method. Such inorganic hybrid material TiO_2-ZnO with a molar ratio of TiO_2: ZnO of 1:1 served for the elaboration of TiO_2-ZnO/PANI nanocomposite by in situ chemical oxidative polymerization of aniline monomers in various amounts using ammonium persulfate. TiO_2-ZnO/PANI nanocomposite particles are of small size nanometric order between 20 and 30 nm, very close to that of pristine TiO_2 and TiO_2/ZnO hybrid material also included in the same range. The doping of TiO_2 with ZnO and the addition of PANI gave the nanocomposite a great thermal stability thanks to the strong interaction between the inorganic hybrid material and the polymeric layer, which led to the restriction of the thermal movement of PANI.

The nanocomposite was designed for the removal of P-Cresol under UV-light and its catalytic activity was compared to that of prestine TiO_2, ZnO and TiO_2/ZnO heterostructure.

The authors report a strong catalytic activity of TiO2-ZnO/PANI nanocomposite under UV light; it degrades P-Cresol to 99% in 6h with a degradation reaction rate constant of 0.9679 min-1, more than twice compared to that of TiO_2/ZnO. As mentioned above, this high activity is directly related to the synergistic effect between the constituents of the nanocomposite resulted in charge separation caused by the transfer of TiO_2/ZnO holes to PANI's HOMO atomic orbital.

The effect of the molar ratio of PANI in the nanocomposite was also studied by evaluating the catalytic efficiency of the nanocomposites prepared at different molar ratios of PANI:TiO_2/ZnO of 0.5:2, 0.1:2 and 5:2 in the degradation of P-Cresol under UV light.

The best activity was recorded with the ratio of 0.5:2 of PANI: TiO_2/ZnO. A thick layer of PANI (5:2) constitute a barrier preventing the catalyst from absorbing light while a thin layer

allows penetration of the UV light to the TiO_2 surface and thus improves the charge transfer at TiO_2/ZnO//PANI interface.

Faraji et al. reported the photocatalytic activity of the Binder-free PANI-WO_3/TiO_2NTs/Ti plates which was fabricated via pulse reverse co-electrodeposition of PANI and WO_3 onto the previously formed TiO_2 NTs/Ti by electrochemical anodic oxidation of Ti plates. Its photocatalytic behavior was tested in the decomposition of organic pollution Methyl Orange (MO) dye under UV light irradiation.The Anodization of Ti plate was carried out in an electrochemical cell containing glycerol/water (75:25, vol.%)+0.5 wt.% NH_4F at 20 V for 2 h. The anodization process was finished by annealing at 450 °C for 2 h in order to crystallize the TiO_2NTs/Ti plates to anatase phase; Then followed by the electrodeposition of of WO_3 under potentiostatic conditions in acidic electrolyte and finally, in situ electro-deposition of PANI on the modified-Ti plate surface. The anodizing allowed to have an attractive tubular surface, the nanotubes are regular of size of about 70 nm that were totally covered by the WO_3/PANI hybrid layer (Figure 11A). As the photocatalytic activity of a catalyst depends on the photo-generated charge transfer, the measurement of the photocurrent electrochemically is important to predict the catalytic efficiency of the materials. The PANI-WO_3/TiO_2NTs/Ti plate exhibits a high photocurrent compared to TiO_2/Ti, WO_3/TiO_2/Ti, and PANI/TiO_2/Ti, so, easy transfer and fast separation efficiency of photogenerated charge. Therefore should have a better activity under UV irradiation (Figure 11B).

The results of the MO degradation mechanism are in agreement with those of photocurrent measurement, ie, PANI-WO_3/TiO_2NTs/Ti nanocomposite exhibits a high photocatalytic performances than those of associated materials. This efficiency attributed the synergetic effect among PANI, WO_3 and TiO_2 NTs, this has led to a reduction of the recombination rate of the photo-generated electron-hole pairs and thus to the improvement of the surface properties of the TiO_2NTs/Ti plates (Figure 11C).

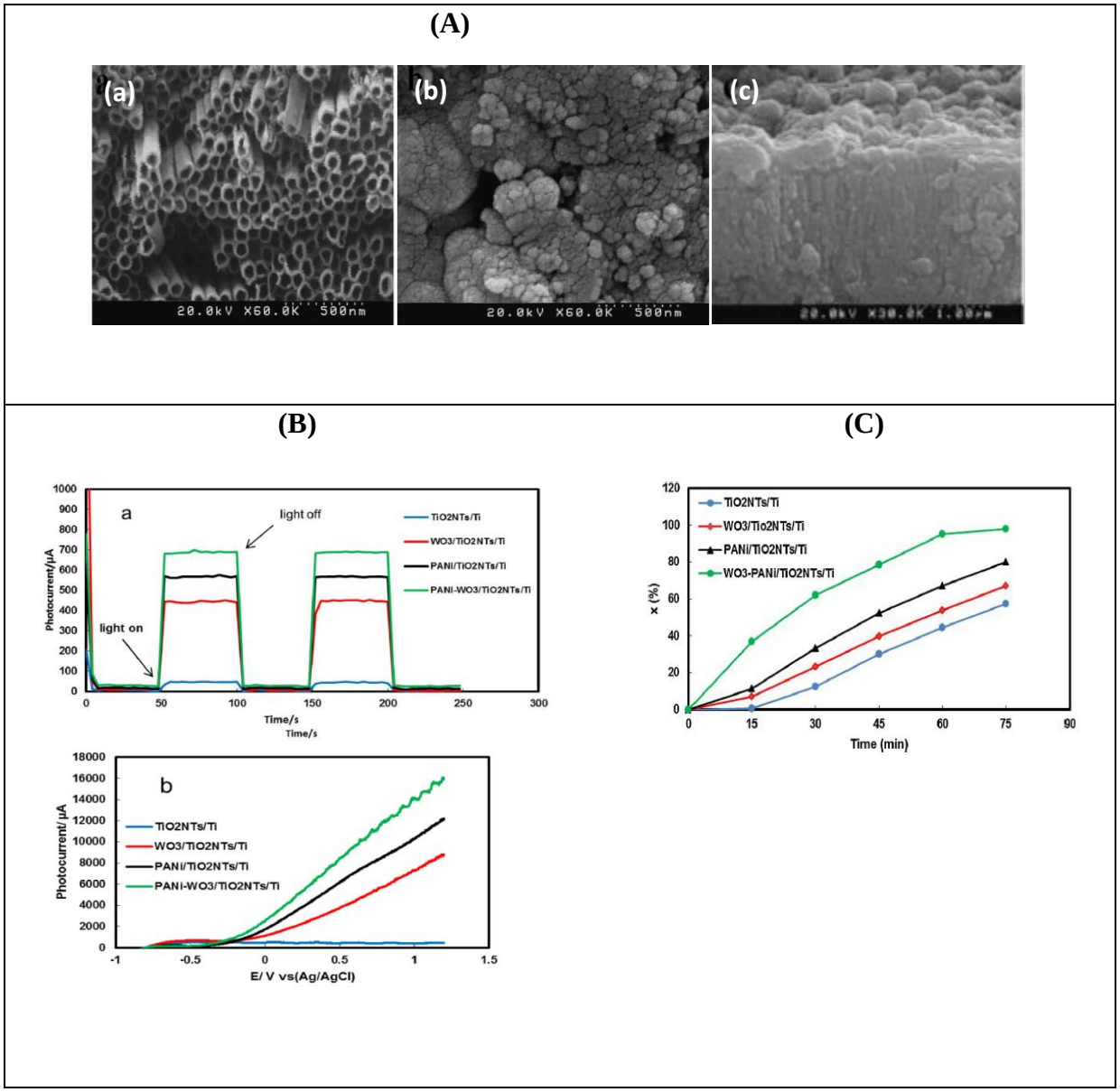

Figure 11. (A) SEM images of bare TiO_2NTs/Ti plate (a), PANI-WO_3/TiO_2NTs/Ti plate (b) and cross section image of PANI-WO_3/TiO_2NTs/Ti plat(c). **(B)** Photocurrent density of the fabricated plates at −0.2 V (a), Linear sweep voltammograms of different obtained plates in 1.0M H_2SO_4 at scan rate of 20 mV/s under UV lamp irradiation (b). **(C)**The degradation curves of MO using PANI-WO_3/TiO_2NTs/Ti, PANI/TiO_2NTs/Ti, WO_3/TiO_2NTs/Ti and bare/TiO_2NTs/Ti plates adapted from [Erreur ! Signet non défini.].

TiO_2/Nb_2O_5/PANI nanocatalyst was successfully prepared via hydrothermal method with in-situ chemical oxidative polymerization of aniline monomer.[124] The authors have shown once again that the TiO_2 doping as well as the combination of TiO_2-based hybrid materials and PANI improves significantly the catalytic performance of the final material, and this by

evaluating the catalytic properties of TiO_2/Nb_2O_5/PANI nanocomposite toward the degradation of Methylene bleu (MB) under visible light at neutral pH.

Compared to the bare TiO_2 and TiO_2/Nb_2O_5, the maximum degradation yield of the dye has been registered after 240 min in the presence of TiO_2/Nb_2O_5/PANI under visible light irradiation.

pH is a very important parameter in photocatalytic processes. The surface charge of the catalysts depends on the pH of the solution to be degraded. The adsorption of the pollutant on the surface of the catalyst promotes its degradation through the interactions between the inorganic species and the PANI. The pH has also an effect on the OH• radicals and $O^{2-\bullet}$ anion radicals which are responsible for any photocatalytic reaction.[125]

The study carried out by the authors with varying pH (5, 6.9, 9, 10) reveals that the best degradation yield of 99% is observed at pH 5 and 9. pH=6.9 is the zero point charge of the catalyst. At alkaline pH, the catalyst surface is negatively charged and inversely positive in acidic conditions. OH• radicals are generated by the reaction of the hydroxide ions with the positive pores of the catalyst surface.[126] In acidic medium, the concentration of OH ions and the concentration of OH• radicals are reduced, which leads to a decrease in the efficiency of the catalyst and the decrease in the degradation reaction rate of the pollutant.[127]

In solution, MB is positively charged. At alkaline pH, the surface of the nanocatalyst adopts the negative charge which promotes the adsorption of the dye on the photocatalyst surface, and acidic pH (pH = 5) will restrict the adsorption. Therefore, the excellent catalytic activity of the photocatalyst is due to the presence of hydroxyl radicals arising from the oxidation of adsorbed water or adsorbed OH^-.

5.3.4. PANI/mixed oxide-TiO_2

Huang et al.[128] prepared a nanocomposite based on $Fe_3O_4/SiO_2/TiO_2$ microspheres coupled with PANI. The $Fe_3O_4/SiO_2/TiO_2$ microspheres were prepared by the sol gel route followed by in situ oxidative polymerization of aniline. They have demonstrated that the effect of PANI in the improving of the catalytic performances of TiO_2 on the one hand and $Fe_3O_4/SiO_2/TiO_2$ microspheres on the other hand is spectacular; and this, by the study of the photo-degradation reaction of MB dye under visible light.

The results obtained in this study are attributed to the different transfer rates of photoinduced carriers and the recombination electron-hole pairs. The narrow band of Fe_3O_4 causes an

increase in the incidence of electron-hole recombination and decrease in photoactivity of the material. While the SiO_2 intermediate layer between Fe_3O_4 core and the TiO_2 shell promotes the photocatalytic activity by decreasing the electronic interactions at the interface of the heterojunctions.

Leng and his collaborators [129] have combined the $CoFe_2O_4$ mixed oxide NPs with TiO_2 NPs by hydrothermal treatment. The heterostructure thus formed was used for the development of PANI/$CoFe_2O_4$-TiO_2 nanocomposite with hierarchical flower form by in situ polymerization of aniline. They suggest two mechanism of transferring charge under irradiation:

Under UV light, TiO_2, PANI, and $CoFe_2O_4$ all can absorb photons to generate electron–hole pairs. The relative energy level of them creates a synergistic effect. The photogenerated electrons in the LUMO of PANI can inject into the CB of TiO_2, and then transfer into the CB of $CoFe_2O_4$. The photogenerated holes in TiO_2 VB can transfer to the HOMO of PANI. (Figure 12a). The photogenerated holes in the VB of TiO_2 can transfer into the VB of $CoFe_2O_4$, and then transfer into the HOMO of PANI. (Figure 12b)

Both mechanisms result in charge separation, thus hindering the process of recombination. Promoting the separation of electron-hole pairs and significantly improves the photocatalytic capacity of nanocomposite

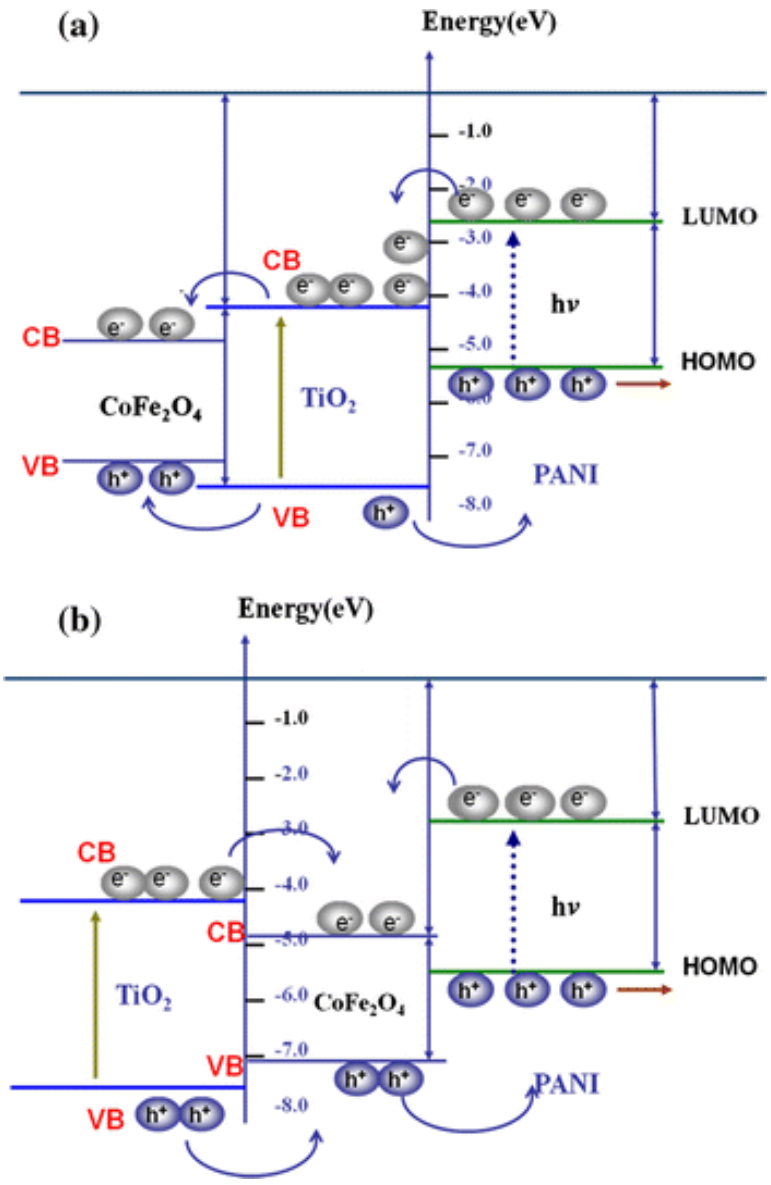

Figure 12. Possible charge carrier transfer mechanism in PANI/$CoFe_2O_4$-TiO_2 system under UV light irradiation adapted from [129].

The same catalytic study as that carried out by Huang et al. [128] was carried out in this study using PANI/$CoFe_2O_4$-TiO_2 nanocomposite as a catalyst, and they came to the same conclusions. The presence of PANI improves significantly the catalytic activity of TiO_2, $CoFe_2O_4$ and the $CoFe_2O_4$-TiO_2 heterostructure. The latter exhibits an excellent catalytic activity under UV and visible light comparing to PANI/TiO_2 and PANI/$CoFe_2O_4$. This efficiency is attributed to the effect of synergy between the different components of the nanocomposite, which improves the charge separation, but also to the ferromagnetic

properties of $CoFe_2O_4$ maintained in the nanocomposite. This promotes its separation from the liquid phase during the reaction by applying an external magnetic field, which makes these materials promising for the photocatalytic treatment of wastewater. While Li[130] related the catalytic efficiency of the nanocomposite photocatalyst $ZnFe_2O_4/TiO_2$/PANI during the photocatalytic decomposition of MO and RhB under UV light, to the interactions between the different components of the nanocomposite as well as its high electrical conductivity. He also points out that the improvement of the catalytic performances of the material did not take place except in the presence of PANI on $ZnFe_2O_4/TiO_2$ surface.

Other studies whose results are in agreement with those mentioned above are carried out by Feizpoor [131] which compared the catalytic activity of TiO_2, $TiO_2/CoMoO_4$ and $TiO_2/CoMoO_4$ coated with the PANI (30%) in the degradation of several organic pollutants namely: MO, MB, RhB and fuchsine, under irradiation of visible light; and Zhao et al.[132] which associated Go-modified $BiVO_4$ to TiO_2 to design a new nanocomposite in combination with PANI. The final Nanocomposite $BiVO_4$-GO-TiO_2-PANI has been used as a photocatalyst in the degradation process of MB and phenol under visible light.

All of these studies lead to a single conclusion that relies on the contribution of the mixed oxide-TiO_2 heterostructure in catalysis process on the one hand, and the spectacular role of PANI in improving the absorption capacity of visible light by TiO_2, and thus the improvement of its catalytic activity under illumination.

Recently, we have demonstrated that some metals oxide make the TiO_2/PANI nanocomposite functional in the dark, such as RuO_2, which has attracted a lot of interest because of its high chemical and thermal stability, its low resistivity, its high resistance to chemical corrosion and its excellent diffusion properties that make it an interesting material in many applications. [133, 134] It has electrical conductive metallic character due to its partial filled metal (d) -oxygen (p) π * band[135,136].

Mixed oxide nanoparticles (NP) RuO_2-TiO_2 prepared by gel sol was modified with diphenylamino groups (DPA) from the diazonium precursor. The grafting method chosen is based on a 4-diphenylamine diazonium salt using ascorbic acid as a reducing agent.

The modification of RuO_2-TiO_2 NPs is followed by the in situ synthesis of polyaniline thus providing the RuO_2/TiO_2-DPA-PANI nanocomposite. As the diazonium salt is a coupling agent, the amount of PANI deposited on the DPA-modified RuO_2-TiO_2 surface is much higher than that deposited on naked RuO_2-TiO_2.

Electrical measurements made by probe four points reveal that the presence of RuO_2 increases the conductivity of the composite material. The conductivity of the heterostructure RuO_2-TiO_2 is much higher than that recorded for pristine TiO_2, and the resistivity heterojunction is three times lower than that of pure TiO_2.

As the in situ polymerization of aniline was doing in ammonium persulfates, the PANI present on the surface of RuO_2-TiO_2 is doped with SO_4^{2-} at 50% and the measured conductivity is 94 S/cm. the results show that the conductivity of the materials obtained increases with the increase of the amount of PANI; it's worth 343 and 384 S/cm for RuO_2-TiO_2/PANI and RuO_2-TiO_2/DPA/PANI respectively.

These results allowed prediction that the catalytic activity of materials containing PANI could be better than pristine RuO_2-TiO_2. This has been confirmed by the study of the degradation of MO reaction. RuO_2-TiO_2/DPA/PANI nanocomposite revealed superior catalytic properties in comparison to RuO_2-TiO_2/PANI and RuO_2-TiO_2 towards the degradation of MO even in the darkness. Such remarkable performance depends on the amount of PANI in the nanocomposites. The electronic displacements at the interface of the heterojunction metal/semi-conductor and the synergistic effect between PANI and RuO_2-TiO_2 nanoparticles result in a reduction of the photo-electron-hole recombination rate as well as a significant catalytic activity of the catalyst in darkness. As a matter of fact, pristine RuO_2/TiO_2 mixed oxide NPs photocatalyze the degradation of MO under simulated sunlight and UV light but not in the dark.

The degradation of OM in the presence of RuO_2-TiO_2/DPA/PANI nanocomposite depends only on the PANI and RuO_2 as TiO_2 is a photocatalyst that activates only under UV light.

PANI is known as an electron donor; in the dark, the electrons that are stored on the LUMO are released and recovered by RuO_2 leaving holes on the HOMO. The electrons and holes are very important in any catalytic process; they promote the formation of $OH^{\bullet}$ radicals and $O_2^{\bullet -}$ anion radicals which are responsible for the decomposition reaction of organic pollutants (Figure 13). [38]

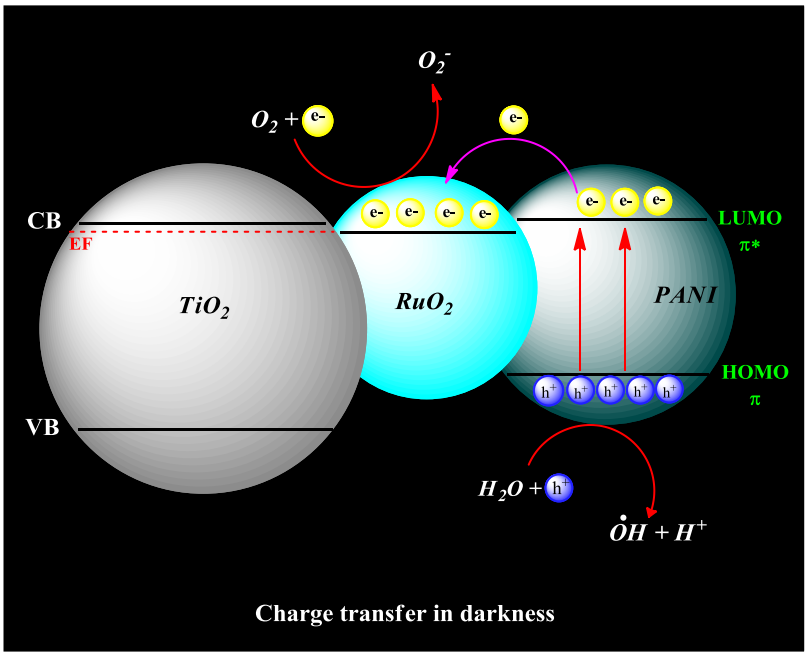

Figure 13. Charge transfer in RuO_2-TiO_2/DPA/PANI nanocomposite in darkness [38].

5.3.5. PANI/graphite-TiO_2

Carbon nanomaterials such as carbon nanotubes, graphene (GN) and graphene oxide (GO) have been widely used to improve the photocatalytic power of TiO_2. They are very effective materials, able to promote charge separation.[137] It has been found that TiO_2-GN heterostructures are good electron sensors, possessing a large storage capacity and a high charge transfer rate. Park et al.[138] has demonstrated that the TiO_2 band gap goes from 3.2 to 2.8 eV by associating with Graphene NPs, which means an improvement in the catalytic activity of TiO_2 under illumination. Stengl et al.[139] prepared TiO_2/GN heterostructure nanocomposite by a one-pot process and revealed its high efficiency towards the decomposition and the mineralization of butane. Similar results were obtained by Zhou et al.[140] who observed a highly efficient degradation of MB under sunlight irradiation. Zhang [141] observed a superior catalytic effect and a stability of TiO_2/GN nanocomposite compared to that of pristine TiO_2 toward the degradation reaction of benzene gas phase and under ambient conditions. However, the doping of TiO_2 with the GN must be studied and optimized, i.e. high or low doping blocks the TiO_2 activity and thus leads to the slowing down of the photocatalytic process.[142] The modification of TiO_2 with graphitic carbon nitride (g-C_3N_4) was also investigated due to its thermal and chemical stability, with a narrow bandgap (2.7 eV). However, the application of g-C_3N_4-TiO_2 heterostructure in heterogeneous catalysis is

limited because of the low absorption of visible light by materials and the low rate of charge transfer by g-C_3N_4. [143]

As mentioned above, the PANI-sensitized TiO_2 increases the absorption of ultraviolet and visible light, in addition to its high electrical conductivity and its good stability under ultraviolet rays. So, the combination TiO_2-GN-PANI should further modify the catalytic and physico-chemical properties of TiO_2 under irradiation.

The table 4 gathers all the works which are based on the synthesis of nanocomposites of type TiO_2-(GN/GO)-PANI as well as their activity in photocatalytic processes, reported in these last decade.

Table 4. Carbon materials-doped TiO_2-PANI nanocomposites used in (photo)catalysis

Nanocomposites	**Applications**	**Irradiation**	**Rate constant (k. min-1). Photo-current (I_p. A/cm^2)**	**References**
PANI–GN–TiO_2	Photoelectrocatalytic water oxidation	Visible light	//	[144]
PANI@TiO_2/GN	Degradation of MB and biological activity	Visible light	k=0.001, 0.001 at pH 3 and 5. 0.004 at pH 7. 0.008 at pH 9.	[142]
PANI-GN-TiO_2	Photo-generated cathodic protection	Intermittent light	Ip =13 A/cm^2	[145]
GO-PANI/TiO_2	Degradation of phenol, biphenol and 2,4-dichlorophenol	Visible light	Ip=3.21 mA/cm^2	[146]
PANI-TiO_2-GN	Oxygen reduction reaction activity and immobilization of bacteria	Without irradiation	//	[147]
PANI/TiO_2/GO	Degradation of Bisphenol A	UV light	I_P=10.5. 10^{-5}A	[148]
PANI-CNT/TiO_2	Degradation of diethyl phthalate	Visible light	k= 4.1.10^{-3}	[149]
PANI−g‑C_3N_4−TiO_2	Photocatalyzed Synthesis of α‑Chloro Aryl Ketones	Visible light	//	[143]

All these studies show that the nanocomposites PANI-TiO_2-GN/GO reveal a great catalytic activity, but we could not carry out a comparative study of the rate constants k and the photo-currant of the nanocomposite with those of pristine TiO_2 and TiO_2-GN/GO heterostructure because the majority of the articles did not report them.

6. Critical opinion

At this stage, we can conclude that the metallic and non-metallic doping of TiO_2 can further shift the bandgap and make the photocatalytic activity of TiO_2 possible under visible light.
The decrease in the value of the band gap varies with the nature of the element doping TiO_2.
Nitrogen, for example, as well as carbon and sulfur have the power to improve the growth orientation during the modification of TiO_2, affect the microstructure surface, induce narrowing of the bandgap down to 2.4 eV and improves the photocatalytic activity of TiO_2 under visible light. (Figure 14a).
This effect was thought to be due to the N atom wish replaces the oxygen of TiO_2 in the substitution case and the visible light response is caused by the occupied N2p delocalized states.[150] The mechanism explaining the origin of the absorption of visible light by N-modified TiO_2 remains under debate up to now.
The metal doping of TiO_2 can introduce an intra-band state close to CB edge, which results in a red shift in bandgap adsorption due to the sub-band gap energies.[151]
The gap of TiO_2 varies with the doping metal; it goes from 3.2 eV to3.16, 3.14, 3.05, 3, 2.6 and 2.2 by the doping with Pb, Sn, Ge, Si, Fe and Fe_2 respectively.[152] (Figure 14b)
The bandgap energy, Fermi level, and d-electron configuration of the electronic structure in TiO_2 can be effectively modulated by the metal doping. The lattice forms a wide range of new energy levels below the CB of TiO_2, resulting from their partial filled d - orbitals, which leads to the red shift of the band gap and increases the power visible light absorption. [153]
The metal ions modify the equilibrium concentration of the charge carriers by trapping electrons and decreasing and sometimes delete the recombination rate of electron-hole pairs, and thus improve the photocatalytic performances of TiO_2.[152]
The co-doping using two or more doping atoms can passivate the impurity bands and reduce the formation of recombination centers by increasing the solubility limit of the dopants. The co-doping can also solve the problem of charge recombination to improve the photocatalytic activity of TiO_2.[152] It can also reduce the TiO_2 bandgap better than the presence

of a single dopant as in the case of doped TiO_2 N which goes from 2.4 to 2.3 eV in the presence of Tungsten (W) as co-dopant. [154] (Figure 14c).

Wang et al.[155] have shown that co-doping TiO_2 with (N,Cu) enhances the photocatalytic effect of TiO_2 in blue methyl degradation process. They found that at the equilibrium, the adsorption of the dye on co-doped TiO_2 photocatalyst surface in darkness reached 7.7% while 5.9% of the dye was adsorbed on N-doped TiO_2 surface. This is attributed to the low specific surface area of N-doped TiO_2 and the improvement of the absorption by the co-doped catalyst could be attributed to its surface modification by Cu doping.

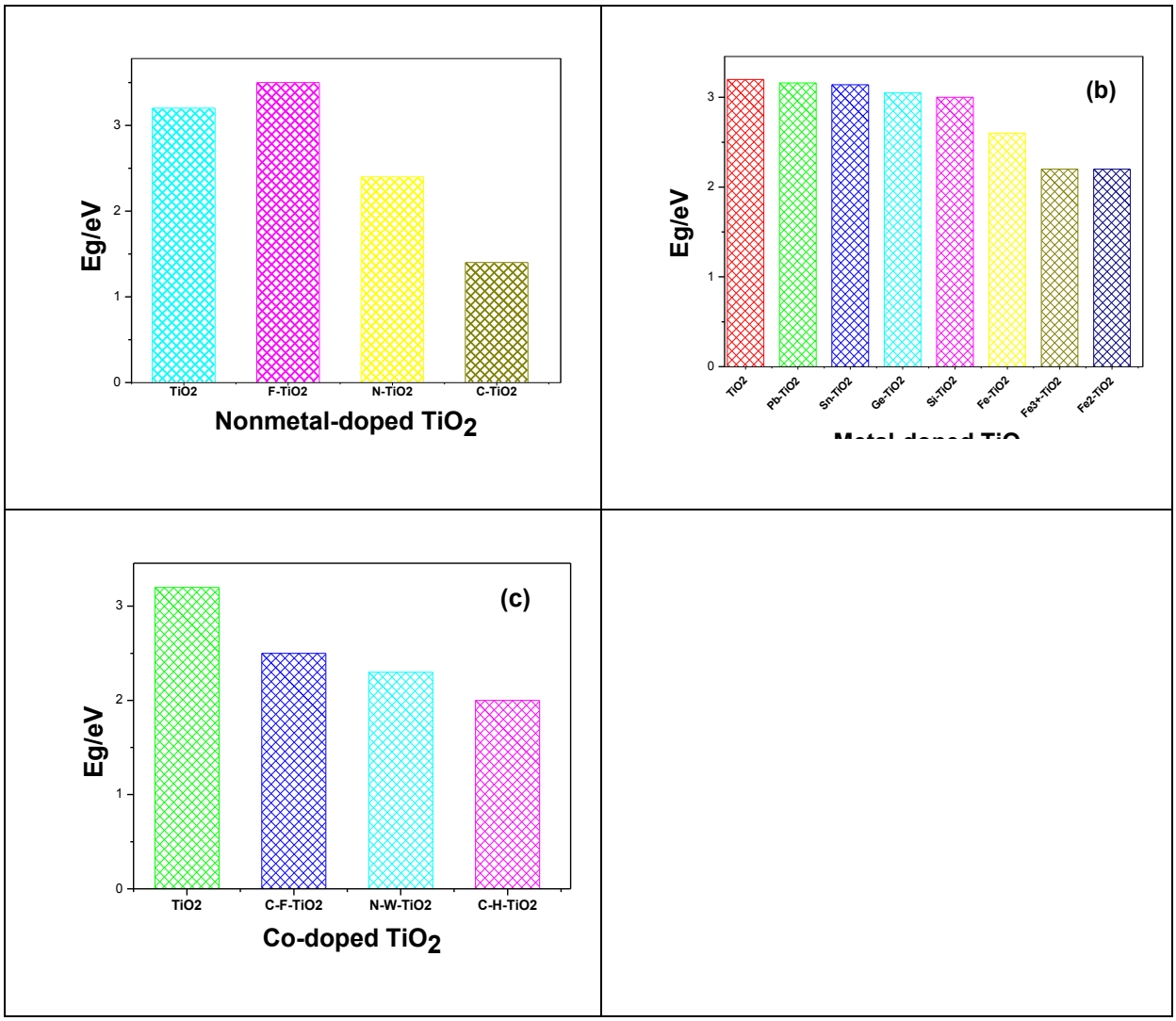

Figure 14. Variation TiO_2 gap energy as a function of the dopant nature.

The modified TiO_2 gap energy also depends on the amount of the modifying element. the integrality of the investigations undertaken on the influence of the quantity of the dopant on the improvement of the catalytic efficiency of TiO_2 indicate that the gap energy decreases with the increase of the percentage of the dopant in the heterostructure, which leads to thus a strong photocatalytic activity in the visible.

Ha et al.[156] showed that the band gap is shrinking when the concentration of N dopant increases. It goes from 3.2 eV to 2.9 eV in the presence of 4Wt% N and 2.4 eV in the presence of 9.4Wt% N. This improves significantly the photocatalytic properties of TiO_2 under visible light. The increase in the catalytic effect is due to the improvement of the absorption capacities of the surface. (Figure 15 a)

Similar conclusions were reported by Fang [157] and Beldjebli [158] in the case of F-modified TiO_2 and Al-doped TiO_2 photocatalyst. (Figure 15b and c)

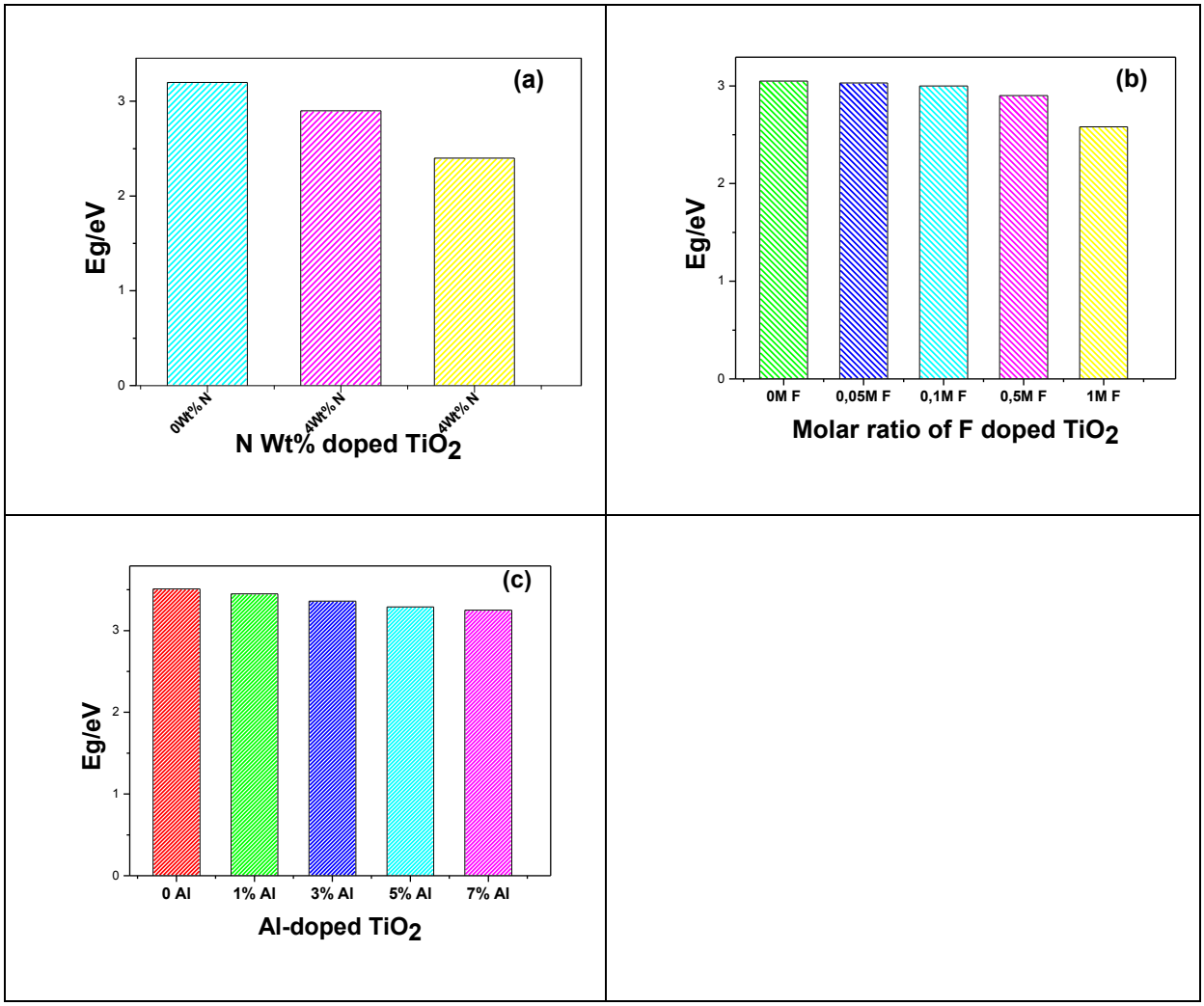

Figure 15. Variation TiO_2 gap energy as a function of the quantity of the dopant in the heterojunction.

Modification of TiO_2 with a metallic or non-metallic element decreases the bandgap and improves the photocatalytic performance of TiO_2, the addition of conductive polymer makes it possible to reduce the gap energy of the catalyst to a much lower value than that of the heterostructure, thus enabling new photocatalytic properties that are superior and better functionalities are obtained in the visible region.

The gap band of TiO_2 goes from 3.2 eV to 2.78 eV by Cu doping and to 2.55eV in the presence of PTh. [101] It is 2.48 eV in the case of $TiO_2/TiO_2/V_2O_5$/PPy nanocomposite.[105] (Figure 16 A and B)

Several publications reported significant shift in the gap band of TiO_2 heterostructure to lower values in the presence of PANI, with an improvement in photocatalytic performance under both UV and visible light. [34,113,121,129]

Jing[144] linked the red shift of the gap band in the case of PANI/GR/TiO_2 nanocomposite compared to GR/TiO_2 to the presence of PANI which extends the absorption to the visible light region. The existence of the p-p * transition of the benzenoid ring, the p-polaron and the p-polaron transition of the quinonoid rings in the PANI structure results in a strong uptake both in the UV and visible. The incorporation of PANI on the surface improves the use of solar energy, produces more electron-hole pairs and eliminates their recombination problems under visible irradiation, and thus increases the photocatalytic activity of the material (Figure 16 C: a,b, c).

It is noted that the photocatalytic activity of the nanocomposites containing conductive polymers strongly depends on the quantity of the latter. The photocatalytic activity of the photocatalyst increases with the increase of the polymerization time of the polymer and therefore its content in the final nanocomposite.[105] (Figure 16C: d)

(A)

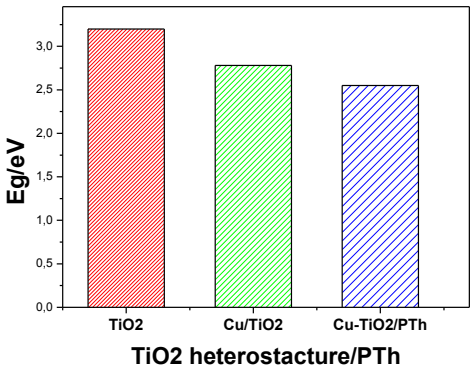
Eg/eV
3,0
2,5
2,0
1,5
1,0
0,5
0,0
TiO2
Cu/TiO2
Cu-TiO2/PTh
TiO2 heterostacture/PTh

(B)

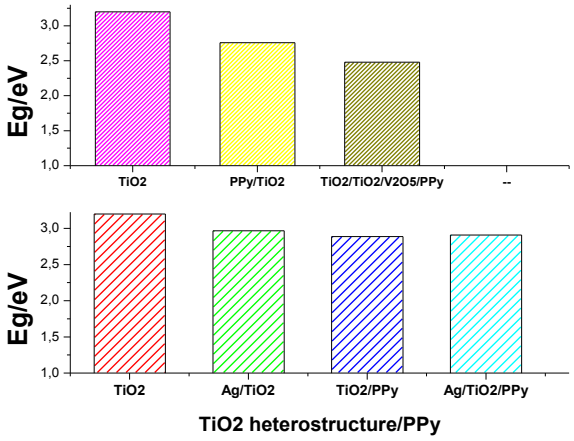
Eg/eV
3,0
2,5
2,0
1,5
1,0
TiO2
PPy/TiO2
TiO2/TiO2/V2O5/PPy
--
Eg/eV
TiO2
Ag/TiO2
TiO2/PPy
Ag/TiO2/PPy
TiO2 heterostructure/PPy

(C)

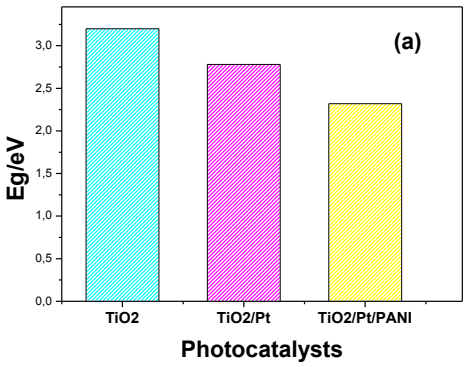
(a)
Eg/eV
3,0
2,5
2,0
1,5
1,0
0,5
0,0
TiO2
TiO2/Pt
TiO2/Pt/PANI
Photocatalysts

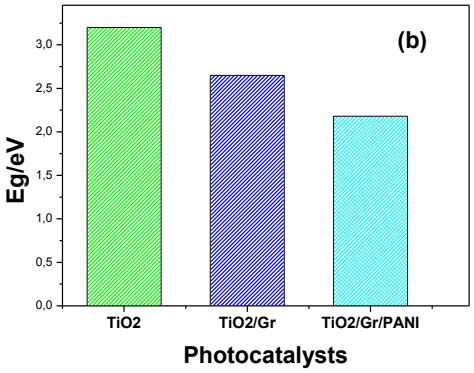
(b)
Eg/eV
3,0
2,5
2,0
1,5
1,0
0,5
0,0
TiO2
TiO2/Gr
TiO2/Gr/PANI
Photocatalysts

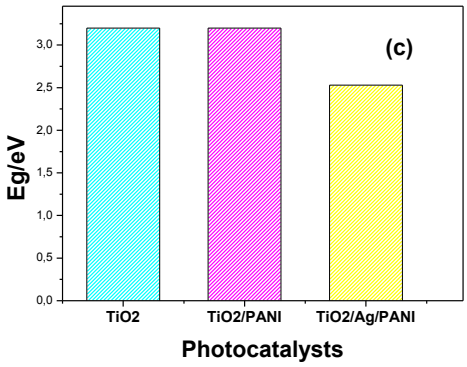
(c)
Eg/eV
3,0
2,5
2,0
1,5
1,0
0,5
0,0
TiO2
TiO2/PANI
TiO2/Ag/PANI
Photocatalysts

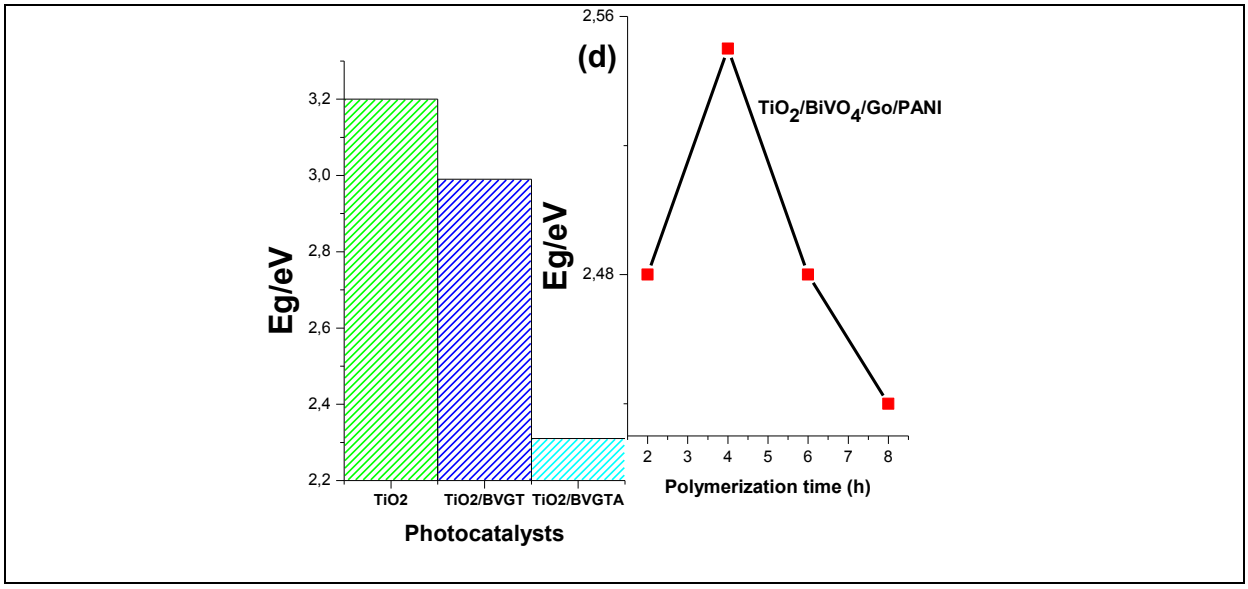

Figure 16. Variation TiO_2 heterostructure gap energy in the presence of conductive polymers PTh (A), PPy (B) and PANI (C: a, b, c, d).

This was the conclusion of several researchers, among them Brooms et al.[123] Their TiO_2/ZnO/PANI hybrid material caused a complete decomposition of P-cresol (99.3%) after 6 h while the degradation rate was 50% in the presence of TiO_2/ZnO heterostructure after the same period of time. They stated that the highest degradation rate of P-cresol was observed in the presence of TiO_2/ZnO/PANI and correlated with aniline to TiO_2/ZnO ratio. The efficiency increased with PANI mass loading in the nanocomposite (Figure 17). This activity is due to the fact that TiO_2/ZnO and PANI both absorb photons at a much faster rate at their interface than TiO_2. PANI is able to absorb visible light, inducing π-π^* transitions.[159] In addition to the synergistic effect of PANI and the mixture (TiO_2/ZnO), which promotes the fast and efficient separation of the charge under irradiation.

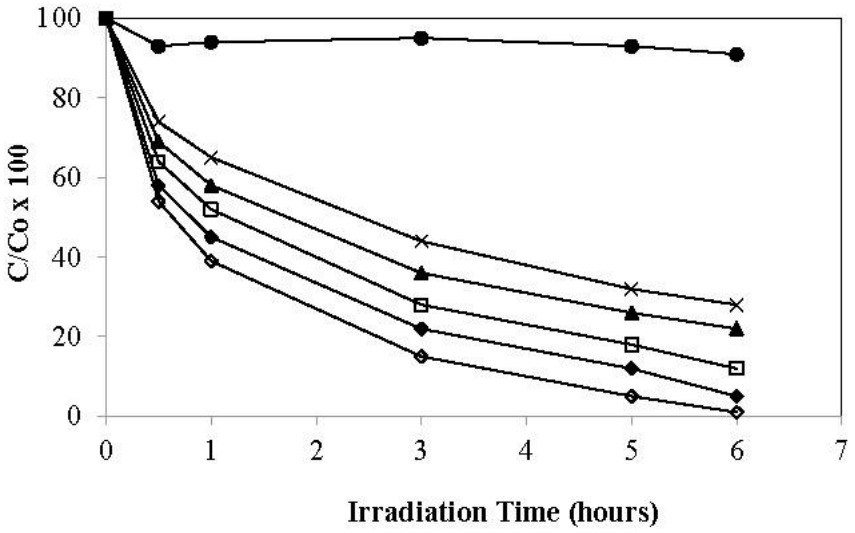

Figure 17. Photocatalytic degradation of P-Cresol (100 ppm) under UV illumination using different catalysts: blank (•), ZnO (□), TiO_2 (Δ), TiO_2/ZnO (▲) and TiO_2/ZnO/PANI (+). Adapted from [123].

The efficiency of TiO_2-based photocatalysts also depends on other factors such as the specific surface area and its porosity. A high specific surface area and a porous structure make it possible to improve the photocatalytic performance of the photocatalysts. They provide more active sites and adsorb more reactive species, which promotes and enhances photocatalytic processes and makes them more efficient.[129] In addition, the porosity of the surface facilitates the transport of reactive molecules and products through the interior space due to interconnected porous networks and promotes light collection due to the enlarged surface and the multiples diffusion in the porous framework. [160]

It has been found that the surface area of TiO_2/$CoFe_2O_4$ heterostructure increases in the presence of conductive polymer. The study carried out by Leng[129] showed that the association of PANI with the heterostructure of TiO_2/$CoFe_2O_4$ allows to have a high specific surface, *i.e.* 58.2, 72.5 and 79.3 m^2/g for pristine TiO_2, TiO_2/$CoFe_2O_4$ and TiO_2/$CoFe_2O_4$/PANI,respectively.

Conclusion

Photocatalysis is a promising paradigm for environmental and energy problem solving in the future. During the past two decades, constant advances in synthesis, modification and application of TiO_2 semiconductors have been reported. This versatile material, at the heart of photocatalysis, is constantly investigated and its properties revisited for possible improvements of its performances, particularly via nanostructuration and hybridation with complementary organic and/or inorganic compounds. In this review, we have described the general strategies of- and recent progress, in the fabrication of nanocomposites based on TiO_2 heterostructure and conductive polymers, in particular polyaniline (PANI), for environmental remediation and wastewater purification during the 2010s years.

We have demonstrated throughout this review that it is possible to develop a very large number of TiO_2 heterostructure/conducting polymer nanocomposite materials with different compositions, morphologies and structures, each with particular physicochemical and photocatalytic properties. These materials are promising candidates for the preservation of the environment in a very efficient and inexpensive way. They show the advantages of the structural and compositional aspects. Generally, these nanocomposites have large specific surface areas with high density of active sites for the degradation reactions of a wide range of organic pollutants. The modification of TiO_2 with another metallic or non-metallic element can effectively reduce the distance required for the transfer of electrons and photogenerated holes. Thus, charge carriers can easily participate in redox reactions on the catalyst surface. In addition, the absorption of light by TiO_2-based nanocomposites during the degradation process of organic pollutants could be improved. The photoactivity zone of TiO_2 shifts towards the visible when associated with a metallic or nonmetallic element and can also be functional in darkness in the presence of conducting polymers, hence increased efficiency with an energy gain. The photocatalytic activity depends strongly on the high roughness, porosity, crystallinity, structure, and surface morphological properties. The nanomaterials based on the TiO_2 heterostructure and conducting polymers are chemically stable, which favors recovery and thus multiple catalysed degradation reaction cycles.

Acknowledgements

FM would like to thank Campus France for the provision of PROFAS B+ fellowship. All authors are indebted to NATO for financial support through the SfP program (CATALTEX project No 984842).

References

[1] J. Im, F. E. Löffler, *Environmental Science & Technology*, 2016, 50, 8403–8416.
[2] M. Sudha, A. Saranya, G. Selvakumar, N. Sivakumar, *International Journal of Current Microbiology and Applied Sciences*, 2014, *3*(2), 670-690.
[3] J. Kanagaraj, T. Senthilvelan, R. C. Panda, S. Kavitha,
Journal of Cleaner Production2015, 89, 1-17
[4] H. He, G.-j. Hu, C. Sun, S.-l. Chen, M.-n. Yang, J. Li, Y. Zhao, H. Wang, China. Environ. Sci. Pollut. Res, 2011, 18, 638–648.
[5] R. A. Elsalamony, *Res Rev J Mat Sci*, *4*(2), 26-50.
[6] A. Pandey, S. Poonam, I. Leela, *International biodeterioration & biodegradation* 59.2 (2007): 73-84.
[7] J. Chen, F. Qiu, W. Xu, S. Cao, H. Zhu, *Applied Catalysis A: General*, 2015, *495*, 131-140.
[8]P. R. GogateA. B. Pandit, Adv.Environ.Res, 2004, 8, 553-597.
[9]P. S. Yap, T. T. Lim, *Applied Catalysis B: Environmental*, 2011, *101*(3-4), 709-717.
[10] K. R. Reddy, M. Hassan, V. G. Gomes, Appl. Catal. A: General. 489 (2015) 1-16.
[11] S. Mahshid, M. Askari, M. Sasani Ghamsari, , Mater. Process. Technol. 189 (2007) 296-300.
[12] X. Z. Wang, Q. Q. Gao, H. T. Zhao, K. Feng, R.g. Guo, Appl. Mech. Mater. 110-116 (2012) 3801-3806.
[13] M. M. Byranvand, A. Nemati Kharat, L. Fatholahi, Z. M. Beiranvand, J. Nanostruct. 3 (2013) 1-9.
[14] S. Oros-Ruiz, R. Zanella, B. Prado, *Journal of hazardous materials*, 2013, *263*, 28-35.
[15] J. Chen. F. Qiu. W. Xu. S. Cao. H. Zhu, Applied *Catalysis A: General*, 2015, *495*, 131-140.
[16] M. Bellardita, A. Di Paola, B. Megna, L. Palmisano, *Journal of Photochemistry and Photobiology A: Chemistry*, 2018, *367*, 312-320.
[17] A. Deng, Y. Zhu, L. Zhou, Y. Lin, Y, *Micro & Nano Letters*, 2018, *13*(1), 12-17.
[18] M. Zeng, Y. Li, M. Mao, J. Bai, L. Ren, X. Zhao, 2015, *ACS Catalysis*, *5*(6), 3278-3286.
[19] M. T. Uddin, Y. Nicolas, C. Olivier, T. Toupance, M. M. Müller, H. J. Kleebe, K. Rachut, J. Ziegler, A. Klein and W. Jaegermann, *J. Phys. Chem C*, 2013, *117*(42), 22098-22110.
[20] B. Cao, G. Li and H. Li, *App.Catal. B: Environ*, 2016, *194*, 42-49.
[21] A. K. Chakraborty, M. E. Hossain, M. M. Rhaman and K. M. A. Sobahan, *J. Environ. Sci*, 2014, *26*(2), 458-465.
[22] J. Tian, P. Hao, N. Wei, H. Cui, H. Liu, 2015, *ACS catalysis*, *5*(8), 4530-4536.
[23] B. A. Bhanvase, T. P. Shende, S. H. Sonawane, *Environmental Technology Reviews*, 2017, *6*(1), 1-14.

[24] H. Dong, G. Zeng, L. Tang, C. Fan, C. Zhang, X. He, Y. He, *Water research*, 2015, *79*, 128-146.
[25] A. Naldoni, M. Allieta, S. Santangelo, M. Marelli, F. Fabbri, S. Cappelli, C. L. Bianchi, R. Psaro, V.J. Dal Santo, Am. Chem. Soc, 2012, 134, 7600−7603
[26] Y. Yang, J. Wen, J. Wei, R. Xiong, J. Shi, C. Pan, ACS Appl. Mater. Interfaces, **2013**, 5, 6201–6207.
[27]W. J. Yu, Y. Cheng, T. Zou, Y. Liu, K. Wu, N. Peng, *Nano*, 2018, *13*(01), 1850009.
[28] R. Kumar, R. El-Shishtawy, M. Barakat, *Catalysts*, 2016, *6*(6), 76.
[29] F. Deng, Y. Li, X. Luo, L. Yang, X. Tu, Coll. Surf. A **2012**, 395, 183–189.
[30] L. Juanbi, X. Qiushi, L. Liangchao, S. Junhai, H. Diqiong, Appl. Surf. Sci, 2015, 331, 108–114.
[31] K.R. Reddy, K. V. Karthik, S.B. Prasad, S.K. Soni, H.M. Jeong, A. V. Raghu, Polyhedron, 2016, 120, 169-174.
[32] M. Sboui, M. F. Nsib, A. Rayes, M. Swaminathan, A. Houas, *Journal of Environmental Sciences*, 2017, *60*, 3-13.
[33] J. Ge, Y. Zhang, Y. J. Heo, S. J. Park, *Catalysts*, 2019, *9*(2), 122.
[34] Y. Shi, D. Yang, Y. Li, J. Qu, Z. Z. Yu, *Applied Surface Science*, 2017, *426*, 622-629.
[35] S. Nasirian, H. M. Moghaddam, *Applied Surface Science*, 2015, *328*, 395-404.
[36] T. J. Brooms, B. Otieno, M. S. Onyango, A. Ochieng, *Journal of Environmental Science and Health, Part A*, 2018, *53*(2), 99-107.
[37] M. O. Ansari, M. M. Khan, S. A. Ansari, M. H. Cho, *New Journal of Chemistry*, 2015, *39*(11), 8381-8388.
[38] F. Mousli, A. Chaouchi, M. Jouini, F. Maurel, A. Kadri, M. M. Chehimi, Catalysts, 2019, 9(7), 578.
[39] J. Low, B. Cheng, J. Yu, *Applied Surface Science*, 2017, *392*, 658-686.
[40] L. Sun, J. Guan, Q. Xu, X. Yang, J. Wang, X. Hu, Polymers, 2018, 10(11), 1248.
[41] M. Q. Hamzah, S. O. Mezan, A. N. Tuama, A. H. Jabbar, M. A. Agam, *International Journal of Engineering & Technology*, 2018, *7*(4.30), 538-543.
[42] E. Dadvar, R. R. Kalantary, H. Ahmad Panahi, M. Peyravi, Journal of Chemistry, 2017.
[43] W. Qing, X. Li, S. Shao, X. Shi, J. Wang, Y. Feng, W. Zhang, Journal of Membrane Science, 2019, 118-138.
[44] I. C. Roata, C. Croitoru, A. Pascu, E. M. Stanciu, Materials Science,2019, 6(3): 335–353
[45] S. Leong, A. Razmjou, K. Wang, K. Hapgood, X. Zhang, H. Wang, Journal of Membrane Science, 2014, 472, 167-184.
[46] U. Riaz, S. M. Ashraf, J. Kashyap, Polymer-Plastics Technology and Engineering,2015, 54(17), 1850-1870.
[47] H. Tai, Y. Jiang, G. Xie, J. Yu, M. Zhao,. *International Journal of Environmental Analytical Chemistry*, 2007, *87*(8), 539-551.
[48] W. Jiang, Y. Wang, A. XieF. Wu, *Journal of Physics D: Applied Physics*, 2016, *49*(38), 385502.
[49] L. Mais, M. Mascia, S. Palmas, A. Vacca, *Separation and Purification Technology*, 2019, *208*, 153-159.
[50] C. P. Athanasekou, V. Likodimos, P. Falaras, *Journal of environmental chemical engineering*, 2018, *6*(6), 7386-7394.
[51] C. H. Nguyen, C. C. Fu, R. S. Juang, *Journal of cleaner production*, 2018, *202*, 413-427.
[52] P. V. L. Reddy, B. Kavitha, P. A. K. Reddy, K. H. Kim, *Environmental research*, 2017, *154*, 296-303.
[53] L. Wenjuan, L. Danzhen, L. Yangming, W. Peixian, C. Wei, F. Xianzhi,S. Yu. J. Phys. Chem. (2012, C 116, 3552-3560.

[54] N. Guo, Y. Liang, S. Lan, L. Liu, J. Zhang, G. Ji, S. Gan, J. Phys. Chem. C, 2014, *118* (32), 18343–18355.
[55] H. Khan, M. G. Rigamonti, G. S. Patience, D. C. Boffito, Applied Catalysis B: Environmental, 2018, 226, 311-323.
[56] Z. Zhao, J. Tian, Y. Sang, A. Cabot, H. Liu, Advanced Materials, 2015, 27(16), 2557-2582.
[57] X. Zhang, Y. Wang, B. Liu, Y. Sang, H. Liu, Applied Catalysis B: Environmental, 2017, 202, 620-641.
[58]Z. Ambrus, N. Balasz, T. Alapi, G. Wittmann, P. Sipos, A. Dombi, K. Mogyorosi, Appl. Catal. B, 81 (2008), pp. 27-37.
[59]T. Tong, J. Zhang, B. Tian, F. Chen, D. He, J. Hazard. Mater., 155 (2008), pp. 572-579.
[60] R. Fiorenza, M. Bellardita, T. Barakat, S. Scirè, L. Palmisano, *Journal of Photochemistry and Photobiology A: Chemistry*, 2018, *352*, 25-34.
[61] D. A. Quang, T. T. T. Toan, T. Q. Tung, T. T. Hoa, T. X. Mau, D. Q. Khieu, *Journal of environmental chemical engineering*, 2018, *6*(5), 5999-6011.
[62] J. C. Cano-Franco, M. Álvarez-Láinez, *Materials Science in Semiconductor Processing*, 2019, *90*, 190-197.
[63] R. Fiorenza, M. Bellardita, T. Barakat, S. Scirè, L. Palmisano, *Journal of Photochemistry and Photobiology A: Chemistry*, 2018, *352*, 25-34.
[64] J. Henych, M. Kormunda, M. Šťastný, P. Janoš, P. Vomáčka, J. Matoušek, V. Štengl, *Applied Clay Science*, 2017, *144*, 26-35.
[65] M. R. D. Khaki, M. S. Shafeeyan, A. A. A. Raman, W. M. A. W. Daud, Journal of Molecular Liquids, 2018, 258, 354-365.
[66] S. Moradi, P. Aberoomand-Azar, S. Raeis-Farshid, S. Abedini-Khorrami, M. H. Givianrad, *Journal of Saudi Chemical Society*, 2016, *20*(4), 373-378.
[67] K. Siwińska-Stefańska, A. Kubiak, A. Piasecki, J. Goscianska, G. Nowaczyk, S. Jurga, T. Jesionowski, Materials, 2018,11(5), 841.
[68] X. Zhang, J. Yuan, J. Zhu, L. Fan, H. Chen, H. He, Q. Wang, *Ceramics International, 2019, 45(9), 12449-12454.*
[69] W. H. Saputera, H. Tahini, M. Sabsabi, T. H. Tan, N. M. Bedford, E. Lovell, J. N. Cui, D. Hart, ACS Catalysis, 2019, 9(3), 2674-2684.
[70] M. V. Dozzi, S. Marzorati, M. Longhi, M. Coduri, L. Artiglia, E. Selli, *Applied Catalysis B: Environmental*, 2016, *186*, 157-165.
[71] P. Eskandari, M. Farhadian, A. R. Solaimany Nazar and B. H. Jeon, *Ind. Eng. Chem. Res*, 2019, 58, 2099−2112.
[72] L. Yao, W. Wang, L. Wang, Y. Liang, J. Fu and H. Shi, *Inter. J. Hydrogen Energy*, 2018, *43*(33), 15907-15917.
[73] H. Wang, Q. Gong, H. Huang, T. Gao, Z. Yuan and G. Zhou, *Mater. Res. Bull*, 2018, *107*, 397-406.
[74] G. Zhang, Y. Zhang, M. Nadagouda, C. Han, K. O'Shea, S.M. El-Sheikh, A.A. Ismail, D.D. Dionysiou, Appl. Catal. B, 2014, 144, pp. 614-621.
[75] X. Lin, D. Fu, L. Hao, Z. Ding. J. Environ. Sci., 25 (2013), pp. 2150-2156.
[76] X. Cheng, X. Yu, Z. Xing. J. hys. Chem. Solids, 74 (2013), pp. 684-690.
[77] S.M. El-Sheikh, G.S. Zhang, H.M. El-Hosainy, A.A. Ismail, K.E. O'Shea, P. Falaras, A.G. Kontos, D.D. Dionysiou. J. Hazard. Mater., 280 (2014), pp. 723-733.
[78] T. S. Natarajan, H. C. Bajaj, R. J. Tayade, *Process Safety and Environmental Protection*, 2016, *104*, 346-357.
[79] J. Li, B. Yan, X. Shao, S. Wang, H. Tian, Q. Zhang, Appl. Surf. Sci., 324 (2015), pp. 82-89.

[80] M. Yang, N. Zhang, Y. Xu, Chem. Soc. Rev., 43 (2014), pp. 8240-8254.
[81]C.P. Athanasekou, S. Morales-Torres, V. Likodimos, G.E.Romanos, L.M. Pastrana-Martinez, P. Falaras, D.D. Dionysiou, J.L. Faria, J.L. Figueiredo, A.M.T. Silva, Appl. Catal. B Environ, 158–159 (2014), pp. 361-372.
[82] M. Safarpour, A. Khataee, V. Vatanpour, J. Membr. Sci., 489 (2015), pp. 43-54.
[83] Y. Gao, M. Hu, B. MiMembrane surface modification with TiO_2–graphene oxide for enhanced photocatalytic performance. J. Membr. Sci., 455 (2014), pp. 349-356.
[84] Y. Zhang, G. Zhang, S. Liu, C. Zhang, X. Xu, Chem. Eng. J., 204–206 (2012), pp. 217-224.
[85] E. Bet-Moushoul, Y. Mansourpanah, K. Farhadi, M. Tabatabaei, *Chemical Engineering Journal*, 2016, *283*, 29-46.
[86] A. S. Roy, K. R. Anilkumar, M. N. A. Prasad, *Journal of Applied Polymer Science*, 2011, *121*(2), 675-680.
[87] U. Riaz, S. M. Ashraf, J. Kashyap, *Polymer-Plastics Technology and Engineering*, 2015, *54*(17), 1850-1870.
[88] C. Zhan, G. Yu, Y. Lu, L. Wang, E. Wujcik, S. Wei, *Journal of Materials Chemistry C*, 2017, *5*(7), 1569-1585.
[89] B. Liu, Y. Fang, Z. Li, S. Xu, *Journal of nanoscience and nanotechnology*, 2015, *15*(2), 889-920.
[90] F. Mousli, A. Chaouchi, S. Hocine, A. Lamouri, M. R. Vilar, A. Kadri, M. M. Chehimi, *Applied Surface Science*, 2019, *465*, 1078-1095.
[91] S. Xu, S. Li, Y. Wei, L. Zhang, F. Xu, *Reaction Kinetics, Mechanisms and Catalysis*, 2010, *101*(1), 237-249.
[92] D. Wang, J. Zhang, Q. Luo, X. Li, Y. Duan, Journal of Hazardous Materials, 2009, 169, 546–550.
[93] S. Xu, L. Gu, K. Wu, H. Yang, Y. Song, L. Jiang, Y. Dan, *Solar Energy Materials and Solar Cells*, 2012, *96*, 286-291.
[94] J. H. Huang, M. A. Ibrahem, C. W. Chu, *Rsc Advances*, 2013, *3*(48), 26438-26442.
[95] X. Li, J. Sun, G. He, G. Jiang, Y. Tan, B. Xue, *Journal of colloid and interface science*, 2013, *411*, 34-40.
[96] N. M. Dimitrijevic, S. Tepavcevic, Y. Liu, T. Rajh, S. C. Silver, D. M. Tiede, The Journal of Physical Chemistry C, 2013, 117(30), 15540-15544.
[97]C. Yang, W. Dong, G. Cui, Y. Zhao, X. Shi, X. Xia, W. Wang, *Electrochimica Acta*, 2017, *247*, 486-495.
[98]C. Yang, W. Dong, G. Cui, Y. Zhao, X. Shi, X. Xia, W. Wang, Electrochimica Acta, 2017, 247, 486-495.
[99] S. Li, C. Du, D. Zhao, J. Zheng, H. Liu, Y. Wang, *Chemistry Letters*, 2015, *44*(4), 568-570.
[100] M. R. Chandra, T. S. Rao, B. Sreedhar, *Chinese Journal of Catalysis*, 2015, *36*(10), 1668-1677.
[101] Chandra, M. R., Rao, T. S., Kim, H. S., Pammi, S. V. N., Prabhakarrao, N., & Manga Raju, I. (2017). *Journal of Asian Ceramic Societies*, *5*(4), 436-443.
[102] Afzal, A., Abuilaiwi, F. A., Habib, A., Awais, M., Waje, S. B., & Atieh, M. A. (2017). *Journal of Power Sources*, *352*, 174-186.
[103] Smirnov, M. A., Sokolova, M. P., Bobrova, N. V., Toikka, A. M., Morganti, P., & Lahderanta, E. (2018). *Journal of energy chemistry*, *27*(3), 843-853.
[104] Yang, Y., Wen, J., Wei, J., Xiong, R., Shi, J., & Pan, C. (2013). *ACS applied materials & interfaces*, *5*(13), 6201-6207.

[105] Piewnuan, C., Wootthikanokkhan, J., Ngaotrakanwiwat, P., Meeyoo, V., & Chiarakorn, S. (2014). *Superlattices and Microstructures*, *75*, 105-117.
[106] X. Zhang, L. Lei. Mater. Lett. 62 (2008) 895–897.
[107] E. Borgarello, J. Kiwi, M. Graetzel, E. Pelizzetti, M. Visca. J. Am. Chem. Soc. 104 (1982) 2996–3002.
[108] K. Iketani, R.D. Sun, M. Toki, K. Hirota, O. Yamaguchi. Mater. Sci. Eng. B 108 (2004) 187–193.
[109] Tiana, F., Jiaa, J., Xua, B., Fua, Z., Liua, J., & Luo, J. (2018, July). In *IOP Conference Series: Materials Science and Engineering* (Vol. 392, No. 3, p. 032030). IOP Publishing.
[110] Nosrati, R., Olad, A., & Maryami, F. (2018). *Journal of Molecular Structure*, *1163*, 174-184.
[111] Murugan, C., & Subramanian, E. (2017). *Indian Journal of Chemistry Section A-Inorganic Bio-Inorganic Physical Theoretical & Analytical Chemistry*, *56*(3), 287-296.
[112] Gnaser, H., Huber, B., & Ziegler, C. (2004). In *Encyclopedia of Nanoscience and Nanotechnology* (Vol. 6, No. 535, pp. 505-535). American Scientific Publishers.
[113] Koysuren, O., & Koysuren, H. N. (2019). *Journal of Macromolecular Science, Part A*, 1-10.
[114] Teh, C. M.; Mohamed, A. R. A review. J. Alloys Compd. 2011, 509, 1648−1660.
[115] Kment, S.; Kmentova, H.; Kluson, P.; Krysa, J.; Hubicka, Z.;Cirkva, V.; Gregora, I.; Solcova, O.; Jastrabik, L. J. Colloid Interface Sci. 2010, 348, 198−205.
[116] Ansari, M. O., Khan, M. M., Ansari, S. A., Raju, K., Lee, J., & Cho, M. H. (2014). *ACS applied materials & interfaces*, *6*(11), 8124-8133.
[117] Zhu, J., Huo, X., Liu, X., & Ju, H. (2015). *ACS applied materials & interfaces*, *8*(1), 341-349.
[118] Panwar, V., & Jain, S. L. (2019). Materials Science and Engineering: C, 99, 191-201.
[119] Soleimani-Lashkenari, M., Rezaei, S., Fallah, J., & Rostami, H. (2018). Synthetic Metals, 235, 71-79.
[120] Roy, S., Payra, S., Challagulla, S., Arora, R., Roy, S., & Chakraborty, C. (2018). ACS Omega, 3(12), 17778-17788.
[121] Liu, X., Lai, H., Li, J., Peng, G., Yi, Z., Zeng, R., Liu, Z. (2019). International Journal of Hydrogen Energy, 44(10), 4698-4706.
[122] Tao, J., Chai, J., Guan, L., Pan, J., & Wang, S. (2015). Applied Physics Letters, 106(8), 081602.
[123] Brooms, T. J., Otieno, B., Onyango, M. S., & Ochieng, A. (2018). Journal of Environmental Science and Health, Part A, 53(2), 99-107.
[124] Zarrin, S., & Heshmatpour, F. (2018). *Journal of hazardous materials*, *351*, 147-159.
[125] Z. Jiang, W. Wei, D. Mao, C. Chen, Y. Shi, X. LV, J. Xie. Nanoscale (2015) 1–14.
[126] M. Jiménez, M.I. Maldonado, E.M. Rodríguez, H.A. Ramírez, E. Saggioro, I. Carra, J.A.S. Pérez. J. Chem. Technol. Biotechnol. 90 (1) (2015) 149–157.
[127] M. Jiménez, M.I. Maldonado, E.M. Rodríguez, H.A. Ramírez, E. Saggioro, I. Carra, J.A.S. Pérez. J. Chem. Technol. Biotechnol. 90 (1) (2015) 149–157.
[128] Huang, X., Wang, G., Yang, M., Guo, W., & Gao, H. (2011). *Materials Letters*, *65*(19-20), 2887-2890.
[129] Leng, C., Wei, J., Liu, Z., Xiong, R., Pan, C., & Shi, J. (2013). Journal of nanoparticle research, 15(5), 1643.
[130] Li, J., Xiao, Q., Li, L., Shen, J., & Hu, D. (2015). Applied Surface Science, 331, 108-114.
[131] Feizpoor, S., Habibi-Yangjeh, A., Yubuta, K., & Vadivel, S. (2019). Materials Chemistry and Physics, 224, 10-21.

[132] Zhao, J., Biswas, M. R. U. D., & Oh, W. C. (2019). Environmental Science and Pollution Research, 26(12), 11888-11904.
[133] J. Tian, X. Hu, N. Wei, Y. Zhou, X. Xu, H. Cui and H. Liu, *Sol. Energy Mater. Sol. Cells*, 2016, *151*, 7-13.
[134] L.A. Näslund, C. M. Sánchez-Sánchez, A. S. Ingason, J. Bäckström, E. Herrero, J. Rosen and S. Holmin, *J. Phys. Chem C*, 2013, *117*(12), 6126-6135.
[135] T. Mitsuhashi and A. Watanabe, *J. Therm. Anal. Calorim*, 2000, *60*(2), 683-689.
[136] J. Riga, C. Tenret-Noel, J. J. Pireaux, R. Caudano, J. J. Verbist and Y. Gobillon, *Phys. Scr*, 1977, *16*(5-6), 351.
[137] Xu, Y. J., Zhuang, Y., & Fu, X. (2010). The Journal of Physical Chemistry C, 114(6), 2669-2676.
[138] Lee, J. S., You, K. H., & Park, C. B. (2012). Advanced Materials, 24(8), 1084-1088.
[139] Stengl, V., Popelková, D., & Vlácil, P. (2011). The Journal of Physical Chemistry C, 115(51), 25209-25218.
[140] Zhou, K., Zhu, Y., Yang, X., Jiang, X., & Li, C. (2011). *New Journal of Chemistry*, *35*(2), 353-359.
[141] Zhang, N., & Xu, Y. J. (2016). *CrystEngComm*, *18*(1), 24-37.
[142] Kumar, R., Ansari, M. O., Parveen, N., Oves, M., Barakat, M. A., Alshahri, A., ... & Cho, M. H. (2016). *RSC Advances*, *6*(112), 111308-111317.
[143] Liu, W., Wang, C., & Wang, L. (2017). Industrial & Engineering Chemistry Research, 56(21), 6114-6123.
[144]Jing, L., Yang, Z. Y., Zhao, Y. F., Zhang, Y. X., Guo, X., Yan, Y. M., & Sun, K. N. (2014). Journal of Materials Chemistry A, 2(4), 1068-1075.
[145] Zhang, W., Guo, H., Sun, H., & Zeng, R. (2017). Applied Surface Science, 410, 547-556.
[146] Cui, W., He, J., Wang, H., Hu, J., Liu, L., & Liang, Y. (2018). Applied Catalysis B: Environmental, 232, 232-245.
[147] Han, T. H., Parveen, N., Shim, J. H., Nguyen, A. T. N., Mahato, N., & Cho, M. H. (2018). Industrial & Engineering Chemistry Research, 57(19), 6705-6713.
[148] Chen, F., An, W., Li, Y., Liang, Y., & Cui, W. (2018). Applied Surface Science, 427, 123-132.
[149] Yuan, C., Hung, C. H., Yuan, C. S., & Li, H. W. (2017). Materials, 10(8), 877.
[150] Q. Gao, Z. Li, M. Li, Y. Liu, C. Song, G. Han. J. Mater. Sci. Eng., 2012, 30(1), 93–97.
[151] W. Q. Fan, H. Y. Bai, G. H. Zhang, Y. S. Yan, C. B. Liu, W. D. Shi. CrystEngComm, 2014, 16, 116–122.
[152] Huang, F., Yan, A., & Zhao, H. (2016). Materials, Mechanisms and Applications; Cao, W., Ed, 31-80.
[153]Y. F. Zhao, C. Li, S. Lu, L. J. Yan, Y. Y. Gong, L. Y. Niu, X. J. Liu. Chem. Phys. Lett., 2016, 647, 36–41.
[154] L. L. Lai, J. M. Wu. J. Mater. Chem. A, 2015, 3, 15863–15868.
[155] X. Wang, Y. Yan, B. Hao, G. Chen. Dalton Trans., 2014, 43, 14054–14060.
[156] S. J. Ha, D. H. Kim, J. H. Moon. RSC Adv., 2015, 5, 77716–77722.
[157]W. Q. Fang, X. L. Wang, H. Zhang, Y. Jia, Z. Huo, Z. Li, H. Zhao, H. G. Yang, X. Yao. J. Mater. Chem. A, 2014, 2, 3513–3520
[158] Beldjebli, O., Bensaha, R., Ocak, Y. S., Amirache, L., & Boukherroub, R. (2019). *Materials Research Express*, *6*(8), 085036
[159]Zhang, L.; Liu, P.; Su, Z. *Polym. Degrad. Stab.* 2006, *91*, 2213–2219.
[160] Qi F, Moiseev A, Deubener J, Weber A (2011) J Nanopart Res 13:1325–1334.

Chapter 2: Diazonium-modified TiO_2/polyaniline core/shell nanoparticles. Structural characterization, interfacial aspects and photocatalytic performances

Diazonium-modified TiO_2/polyaniline core/shell nanoparticles. Structural characterization, interfacial aspects and photocatalytic performances

Fatima Mousli, Ahcène Chaouchi, Smain Hocine, Aazdine Lamouri, Manuel Rei Vilar, Abdelaziz Kadri, Mohamed M. Chehimi

Reference

F. Mousli, A. Chaouchi, S. Hocine, A. Lamouri, M.R. Vilar, A. Kadri, M. M. Chehimi, Diazonium-modified TiO_2/polyaniline core/shell nanoparticles. Structural characterization, interfacial aspects and photocatalytic performances. *Applied Surface Science*, *465 (2019)* 1078-1095.

Graphical abstract

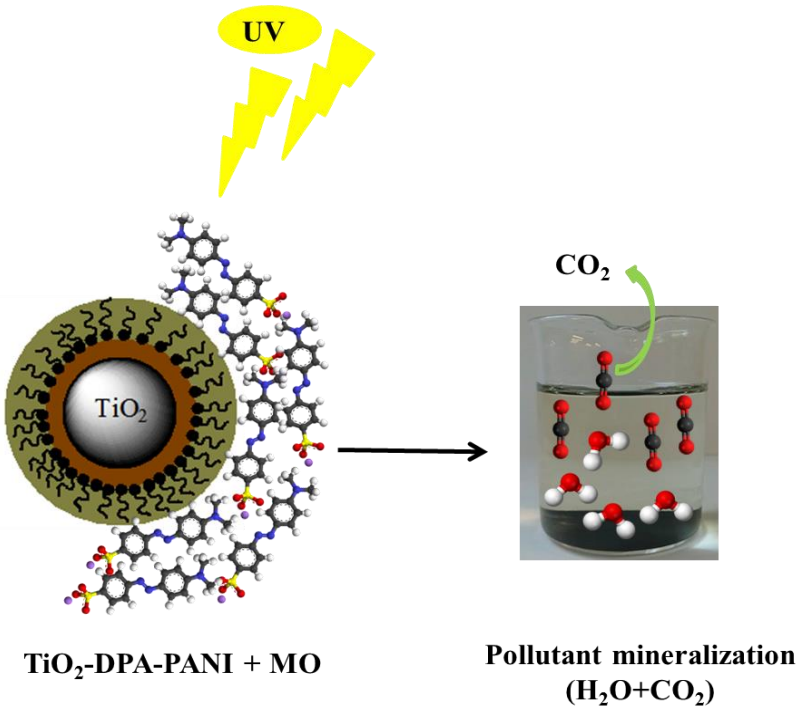

Aim of the paper

This paper investigates the role of diazonium salt modification of TiO_2 nanoparticle surface in the design of novel TiO_2/conductive polymer nanocomposite photocatalysts by in situ oxidative polymerization of the corresponding monomer for the mineralization of organic pollutants model.

Method

TiO_2 nanoparticles (NPs) were functionalized with diphenyl-amino (DPA) groups from 4-diphenylamine diazonium salt precursor, reduced with ascorbic acid to provide radicals that modified the NPs and further served for in situ synthesis of polyaniline (PANI) that resulted in TiO_2/DPA/PANI nanocomposite used in photocatalysis.

Results

Physico-chemical characterization tools confirmed the diazonium modification of TiO_2 NPs and highlighted the effect of such a surface modification on the loading and covalent attachment of PANI to the modified surface. XPS study brought strong supporting evidence for a core/shell structure (TiO_2-DPA being the core, and PANI the shell). The TiO_2-DPA-PANI nanocomposite exhibited excellent catalytic performances which depend on the amount of PANI on the surface of TiO_2 NPs. The results obtained underline the spectacular role of diphenylamine tetrafluoroborate diazonium salt in the coating of high quantity of PANI and in the stability of the formed nancomposite photocatalysts.

Significance

This study brings strong supporting evidence for the vital role of diazonium salts in the making of new generation photocatalysts with remarkable performances that are tuned by the fine control over interfacial chemistry.

Diazonium-modified TiO_2/polyaniline core/shell nanoparticles. Structural characterization, interfacial aspects and photocatalytic performances

Fatima Mousli[1,*], Ahcène Chaouchi[2], Smain Hocine[2], Aazdine Lamouri[3], Manuel Rei Vilar[3], Abdelaziz Kadri[1], Mohamed M. Chehimi[3,4*]

[1] Laboratoire de Physique et Chimie des Matériaux (LPCM), Faculté des Sciences, Université Mouloud Mammeri, Tizi-Ouzou 15000, Algeria.
[2] Laboratoire de Chimie Appliquée et Génie Chimique, Université Mouloud Mammeri, Tizi-Ouzou 15000, Algeria
[3] Univ Paris Diderot, Sorbonne Paris Cité, ITODYS, UMR CNRS 7086, 15 rue JA DeBaïf, 75013 Paris, France
[4] Université Paris Est, CNRS, ICMPE (UMR 7182), 94320 Thiais, France

Abstract

Dyes are important in many industrial sectors but represent a threat if they are discharged in waste water. In this global concern, novel TiO_2-polymer nanocomposites were designed for the removal of methyl orange (MO), a model pollutant. In this process, polyaniline (PANI) was prepared by in situ polymerization of aniline on TiO_2 nanoparticles grafted with 4-diphenylamine (DPA) groups from diazonium salt. PANI loading was very high on diazonium-modified TiO_2 and withstood leaching in polar solvents compared to the low loading and poor adhesion noted for bare TiO_2.

TiO_2-DPA-PANI efficiently catalyzed the degradation of MO in aqueous media under UV light. Total discoloration of MO solutions was achieved without any spectral evidence for organic byproducts thus suggesting complete mineralization of the dye. The degradation rate constant (K_{app}) was 0.133 min^{-1} for TiO_2-DPA-PANI nanocomposite, much higher than 0.059 and 0.085 min^{-1} found for TiO_2 and TiO_2-PANI, respectively. This clearly stresses the role of PANI for improving the activity of the photocatalyst and for protecting TiO_2 under UV light. Indeed, TiO_2-DPA-PANI could be recycled 5 times without any loss in the photocatalytic activity, whereas TiO_2-PANI could be recycled only 3 times and the bare TiO_2 reused once.

This work highlights the major role of diazonium salts in the design of novel photocatalysts for the mineralization of organic dye pollutants.

Keywords: titanium dioxide, diazonium salts, polyaniline, nanocomposites, photocatalysis, mineralization.

Corresponding authors
F. Mousli : fatima.mousli@yahoo.fr; M. M. Chehimi : chehimi@icmpe.cnrs.fr

1. Introduction

Recent years witnessed quantum jump in technological development based on a variety of non-biodegradable organic materials. Their production at industrial scale has adverse effects on humans, animals and environment due to pollution by their side and/or waste products [1,2]. For example, the leather and textile industries (among others) employ various chemicals including dyes which can be wasted if they are not managed properly [3,4,5]. In this situation, chemical wastes heavily contribute to the contamination of waters and the deterioration of the environment [6] as they are difficult to biodegrade [7]. Numerous studies that were devoted to water purification led to an improvement in the oxidative degradation processes of organic compounds. Particularly, heterogeneous photocatalysis is an attractive for pollution problem solving because it permits to degrade organic matter into elementary and less toxic products. Time and efforts were spent to develop semiconductor photocatalysts with high performances for the removal of various pollutants in water and air [8]. Among the various metal oxide semiconductors, titanium dioxide (TiO_2) has been widely used in this regard [9,10,11]; it has indeed attracted a great deal of interest due to its physical and chemical stability [12], high photocatalytic activity [13,14,7] photostability [15,16], high dielectric constant [17], physical, optical and electrical properties [18], low cost and non-toxicity [8,19]. It is the most successful UV-active photocatalyst.

TiO_2 exists in three crystallographic phases namely rutile, brookite and anatase; the latter has excellent catalytic properties due to the slightly higher Fermi level and its low oxygen adsorption capacity [11]. It has been reported that the properties of titania are related to the particles size and their morphology [6] which depend on the operating mode and conditions. Several processes have been reported on the preparation of TiO_2 such as hydrothermal method [20], solvent evaporation [21], chemical vapor deposition (CVD), sonochemical method [22], hydrolysis [6], combustion [23], chemical precipitation [24], electrodeposition [25] and sol-gel [17,26,27] which is the most efficient approach to prepare nanoparticles of TiO_2. However, one difficulty with these oxide NPs is to control their aggregation, dispersion and colloidal stability in organic and aqueous media or in polymeric matrices [28,29]. Towards this end, and in order to optimize these important features, one could undertake surface functionalization of nanoparticles using e.g. thiols and citrate [30], carboxyl group [31], phosphates and phosphonates [32] and amines [33]. In addition to these classical strategies, the recent years witnessed the emergence of aryl diazonium salts as unique chemical series for the functionalization of broad range of nanomaterials [34]. This strategy is quasi universal as it concerns a variety of materials such as CNTs [35] and graphene [36],

diamond [37], polymers [38], gold nanoparticles [39], ITO [40], sensing electrodes [41], and Ti/TiO_2 [42] or TiO_2 [43]. It has been demonstrated that a covalent bond is formed between the substrate and the aryl groups during the functionalization reaction resulting in C-C [44,45], metal-C [46,47,48] or metal-O-C bonds [48], or even Au-N=N in the case of gold [49].

Aryl diazonium salts can be attached to the particles by two main methods: isolated aryl diazonium salts using reducing agents; and in situ generated of aryl diazonium salts from the corresponding aromatic amine in the presence of sodium nitrite in acidic medium. In the neutral and alkaline medium, these salts produce diazohydroxides and diazoates [50]. The chemical surface modification with aryl diazonium salts can be produced in different media (aqueous, organic, ionic liquid) [51]. It allows the introduction of several functional groups at the surface, some of them able to bridge two distinct materials [52].

As coupling agents, diazonium salts are more and more employed in order to provide aryl-modified materials serving as macroinitiator for in situ polymerization methods. Mesnage et al. [29] prepared a nanocomposite based on TiO_2 NPs by polymerization of 2-hydroxyethyl methacryalte initiated by nitrobenzendiazonium salt. Inspired by the work of Santos et al. [53] on the preparation of polyaniline (PANI) films at the surface of glassy carbon electrodes electrografted with diphenylamino groups from diazonium precursors, Mekki et al. [54] designed a MWCNT-PANI nanocomposite. The oxidative polymerization of aniline was initiated by the 4-diphenylamine diazonium grafted onto the surface of the MWCNTs by in situ generation.

In this work, we reasoned that bridging the gap between polymer grafting to TiO_2 particles [29] and PANI grafting to sp^2 carbon materials [53,54], one could prepare robust TiO_2-PANi nanocomposites in an original way that has not been described previously.

PANI is most widely studied because it has a broad range of tunable properties derived from its structural flexibility [55,56,57]; it presents interesting electronic, thermoelectronic, and optical properties properties hence the variation of these applications [58]. It has a high absorption coefficient and a high mobility of charge carriers [59]. These characteristics make it an interesting material to improve the charge separation effect as well as the catalytic activity of a catalyst [60]. Given the photocatalytic nature of TiO_2 and the redox properties of PANI, one would end up with a functional nanocomposite of interest for environmental applications. In this work, the role of diazonium compounds is to ensure excellent adhesion of

large amount of PANI to the underlying TiO_2; this has not been addressed previously and worth to be reported as we shall demonstrate later in this work.

In the following, we shall describe the synthesis of the diazonium salt of DPA and its use to functionalize non-commercial TiO_2 nanoparticles. Diazonium-modified TiO_2 particles served as particulate platform for the grafting of PANI by in situ oxidative polymerization and design of the final TiO_2-DPA-PANI nanocomposite. We employed a range of analytical tools to account for the structural analysis of TiO_2 and monitoring changes of its surface chemical upon diazonium pre-treatment and PANI grafting. As far as the photocatalytic performances are concerned, methyl orange was used as model organic pollutant to probe the efficiency of the composite photocatalysts to degrade this azo dye. Untreated TiO_2 and TiO_2-PANI nanocomposite prepared without any diazonium salts served as reference photocatalysts for TiO_2-DPA-PANI.

2.Experimental

2.1 Reagents

Titanium isopropoxyde (TIPT, Aldrich, 99% purity), methanol (99.9%), ethanol (99.9%). N-phenyl-p-phenylenediamine (Alfa Aesar, 98% purity), HBF_4 (48%), ascorbic acid, sodium nitrite (Alfa Aesar, purity 99%), ammonium persulfate (APS, Aldrich, 98% purity), nitric acid (Carlo Erba, 60% purity) and aniline (Aldrich, 99.5% pure). Polar and non-polar solvents (all Aldrich products) were used as-received for adhesion testing: dimethylformamide (DMF), N-methyl-2-pyrrolidone (NMP), tetrahydrofuran (THF), hexafluoropropan-2-ol (HFIP), dimethyl sulfoxide (DMSO), chloroform, 1,2-dichloroethane, xylene and toluene, methyl orange (Sigma-Aldrich). The reagents were used without any further purification. All aqueous solutions were prepared using ultrapure water. Aldrich, Alfa Aesar and Carlo Erba reagents were produced in Germany, France, China and USA.

2.2. Catalyst preparation

TiO_2 nanoparticles (NPs) were prepared by dissolving the TIPT (148 ml, 0.5 mol) in a a solvent mixture of ethanol (146 ml, 2.5 mol) and methanol (21 ml, 0.5 mol). The mixture thus obtained is stirred for 30 min, then 20 ml of H_2O are added and refluxed at 60°C for 15h. The gel was then centrifuged and washed several times with ethanol and water. The resulting product was dried at 100°C for 24h and calcined at 550°C for 150 min (this is an ideal temperature for obtaining anatase [61]). It is worth to note that for the synthesis of TiO_2 nanoparticles, the amount of reagents were calculated in order to have approximately 3g of

TiO_2 powder without significant losses. TIPT hydrolyzes in water while it is highly soluble in alcohol; EtOH and MeOH play both the roles of solvents and reducing agents for TIPT; their presence in excess in the solution does not affect the final product. As the boiling temperature of EtOH is 79 °C and that of MeOH is 65 °C, therefore MeOH starts boiling as soon as the temperature of the mixture reaches 65 °C; this actually can drastically change the composition of the synthesis solution. For this reason, the synthesis temperature was set to 60 °C.

2.3. Synthesis of 4-diphenylamine diazonium tetrabuoroborate

The method employed for the synthesis of 4-diphenylamine diazonium tetra- fluoroborate (DPA) was according to the conditions reported in [62]. N-phenyl-p-phenylenediamine (0.45g, 2.44 mmol) was dissolved in 5 mL of HBF_4 (aqueous solution 48%), cooled in an ice bath and stirred for 15 min, then sodium nitrite (0.45 g, 6.52 mmol) was added to the mixture which was kept under vigorous stirring for 1h. 60 mL of CH_2Cl_2 was added in order to crystallize the mixture and separate the phases. the crystallized precipitate was filtered and washed with copious amounts of cold ether. The diazonium salt (Scheme 1) was then dried and kept at low temperature.

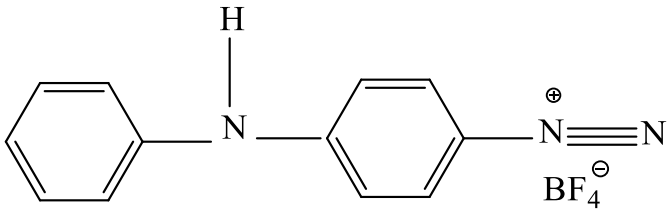

Scheme 1. Structure of 4- diphenylamine diazonium tetrafluoroborate

^{1}H NMR (DMSO) δ (ppm): 8.3 (d, CH-C**H**-C (N_2^+, BF4$^-$)), 7.51(d, CH, C**H**, C (N-H)), , 7.33(d, CH-C**H**-C (N-H)), 7.14(d, CH-C**H**-CH), 10.58(s, C-N**H**-C).

2.4. Diazonium-modification of TiO_2

Three strategies were adopted to attach DPA to the surface of TiO_2 NPs.

2.4.1. With in situ generated aryl diazonium salt

To start, 40 mg (0.5 mmol) of TiO_2 is added in 5 mL of H_2O and sonicated for 15 min. 35 mg, (0.19 mmol) of N-phenyl-p-phenylenediamine was dissolved in 5 mL of HBF_4, cooled in ice bath and stirred for 15 min, then the suspension of TiO_2 was added slowly under stirring for 20 min. After that, an aqueous solution of $NaNO_2$ (50 mg, 0.72 mmol in 3 mL H_2O) was added dropwise. The mixture is kept under stirring at 0°C for 1h. The resulting precipitate was separated from the solution with centrifugation and washed with water+ethanol, and then dried at room temperature.

2.4.2. With isolated aryl diazonium salt

An aqueous suspension of TiO_2 (30 mg, 0.37 mmol in 2mL of H_2O) was stirred with an ultrasonic probe for 20 min, then added to an aqueous solution of diazonium salt (0,28g, 1.04 mmol in 5 mL H_2O). The suspension was stirred at 0°C for 15 min, after which, the reducing agent (ascorbic acid, 0,4g, 2.27 mmol in 3mL H_2O) was added dropwise and the mixture left to stir for 1h. The suspension was then centrifuged and washed several times with ethanol then with water. The final product was dried at room temperature overnight.

2.4.3. With diazoate

40 mg (0.5) mmol of TiO_2 was first sonicated for 15 min in 5 mL H_2O and 5 mL of ethanol, then, 2 mL of NaOH (0.5 $mol.L^{-1}$) was added to adjust the pH under stirring for 10 min. 10 g (0.03 mol) of DPA dissolved in 5 mL of H_2O was added to the suspension. The mixture was left to react under stirring for 1h. The result suspension was then centrifuged and washed several times with ethanol and water then dried at room temperature.

2.5. Synthesis of TiO_2-DPA-PANI nanocomposites

The synthesis of TiO_2-PANI nanocomposite was carried out according to the procedure adopted by Jlassi et al. [62]. 30 mg (0.37 mmol) of TiO_2 was dispersed in 20 mL of acetonitrile and sonicated for 10 min. The anilinium cation was prepared by mixing aniline (0.3 g, 3.23 mmol) with (0.1 g, 1.51 mmol) nitric acid. The mixture was left under magnetic stirring for 1 h. The suspension of TiO_2 was added to the anilinium cation solution and cooled in an ice bath and stirred for more than 2 h. Thereafter, aqueous solution of APS (0,4g, 1.75 mmol in 5mL H_2O) was added dropwise using a micropipette. The suspension was kept under ultrasonication for 5 min and then with constant stirring for 3h to allow the oxidative polymerization to proceed. The TiO_2/PANI nanocomposite was centrifuged and washed several times with methanol and de-ionized water to remove un-reacted monomers and oxidant. The final product was dried at room temperature overnight. The same protocol was

adopted for the preparation of TiO_2/DPA/PANI nanocomposite using TiO_2/DPA (30 mg, 0.076 mmol). We found this protocol very efficient in the case of TiO_2 as it was for diazonium-intercalated clay.

2.6. Characterization

X-ray diffraction (XRD) was used for crystal phase identification of different nanopowders and estimation of the crystallite size of TiO_2 nanoparticles. The measurements were performed using a diffractometer (Bruker AXS D8 Advance, CuKα radiation λ=1.5418 A°). The XRD profile was measured in 2θ range 10°-90° with a step width of 0.02° and collection time of 5s.

The optical properties of TiO_2 NPs were investigated by UV-visible spectroscopy using a Thermofisher Evolution 220 apparatus.

The morphology and the composition of TiO_2 NPs and TiO_2-PANI nanocomposites were checked with a Merlin Carl Zeiss apparatus fitted with energy dispersive X-ray (EDX) analyzer. Samples were metallized with platinum in order to eliminate charging effects.

FTIR spectra were investigated using a Bruker apparatus operating in ATR mode with a wave number range 4000 - 400 cm^{-1}. Raman spectroscopy was carried out using Horiba Lab RAM HR Evolution operating at 638 nm. NMR spectra was recorded by Brucker AM 300 MHz instrument.

X-ray photoelectron spectra were recorded using a K Alpha apparatus (Thermo Fisher Scientific, Al X-ray source h = 1486.6 eV; spot size = 400 µm). Charge compensation was achieved using a flood gun. The composition was determined using the manufacturer's sensitivity factors.

The photocatalytic activity of TiO_2-DPA-PANI nanocomposite was evaluated by the photodegradation of MO in darkness and under UV irradiation. TiO_2 and TiO_2 nanocomposites (TiO_2-PANI, TiO_2-DPA-PANI) (10 mg in 50 ml), were first dispersed in aqueous solution of methyl orange (50 $mg.L^{-1}$) then stirred in the dark for 50 min before the addition of 1 mL of H_2O_2 and irradiation to reach equilibrated adsorption. The UV irradiation was generated by UVA CUBE 100 (Honle UV technology).

3. Results and discussion

3.1. General route for the making of TiO_2-PANI nanocomposites

Figure 1 shows the general strategy for making nanocomposites made of TiO_2 and PANI synthesized in the presence of TiO_2 (Figure 1A, Upper level) and the digital photographs of the main samples of this work (Figure 1B, Lower level). As part of our ongoing projects on diazonium modification of a large range of materials (metals, ceramics, polymers, sp^2 carbon), herein our main objective is to deeply investigate the role of diazonium pre-treatment of TiO_2 prior to in situ polymerization of aniline. In order to highlight this effect, it was also necessary to synthesize TiO_2-PANI reference composite by in situ oxidative polymerization of aniline in the presence of pristine TiO_2. In Figure 1A, we thus show the two pathways adopted in this work: synthesis of PANI in aqueous solution, in the presence of pristine and diazonium-modified TiO_2.

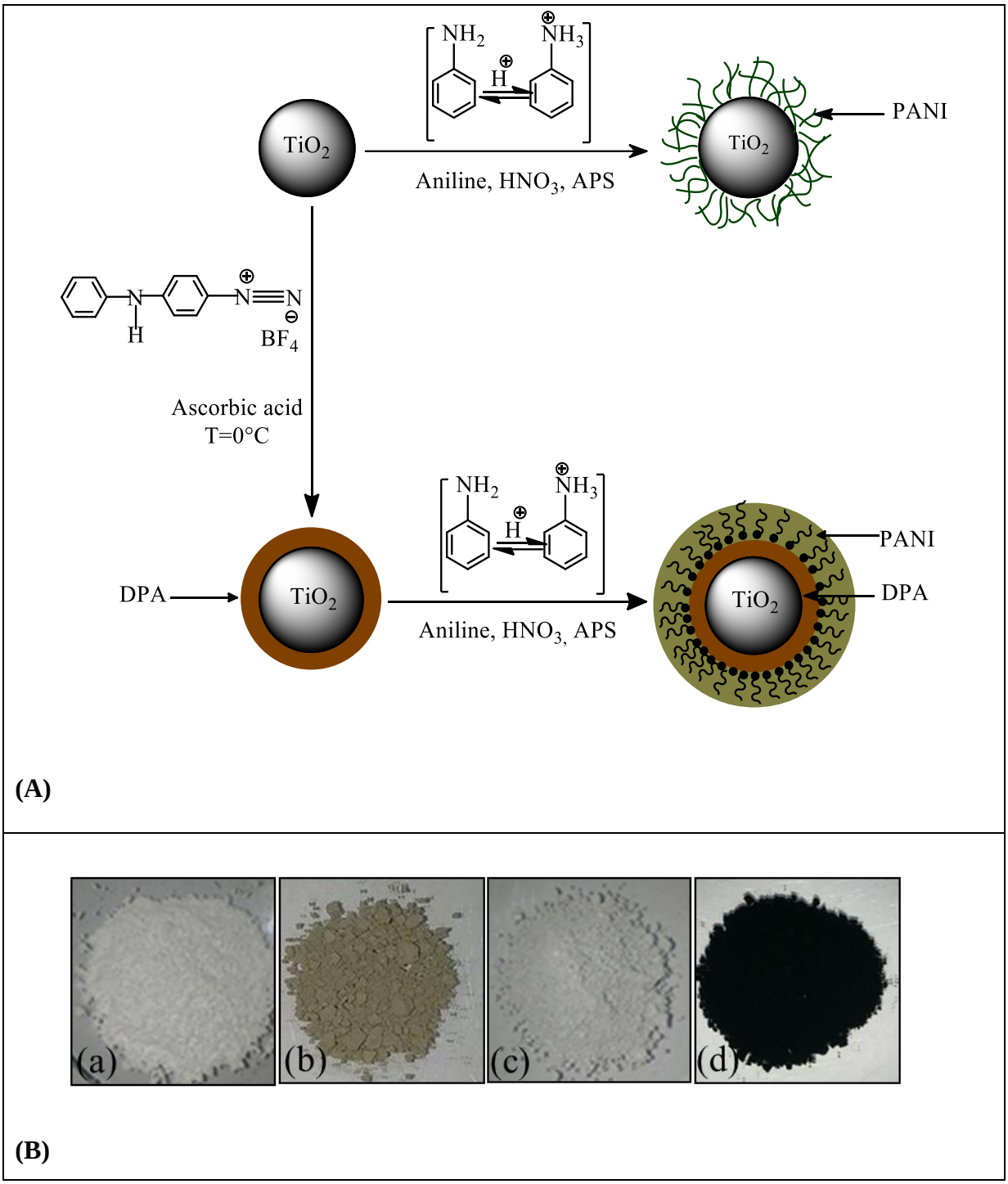

Figure 1. Upper level (A): General pathway for TiO_2-DPA-PANI and TiO_2-PANI nanocomposites. Lower level (B): digital photographs of TiO_2 (a), TiO_2-DPA (b), TiO_2-PANI (c), and TiO_2-DPA-PANI (d).

Figure 1B (lower level) displays digital photographs of the products under test strating from pristine TiO_2 (Figure 1Ba). The effect of diazonium modification of TiO_2 powder is visible with the naked eye (Figure 1Bb) in the sense that the powder turns from white to pale green color. Surprisingly, and despite the deep green color of conductive PANI, TiO_2-PANI

powders is hardly distinguishable from TiO_2 (Figure 1Bc); the composite powder is only slightly light grey colored. For similar nanocomposite but prepared with diazonium-modified TiO_2 a striking contrast is visible in Figure 1Bd in the sense that the TiO_2-DPA-PANI nanocomposite turns to very dark green, which is quasi the color of PANI (shown in inset of Figure 1Bd). It follows that DPA has a tremendous effect on the optical properties of the final TiO_2/PANI-based nanocomposites.

3.2. Nanocomposite formation mechanism

The modification of metal oxides with diazonium salts usually leads to interfacial M-O-C bonds [48,63] as demonstrated by means of surface specific analytical methods such as XPS and time of flight secondary ion mass spectroscopy (ToF-SIMS) and supported by computational chemistry [64]. However, the mechanisms is yet to be demonstrated. Herein, we hypothesize that such interfacial groups exists (Ti-O-C) and consider the polymerization of aniline proceeds at the DPA groups anchored to TiO_2 by covalent bonds. In the light of previously published results on the attachment of aryl groups to TiO_2 via Ti-O-C group [42] and the in situ polymerization of aniline at the surface of MWCNT-DPA reported by Mekki et al. [54], one can reason that the TiO_2-aryl-PANI interface be Ti-O-C_6H_4-NH-C_6H_4-PANI. Figure 2 describes the stepwise initiation and growth of PANI chains at the surface of TiO_2-DPA.

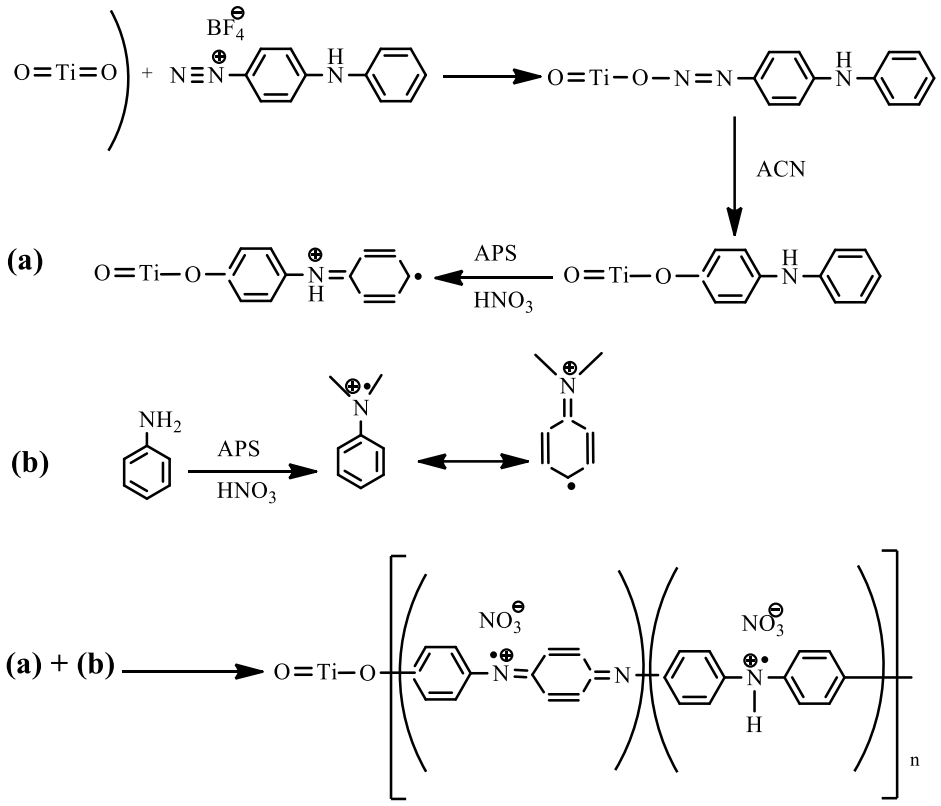

Figure 2. Chemical route for preparing (A) TiO_2-PANI, and (B) TiO_2-DPA-PANI nanocomposites. The growth of polyaniline at the surface of TiO_2-DPA is dispalyed in (C).

Hereafter, we shall characterize the TiO_2 starting material prepared by sol-gel process and then proceed to the characterization and photocatalytic performances of its corresponding nanocomposites. Note however that diazonium modification of surfaces can be conducted with isolated or in situ generated diazonium compounds in aqueous acidic media, eventually with diazoates resulting from alkaline treatment of diazonium compounds. These three main strategies will be evaluated in the case of the TiO_2 nanoparticles under test.

3.3. TiO_2 characterization

Figure 3 displays XRD pattern, UV-vis spectrum and SEM micrographs of the TiO_2 NPs designed along the sol-gel protocol described above. The diffractogram in Figure 3a exhibits peaks expected for TiO_2 in its anatase form: 2θ = 25.4°, 37.1°, 37.9°, 38.7°, 48.1°, 54.2°, 55.2°, 62.9°, 68.7°, 70.3°, 74° and 76.03° related to TiO_2 reflections in planes (1 0 1), (1 0 3), (0 0 4), (1 1 2), (2 0 0), (1 0 5) , (2 1 1), (2 0 4), (1 1 6), (2 2 0), (2 1 5) and (3 0 1), respectively.

The crystallite size of TiO_2 is estimated from the line broadening of the most intense peak of anatase (101) using the Debye–Scherrer's formula [65]:

$$d_{DRX} = \frac{K\lambda}{B\cos\theta}$$

where **d** is the crystallite diametr, **λ** the wavelength of the X-ray radiation (Cu K = 0.15406 nm), **k** is a constant taken as 0.94, **θ** is the Bragg diffraction angle and **B** is the line width at half maximum intensity [65,66]. The crystallite size was about 6 nm.

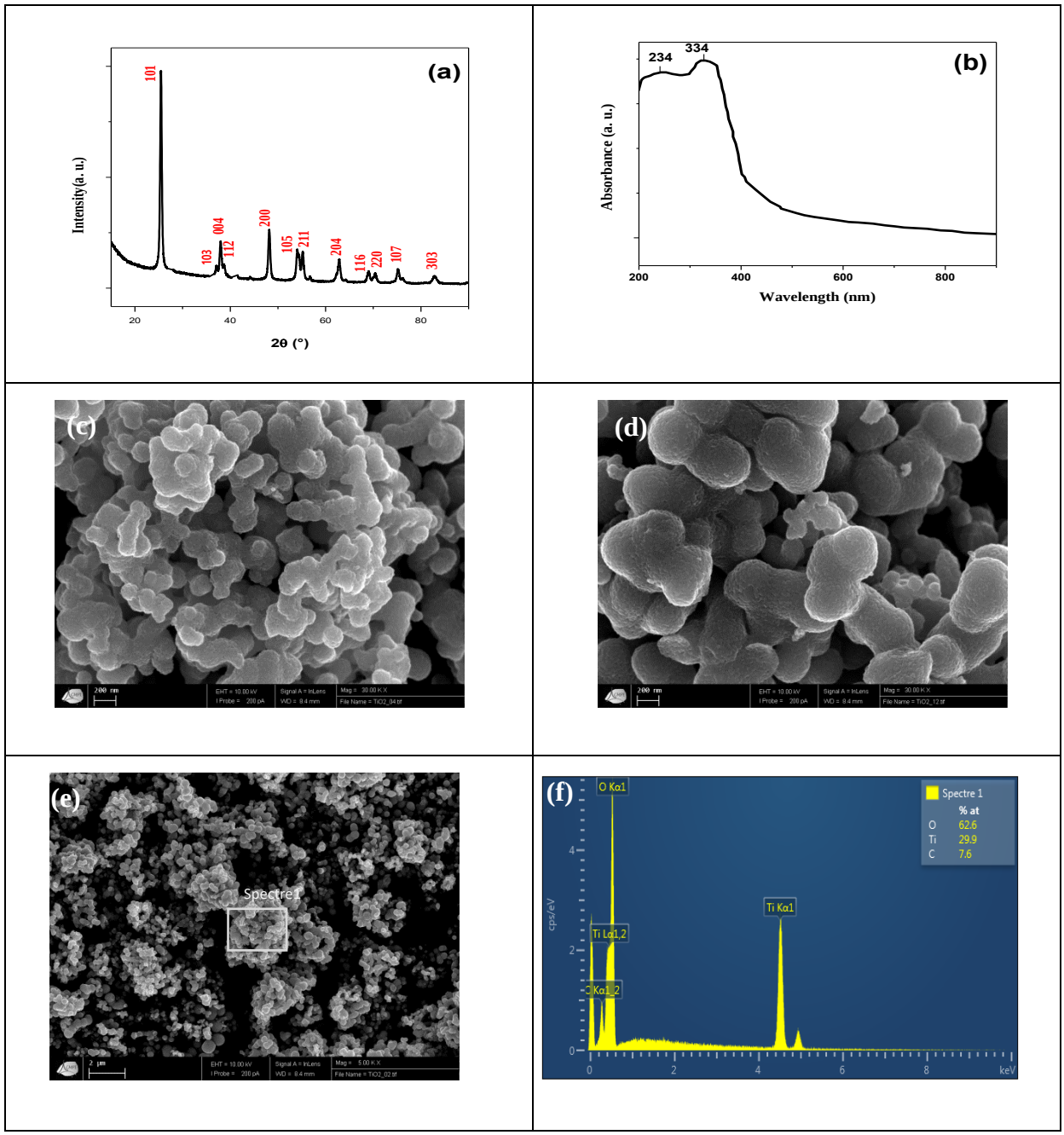

Figure 3. Characterization of TiO_2 NPs by XRD (a), UV-vis spectroscopy (b), and SEM imaging at various magnifications (c-e) with elemental spectrum (f).

UV analysis was carried out in order to determine the valence state and the coordination of the Ti ions in the solid structure. Figure 3b displays the UV-visible spectrum of TiO_2 which exhibits absorption bands at 200 nm and 400 nm, they are characteristic of an electron transition d-d between Ti^{4+} and an O^{2-} ligand present in the anatase phase. The first band between 200 nm and 270 nm corresponds to the transition of Ti^{4+}in a tetrahedral environment where as the second band between 290 nm and 350 nm is characteristic of Ti^{4+} in an octahedral environment [67]

Based on the absorption spectra, the band gap energy (Eg) of the TiO_2 was calculated using:

$$\alpha(h\upsilon) = A(h\upsilon\text{-}Eg)^n$$

were α,υ, Eg and A are the absorption coefficient, light frequency, band gap energy, and A constant respectively.

(n) is determined by the type of optical transition of semiconductor (n=1/2 for direct transition and n=2 for indirect transition). The band gap energy of TiO_2 nanopowders as calculated by extrapolating a straight line to the abscissa axis in the $(\alpha h\upsilon)^2 = f(h\upsilon)$ plot, where α is zero, for $Eg = hv$ is 3.2 eV, in line with the literature [68,69,70, 71].

The morphology of calcined oxide powder observed by SEM is shown in Figures 3c-d at various magnifications. The pictures **s**how that the TiO_2 NPs are spherical with strong agglomeration.

The EDX spectrum (Figures 3f) obtained reveals that TiO_2 was pure phase without any other Impurities. the percentage of O_2 is twice that of Ti, this also confirms the formation of titanium dioxide.

3.4. Appraisal of methods for TiO_2 diazonium modification

In order to select the ideal process for the grafting of DPA on the surface of TiO_2, we have characterized the modified TiO_2 products by IR, Raman and XPS after modification with in situ generated and isolated diazonium salts, as well as with diazoates formed in alkaline medium (pH=12). The main results are summarized in Table 1.

Table 1. Characteristic features of TiO_2 nanoparticles modified in various conditions.

Characterization techniques / Process	FTIR	Raman	XPS (C+N)/Ti
Grafting in situ	Appearance of $\upsilon_{N\equiv N}$	No shift	23.8
Grafting with isolated DPA	No band at 2232 cm^{-1} Aromatic core bands appear	Red shift	6.6
Diazoate	No band at 2232 cm^{-1} Appearance of aromatic core bands	Red shift	0.3

The characterization results revealed that the in situ grafting of the DPA did not take place, this is confirmed by the appearance of the IR band located at 2232 cm^{-1} corresponding to the ungrafted diazonium. Moreover, no shift of the TiO_2 characteristic bands was recorded by Raman, thus confirming that no reaction occurred between the DPA diazonium and TiO_2. In XPS, we have noted a sharp F1s peak centred at 685 eV and assigned to BF_4^- counter-ion. The high (C+N)/Ti atomic ratio accounts thus for diazonium salts physisorbed on the nanoparticles. It resisted thorough washing process.

The modification with isolated diazonium salt that was reduced using ascorbic acid, in the presence of the TiO_2 nanoparticles, gave the best results. Indeed, the IR spectrum of TiO_2-DPA lacks the $\upsilon_{N\equiv N}$ band of diazonium salt, suggesting the grafting of DPA aryl groups to TiO_2. This is confirmed by a Raman shift of the characteristic TiO_2 band on going from the bare to the grafted nanoparticles. The XPS (C+N)/Ti atomic ratio is ~6.6.

For the diazoate modification, we have noted similar trends in the IR and Raman results with the exception of a much lower (C+N)/Ti atomic ratio of ~0.3.

The results obtained so far, dictated the choice of the use of isolated diazonium salts for the grafting of TiO_2 nanoparticles with 4-diphenylamine groups using ascorbic acid as a reducing agent for the diazonium. The nanoparticles modified in this way were further used for the making of TiO_2-DPA-PANI nanocomposites.

3.5. Design and characterization of TiO_2-DPA-PANI nanocomposite and related compounds

3.5.1. FTIR and Raman vibrational studies

TiO_2-PANI nanocomposites prepared were first characterized by IR. Figure 4 displays IR spectra of the nanocomposites and the reference compounds TiO_2 NPs, DPA diazonium salt and PANI powder. The spectrum of untreated TiO_2 NPs (Figure 4a) displays three characteristics bands at 480, 640 and 850 cm^{-1} corresponding to Ti=O, Ti-O-Ti and Ti-O, respectively. DPA spectrum (Figure 4b) exhibits characteristic bands of the diazonium salt powder in the 3350-1400 cm^{-1} region. The vibration band located at 3340 cm^{-1} is assigned to N-H vibration; 2232 cm^{-1} is due to N≡N stretching mode, the bands at 1590 cm^{-1} and 1610 cm^{-1} are assigned to the aromatic C=C stretching in addition to the band at 1180 cm^{-1} which is relative to C-H benzene ring stretching band. The spectrum of TiO_2-DPA (Figure 4c) appears to be a combination of the spectrum of pure TiO_2 and DPA. The spectrum displays bands at 1510 cm^{-1} and 1690 cm^{-1} which are assigned to the aromatic C=C stretching vibrations [72], in addition to the characteristic bands of TiO_2. It is noted that the vibrating band situated at 2232 cm^{-1} corresponding to the N≡N stretching mode does not appear on the spectrum, thus confirms the grafting of the diazonium-derived aryl groups to TiO_2 surface. The spectrum of PANI (Figure 4d) exhibits bands centred at 3330 and 3620 cm^{-1} assigned to N-H stretching [73] and strongly adsorbed H_2O molecules [74], respectively. As mentioned above, a similar band in the spectrum of TiO2-DPA (Figure 4b) is located at 3340 cm^{-1} and assigned to N-H. The band that apears at 3112 cm^{-1} is attributed to N-H stretching vibration for intramolecular hydrogen bonded NH groups; this type of bonds is well known to induce a red shift in IR spectra. The peak at 1570 cm^{-1} is ascribed to C=N stretching of quinoid vibrations [75]**.** The bands at 1489 cm^{-1} and 1426 cm^{-1} are assigned to N-N and C=C aromatic ring stretching of the benzenoid vibration. The peaks centred at 1315 cm^{-1} and 779 cm^{-1} are relative to C-N^+ stretching vibration. The band appearing at 1140 cm^{-1} is assigned to the "electron-like band"; it accounts for the conductivity of PANI [76]. Furthermore, the band at 1026 cm^{-1} is due to the in plane bending of C-H. It is noted that the bands located between 2100 and 2300 cm^{-1} in the spectra of TiO_2 and PANI are attributed to the atmospheric CO_2. The spectrum of TiO_2-PANI (Figure 4e) gathers all TiO_2 bands with only two characteristic peaks of PANI, located at 1061 cm^{-1} and 1315 cm^{-1}. In addition, a new band appeared between 1020 cm^{-1} and 1040 cm^{-1} corresponding to Ti-O-C [77]. This band was also observed by Yuzhen et al [75] . In the case of the synthesis of PANI in the presence of DPA-modified TiO_2, the resulting TiO_2-DPA-PANI nanocomposite exhibits various vibration modes of PANI located between 750 and 3200 cm^{-1} but shifted toward higher wavenumbers (Figure 4f). Katoch et al. [78]

attributed this shift to the formation of a chemical bond between TiO_2 NPs and PANI and the existence of molecular interactions between them. The peak position of pure PANI and the nanocomposites TiO_2-PANI and TiO_2-DPA-PANI are gathered in Table 2.

Table 2. Peak positions of pure PANI and the TiO_2-PANI nanocomposites in the FTIR Spectra.

Bonds / materials	C-H plane bonding (cm^{-1})	C-C (benzoid rig) (cm^{-1})	C-N (quinoid ring) (cm^{-1})	N-H (quinoid ring) (cm^{-1})
PANI	1026	1426	1570	3112
TiO_2-PANI	1061	-	-	-
TiO_2-DPA-PANI	1061	1478	1578	3221

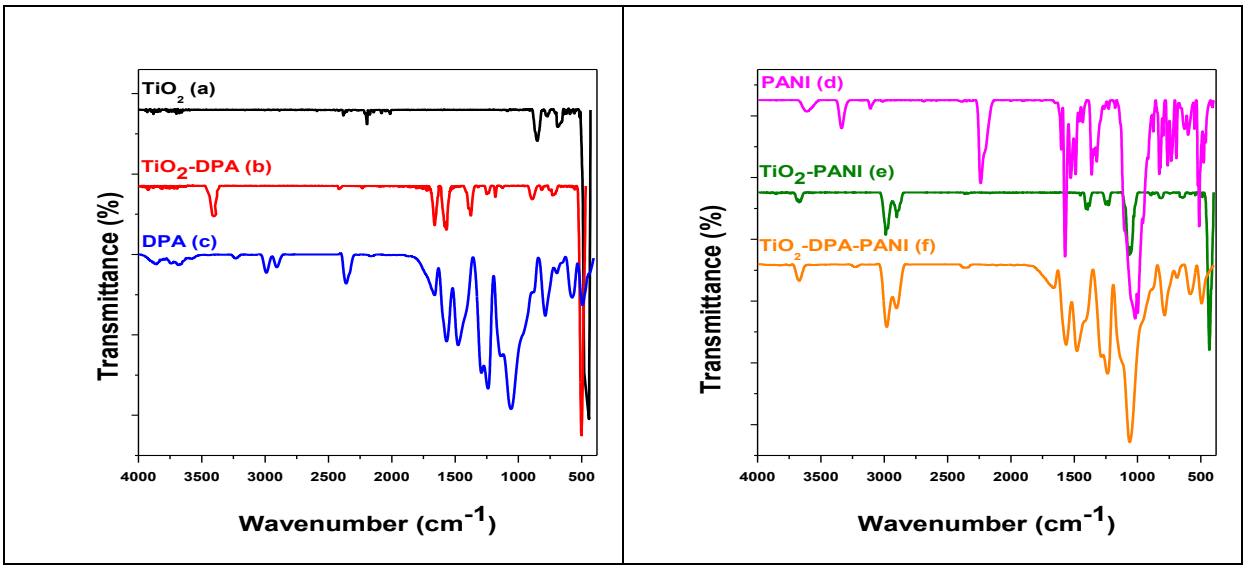

Figure 4. FTIR spectra of (a) TiO_2, (b) TiO_2-DPA, (c) DPA diazonium, (d) PANI, (e) TiO_2-PANI, and (f) TiO_2-DPA-PANI nanocomposite.

Figure 5 shows the Raman spectra of TiO_2, TiO_2-PANI and TiO_2-DPA-PANI nanocomposite. TiO_2 nanoparticles spectrum display caracteristic bands at 144 (E_g), 197 (E_g), 398 (B_{1g}), 514 (A_{1g}), 639 (E_g). From the PANI spectrum, the band situated at 1484 cm^{-1} is assigned to the C-N stretching vibration from benzenoid ring while the peak observed at 1319 cm^{-1} is due to the C-N stretching from quinoid structure. The pic located at 1596 cm^{-1} is due to C-C stretching from quinoid ring [62]. The coating of PANI onto TiO_2 NPs does not exhibit any shift of the TiO_2 characteristic bands but the addition of DPA caused a red shift of the bands characteristic of TiO_2 and an increase in the intensity, indicating a successful modification of

TiO_2 NPs by DPA. Typical Raman spectra of TiO_2-DPA-PANI nanocomposite stresses the spectacular role of DPA in the nanocomposite. The peaks corresponding to TiO_2 and PANI are broad, intense and red shifted. This confirms the insertion of the polymer on the TiO_2-DPA surface.

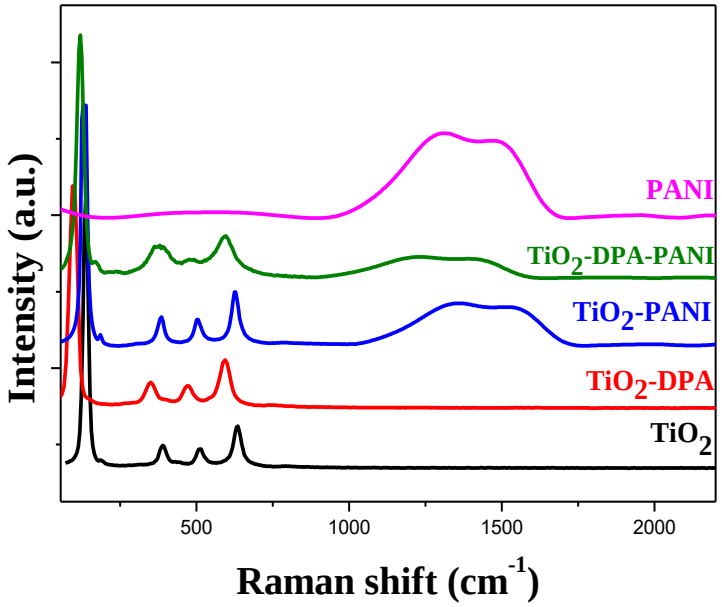

Figure 5. Raman spectra of TiO_2, TiO_2-DPA, PANI, TiO_2-PANI and TiO_2-DPA-PANI nanocomposites

3.5.2. UV-vis

UV-vis diffuse reflectance spectra of TiO_2-PANI and TiO_2-DPA-PANI nanocomposites are presented in Supplementary Material SM1. A broadening of the two TiO_2 absorption bands with a slight decrease in absorption was recorded due to the presence of a small amount of PANI. This conductive polymer has good absorption in the UV range as well as in the visible spectral region [79]. The spectrum obtained in the case of TiO_2-DPA-PANI nanocomposite is almost similar to that of PANI presented by Wahyuni et al [80] with the presence of a band around 469 nm corresponding to the π-π* transition in the polymer chain [81]. The increase of the right part of the spectrum in the infrared region indicates a delocalization of the carriers n-π* [82].

The band gap energy of TiO_2-PANI and TiO_2-DPA-PANI nanocomposite was calculated by extrapolating a straight line to the abscissa axis in the $(\alpha h\upsilon)^2 = f(h\upsilon)$ plot. The band gaps were found to be 2.23 and 1.30 eV for these nanocomposites, respectively.

3.5.3. XRD

TiO_2-DPA, TiO_2-PANI, TiO_2-DPA-PANI nanocomposites were characterized by X-ray diffraction. The diffractograms are shown in the Supplementary Material SM2.

The diffractogram of TiO_2-DPA and that of TiO_2-PANI nanocomposite are almost similar to those of TiO_2 anatase shown in Figure 3a, with a slight broadening of the corresponding peaks. The diffractogram of TiO_2-DPA-PANI nanocomposite displays less intense TiO_2 anatase peaks with a diffuse signal between 20 and 30 ° which is likely to be due to an amorphous phase of polyaniline.

3.5.4. SEM-EDS

The morphology and the elemental composition of the nanopowders (TiO_2-DPA, TiO_2-PANI and TiO_2-DPA-PANI) were obtained by SEM-EDS (Figure 6). The SEM images of DPA-modified TiO_2-DPA (Figures 6a-b) show a change in the structure and the morphology of TiO_2 NPs. The introduction of organic matter is very clear and confirmed by the appearance of nitrogen (N) from the diazonium salt (Figure 6c, N=5.3 at.%) and the decrease of Ti and O percentages on the corresponding EDS spectrum (Figure 6c).

The images recorded for the TiO_2-PANI nanocomposite (Figures 6d-e) are similar to those recorded for pristine TiO_2 NPs. The amount of PANI inserted on the TiO_2 surface is very small or even negligible and this is confirmed by the absence of nitrogen and the sulfur of the doping anion of the polymer in the analyzed zone. As a matter of fact, this is in line with the pale color of TiO_2-PANI (see digital photograph in Figure 1Bc), showing quasi no change in the color of TiO_2 after in situ polymerization of aniline.

In contrast, Figures 6g-h display a surface of TiO_2-DPA-PANI with a globular and porous morphology due to PANI. The corresponding EDS spectrum (Figure 6i) has peaks assigned to TiO_2 NPs and that of nitrogen (10.4 at.%) and sulfur of the doping anion (0.7 at.%).

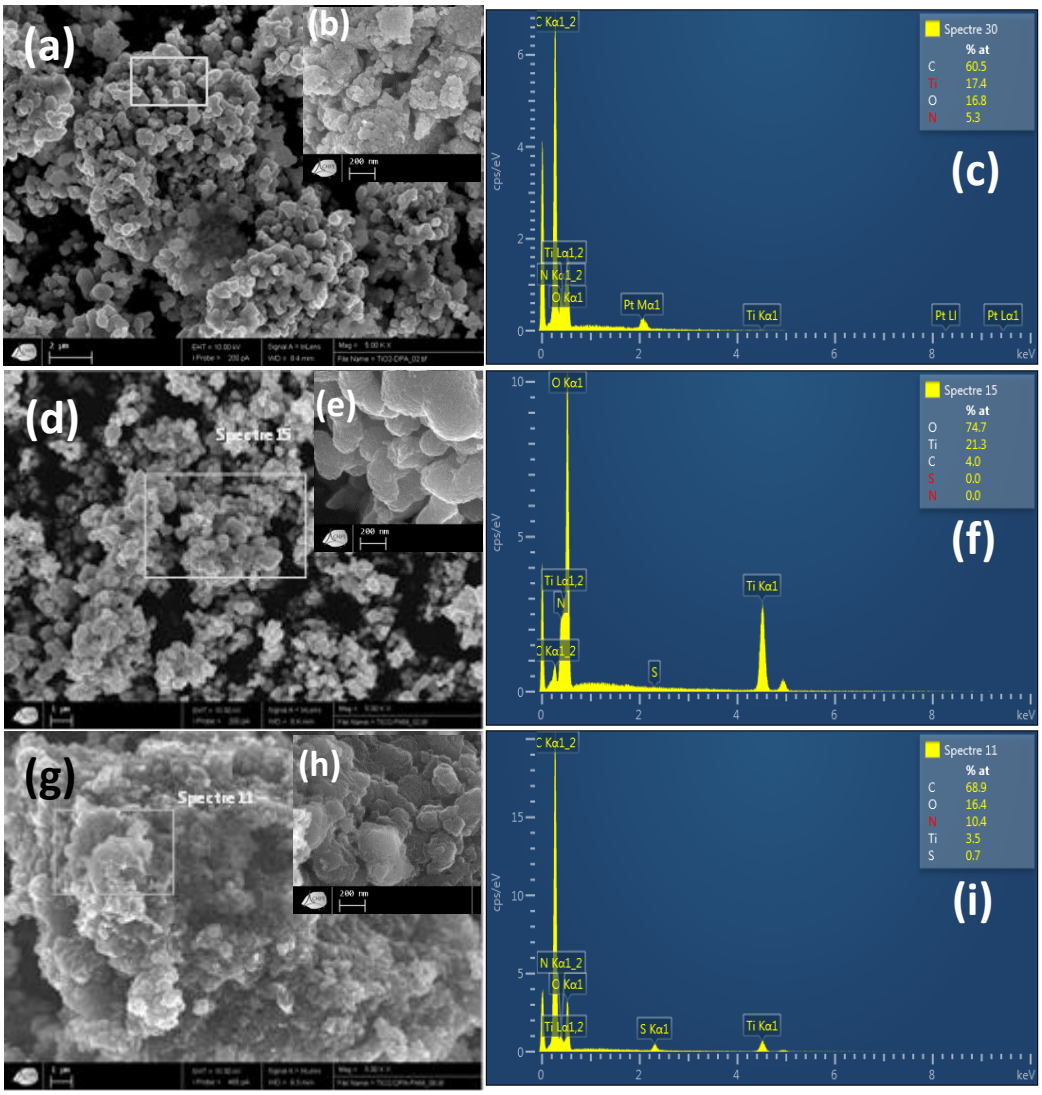

Figure 6. SEM images (a,b,d,e,g,h) and elemental spectra (c,f,i) of TiO_2-DPA (upper panel, a-c), TiO_2-PANI (central panel, d-f) and TiO_2-DPA-PANI (lower panel,g-i) nanocomposites. Low magnification SEM images are insets of the high resolution images.

3.5.5. XPS

Figure 7 displays survey spectra (Figure 7A) and the surface composition in at.% of the TiO_2-DPA-PANI and related compounds. In Figure 7A, TiO_2 exhibits two prominent Ti2p ($Ti2p_{3/2}$ centred at 459.4 eV) and O1s (530.7 eV) signals and a minor C1s peak at 285 eV due to unavoidable adventiotious hydrocarbon contamination. Clear change of the surface of TiO_2 is testified by the TiO_2-DPA survey spectrum which shows C1s peak as intense as that of the Ti2p doublet. The diazonium bears an amino group which yields an N1s peak at 399.7 eV. The in situ synthesis of PANI in the presence of bare TiO_2 is quasi-similar to that of bare TiO_2 therefore indicating a low extent of PANI deposition. This is in line actually with the pale

color of TiO_2-PANI powder displayed in Figure 1Bc. In contrast, TiO_2-DPA-PANI has a survey spectrum lacking Ti2p doublet indicating a complete coverage of the nanoparticles with PANI top layer (Figure 7A); the spectrum is similar to that of pure PANI reported in the literature [54,83]. S2p at 168.1 eV accounts for PANI top layer dopant.

Figure 7B displays O1s regions from TiO_2 (Figure 7Ba) and TiO_2-DPA (Figure 7Bb); both are fitted with 3 components centred at 530.4, 532.0-532.2 and 533.6 eV assigned to TiO_2, TiO_2 surface hydroxide [42] and/or Ti_2O_3 [84], and C-O, respectively. Interestingly, the intensity of the high binding energy component assigned to C-O bonds relative to the sum of the peak areas of the signals at 530.4 and 532.0-532.2 eV increases from 6.5 to 13.4% upon aryl grafting to TiO_2. This results supports the hypothesis of a chemical reaction between the diazonium and the oxide leading to Ti-O-C interfacial bond.

Bar graphs shown in Figure 7C permit to quantitatively track changes at the surface of TiO_2. The C/Ti ratio dramatically increases from 0.6 to 5.8 on going from TiO_2 to TiO_2-DPA, and similar trend is observed for N/Ti ratio (0 and 0.7, respectively). N/Ti for TiO_2-PANI is 0.01 significantly smaller than that of TiO_2-DPA. For the final nanocomposites TiO_2-DPA-PANI, Ti content could not be quantified due to a noisy Ti2p region lacking Ti2p, whereas C/N = 6.5 less than 10% higher than the theoretical value of 6, whilst S/N=0.22, similar to 0.24 obtained for pure PANI.

These results indicate that the diazonium modification of TiO_2 permits to coat PANI at an extent sufficient to completely screen the underlying TiO_2. Hence, the effective role of diazonium compounds as coupling agents for polymers to materials surfaces [29,53,54,62,85,86], and for obtaining herein a TiO_2-DPA (core)/PANI (shell) structure as judged from the gradual attenuation of TiO_2 XPS peaks.

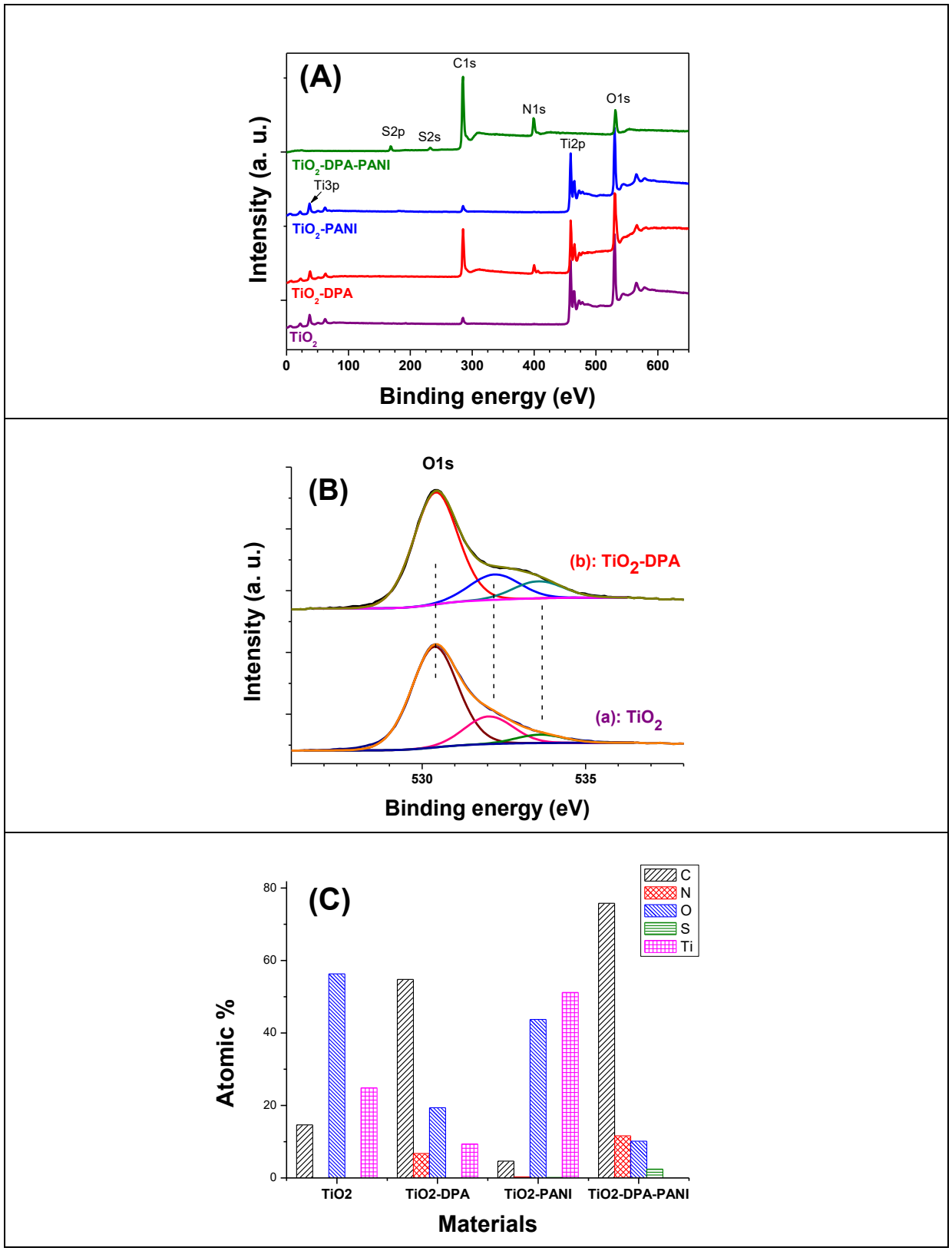

Figure 7. (A) XPS survey scan of TiO_2, TiO_2-DPA, PANI, TiO_2-PANI and TiO_2-DPA-PANI nanocomposites; (B) peak-fitted high resolution O1 spectra from TiO_2 (a) and TiO_2-DPA (b); (C) surface composition (in at.%) of the materials under test.

3.6. Adhesion of PANI to TiO_2 nanoparticles

The adhesion of PANI to the surface of TiO_2 NPs was investigated by testing its solubility in various organic polar (DMF, NMP, THF, HFIP and DMSO), and non-polar solvents (chloroform, 1,2-dichloroethane, xylene, toluene). It is to note that the solubility of PANI is influenced by its basic thermodynamic properties [87], interaction among polymer chains and the associated counter ions and the solvent [88]. The solutions of PANI in different solvents are shown in Figure 8. The pictures prove that the PANI was highly soluble in DMSO, NMP, HFIP and THF as reported elsewhere [89,90]; partially soluble in DMF and toluene; and insoluble in chloroform, 1, 2-dichloroethane and xylene (Figure 8A). TiO_2-PANI nanocomposite exhibits the same behavior *ca* PANI is easily leached from the TiO_2-PANI nanocomposites. This suggests that there is a weak bond between the conductive polymer and the TiO_2 which results in failure of PANI to TiO_2 adhesion (Figure 8B). In contrast, in the presence of DPA, the adhesion of the PANI has improved considerably; the polymer is insoluble in the solvent except a slight staining of DMSO which may be due to the dissolution of PANI chains that are loosely bound to TiO_2 (Figure 8C).

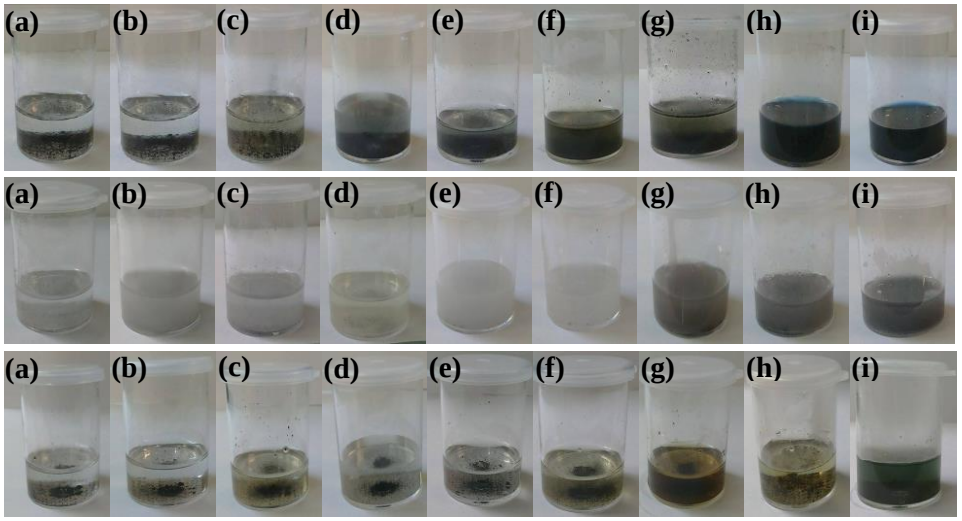

Figure 8 . Digital photographs of solutions of (**A**):PANI, (**B**): TiO_2-PANI, (**C**): TiO_2-DPA-PANI in : (a) Chloroform , (b) 1,2-dichloroethane , (c) Xylene, (d) Toluene, (e) DMF, (f) THF, (g) HFIP , (h) NMP, (i) DMSO .

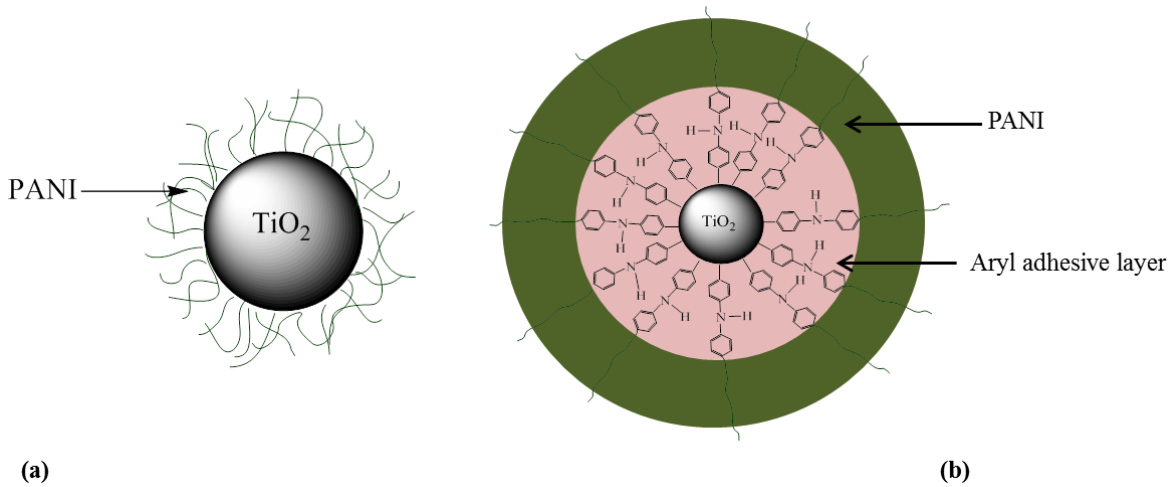

Figure 9. Schematic illustration of the core/shell structure of TiO_2/PANI nanoparticles: (a) TiO_2-PANI prepared without diazonium, and (b) TiO_2-DPA-PANI.

Considering the adhesion testing results reported so far, one can suggest the following "molecular picture" of the situation at the interface between the TiO_2 core and the PANI shell (Figure 9). In the absence of any diazonium-pretreatment most probably PANI chains are loosely bound to the surface with a minimal density, whereas after DPA-modification, the chains grow perpendicular to the surface with the covalent anchor site being the second phenyl group starting from the surface. The attachment of aryl groups to TiO_2 grown on Ti by anodization was suggested to be via the oxygen atoms from TiO_2. It is thus likely that the primary adhesion, between aryl groups and TiO_2, occurs via the interfacial group Ti-O-C in the Ti-O-aryl chemical environment. This primary adhesion is important for the second step of the process of making TiO_2-DPA-PANI in the sense it ensures adhesion of PANI via covalent bonds. Indeed, as demonstrated elsewhere, PANI was most probably covalently bound to DPA-modified glassy carbon electrodes [53]. Similarly, DPA ensures attachment of uniform coating of PANI to MWCNTs [54] and to bentonite lamellae [62]. In the latter case, intercalation of clay by DPA triggered exfoliation of the clay when aniline was polymerized in the presence of DPA-modified bentonite therefore resulting in remarkable exfoliated, conductive clay/PANI nanocomposites employed as reinforcement of epoxy resin [91].

Herein, the DPA modification appears again as unique "molecular glue" for attaching PANI chains to a particulate support, namely TiO_2. Not only the loading is high, mostly due to covalent bonding of PANI to TiO_2 but such covalent bond results in remarkable adhesion of PANI which withstands the attack of strong polar solvents. It is well known for example that NMP is a paint remover employed in testing paint adhesion and that HFIP has been used to coat PANI on chromatographic support by Al-Saïgh and co-workers [92].

3.7. Photocatalytic performances of TiO_2-DPA-PANI

At this stage, it is important to stress that pH is an important parameter in the study of the photocatalyzed degradation of MO due to the fact that this dye is a pH indicator. As a matter of fact, Smith et al. [93] on the one hand, and Niu [94], on the other hand, investigated the degradation of MO using TiO_2 as a nanocatalyst at different pH solutions and found the degradation rate to decrease with increasing pH. This conclusion was also reached by Zhenghua *et al.* [95] who used Fe_3O_4@SiO_2@TiO_2 microspheres as photocatalyst for the decomposition of the same dye. Elsewhere, Chen et al [96] reported that in acid medium (< 2) MO is transformed into quinone which is more toxic and difficult to degrade than the parent molecule. Based on what was reported by these and other researchers, we chose to work at pH 6.5 in order to drastically limit any formation of quinonic form of MO. The addition of H_2O_2 is expected to enhance the reaction by the formation of cation and anion radicals in solution during the dye decomposition process.

3.7.1. General aspects of the photocatalyzed degradation of methyl orange

Methyl orange solutions with and without catalysts (TiO_2, TiO_2-PANI, TiO_2-DPA-PANI) were first stored in the dark 50 min to any photocatalytic degradation experiment then exposed to UV light. No discoloration of the solutions occurred in the dark (Figure 10A) meaning that no degradation has taken place under these conditions and that the powders have no catalytic effect in darkness.

The exposure of aqueous solutions of MO to UV irradiation in absence and presence of catalysts caused complete discoloration of the dye solution containing TiO_2 NPs, TiO_2-PANI or TiO_2-DPA-PANI nanocomposites after 20 min.There is a clear role of the catalysts in activating the process of degradation of the dye (Figure 11B), likely due to complete mineralization of the dye. Indeed, as illustrated in Figure 11, one can note the disappearance of the absorbance bands characteristic of the phenyl group, which is usually found between 250 and 300 nm and the band located between 400 and 500 nm characteristic of the azo group (Figure 11).

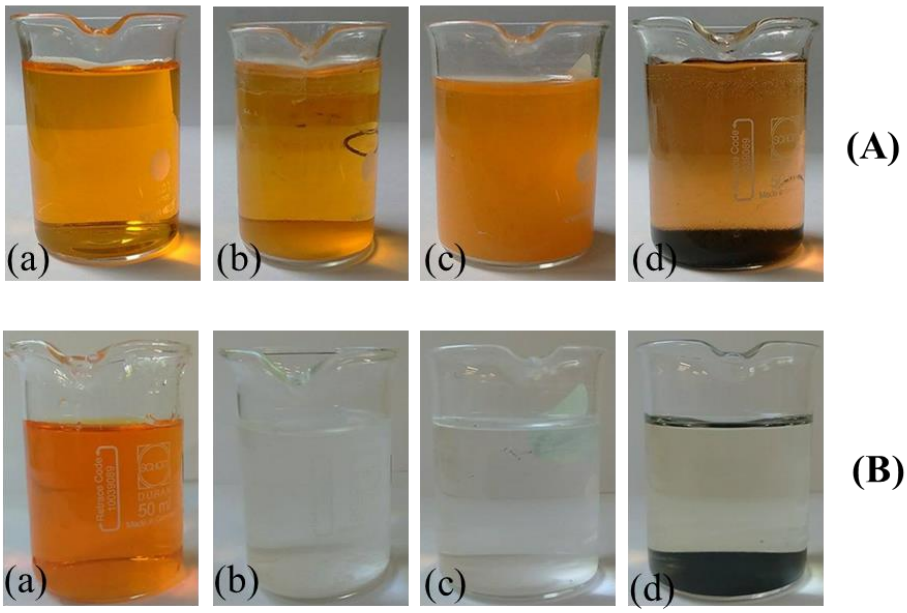

Figure 10. Digital photographs of methyl orange after (A) storage in the dark, (B) UV irradiation. (a) Without catalyst, (b) TiO_2, (c) TiO_2-PANI, (d) TiO_2-DPA-PANI.

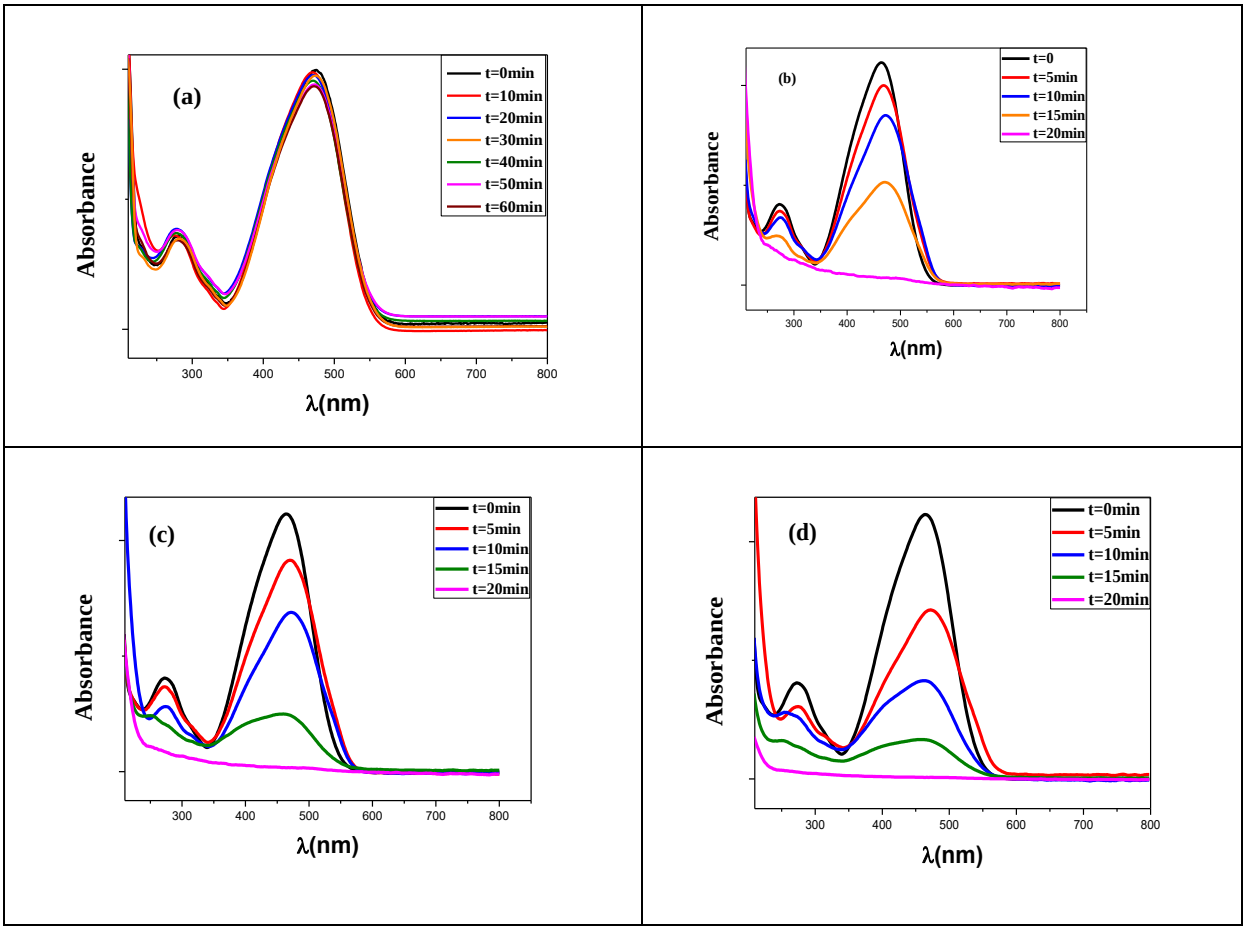

Figure 11. UV-vis absorption spectra of MO solutions for various periods. (a) without catalyst, (b) TiO_2, (c) TiO_2-PANI, (d) TiO_2-DPA-PANI**.**

Kinetic studies of the degradation of methyl orange

The percentage of degradation was calculated using **[97]:**

$$\% = \frac{C^\circ - C}{C^\circ} * 100$$

Table 3 reports the extent of degradation of the dye (in molar %).

Table 3. Degradation extent (%) of methyl orange with different catalysts.

t (min) / catalysts	5 min	10 min	15 min	20 min
No photocatalyst	_	1.89	_	2
TiO_2	10.1	23.9	53.8	98.0
TiO_2-PANI	18.0	38.1	77.5	98.6
TiO_2-DPA-PANI	36.2	62.8	85.1	99.5

The degradation percentage of MO is higher with TiO_2-PANI compared to that obtained with pure TiO_2 nanoparticles. This is probably due to the amount of conductive polymer loaded on the nanocatalyst surface and its role during the photocatalyzed reaction. Salem *et al.* [98] and Reddy *et al.* [59] have also concluded that the TiO_2-PANI nanocomposite has a much greater photocatalytic effect than pure TiO_2. The highest percentage of degradation was obtained in the presence of TiO_2-DPA-PANI; this is illustrated by a percentage which is twice higher than that obtained with TiO_2-PANI (see values for 5 and 10 min reaction). The improved catalysis rate is now undoubtly due to the amount of polymer contained in the composite. As the loading of PANI is intimately linked to the diazonium coupling agent, it is clear that the diazonium salt of DPA plays a vital role in the design of highly active photocatalyst based on PANI-grafted TiO_2.

The kinetic of discoloration of MO dye by the various photocatalysts was investigated (Figure 12). After 20 minutes of irradiation, the degradation of MO solution containing no catalyst is negligible. In the presence of TiO_2, the discoloration is remarkable but less rapid than with TiO_2-PANI and TiO_2-DPA-PANI nanocomposites. The kinetics is even faster than in the case of Ag Nanoparticles-TiO_2 nanofiber composite photocatalyst employed to degrade MO under UV illumination [99], if one has to compare the coating of TiO_2 with two different types of conductive materials, that is metallic nanoparticles and conductive polymers. This confirms the synergetic effect of PANI in photocatalyzing the degradation of the dye. The TiO_2 nanoparticles, TiO_2-PANI and TiO_2-DPA-PANI nanocomposites are responsible for this photoactivation as we have discussed above. They absorb UV radiation to give rise to very reactive species that will lead to the degradation of the dye in solution.

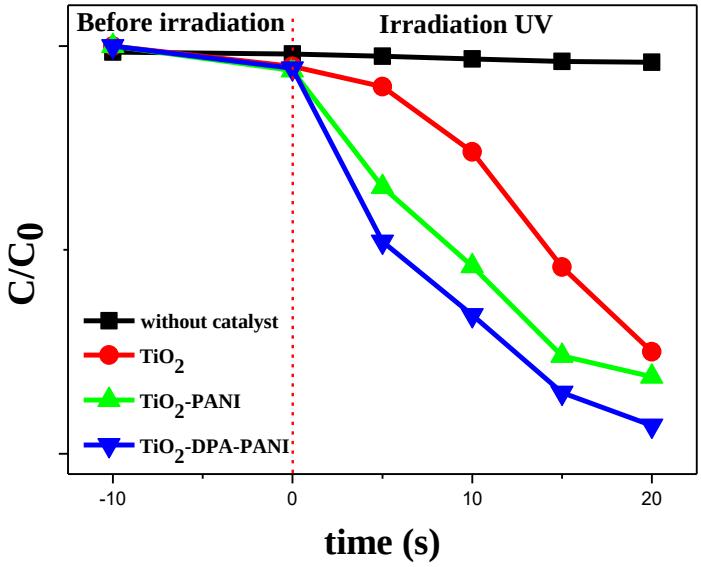

Figure 12. Kinetics of degradation of methyl orange solution (C= 50 mg.L^{-1}).

The experimental data shown in Figure 11 were fitted to the pseudo first order rate law:

$$-\frac{d[C]}{dt} = K[C]$$

where, K (min^{-1}) is the apparent rate constant and C is the concentration of MO.
The linearization form is given by:

$$Ln\ \frac{C}{Co} = -Kt$$

where, C_0 is the initial concentration. All Ln(C/C_0) vs t(min) plots (Figure 13) are linear with correlation coefficients of 0.9627, 0.9851, 0.9954 for TiO_2, TiO_2-PANI and TiO_2-DPA-PANI, respectively. The photodegradation of the dye thus obeys pseudo-first-order kinetics as reported for other photocatalytic systems [97,100].

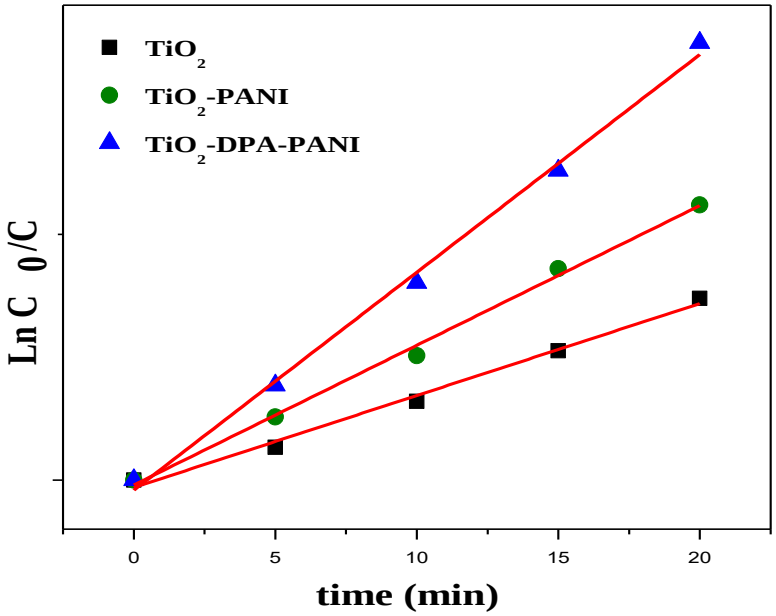

Figure 13. First order linear transforms of the degradation of methyl orange under UV-irradiation.

The values of *K*, computed from the linear correlations, equal 0.059, 0.0853 and 0.133 min^{-1} for the catalyzed reaction using TiO_2, TiO_2-PANI and TiO_2-DPA-PANI, respectively. This result clearly shows that the OM dye degrades more rapidly in the presence of TiO_2-PANI and TiO_2-DPA-PANI.

Generally, the activity of a photocatalyst depends on several parameters such as particle size and surface area, adsorption capacity, light-response range, and the recombination time of photogenerated charge carriers [11]. It is thus reasonable to deduce that the increased photodegradation rate of MO with TiO_2-PANI and TiO_2-DPA-PANI nanocomposite photocatalysts is due to the PANI top layer. Huyen et al. [101] have reported that TiO_2 acts as a counter ion in the TiO_2-PANI nanocomposite. This interaction may cause a displacement of the electrons from the valence band (HOMO) to the conductive strip (LUMO) of the PANI, which increases its conductance [101]. This may be the cause of the acceleration of the dye photodegradation by increasing the number of adsorption sites.

Table 4 compares the performances of the photocatalysts prepared so far with (TiO_2-DPA-PANI) and without diazonium modification of the underlying TiO_2 particles (TiO_2-PANI). The actual rate constants are far higher than those previously reported in the literature for

similar systems tested in the photocatalyzed degradation of MO. More importantly, the diazonium interface chemistry step in the construction of the final nanocomposites has profound, positive effect as it is induces a rate constant as high as 133×10^{-3} min^{-1}.

Table 4. Degradation of methyl orange using various TiO_2-PANI based photocatalysts under UV light.

Materials	**Experimental Conditions**	**Initial MO concentration ($mol.L^{-1}$)**	**Rate constant (min^{-1})**	**Refs.**
TiO_2, P25 m=0.8g in 1L of MO	T_{room} pH=3 t=360 min λ<365 nm	50 $mg.L^{-1}$	0.87×10^{-2} min^{-1}	**[102]**
TiO_2/PANI m=0.05g in 20 ml of MO	T_{room} pH=6 t=160 min λ<400 nm	80 $mg.L^{-1}$	0.6×10^{-3} min^{-1}	[103]
TiO_2/PANI m= 0.08g in 150 ml of MO	T_{room} t= 6h λ=254 nm	20 ppm	41.4×10^{-3} min^{-1}	[104]
TiO_2/PANI m= 0.01g in 50 ml of MO	T=25°C T=120 min λ>400 nm	10 $mg.L^{-1}$	3.7×10^{-3} min^{-1}	[105]
TiO_2-PANI m=10 mg in 50 ml of MO	T_{room} T=20 min λ=382 nm, (power density ~13 mW/cm^2)	C= 50 $mg.L^{-1}$	85.3×10^{-3} min^{-1}	This work
TiO_2-DPA-PANI m=10 mg in 50 ml of MO	T_{room} T=20 min λ=382 nm, (power density ~13 mW/cm^2)	C= 50 $mg.L^{-1}$	133×10^{-3} min^{-1}	This work

3.7.2. Mineralization

The degradation of organic pollutants by oxidation processes can lead to the formation of other compounds which may be more toxic than the parent molecule and thus contribute again to water and environmental pollution. Therefore, it is necessary to identify the degradation products formed after the photocatalytic reaction. The identification of the formed products was carried out by infrared spectroscopy (Figure 14).

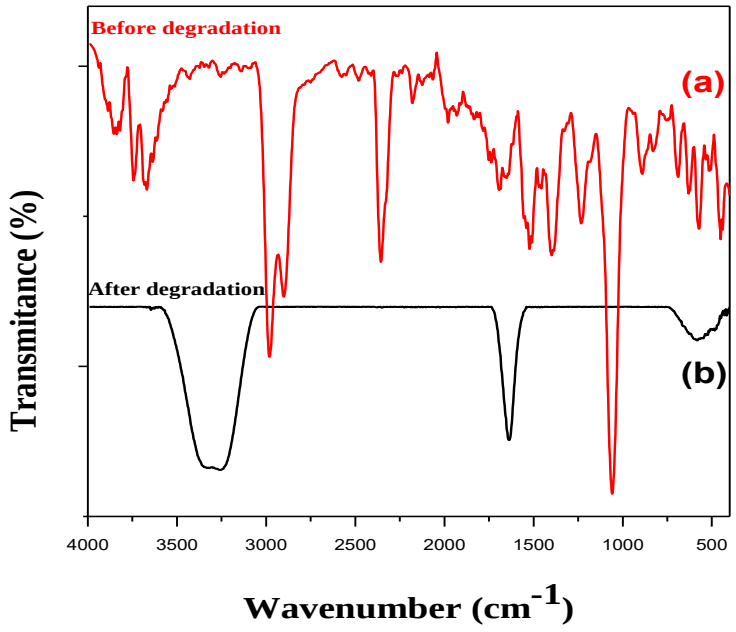

Figure 14. FTIR spectra of methyl orange solution before (a), and after photocatalyzed degradation using TiO_2-DPA-PANI (b).

Figure 14 exhibits a net difference between the IR spectra of the MO solution before degradation and that of the discolored solution after expose to UV light in the presence of TiO_2-DPA-PANI for 20 min. In the spectra of initial MO (Figure 14a), the –S=O band is centred at 1380 cm^{-1}. The bands located at 570, 623 and 697 cm^{-1} are assigned to –C-S vibrations [106]. The spectrum displays two aromatic ring stretching vibration peaks at 840 and 1030 cm^{-1}. The –N=N stretching is found at 1426 cm^{-1} [107]. The bands at 1225 and 1170 cm^{-1} are due to -C-N vibrations. The peak situated at 2905 cm^{-1} accounts for asymmetric –CH_3 stretching vibration. After the photocatalyzed reaction, the spectrum exhibits two broad peaks between 2200 and 3340 cm^{-1} corresponding to OH and H_2O vibrations, respectively [108]. The disappearance of the peaks situated between 440 and 680 cm^{-1} and the peaks corresponding to the azo structure of the dye, indicates the total destruction of azo bands. The

spectrum of MO solution after decolourization displays two bands (Figure 14b): the first one at 3263 cm^{-1} is attributed to –OH stretching in water molecules, whereas the second one at 1636 cm^{-1} could be due to HCO_3^- [109] arising from the reaction of CO_2 with water upon mineralization of methyl orange.

3.7.3. Recovery and stability of the photocatalysts

The pure TiO_2 and its TiO_2-PANI and TiO_2-DPA-PANI nanocomposites were washed several times with ethanol and de-ionized water and dried at room temperature overnight prior to re-use in new experiments with fresh MO solutions (50 $mg.L^{-1}$). The efficiency test by recycling shows that the TiO_2 nanoparticles retains the same photocatalytic performances after two tests, four tests for the TiO_2-PANI and six tests for TiO_2-DPA-PANI nanocomposite (Figure 15A). Figure 15B plots the kinetic constants versus the experiment run number for the photocatalyzed degradation reaction of the dye using the three TiO_2-based materials. It is worth to note that the degradation rate of MO in the presence of reused TiO_2-PANI is larger than that obtained with fresh TiO_2. This is exacerbated in the case of the ternary TiO_2-DPA-PANI nanocomposite. As a matter of fact the latter is not only stable after 6 uses but gives significantly higher degradation rate.

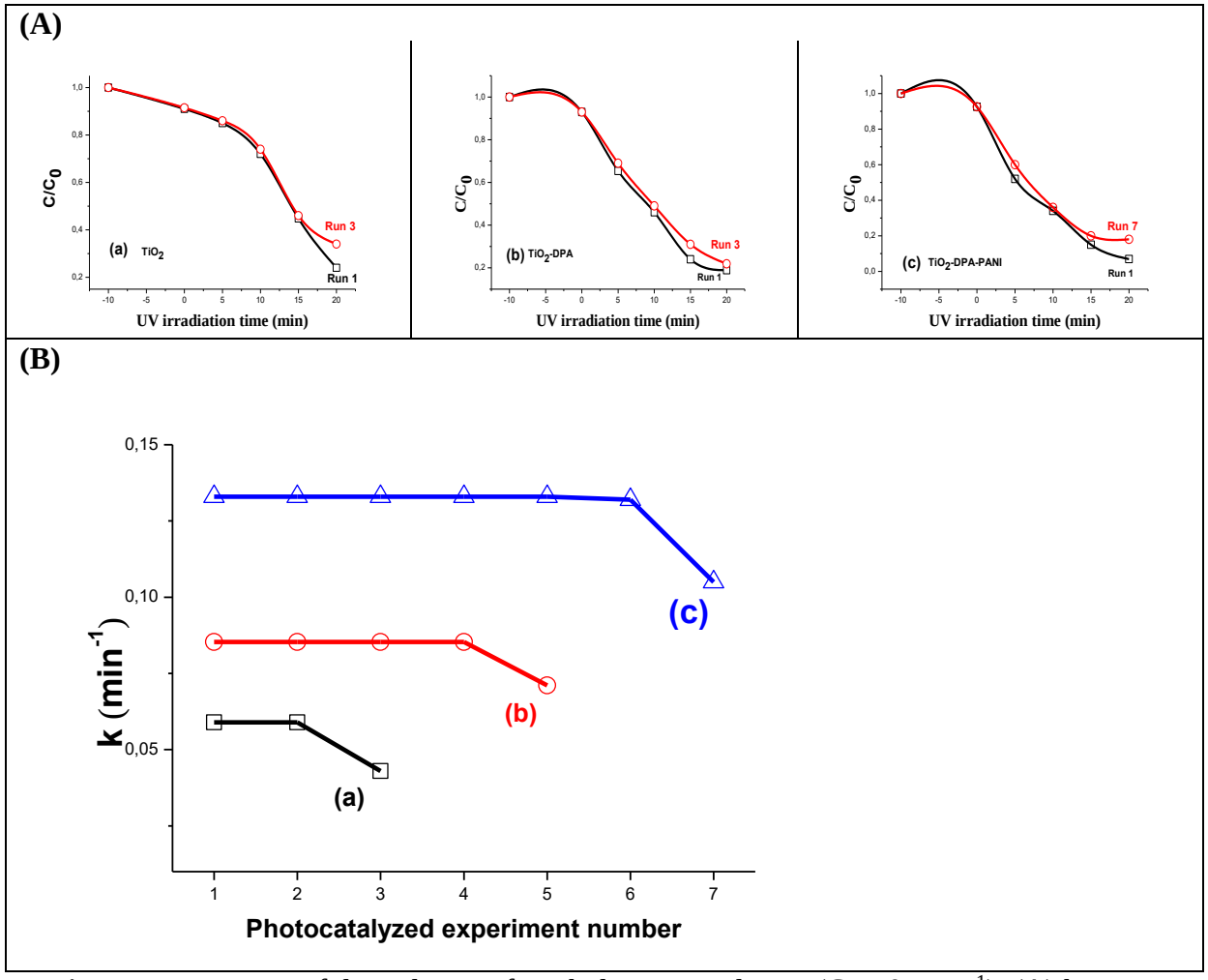

Figure 15. Kinetics of degradation of methyl orange solution (C= 50mg.L^{-1}): (A) kinetics plots obtained at first and last runs with the same catalysts TiO_2 (a), TiO_2-PANI (b) and TiO_2-DPA-PANI (c). (B): Plots of kinetic constants-*vs*-photocatalyzed experiment number for TiO_2 (a), TiO_2-PANI (b) and TiO_2-DPA-PANI (c).

3.7.4. Possible mechanisms of methyl orange photocatalyzed degradation

The recombination rate of the electron-hole pairs photogenerated is a very important factor in studying the photocatalytic activity of a catalyst [110]. PANI-TiO_2 and TiO_2-DPA-PANI composites have much lower recombination rate of electron–hole pairs. The recombination of photogenerated charge was greatly hampered by the introduction of PANI, which showed that the separation efficiency of the photogenerated electron–hole pairs in the nanocomposites was higher than that in pure TiO_2. Consequently, when the PANI–TiO_2 and TiO_2-DPA-PANI catalysts are exposed to the UV light, they show a higher photocatalytic activity than the TiO_2 samples, which stresses the interest of the composites. PANI is constantly donating electrons and accepting holes from TiO_2, and a series of active species such as holes $O^{\bullet 2-}$ and $OH^{\bullet}$ are

successively generated in the photocatalytic process. The detailed photodegradation mechanism of the dye and charge transfer in TiO_2-PANI nanocomposite under UV irradiation are illustrated by the set of steps (Step 1 to 3) and corresponding equations (1)-(8), as well as by Figure 16.

The decomposition process of MO in the presence of H_2O_2 under irradiation can occur in accordance with the mechanism described below.

In ***Step 1***., active radicals are generated:

$$TiO_2\text{-}PANI + h\nu \longrightarrow h_{VB}^{+} + e_{CB}^{-} \quad \textbf{(1)}$$

$$h_{VB}^{+} + H_2O \longrightarrow H^{+} + HO^{\bullet} \quad \textbf{(2)}$$

$$H_2O_2 + h\nu \longrightarrow 2HO^{\bullet} \quad \textbf{(3)}$$

Step 2.The dissolved oxygen gives a radical anion under the action of the UV-light:

$$O_2 \longrightarrow O_2^{*} \quad \textbf{(4)}$$

$$O_2^{*} + 1e^{-} \longrightarrow O_2^{\ominus\bullet} \quad \textbf{(5)}$$

$$O^{\ominus}\!-\!O^{\bullet} \xrightarrow{H_2O} H\!-\!O\!-\!O^{\bullet} + OH^{\ominus} \quad \textbf{(6)}$$

The degradation mechanism of MO is very complex. In the degradation mechanism , several degradation products occur:

$$HO^{\bullet} + C_{14}H_{14}N_3NaO_3S \longrightarrow (C_aH_bN_cN_dO_eS_f)^{\bullet} + H_2O \longrightarrow CO_2 + H_2O + SO_4^{2-} + NO^{3-} \quad \textbf{(7)}$$

The active radical species ($HO^{\bullet}$) oxidize the MO molecule to the several organic radical molecules and then lead to the final products (CO_2, H_2O, SO_4^{2-} and NO_3^{-}) through the successive reactions [111,112] displayed in Step 3.

Step 3.

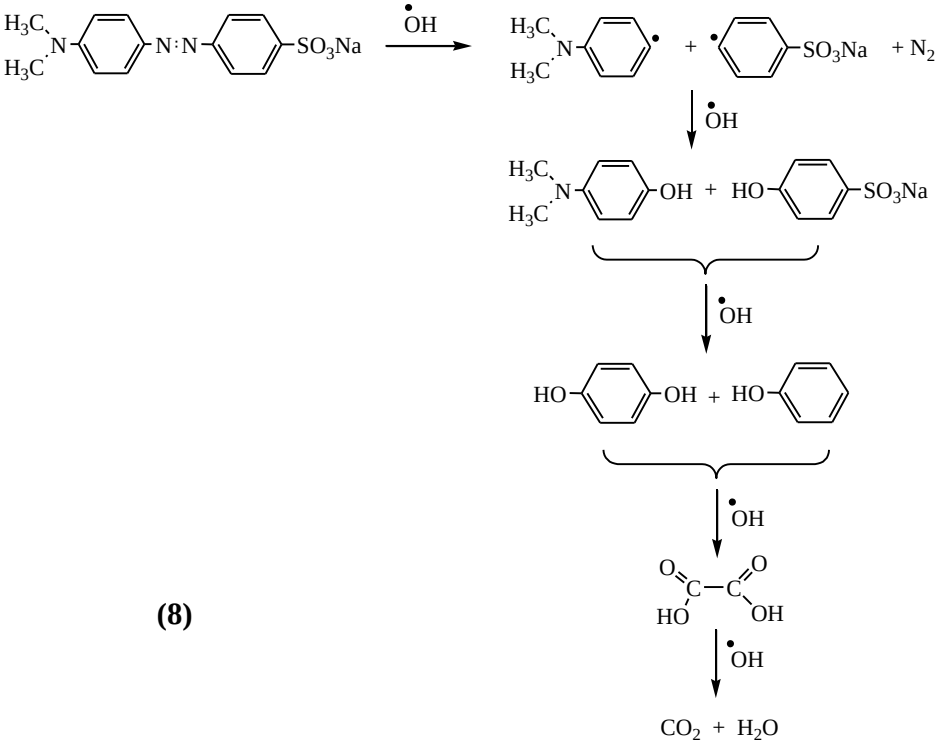
OH
+ N2
OH
OH
OH
OH
CO2 + H2O

(8)

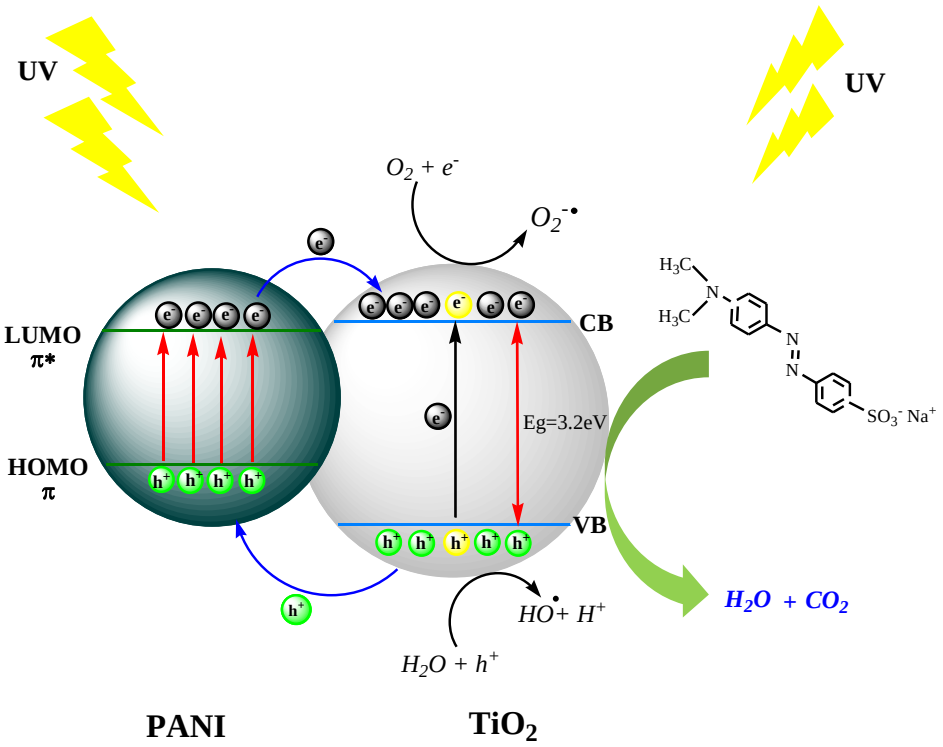
UV
UV
O2 + e-
O2-•
LUMO
π*
HOMO
π
CB
VB
Eg=3.2eV
H2O + CO2
HO• + H+
H2O + h+
PANI
TiO2

Figure 16. Suggested mechanism of degradation of methyl orange (upper panel). charge transfer in TiO_2-PANI nanocomposite under UV irradiation (lower panel).

The set reactions (1) to (8) is illustrated in Figure 16. As discussed by Huyen [101], Nakata [113] and Guo [103], under UV irradiation, TiO_2 and PANI generate electron-hole pairs. The generated electrons which are excited in the velence band (VB) of TiO_2 move towards the conduction band (CB), leaving holes behind in VB These holes leave the VB of TiO_2 to join the HOMO of PANI; the latter transfers electrons from the the LUMO towards the CB of TiO_2 under the effect of the UV light.

The holes and the e^- photogenerated are the most important species in the photocatalytic processes because they are at the origin of the formation of the active species ($O_2^{-\bullet}$, $OH^\bullet$) which are responsible for the decomposition of the organic molicules [103]. The holes generated react with dissolved oxygen peroxide or H_2O to produce the $OH^\bullet$ radicals, which are responsible for the oxidation of MO. In addition, the O_2 molecules adsorbed on the surface of the catalyst capture an e^- giving rise to $O_2^{-\bullet}$ anion radicals which also participate in the photodegradation of the dye molecules [114].

The formed reactive species ($O_2^{-\bullet}$, $OH^\bullet$) are responsible for the degradation of the MO by oxidation under UV light, thus yielding H_2O and CO_2 molecules as well as $SO_4^=$ and NO_3^- stemming from the complete mineralization of MO.

Conclusion

TiO_2-DPA-PANI nanocomposites were prepared by in situ oxidative polymerization of aniline in the presence of a diazonium-modified TiO_2 particles. This strategy provided TiO_2-DPA-PANI nanocomposite photocatalysts that were tested in the degradation of methyl orange dye, taken as a model pollutant. A range of physico-chemical characterization tools permitted to confirm the diazonium modification of TiO_2 and more importantly to highlight the effect of such a surface modification on the loading and covalent attachment of PANI. XPS study brought strong supporting evidence for a core/shell structure (TiO_2-DPA being the core, and PANI the shell). The TiO_2-DPA-PANI nanocomposite exhibited excellent catalytic performances which depend on the amount of PANI on the surface of TiO_2 NPs. The results obtained so far underline the spectacular role of diphenylamine tetrafluoroborate diazonium salt in the coating of high quantity of PANI and in the stability of the formed nancomposite photocatalysts. The synergistic effect at the interface of the n-p (TiO_2-PANI) heterojunction

formed by this association leads to the separation of the elctron-hole pairs which is the origin of the improvement of the catalytic properties of TiO_2 NPs in the degradation of methyl orange. We have achieved high apparent kinetic constant (0.133 min^{-1}) attributed to the important loading of PANI on TiO_2-DPA. Another salient feature of the diazonium-pretreatment step lies in the thick coating of PANI that protects the underlying TiO_2 and thus permits to recycle the final TiO_2-DPA-PANI nanocomposite up to 5 times without any loss in the photocatalytic activity.

This paper brings strong supporting evidence for the vital role of diazonium salts in the making of new generation photocatalysts with remarkable performances that are tuned by the fine control over interfacial chemistry.

Acknowledgements
FM would like to thank Campus France for the provision of PROFAS B+ fellowship. All authors are indebted to NATO for financial support through the SfP program (CATALTEX project No 984842).

References

[1] R. P. Schwarzenbach, T. Egli, T. B. Hofstetter, U. v. Gunten, B. Wehrli, Global water pollution and human health, Annu. Rev. Environ. Resour. 35 (2010) 109–36.
[2] J. Im, F. E. Löffler, Fate of bisphenol a in terrestrial and aquatic environments, Environ. Sci. Technol., 50 (2016) 8403–8416.
[3] J. Kanagaraj, T. Senthilvelan, R. C. Panda, S. Kavitha, Eco-friendly waste management strategies for greener environment towards sustainable development in leather industry: a comprehensive review. J. Clean. Prod. 89 (2015) 1-17.
[4] P. A. Carneiro, G. A. Umbuzeiro, D. P. Oliveira, M. Valnice, B. Zanoni, Assessment of water contamination caused by a mutagenic textile effluent/dyehouse effluent bearing disperse dyes. J. Hazard. Mater. 174 (2010) 694–699.
[5] H. He, G.-j. Hu, C. Sun, S.-l. Chen, M.-n. Yang, J. Li, Y. Zhao, H. Wang, Trace analysis of persistent toxic substances in the main stream of Jiangsu section of the Yangtze River, China. Environ. Sci. Pollut. Res. 18 (2011) 638–648.
[6] A. Azizullah, M. N. K. Khattak, P. Richter, D.-P. Häder, Water pollution in Pakistan and its impact on public health — A review. Environ. Int. 37 (2011) 479–497.
[7] V. K. Gupta, Suhas, Application of low-cost adsorbents for dye removal – A review. J. Environ. Manage. 90 (2009) 2313–2342.
[8] **A.** Fujishima, T. N. Rao, D. A. Tryk, Titanium dioxide photocatalysis, Photochem. Photobiol. C 1 (2000) 1–21.
[9] A. L. Linsebigler, G. Q. Lu, J. T. Yates, Photocatalysis on TiO_2 surfaces-principles, mechanisms and selected results, Chem. Rev. 95 (1995) 735–758.
[10] A. Fujishima, X. Zhang, D. A. Tryk, TiO_2 photocatalysis and related surface phenomena, Surf. Sci. Rep. 63 (2008) 515–582.
[11] M. A. Henderson, A surface science perspective onTiO_2 photocatalysis, Surf. Sci. Rep.

66 (2011) 185–297.
[12] X. Z. Wang, Q. Q. Gao, H. T. Zhao, K. Feng, R.g. Guo, Synthesis of nano TiO_2/CTMAB-expanded perlite applied to the degradation of methyl orange, Appl. Mech. Mater. 110-116 (2012) 3801-3806.
[13] K. R. Reddy, M. Hassan, V. G. Gomes, Hybrid nanostructures based on titanium dioxide for enhanced photocatalysis, Appl. Catal. A: General. 489 (2015) 1-16.
[14] S. Mahshid, M. Askari, M. Sasani Ghamsari, Synthesis of TiO_2 nanoparticles by hydrolysis and peptization of titanium isopropoxide solution, Mater. Process. Technol. 189 (2007) 296-300.
[15] C. Burda, Y. Lou, X. Chen, A. C. S. Samia, J. Stout, J. L. Gole, Enhanced nitrogen doping in TiO_2 nanoparticles. Nano Lett. 3 (2003) 1049-1051.
[16] A. Su., B. Y. Hong, C. M. Tseng. Sol-gel preparation and photocatalysis of titanium dioxide, Catal. Today. 96 (2004) 119-126.
[17] A. Saleh, F. Abd Rasin, M. Ali Ameen, TiO_2 nanoparticles prepared by sol-gel, Mater. Sci. Eng. 3 (2009) 81-83.
[18] M. M. Byranvand, A. Nemati Kharat, L. Fatholahi, Z. M. Beiranvand. A Review on synthesis of nano-TiO_2 via different methods, J. Nanostruct. 3 (2013) 1-9.
[19] G. S. Mital, T. Manoj. A review of TiO_2 nanoparticles, Rev. Sci. Bull. 56 (2011) 1639–1657.
[20] A. E. Shalan, M. M. Rashad, Y. Yu, L. M. Cantu, M. S. A. A. Mottaleb, Controlling the microstructure and properties of titania nanopowders for high efficiency dye sensitized solar cells, Electrochim. Acta. 89 (2013) 469-478.
[21] W. Fumin, S. Zhansheng, G. Feng, A. Motonarib, Morphology control of anatase TiO_2 by surfactant-assisted hydrothermal method, Chem. Eng. 15 (2007) 754–759.
[22] H. Arami, M. Mazloumi, R. Khalifehzadeh, S.K. Sadrnezhaad, Sonochemical preparation of TiO_2 nanoparticles, Mat. Lett. 61 (2007) 4559–4561.
[23] F. A. Deorsola, D. Vallauri, Synthesis of TiO_2 nanoparticles through gel combustion process, J. Mater. Sci. 43 (2008) 3274–3278.
[24] T. Phonkhokkong, T. Thongtem, S. Thongtem, A. Phuruangrat, W. Promnopas, Synthesis and characterization of TiO_2 nanopowders for fabrication of dye sensitized solar cells, Digest J. Nanomater. Biostruct. 11 (2016) 81-90.
[25] W. Tan, J. Chen, X. Zhou, J. Zhang, Y. Lin, X. Li, X. Xiao, Preparation of nanocrystalline TiO_2 thin film at low temperature and its application in dye-sensitized solar cell, J. Solid. State. Electrochem. 13 (2009) 651-656.
[26] S. Riaz, A. Akbar, M. Imran, S. Naseem, Synthesis and characterization of TiO_2 nanoparticles, Adv. Nano, Biomechanics, Robotics Energy Res. 13 (2013) 353-360. http://www.i-asem.org/publication_conf/anbre13/M5A.8.MS541_1021F.pdf last accessed 30 August 2017.
[27] M. H. Bazargan , M. M. Byranvand , A. N. Kharat, Preparation and characterization of low temperature sintering nanocrystalline TiO_2 prepared via the sol gel method using titanium (IV) butoxide applicable to flexible dye sensitized solar cell, Int. J. Mat. Res. 103 (2012) 347-351.
[28] N. Griffete, F. Herbst, J. Pinson, S. Ammar, C. Mangeney. Preparation of water-soluble magnetic nanocrystals using aryl diazonium salt chemistry, J. Am. Chem. Soc 133 (2011) 1646-1649.
[29] A. Mesnage, M. A. Majied, P. Simon, N. H. Boime, P. Jégou, G. Deniau, S. Palacin. Grafting polymers to titania nanoparticles by radical polymerization initiated by diazonium salt, J. Mater. Sci. 46 (2011) 6332- 6338.
[30] S. Y. Lin, Y. T. Tsai, C. C. Chen, C. M. Lin, C.H. Chen, Two-step functionalization of

neutral and positively charged thiols onto citrate-stabilized au nanoparticles, J. Phys. Chem. B. 108 (2004) 2134-2139.
[31]. S. Yu, G. M. Chow. Carboxyl group (–CO2H) functionalized ferrimagnetic iron oxide nanoparticles for potential bio-applications, J. Mater. Chem. 14 (2004) 2781-2786.
[32] C. Yee, G. Kataby, A. Ulman, T. Prozorov, H. White, A. King, M. Rafailovich, J. Sokolov, A. Gedanken. Self-assembled monolayers of alkanesulfonic and phosphonic acids on amorphous iron oxide nanoparticles, Langmuir. 15 (1999) 7111-7115.
[**33**] J. Rockenberger, E. C. Scher, A. P. Alivisator. A new nonhydrolytic single-precursor approach to surfactant-capped nanocrystals of transition metal oxides, J. Am. Chem. Soc. 121 (1999) 11595-11596.

[34] A. A. Mohamed, Z. Salmi, S. A. Dahoumane, A. Mekki, B. Carbonnier, M. M. Chehimi, Functionalization of naomaterials with aryldiazonium salts, Adv. Colloid Interface Sci. 225 (2015)16-36.
[35] M. M.Chehimi, J. Pinson, Z. Salmi, Carbon nanotubes: surface modification and applications. In: J. Pinson, M. M. Chehimi (Eds.) Applied Surface Chemistry of Nanomaterials. Hauppauge (NY): Nova Science Publishers; 2013, Chap. 4, pp. 95-143.
[36] M. Radtke, A. Ignaszak, A surface grafting of carbon allotropes with in-situ generated 3-aryl diazonium chlorides: electrochemical kinetic studies, Electroanalysis 28 (2016) 2900–2909.
[37] S. Orefuwa, M. El Naggar, I. Shehadi, M. M. Chehimi, A. A. Mohamed, Modification of nanodiamonds with gold nanoparticles, J. Nanosci. Nanotechnol. 17 (2017) 4063-4068.
[38] D. Hetemi, J. Pinson, Surface functionalisation of polymers, Chem. Soc. Rev. 46 (2017) 5701-5713.
[39] S. A. Orefuwa, M. Ravanbakhsh, S. N. Neal, J. B. King, A. A. Mohamed, Robust organometallic gold nanoparticles, Organometallics 33 (2014) 439–442.
[40] M. Lo, A. K. D. Diaw, D. Gningue-Sall, J.-J. Aaron, M. A. Oturan, M. M. Chehimi, The role of diazonium interface chemistry in the design of high performance polypyrrole-coated flexible ITO sensing electrodes, Electrochem. Commun. 77 (2017) 14–18.
[41] C. M. Cao, Y. Zhang, C. Jiang, M. Qj, G. Z. Liu, Advances on aryldiazonium salt chemistry based interfacial fabrication for sensing applications, ACS Appl. Mater. Interfaces 9 (2017) 5031-5049.
[42] D. Quinton, A. Galtayries, F. Prima, S. Griveau, Functionalization of titanium surfaces with a simple electrochemical strategy, Surf. Coat. Technol. 206 (2012) 2302-2307.
[43] S. Palmas, A. Da Pozzo, M. Mascia, A. Vacca, P. C. Ricci, Sensitization of TiO_2 nanostructures with Coumarin 343, Chem. Eng. J. 211–212 (2012) 285–292.

[44] C. Combellas, F. Kanoufi, J. Pinson, F.I. Podvorica, Time-of-flight secondary ion mass spectroscopy characterization of the covalent bonding between a carbon surface and aryl groups, Langmuir. 21 (2005) 280–286.

[45] F. Brisset, J.Vieillard, B. Berton, S. Morin-Grognet, C. Duclairoir-Poc, F. Le Derf, Surface functionalization of cyclic olefin copolymer with aryldiazonium salts: A covalent grafting method. Appl. Surf. Sci. 329 (2015) 337-346.
[46] K. Boukerma, M. M. Chehimi, J. Pinson, C. Blomfield, X-ray photoelectron spectroscopy evidence for the covalent bond between an iron surface and aryl groups attached by the electrochemical reduction of diazonium salts, Langmuir 19 (2003) 6333-6335.

[47] A. Adenier, M. C. Bernard, M. M. Chehimi, E. Cabet-Deliry, B. Desbat, O. Fagebaume, J. Pinson, F. Podvorica, Covalent modification of iron surfaces by electrochemical reduction of aryldiazonium salts, J. Am. Chem. Soc. 123 (2001) 4541–4549.

[48] Y. Aït Atmane, L. Sicard, A. Lamouri, J. Pinson, M. Sicard, C. Masson, S. Nowak, P. Decorse, J.-Y. Piquemal, A. Galtayries, C. Mangeney. Functionalization of aluminum nanoparticles using a combination of aryl diazonium salt chemistry and iniferter method. J. Phys. Chem. C 117 (2013) 26000−26006.
[49] A. Mesnage, X. Lefèvre, P. Jégou, G. Deniau, S. Palacin, Spontaneous grafting of diazonium salts: chemical mechanism on metallic surfaces. Langmuir 28 (2012) 11767–11778.
[50] F. I. Podvorica, F. Kanoufi, J. Pinson, C. Combellas, Spontaneous grafting of diazoates on metals, Electrochim. Acta 54 (2009) 2164-2170.
[51] P. Actis, G. Caulliez, G. Shul, M. Opallo, M. Mermoux, B. Marcus, R. Boukherroub, S. Szunerits, Functionalization of glassy carbon with diazonium salts in ionic liquids, Langmuir. 24 (2008) 6327–6333.
[52] S. Mahouche-Chergui, S. Gam-Derouich, C. Mangeney, M. M. Chehimi, Aryl diazonium salts: a new class of coupling agents for bonding polymers, biomacromolecules and nanoparticles to surfaces. Chemical Society Reviews, 40 (2011) 4143-4166.
[53] L. M. Santos, J. Ghilane, C. Fave, P.-C. Lacaze, H. Randriamahazaka, L. M. Abrantes, J.-C. Lacroix, Electrografting polyaniline on carbon through the electroreduction of diazonium salts and the electrochemical polymerization of aniline. J. Phys. Chem. C. 112 (2008) 16103–16109.
[54] A. Mekki, S. Samanta, A. Singh, R. Mahmoud, M. M. Chehimi, D. K. Aswal, Core/shell protuberance-free multiwalled carbon nanotube/polyaniline nanocomposites via interfacial chemistry of aryl diazonium salts, J. Colloid Interface Sci. 418 (2014) 185-192.
[55] K. R. Reddy, K. P. Lee, A. I. Gopalan, Novel electrically conductive and ferromagnetic composites of poly (aniline-co-aminonaphthalenesulfonic acid) with iron oxide nanoparticles: Synthesis and characterization, J. appl. Polym Sci. 106(2) (2007) 1181-1191.
[56] K. R. Reddy, K. P. Lee, A. I. Gopalan, A. M. Showkat, Facile synthesis of hollow spheres of sulfonated polyanilines, Polym. J. 38(4) (2006) 349.
[57] K. R. Reddy, B. C. Sin, K. S. Ryu, J. C. Kim, H. Chung, Y. Lee, Conducting polymer functionalized multi-walled carbon nanotubes with noble metal nanoparticles: synthesis, morphological characteristics and electrical properties, Synth. Met. 159(7-8) (2009) 595-603.
[58] K. R. Reddy, K. P. Lee, Y. Lee, A. I. Gopalan, Facile synthesis of conducting polymer–metal hybrid nanocomposite by in situ chemical oxidative polymerization with negatively charged metal nanoparticles, Mater. Lett. 62(12-13) (2008) 1815-1818.
[59] K.R. Reddy, K. V. Karthik, S.B. Prasad, S.K. Soni, H.M. Jeong, A. V. Raghu, Enhanced photocatalytic activity of nanostructured titanium dioxide/polyaniline hybrid photocatalysts. Polyhedron, 120 (2016) 169-174.
[60] L. Juanbi, X. Qiushi, L. Liangchao, S. Junhai, H. Diqiong, Novel ternary composites: Preparation, performance and application of $ZnFe_2O_4/TiO_2$/polyaniline, Appl. Surf. Sci.331 (2015) 108–114.
[61] Y. Bessekhouad, D. Robert, J. V. Weber, Preparation of TiO_2 nanoparticles by Sol-Gel route. Int. J. Photoenergy. 5 (2003) 153-158. DOI: 10.1155/S1110662X03000278
[62] K. Jlassi, A. Mekki, M. Benna-Zayani, A. Singh, D. K. Aswal, M. M. Chehimi, Exfoliated clay/polyaniline nanocomposites through tandem diazonium cation exchange reactions and in situ oxidative polymerization of aniline. RSC Adv. 4 (2014) 65213-65222.
[63] R. Bangle, R. N. Sampaio, L. Troian-Gautier, G. J. Meyer, Surface Grafting of Ru (II) Diazonium-Based Sensitizers on Metal Oxides Enhances Alkaline Stability for Solar Energy Conversion. ACS applied materials & interfaces, 10(3) (2018) 3121-3132.

[64] K. Brymora, J. Fouineau, A. Eddarir, F. Chau, N. Yaacoub, J.M. Grenèche, F. Calvayrac,Grafting of diazonium salts on oxides surface: formation of aryl-O bonds on iron oxide nanoparticles. *J. Nanopart. Res*, *17*(11) (2015), 438.
[65] S. Mahshid, M. Askari, M. Sasani Ghamsari, Synthesis of TiO_2 nanoparticles by hydrolysis and peptization of titanium isopropoxide solution, J. Mater. Process. Technol. 189 (2007) 296-300.
[66] G. Oskam, A. Nellore, R. Lee Penn, P. C. Searson, The growth kinetics of TiO_2 nanoparticles from titanium (IV) alkoxide at high water/titanium ratio, Phys. Chem. B 107 (2003) 1734–1738.
[67] T. Barakat, Oxydation des composés organiques volatils en présence de catalyseurs Au et/ou Pd déposé sur TiO2 nanostructuré dopé. PhD Thesis, Université du Littoral Côte d'Opale, Dunkerque, France (in French), 2012. https://tel.archives-ouvertes.fr/tel-00916578/ last accessed 30 August 2017.
[68] W. Li, Y. Wang, H. Lin , S. Ismat Shah, C. P. Huang, D. J. Doren, Sergey A. Rykov, J. G. Chen and M. A. Barteau, Band gap tailoring of Nd^{3+} doped TiO_2 nanoparticles, Appl. Phys. Lett. 83 (2003) 4143-4145.
[69] C. Burda, Y. Lou, X. Chen, A. C. S. Samia, J Stout, J. L. Gole, Enhanced nitrogen doping in TiO_2 nanoparticles, Nano Lett. 8 (2003) 1049-1051.
[70] S. Valencia, J. M. Marín, G. Restrepo, Study of the bandgap of synthesized titanium dioxide nanoparticles using the sol-gel method and a hydrothermal treatment, Open Mater. Sci. J. 4 (2010) 9-14.
[71] J. Li, L. Zhu, Y. Wu, Y. Harima, A. Zhang, H. Tang, Hybrid composites of conductive polyaniline and nanocrystalline titanium oxide prepared via self-assembling and graft polymerization, Polym. 47 (2006) 7361-7367.
[72] M. Joselevich, F. J. Williams, Synthesis and characterization of diazonium functionalized nanoparticles for deposition on metal surfaces, Langmuir. 24 (2008) 11711-11717.
[73] L. Zhang, P. Liu, Z. Su, Preparation of PANI–TiO_2 nanocomposites and their solid-phase photocatalytic degradation, Polym. Degrad. Stab. 91(2006), 2213-2219.
[74] J. L. Bishop, C. M. Pieters, J. O. Edwards, Infrared spectroscopic analyses on the nature of water in montmorillonite, Clays Clay Miner. 42 (1994) 702-716.
[75] L.Yuzhen, Y. Yuan, W. Liangzhuan Wu, Z. Jinfang, Processable polyaniline/titania nanocomposites with good photocatalytic and conductivity properties prepared via peroxo-titanium complex catalyzed emulsion polymerization approach, Appl. Surf. Sci. 273 (2013) 135–143.
[76] S. Quillard, G. Louarn, S. Lefrant, A.G. MacDiarmid, Vibrational analysis of polyaniline: A comparative study of leucoemeraldine, emeraldine, and pernigraniline bases, Phys. Rev. B. 50 (1994) 12496-12508.
[77] C.J. Barbe, M.A. Harmer, G.W. Scherer, Sol–gel synthesis of potassium titanyl phosphate: solution chemistry and gelation, J. Sol-Gel Sci. Technol. 9 (1997) 183–199.
[78] A. Katoch, M. Burkhart, T. Hwang, S. S. Kim, Synthesis of polyaniline/TiO2 hybrid nanoplates via a sol-gel chemical method, J. Chem. Eng. 192 (2012) 262-268.
[79] Li, X., Wang, D., Cheng, G., Luo, Q., An, J., & Wang, Y. (2008). Preparation of polyaniline-modified TiO2 nanoparticles and their photocatalytic activity under visible light illumination. *Applied Catalysis B: Environmental*, *81*(3-4), 267-273.
[80] S. Wahyuni, E.S. Kunarti, R.T. Swasono, I. Kartini, Characterization and photocatalytic activity of TiO_2 (rod)-SiO_2-polyaniline nanocomposite. Indones. J. Chem. 18 (2018) 321-330.
[81] S. Masid, R. Tayade, N. N. Rao, Efficient visible light active polyaniline/TiO_2 nanocomposite photocatalyst for degradation of Reactive Blue 4, Int. J. Photocatal. Photon 119 (2015) 190-203.

[82] S. Min, F. Wang, Y. Han, An investigation on synthesis and photocatalytic activity of polyaniline sensitized nanocrystalline TiO2 composites. Journal of Material Science, 42 (2007) 9966-9972.
[83] S. N. Kumar, F. Gaillard, A. Sartre, High-resolution XPS studies of electrochemically synthesized conducting polyaniline films, Synth. Met. 36 (1990) 111-127.

[84] M.V. Kuznetsov, J.F. Zhuravlev, V.A. Gubanov, J. Electron Spectrosc. Relat. Phenom. 58, (1992) 169-176.
[85] Z. Salmi, S. Gam-Derouich, S. Mahouche-Chergui, M. Turmine, M. Chehimi, On the interfacial chemistry of aryl diazonium compounds in polymer science, Chem. Pap. 66 (2012) 369-391.

[86] K. Shimizu, K. Malmos, J. Hinke, S. U. Pedersen, K. Daasbjerg, M. Hinge, Durability of PEEK adhesive to stainless steel modified with aryldiazonium salts, Int. J. Adhes. Adhes. 51(2014) 1-12.

[87] B. Wessling , Polyaniline on the metallic side of the insulator-to-metal transition due to dispersion: the basis for successive nano-technology and industrial applications of organic metals, Synth. Met. 102 (1999) 1396-1399.

[88] S. Bilal. S. Gul**.** R. Holze, A.H. Ali Shah**,** An impressive emulsion polymerization route for the synthesis of highly soluble and conducting polyaniline salts**,** Synth. Met. 206 (2015) 131-144.
[89] N. Biçak, B. F. Şenkal, E.Sezer, Preparation of organo-soluble polyanilines in ionic liquid, Synth. Met. 155 (2005) 105-109.
[90] Y. Wang, H. Zheng, L. Jia, H. Li, T. Li, K. Chen, Y. Gu, J. Din, Optimizing the polymerization conditions of soluble polyaniline doped with itaconic acid, J. Macromol. Sci. A Pure Appl. Chem. 51 (2014) 577-581.

[91] K. Jlassi, S. Chandran, M. A Poothanari, M. B. Zayani, S. Thomas, M. M. Chehimi, Clay/polyaniline hybrid through diazonium chemistry: conductive nanofiller with unusual effects on interfacial properties of epoxy nanocomposites, Langmuir. 32 (2016) 3514–3524.
[92] A. Al-Ghamdi, Z. Y. Al-Saigh, A surface and thermodynamic characterization of conducting polymers by inverse gas chromatography: I. Polyaniline, J. Chromatogr. A 969 (2002) 229-243.
[93] Y. R. Smith, A. Kar, V. Subramanian, Investigation of physicochemical parameters that influence photocatalytic degradation of methyl orange over TiO_2 nanotubes, Indus & Eng. Chem. Res. 48(23) (2009) 10268-10276.
[94] P. Niu, Photocatalytic Degradation of methyl orange in Aqueous TiO_2 suspensions, Asian. J. Chem. 25 (2013) 1103-1106.
[95] Z. Wang, L. Shen, S. Zhu, Synthesis of core-shell@ microspheres and their application as recyclable photocatalysts, Int. J. Photoenergy. (2012) Article ID 202519, 6 page, DOI: 10.1155/2012/202519.
[96] L. C. Chen, F. R. Tsai, C. M. Huang, Photocatalytic decolorization of methyl orange in aqueous medium of TiO_2 and Ag–TiO_2 immobilized on γ-Al_2O_3, J. Photochem. Photobiol A: Chem. 170 (2005) 7-14.
[97] T. A. Saleh, V. K.Gupta, Photo-catalyzed degradation of hazardous dye methyl orange by use of a composite catalyst consisting of multi-walled carbon nanotubes and titanium dioxide, J. Colloid Interface Sci. 371 (2012) 101-106.
[98] M.A. Salem, A.F. Al-Ghonemiy, A.B. Zaki, Photocatalytic degradation of allura red and quinoline yellow with Polyaniline/TiO_2 nanocomposite, Appl. Catal. B. Environ. 91 (2009) 59–66.

[99] K. R. Reddy, K. Nakata, T. Ochiai, T. Murakami, D. A. Tryk, A. Fujishima, Facile fabrication and photocatalytic application of Ag nanoparticles-TiO_2 nanofiber composites, J. Nanosci. Nanotechnol. 11 (2011) 3692–3695.
[100] N. Barka, A. Assabbane, A. Nounah, A. Albourine, Y. Ait-Ichou, Degradation photocatalytique de deux colorants séparés et en mélange binaire par TiO_2-supporté, Sci. Technol. 27B (2008) 09-16. http://revue.umc.edu.dz/index.php/a/article/view/126 last accessed 30 August 2017.
[101] D. N. Huyen, N. T.Tung, N. D. Thien, L. H. Thanh, Effect of TiO_2 on the gas sensing features of TiO_2/PANi, Sensors 11 (2011) 1924–1931.
[102] N. Guettai, H.A. Amar, Photocatalytic oxidation of methyl orange in presence of titanium dioxide in aqueous suspension. Part I: Parametric study. Desalination, 185(1-3) (2005) 427-437.
[103] N. Guo, Y. Liang, S. Lan, L. Liu, J. Zhang, G. Ji, S. Gan, Microscale hierarchical three-dimensional flowerlike TiO_2/pani composite: synthesis, characterization, and its remarkable photocatalytic activity on organic dyes under uv-light and sunlight irradiation, J. Phys. Chem. C. *118* (32) (2014) 18343–18355.
[104] Y. Lin, D. Li, J. Hu, G. Xiao, J. Wang, W. Li, X. Fu, highly efficient photocatalytic degradation of organic pollutants by PANI-modified TiO_2 composite, J. Phys. Chem. C, 116 (9) (2012) 5764–5772.
[105] A. Olad, S. Behboudi and A. A. Entezami, Preparation, characterization and photocatalytic activity of TiO_2/polyaniline core–shell nanocomposite, Bull. Mater. Sci. 35(5) (2012) 801–809.
[106] G. K. Parshetti, A. A. Telki, D. C. Kalyani, S. P. Govindwar, Decolorization and detoxification of sulfonated azo dye methyl orange by kocuria rosea MTCC 1532, J. Hazard. Mater. 176 (2010) 503-509.
[107] Y. Liu, D. Sun, Development of Fe_2O_3-CeO_2-TiO_2/γ-Al_2O_3 as catalyst for catalytic wet air oxidation of methyl orange azo dye under room condition, Appl. Catal. B Environ. 72 (2007) 205-211.
[108] M. S. Babushkina, L. P. Nikitina, A. G. Goncharov, N. I. Ponomareva, Water in the structure of minerals from mantle peridotites as controlled bythermal and redox conditions in the upper mantle, Geol. Ore Deposits 51 (2009) 712–722.
[109] E. Garand, T. Wende, D. J. Goebbert, R. Bergmann, G. Meijer, D. M. Neumark, K. R. Asmis, Infrared spectroscopy of hydrated bicarbonate anion clusters: $HCO_3^-(H_2O)_{1-10}$. J. Am. Chem. Soc. 132 (2010) 849–856.
[110] C. Qi, H. Qinqin, L. Mengmeng, L. Xueting , W. Jin, L. Jianping, The vital role of PANI for the enhanced photocatalytic activity of magnetically recyclable N–$K_2Ti_4O_9$/$MnFe_2O_4$/ PANI composites, Appl. Surf. Sci. 311 (2014) 230–238.
[111] C. Baiocchi, M.C. Brussino, E. Pramauro, Characterization of methyl orange and its photocatalytic degradation products by HPLC/UV–VIS diode array and atmospheric pressure ionization quadrupole ion trap mass spectrometry. Int. J. Mass Spectrom. 214 (2002) 247-256.
[112] K.H. Hu, X.G. Hu, Y.F. Xu, Synthesis of nano-MoS_2/TiO_2 composite and its catalytic degradation effect on methyl orange, J. Mater. Sci. 45 (2010) 2640-2648 .
[113] K. Raghava Reddy, K. Nakata, T. Ochiai, T. Murakami, D. A. Tryk, A. Fujishima, Nanofibrous TiO_2-core/conjugated polymer-sheath composites: synthesis, structural properties and photocatalytic activity, J. Nanosci. Nanotechnol. 10 (2010) 7951–7957.
[114] L. Wenjuan, L. Danzhen, L. Yangming, W. Peixian, C. Wei, F. Xianzhi,S. Yu. Evidence or the active species involved in the photodegradation process of methyl orange on TiO_2, J. Phys. Chem. C 116 (2012) 3552-3560.

SUPPLEMENTARY MATERIAL

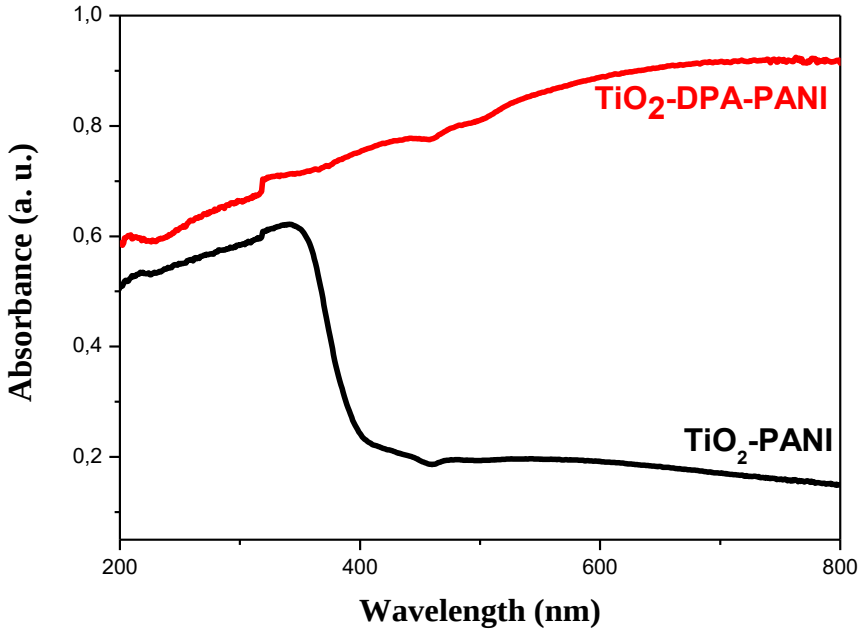

Supplementary Material SM1. UV-vis spectra of TiO_2-PANI and TiO_2-DPA-PANI nanocomposites.

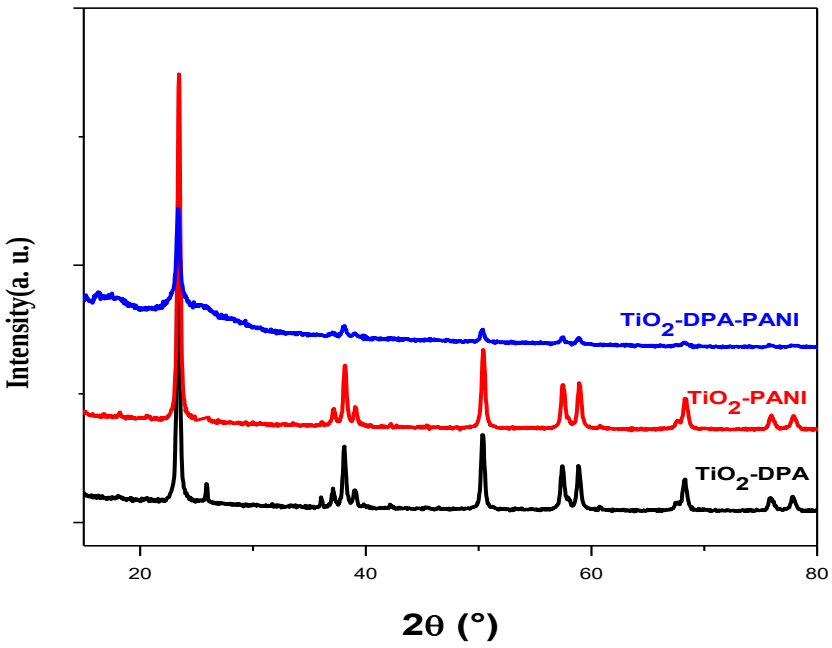

Supplementary Material SM2. XRD patterns of TiO_2-DPA, TiO_2-PANI and TiO_2-DPA-PANI nanocomposites.

Chapter 3: Polyaniline-grafted RuO_2-TiO_2 heterostructure for the catalyzed degradation of organic pollutants in darkness

Cover story

The cover illustrates a metal–semiconductor/polyaniline nanocomposite with spectacular catalytic properties. The nanocomposites catalyze the decomposition of methyl orange (MO) in darkness. Indeed, the RuO_2–TiO_2 mixed oxide is an excellent photocatalyst under visible light, while the nanocomposite RuO_2–TiO_2/aryl/polyaniline exhibits unique, fast catalytic performance in the dark. Total discoloration of MO was noted without any spectral evidence for organic products, thus suggesting complete mineralization of the dye. This activity does not only depend on the components that constitute these materials but also on the subtle interface chemical composition which is driven by diazonium modification of RuO_2–TiO_2

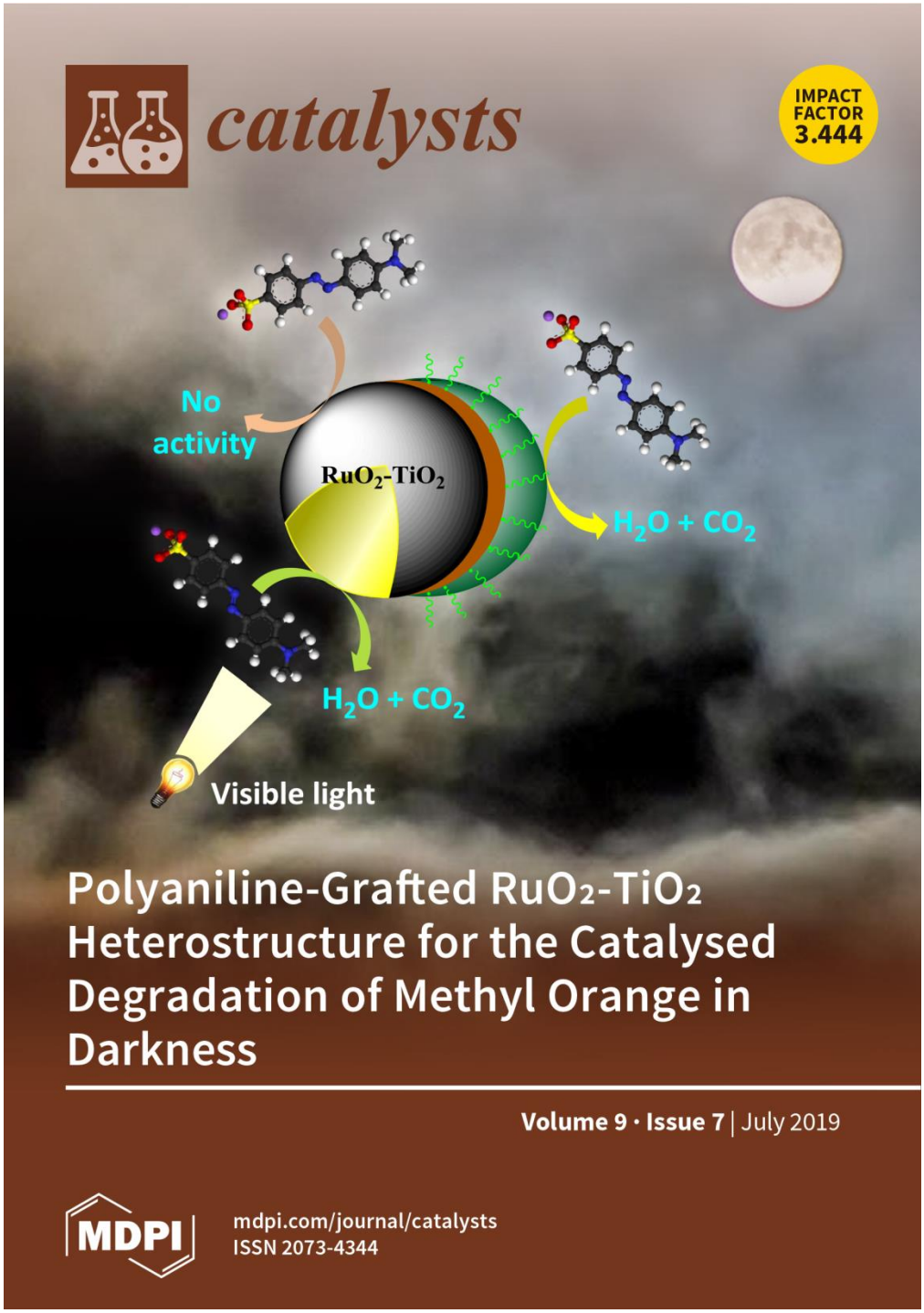

Polyaniline-grafted RuO_2-TiO_2 heterostructure for the catalysed degradation of organic pollutants in darkness

Fatima Mousli, Ahcène Chaouchi, Mohamed Jouini, François Maurel,
Abdelaziz Kadri, Mohamed M. Chehimi

Refernce

F. Mousli, A. Chaouchi, M. Jouini, F. Maurel, A. Kadri, M. M. Chehimi, M. M. Polyaniline-Grafted RuO_2-TiO_2 heterostructure for the catalysed degradation of methyl orange in darkness. *Catalysts 9 (7) (2019) 578.*

Graphical abstract

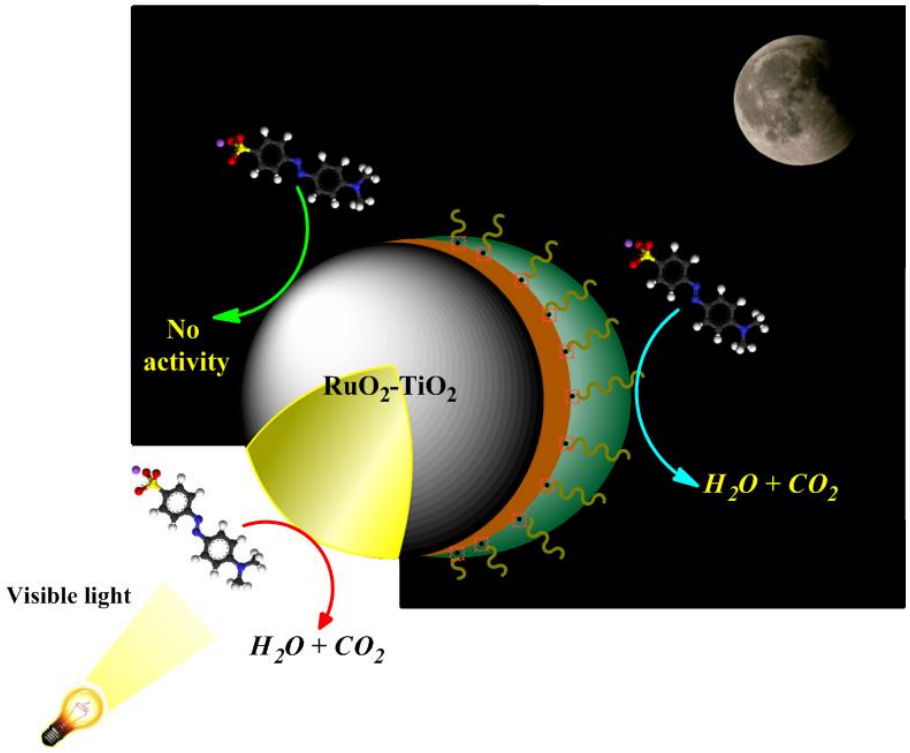

Aim of the paper

This paper aims at investigating the advantage of doping TiO_2 nanoparticles with RuO_2 metal and the effect of this heterojunction metal-semi-conductor (n) on catalytic processes. It also interrogates the role of diazonium salt in the design of nanocomposites of conductive polymer and RuO_2-TiO_2 mixed oxide for the fast catalyzed degradation of pollutants.

Method

The initial experimental approach consists of the synthesis of the isolated diazonium salt 4-diphenylamine tetrafluoroborate (DPA) by chemical route. The salt was to modify the surface of RuO_2-TiO_2 mixed oxide prepared via sol-gel. The second step is devoted to the development of nanocomposites of RuO_2-TiO_2/DPA/Polyaniline and RuO_2-TiO_2-Polyaniline form by in situ oxidative polymerization of the aniline monomer in the presence of functionalized and non-functionalized oxide nanoparticles. The reactivity of the products thus obtained was tested in the methyl orange decomposition reaction in darkness and under visible light.

Results

Through this study, we have demonstrated that the association combining metal-semiconductor n heterostructure and conductive polymer offers spectacular properties to the final materials. The nanocomposites are very reactive in the decomposition of methyl orange dye in darkness; this activity depends on the presence of PANI on the one hand, and its amount in the final nanocomposite, on the other hand. The doping of TiO_2 with RuO_2 metal has improved significantly the catalytic performances of TiO_2 and shifted its photoactivity zone towards the visible range.

Significance

This study underline the spectacular role of diphenylamine tetrafluoroborate diazonium salt in the coating of high quantity of PANI with a strong adhesion to the surface of the mixed oxide nanoparticles, which gives the final nanocomposite a better thermal and chemical stability and especially a better catalytic activity even in darkness.

Polyaniline-grafted RuO_2-TiO_2 heterostructure for the catalysed degradation of organic pollutants in darkness

Fatima Mousli[1,2,3]*, Ahcène Chaouchi[4], Mohamed Jouini[2], François Maurel[2], Abdelaziz Kadri[1], Mohamed M. Chehimi[3,]*

[1] Laboratoire de Physique et Chimie des Matériaux (LPCM), Faculté des Sciences, Université Mouloud Mammeri, Tizi-Ouzou 15000, Algeria.
[2] Sorbonne Paris Cité, Université Paris Diderot, CNRS, ITODYS (UMR 7086), 75013 Paris, France
[3] Université Paris Est, CNRS, ICMPE (UMR 7182), 94320 Thiais, France
[4] Laboratoire de Chimie Appliquée et Génie Chimique, Université Mouloud Mammeri, Tizi-Ouzou 15000, Algeria

Abstract

This work describes the design of novel metal/semi-conductor/polymer nanocomposite for catalyzed degradation and mineralization of model organic dye pollutants in darkness.
RuO_2-TiO_2 nanoparticles (NPs) were modified with diphenyl-amino (DPA) groups from 4-diphenylamine diazonium salt precursor, reduced with ascorbic acid to provide radicals that modified the NPs and further served for in situ synthesis of polyaniline (PANI) that resulted in RuO_2/TiO_2-DPA-PANI nanocomposite. Excellent adhesion of PANI to RuO_2/TiO_2-DPA was noted but not in the case of pristine RuO_2-TiO_2. This stresses the central role of diazonium compounds to tether PANI to the underlying heterostructure.
RuO_2-TiO_2/DPA/PANI revealed superior catalytic properties in the degradation of Methyl Orange compared to RuO_2-TiO_2/PANI and RuO_2-TiO_2. Interestingly, it is active even in darkness due to high PANI mass loading. In addition, PANI constitutes a protective layer of RuO_2-TiO_2 NPs that permitted to reuse RuO_2-TiO_2/DPA/PANI 9 times whereas RuO_2-TiO_2/PANI and RuO_2-TiO_2 were reused 7 and 5 times, respectively. The electronic displacements at the interface metal/semi-conductor heterojunction under visible light and the synergistic effects between PANI and RuO_2 result in the separation of electron-hole pairs and the reduction of its recombination rate as well as a significant catalytic activity of RuO_2-TiO_2 and RuO_2-TiO_2/DPA/PANI under simulated sunlight and in darkness, respectively.

Keywords:
RuO_2-TiO_2, diazonium salt, polyaniline, nanocomposite, catalysis, darkness.

Corresponding authors
F. Mousli : fatima.mousli@yahoo.fr ; M. M. Chehimi : chehimi@icmpe.cnrs.fr

I. Introduction

The development of photocatalytic materials that are active both under visible light and in the dark constitute the subject of numerous studies targeted for environmental applications [1]. Since the last decade, titanium dioxide (TiO_2) has attracted much attention due to its great potential applications and its physico-chemical and catalytic properties [2,3,4]. It is a multifunctional semiconductor and one of the most promising materials for heterogeneous photocatalysis under UV irradiation. However, the use of TiO_2 is limited due to high recombination rate of photoinduced electron-hole pairs produced during photocatalytic processes, few surface active sites, light harvesting ability and the negligible absorbance of visible light [5,6,7]. In this challenging context, efforts have been focused on the development of new materials with a lower electron-hole pair recombination rate and a strong absorption of sunlight. This involves combining the TiO_2 with another material that has a narrow band gap [8]. As a result, several TiO_2-based heterostructures have been designed in different forms such as: semiconductor n/semiconductor n: TiO_2-SnO_2 [9], TiO_2-WO_3 [10], TiO_2-ZnO [11], SiO_2-TiO_2 [12] semiconductor n/semiconductor p: TiO_2-Fe_2O_3 [13], TiO_2-Cu_2O [14], TiO_2-NiO [15] and noble metal/semiconductor n: Au-TiO_2 [16], Ag-TiO_2 [17], Pt-TiO_2 [18] Particularly, the metal/semiconductor n combination is widely investigated in various applications; the noble metals impart to the heterostructure a good electrocatalytic performance and super capacitive properties [19,20]. Among the numerous materials that could be combined with TiO_2 and serve to improve its catalytic performances, RuO_2 has raised much interest owing to its chemical and high thermal stability, low resistivity, high resistance to chemical corrosion, and its excellent diffusion properties make it an interesting material in numerous applications [21,22]. RuO_2 and TiO_2 have the same tetravalent cations; the different electron configurations between Ti and Ru create different physico-chemical properties in the oxides. TiO_2 is n-type semiconductor while RuO_2 has electrical conductive metallic character [23] due to its partially filled metal (d)-oxygen (p) π^* band [24]. The combination between RuO_2 and TiO_2 or metal/semiconductor generally leads to the formation of the Schottky barrier which results in the improvement of the catalytic performances of the heterostructure, due to the difference in Fermi levels of the two materials [25]. Actually, the conductivity of TiO_2 increases owing to the presence of RuO_2 which favors the electronic exchange at the interface and thus increases the kinetics of the reactions in which it is involved [6]. It is noteworthy that a small percentage of RuO_2 relative to that of TiO_2 in the RuO_2-TiO_2 heterostructure (*e.g.* 10%) is sufficient to impart high conductivity, chemical and thermal stability and more importantly greater

catalytic activity. This is an important economical aspect given the cost of ruthenium-based compounds. Due to these salient features, the conducting RuO_2-TiO_2 heterostructure is explored in the development of supercapacitors [21], electrode for chlorine electrogeneration [26] as well as pigments, fillers, electro-resistor films for electrodes, or dielectric device catalyst supports [27,28].

So far, and despite the above-mentioned interest of RuO_2-TiO_2 mixed oxide NPs, very few studies have been undertaken to evaluate their photocatalytic properties [6,21,22,29]. The catalytic activity of this heterostructure is related to the size of the particles, their morphology, and the specific surface area, which are dependent on the mode and the conditions of synthesis.

Several methods have been reported on the synthesis of RuO_2-TiO_2 in different forms. For example, Houšková et *al.*[30] prepared TiO_2 particles doped with RuO_2 by hydrolysis process for gas phase photodecomposition of acetone. Amama et *al.* [31] prepared this mixed oxide by impregnation for the photo-oxidation of trichloroethylene in aqueous medium. The majority of the research works are based on the synthesis of RuO_2-TiO_2 powders or films on plates of Ti or on other substrates by the sol gel route [21,25,32]. According to Panic et *al.* [33,34], anodes prepared by sol gel route have a considerably longer life service than those prepared by thermal decomposition. In addition, it is the most efficient approach for preparing nanoscale materials with a large specific surface area and important catalytic activity.

To enhance the electrical conductivity, the stability of (photo)catalysts and their photocatalytic efficiency, researches were directed towards the design of TiO_2-based polymer nanocomposites. However, there are no reports on RuO_2-TiO_2/polymer nanocomposite catalysts although TiO_2/polypyrrole [35] and TiO_2/polyaniline [36,37] were demonstrated to be efficient composite catalysts owing to the high absorption coefficient and a high mobility of charge carriers of TiO_2. These characteristics make it possible to improve the charge separation and therefore the catalytic performance of TiO_2-based catalytic materials [38]. There is thus room for investigating the design and catalytic properties of RuO_2-TiO_2/polymer nanocomposites. Indeed, recently we have revisited the design of TiO_2/polyaniline composite photocatalysts [39] by considering the mass loading of polyaniline (PANI) and its effect on the photocatalyst efficiency. To address this point, we have modified the underlying TiO_2 NPs with aryl diazonium salts and found not only much larger loading of PANI but also we have achieved remarkable recovery of the composite photocatalyst. Actually, diazonium salts emerged as versatile and efficient coupling or surface modifier agents of practically all types of materials (metals, semi-conductors, polymers, ceramics…) [40]. Their use for surface

functionalization is particularly interesting and easily applicable to nanomaterials [41] such as electrocatalysts [42] and photocatalysts [39]. In addition and of relevance to this work, diazonium compounds act as unique coupling agents for polymers to surfaces [43,44]. Despite the remarkable performances achieved by grafting PANI to diphenylamine (DPA)-modified TiO_2, the final composite TiO_2-DPA-PANI was active under UV light only for the photocatalyzed degradation of Methyl Orange.

Returning to RuO_2-TiO_2 mixed oxide and its photocatalytic activity in the visible light, we reasoned that DPA modification would result in excellent adhesion of PANI and superior photoactivity under visible light conditions. In routine photocatalysis testing, all photocatalysts are actually incubated in the dark with the test solution of the model molecule to be degraded prior to exposure to UV or visible light. Surprisingly, RuO_2-TiO_2 mixed oxide NPs coated with PANI through a DPA aryl layer (hereafter, RuO_2-TiO_2/DPA/PANI), were found to completely degrade MO. This unpredicted result and thus good example of serendipity led us to conduct a thorough study on the catalytic properties of RuO_2-TiO_2/DPA/PANI under dark and to compare the catalytic properties to those of bare RuO_2-TiO_2 mixed oxide and RuO_2-TiO_2/PANI.

In this work, RuO_2-TiO_2 mixed oxide NPs were prepared and modified with aryl diazonium compounds from the diphenylamine precursor and subsequently grafted with in situ prepared polyaniline. The final nanocomposite, denoted RuO_2-TiO_2/DPA/PANI, was evaluated as a nanocatalyst of the degradation of Methyl Orange taken as a model organic pollutant. To highlight the role of both the diazonium modification step and the importance of polyaniline in the performances of the nanocomposite catalyst, the following reference compounds were also prepared and tested: pristine RuO_2-TiO_2 and RuO_2-TiO_2/PANI nanoparticles. The RuO_2-TiO_2/DPA/PANI nanocomposite and related materials were thoroughly characterized by infrared and Raman spectroscopy, SEM/EDS, UV-Vis, XRD, TGA and XPS. The photocatalytic performances were investigated under dark and under simulated sunlight. The extent of residual Methyl Orange after catalyzed reaction was determined by UV-vis spectroscopy.

Whilst much has been said about TiO_2 and TiO_2-based mixed oxide photocatalysts, to the very best of our knowledge:

(i) no work has been undertaken on the combination of RuO_2-TiO_2 mixed oxide with conductive polymers,

(ii) no strategy has been reported so far to take advantage of the synergetic effects of surface functionalization of RuO_2-TiO_2 using diazonium salts and post grafting with conductive polymers in view of making a new generation of (photo)catalysts.

By bridging the best of two worlds: *ca* visible light active RuO_2-TiO_2 photocatalysts, and diazonium coupling agents for the attachment of conductive polymers able of charge transfer, we do provide unique heterostructure with catalytic activity under darkness. This is what has motivated this in-depth study.

2 Experimental

2.1 Chemicals

The following chemicals were used as received: $RuCl_3.xH_2O$ (Sigma-Aldrich 98%), TiO_2 anatase nanoparticles (prepared by sol-gel [39]), H_2O_2 (14%), ethanol (99.9%), N-phenyl-p-phenylenediamine (Alfa Aesar, 98% purity), HBF_4 (48%), ascorbic acid, sodium nitrite (Alfa Aesar, purity 99%), ammonium persulfate (APS, Aldrich, 98% purity), nitric acid (Carlo Erba, 60% purity), aniline (Aldrich, 99.5% pure), Methyl Orange (Sigma-Aldrich) and the solvents that are Aldrich products: dimethylformamide (DMF), N-methyl-2-pyrrolidone (NMP), tetrahydrofuran (THF), hexafluoropropan-2-ol (HFIP), dimethyl sulfoxide (DMSO), chloroform, 1,2-dichloroethane, xylene and toluene. All aqueous solutions were prepared using deionized water.

2.2. Methods

2.2.1. Preparation of RuO_2-TiO_2 powders

RuO_2-TiO_2 nanoparticles were prepared by sol gel route and reflux process. 5g (62.6 mmol) of TiO_2 nanoparticles prepared in the first stage [39], were dissolved in a mixture of 0.3g (1.34 mmol) of $RuCl_3.xH_2O$, 20 mL of hydrogen peroxide (14%) and 10 mL of ethanol. A black colloidal suspension is obtained; this solution is heated under ultrasound operating at a frequency of 50 kHz for 2 hours at 60°C in order to disaggregate the particles. After this period of time, 40 mL of distilled water are added drop wise to the solution. The suspension was stirred magnetically and refluxed for 20 hours at 60°C. The resulting gel was dried at 100°C for 24 hours and calcined at 500°C for 90 min in order to complete the conversion of $RuCl_3$ to RuO_2

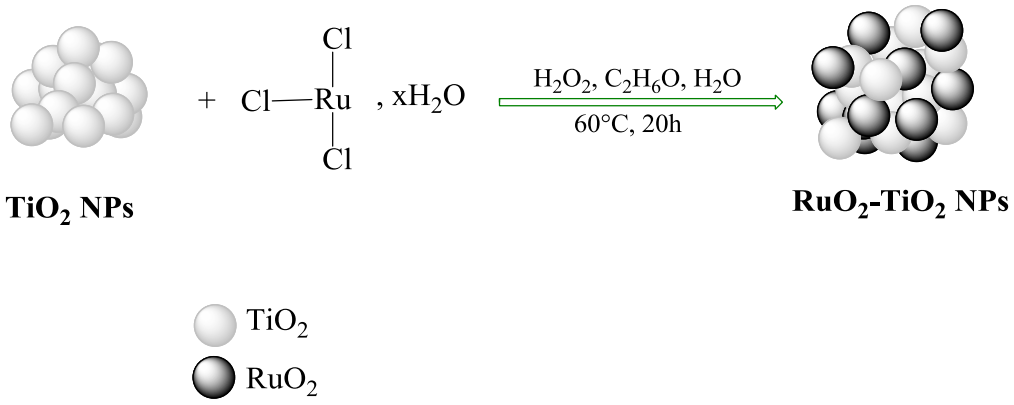

Scheme 1. Synthetic route for the preparation of RuO_2-TiO_2 nanoparticles.

2.2.2. Synthesis of 4-diphenylamine diazonium tetrafluoroborate

The synthesis of 4-diphenylamine diazonium tetrafluoroborate carried out according to our previous work [39]. Typically, 0.45 g (2.44 mmol) of N-phenylendiamine was introduced into 5 mL of HBF_4 (aqueous solution 48%), stirred at 0°C for 15 min. Then 0.45g (6.52 mmol of sodium nitrite was appended to the solution under continuous stirring for 60 min; after that, 60 mL of CH_2Cl_2 was added to the mixture in order to separate the phases by crystallization. The filtered precipitate is rinsed with ice-cold ether and then dried and kept at low temperature.

2.2.3. Preparation of RuO_2-TiO_2/PANI, RuO_2-TiO_2/DPA/PANI nanocomposites

The functionalization of RuO_2-TiO_2 mixed oxide nanoparticles as well as the polymerization of PANI on the surface of RuO_2-TiO_2 NPs and RuO_2-TiO_2/DPA were carried out according to the conditions reported in ref. [39].

We reported three chemical methods of grafting of 4-diphenylamine diazonium tetrafluoroborate on the surface of TiO_2 nanoparticles. These methods are based on the functionalization of the nanoparticles by in situ generation of aryl diazonium salt, grafting of isolated aryl diazonium and the grafting of isolated diazonium salt in basic medium (diazoate). However, grafting with isolated diazonium salts appears to be the most effective method for modifying TiO_2 nanoparticles. Therefore, it was chosen to modify the nanoparticles of RuO_2-TiO_2 mixed oxide according to the same protocol adopted for the modification of TiO_2 nanoparticles.

The strategy used for the preparation of the RuO_2-TiO_2/DPA/PANI nanocomposite is based on two different protocols. The first pathway consists in grafting of the isolated aryl 2

diazonium molecule previously obtained on the RuO_2-TiO_2 mixed oxide surface: 30 mg of RuO_2-TiO_2 NPs (0.14 mmol) was dispersed in 2 mL of water and sonicated for 20 minutes, then an aqueous solution of diazonium salt (0.28g, 1.04 mmol in 5 mL of H_2O) was poured drop wise with stirring at 0 °C for 15 min, after which, the reducing agent (ascorbic acid 0.4g, 2.27 mmol in 3 mL of H_2O) was added drop wise. The reaction mixture was further stirred for 90 min. The modified nanoparticles was centrifugally separated and washed several time with ethanol then with water, and then dried at room temperature overnight. The second is based on the chemical polymerization of the aniline monomer on the surface of RuO_2-TiO_2 nanoparticles already functionalized with 4-diphenylamine tetrafluoroborate diazonium salt. 0.3 g, (3.23 mmol) of aniline monomer was mixed with nitric acid (0.1g, 1.51 mmol) and stirred for 60 min to form the anilinium cation; to this solution, there was added a suspension of RuO_2-TiO_2/DPA (30 mg, 0.062 mmol) dispersed in 20 mL of acetonitrile ultrasontricated for 10 min, cooled and stirred in ice bath for 120min. After this time, the initiator (0.4g, 1.75 mmol APS in 5 mL of H_2O) was added dropwise to the above mixture. The reaction was followed by vigorous stirring for 3h. The resulting precipitate was collected with centrifugation and washed several times with methanol and di-ionized water to remove any un-reacted species then dried at room temperature for 24h. The in situ oxidative polymerization of aniline on the surface of RuO_2-TiO_2 was performed following the same approach using the non-functionalized RuO_2-TiO_2 mixed oxide nanoparticles.

2.2.4. Catalytic and photocatalytic activity

The catalytic and photocatalytic activity of the various elaborated nanocatalysts were examined by the decomposition of Methyl Orange (MO) in the dark and under visible light. In a typical experiment, to prepared aqueous solutions of Methyl Orange (50 mg/l) catalysts (RuO_2-TiO_2 or RuO_2-TiO_2/PANI or RuO_2-TiO_2/DPA/PANI) were added (10 mg in 50 mL of MO solution, pH=5.5). The degradation of Methyl Orange was also carried out without catalyst under irradiation in order to observe the effect of visible light on the degradation of the MO. A first sample was taken at the end of the absorption period, without light and just before the light was turned on, and analyzed by UV-Vis to determine the non-adsorbed dye concentration in solution. UV light was provided by UVA CUBE 400 (Honle UV technology) and the tests were carried out at room temperature.

2.3. Characterization and instrumentation

The different phases constituting the RuO_2-TiO_2 NPs, RuO_2-TiO_2/DPA and RuO_2-TiO_2/PANI nanocomposites prepared have been identified using a diffractometer (BRUKER AXS D8 ADVANCE, CuKα radiation λ=1.5418 A°). Surface morphology, distribution of particles and the composition of the samples were checked with a Merlin Carl Zeiss apparatus fitted with energy dispersive X-ray (EDS) analyzer. UV-vis absorbance spectra of the catalysts and MO solution after degradation were measured at room temperature in the wavelength range of 200-800 nm using EVOLUTION 220 UV-Visible spectrometer.

Raman was recorded with Horiba Lab RAM HR Evolution operating at 638 nm at room temperature. Infrared transmittance spectra were assigned using a BRUKER spectrometer operating in ATR mode ranging from 4000 to 400 cm^{-1}.

Thermogravimetric analysis (TGA) was performed on a Setaram instrument Setsys Evolution 16 thermobalance by heating the samples at a rate of 10°C.min^{-1} from 10 to 800 °C under a flow of air at 20 mL.min^{-1}. X-ray photoelectron spectroscopy analysis (XPS) was performed using K Alpha system (Thermo Fisher Scientific, monochromated Al X-ray source hυ= 1486.6 eV; spot size = 400 μm). A flood was used for charge compensation and the composition was determined using manufacturer's sensitivity factors.

Other analyzes were performed for RuO_2-TiO_2 mixed oxide only:

The zeta potential measurement was performed to predict the emulsion stability using a zetasizer nano (Malvern Man0485-1.1) that measures the electrophoretic migrations. The measurement was carried out with a suspension consisting of RuO_2-TiO_2 (1 g/l) introduced in 10^{-2} NaCl solution and conducted at different pH of solution adjusted with NaOH and HCl for alkaline and acidic medium respectively. Each measurement is made three times and the size distribution is the average of the three measurements for the consecrated sample.

In order to determine the resistivity of the heterostructure RuO_2-TiO_2 at room temperature, Four Point Resistivity measurement was carried out using KEITHLEY 2601 B source mater by imposing a current of 0.1 mA. The dielectric properties of RuO_2-TiO_2 mixed oxide are also studied by electrical impedance spectroscopy using an impedancemeter HP 4284A. A pellet of RuO_2-TiO_2 is metalized by a very thin layer of silver paste on both sides to ensure contact with the electrodes of the measuring apparatus. The impedance measurements were carried out in the frequency ranging from 100 Hz to 1 MHz and several temperatures under low excitation (1V).

3. Results and discussion

3.1. General strategy of designing RuO_2-TiO_2/PANI nanocomposites

RuO_2-TiO_2/PANI nanocomposites were prepared in four steps: (i) sol-gel synthesis of TiO_2 followed by (ii) RuO_2 doping (via sol-gel method), then the mixed oxide was (iii) grafted with DPA aryl nano-layer from diazonium precursor; (iv) the RuO_2-TiO_2/DPA served as substrates for the in situ synthesis of PANI. It is to note that the sol-gel route for the mixed oxide was selected due to its simplicity and the preparation of the catalyst in high yield.

Figure 1 schematically displays the general pathway of making RuO_2-TiO_2/PANI nanocomposites (Fig. 1A, upper panel) and digital photographs of the different materials prepared (Fig. 1B, lower panel). First, the nanoparticles of RuO_2-TiO_2 mixed oxide were functionalized with isolated 4-diphenylamine diazonium tetrafluoroborate at 0°C in the presence of the diazonium reducing agent vitamin C. The DPA layer formed on the surface of RuO_2-TiO_2 NPS acts as surface-attached initiator for the in situ oxidative polymerization of aniline. It was necessary to prepare the RuO_2-TiO_2/PANI nanocomposite by polymerizing the aniline monomer under the same conditions on the surface of the pristine mixed oxide NPs in order to account for the role of DPA as a coupling agent.

Figure 1B shows digital photographs of the main simples pristine (Ba) and modified (Bb, Bc, Bd). The functionalization of RuO_2-TiO_2 mixed oxide nanopowders with diazonium salt is manifested by a change in color from dark gray to pale green (Fig. 2Bb). A slight, even negligible change in color has been observed for RuO_2-TiO_2/PANI nanocomposite, despite the striking color of PANI (Fig. 1Bc). The gray color of the RuO_2-TiO_2 nanoparticles is no longer visible by observing the nanopowders of RuO_2-TiO_2/DPA/PANI, the dark green color of the PANI covers all the RuO_2-TiO_2 powder previously modified with DPA (Fig. 1Bd), this reflects the spectacular role of DPA salt in the process of polymerization of the polymer on the surface of RuO_2-TiO_2 heterojunction as well as its effect on the optical properties of the nanocomposite formed.

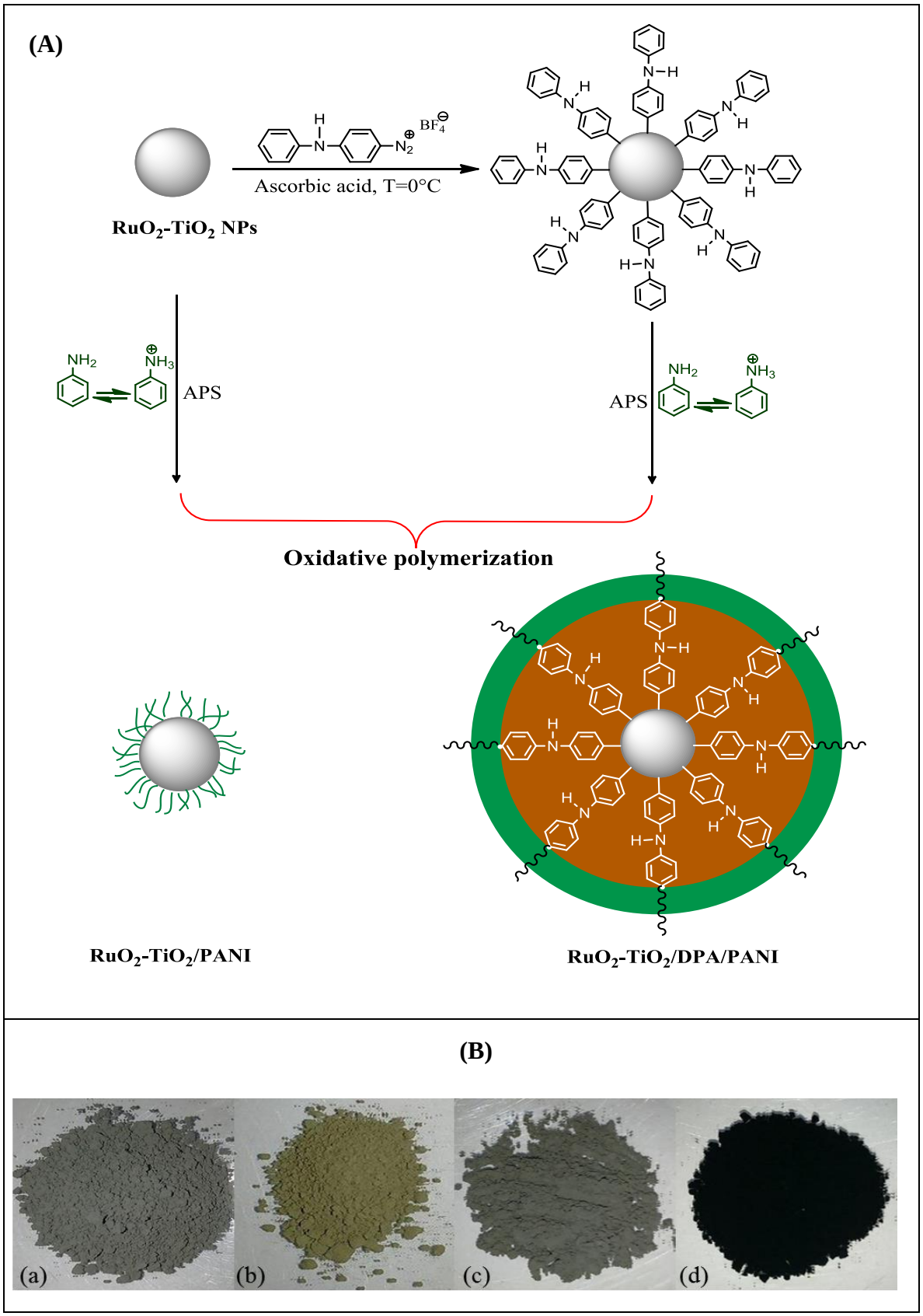

Figure 1. Synthesis of RuO_2-TiO_2/PANI nanocomposite (Upper panel: Fig. 2A) and digital photographs of pristine RuO_2-TiO_2 (a), RuO_2-TiO_2-DPA (b), RuO_2-TiO_2-PANI (c), and RuO_2-TiO_2-DPA-PANI (d) (Lower panel: Fig. 2B).

3.2. RuO_2-TiO_2 characterization

3.2.1. Point of Zero Charge (PZC) of RuO_2-TiO_2 by zeta potential measurement

The Point of zero charge (PZC) is the pH at which the surface of a particle is electrically neutral [45]. Figure 2 depicts the evolution of the zeta potential in the pH ranging from 1.5 to 13 for RuO_2-TiO_2 heterojunction NPs. The plot shows that the PZC of the RuO_2-TiO_2 heterostructure is 5.8. The value of PZC of RuO_2-TiO_2 NPs decreased compared to those of TiO_2 anatase reported in the literature. Li et *al.* [46] have marked the PZC for pure TiO_2 anatase at pH = 7, this result is similar to that found by Song et *al.*[47]. Uchikoshi [48] reported another value which is about 6.7. These values remain dependent on the working conditions namely the measuring device, the electrolyte support and the nature of the material.

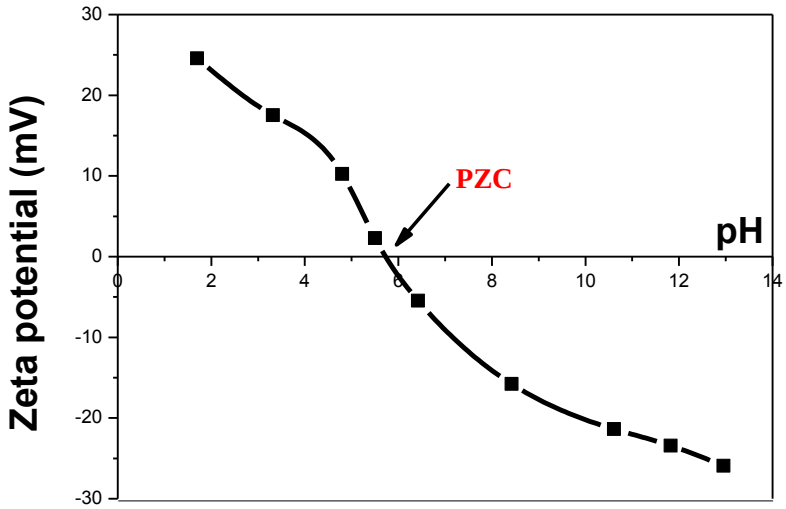

Figure 2. Variation of the zeta potential of RuO_2-TiO_2 NPs dispersed in NaCl as a function of the pH.

3.2.2. Dielectric characterization

Electrical impedance spectroscopy has been widely used to study the charge transport behavior of nanocrystalline materials, providing information on the electrical and structural properties of materials. For a detailed study of charge transport properties of RuO_2-TiO_2 mixed oxide nanoparticles as a function of temperature, the impedance measurements were carried out in the frequency region from 100 Hz to 1 MHz. The electrical properties of the RuO_2-TiO_2 heterojunction have not yet been studied. The combination of ruthenium oxide

with a metallic character and titanium dioxide semiconductor (n) generates original electrical characteristics different from those of simple and spinel oxides.

Figures 3a and 3b display the variation of the real part (Z') and imagines part (Z") of impedance versus frequency (10^3 to 10^6 Hz) at different temperatures. The plots show a sigmoidal variation as a function of frequency in the low frequency region followed by saturation in the high frequency region. These results represent the mixed nature of polarization behavior in the material. The converge of all Z' and Z'' curves at high frequency indicates a possibility of the release space charge in the RuO_2-TiO_2 material, as a result of lowering in the barrier properties of the material. The curves indicate that the electrical conduction increases with rise in temperature, this variation depends on the release of the space charge. In the low frequency region, a very strong dependence of the impedance of the material as a function of frequency and temperature has been recorded, this may be related to a change in the charge order model under the effect of temperature; this effect shows also a noticeable change in its behavior in the low frequency region. A decreasing trend of Z' temperature rise suggests the presence of negative temperature coefficient of resistance (NTCR) in the material in the low frequency region but tends to merge in the high frequency region at almost all temperatures. These results indicate a possibility of increase in alternating current (ac) conductivity with increasing temperature in the high frequency region, possibly due to the release of space charge.

Figure 3 (c) shows the frequency dependence of the relative dielectric permittivity of RuO_2-TiO_2 sample at different temperature and frequency. The dependent dielectric permittivity of the RuO_2-TiO_2 material decreases with increasing of temperature and frequency. This phenomenon can be attributed to the different dipole orientations by charge carriers bounded at different localized states [49,50]. The electron can hop between a pair of these centers under the action of an alternating current field, leading to the reorientation of an electric dipole. This process conducted to a change in the dielectric permittivity. Therefore the increase in the dielectric permittivity with decreasing frequency can be attributed presence of the space charges in the material [51].

Figure 3 (d) displays the frequency dependence of the imaginary part of the relative dielectric permittivity of RuO_2-TiO_2 at various temperatures and frequencies. The curves show that, the imaginary part of the relative dielectric permittivity increased with increasing temperature. However, the imaginary part of the relative dielectric permittivity decreased as the frequency increased. As high frequency, the imaginary part of the relative dielectric permittivity

measured at different temperature ranges converge to similar values, this is probably due to the small value of the conductance compared with the rapidly increased angular frequency ranges. Usually metal oxide materials can be expressed n-type semiconductor due to their oxygen vacancies, therefore free electrons from the metal sites can be easily released by high temperature; so, imaginary part of relative dielectric permittivity has closed relationship with the conductance. As results, the imaginary part of relative dielectric permittivity of RuO_2-TiO_2 composition at the high temperature near the low frequency has high values.

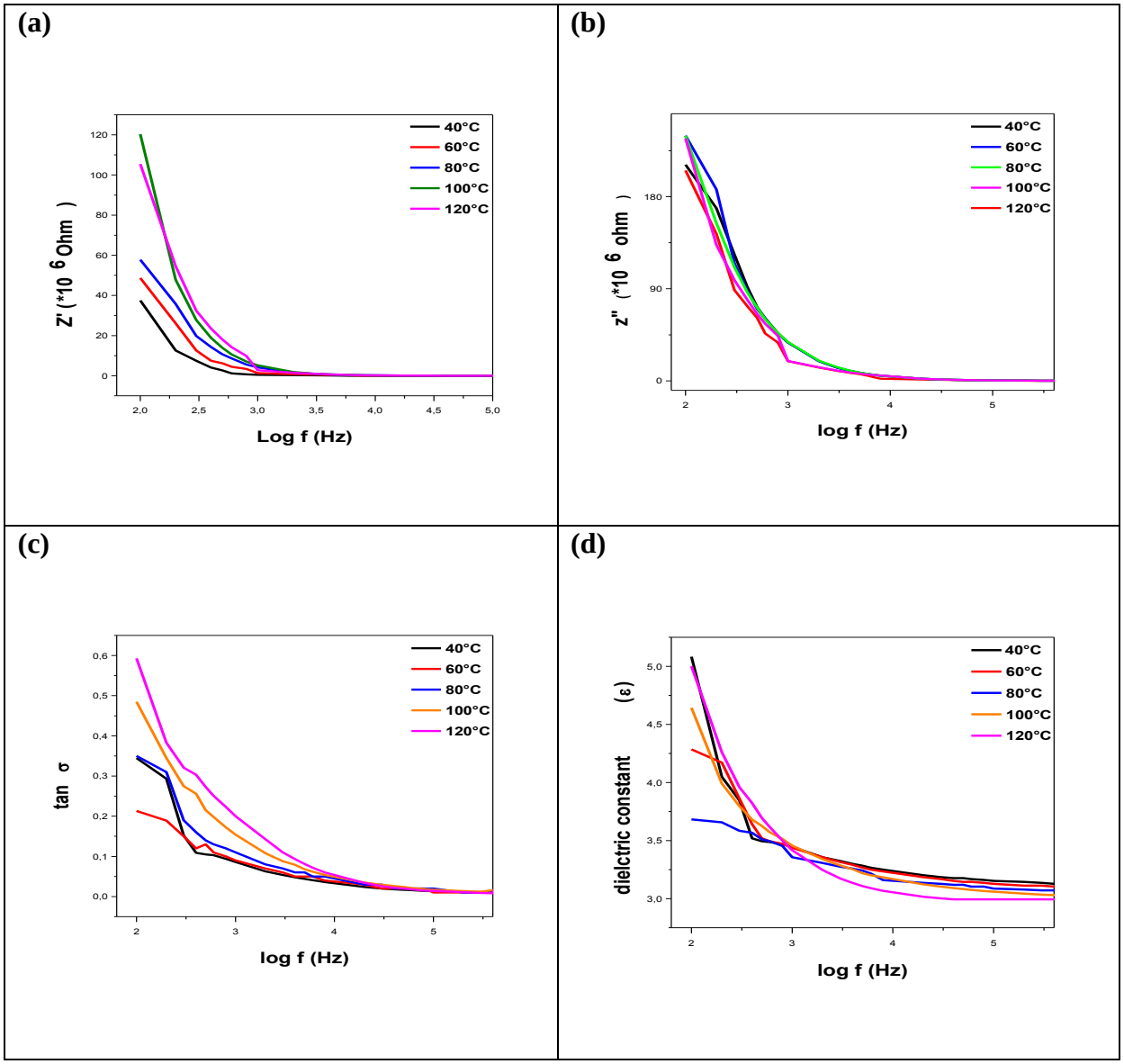

Figure 3. Frequency dependence of (a) Z', (b) Z", (c) relative dielectric permittivity and (d) imaginary part of the relative dielectric permittivity.

3.3. Characterization of RuO_2-TiO_2/PANI nanocomposites

3.3.1. Resistivity by Four Point Probe Measurements

During the catalytic processes, the electrons which are on the surface interact during the whole time of the catalyzed reaction inducing the formation of an electric current. It is therefore possible to correlate the catalytic efficiency of solid catalysts by measuring the electronic conductivity within the materials.

The resistivity of material can be determined using Four Point Probe method and calculated by applying the following relation:

$$R = \frac{V}{I} = K.\frac{\rho}{e} \qquad (1)$$

where: R is the resistance (Ω), ρ the resistivity (Ω. m), e the thickness of the pellet (cm) and K the dimensionless coefficient characteristic of 2D geometry (shape of contours, position of contacts).

$$K = \frac{Ln\ 2}{\pi} \qquad \frac{1}{K} = 4.532$$

$$\rho = \frac{V \times e \times \pi}{I \times Ln2}$$

The conductivity is given by:

$$\sigma = \frac{1}{\rho}$$

Table 1 summarizes the results obtained for the various catalysts at similar pellet thickness.

Table 1. Conductivity and resistivity of pure TiO_2 and RuO_2-TiO_2-based nanocatalysts.

Materials	e (cm)	R (Ω)	ρ (Ω. cm)	σ (S/cm)
TiO_2	0.20	0.0119	0.0109	91.7
RuO_2-TiO_2	0.23	0.0030	0.0032	317
PANI	0.21	0.0111	0.0106	94
RuO_2-TiO_2/PANI	0.23	0.0028	0.003	343
RuO_2-TiO_2/DPA/PANI	0.24	0.0024	0.0026	384

The resistivity of the RuO_2-TiO_2 heterostructure and related materials was studied on compressed materials pellets by setting a current of 0.1 mA at room temperature. The results highlight the effect of RuO_2 on the conductivity of RuO_2-TiO_2 NPs by comparing the results obtained with those of pure TiO_2, as well as the effect of PANI on the conductivity of nanocomposites by comparing pure RuO_2-TiO_2 NPs.

Ruthenium dioxide is widely known for its low resistivity and high conductivity which has allowed it to be ranked among the best conductive oxides at room temperature [52,53,54]. As a result, the resistivity of RuO_2-TiO_2 heterojunction is three times lower than that of pure TiO_2, the results showed also that the conductivity of the mixed oxide RuO_2-TiO_2 is much higher than that recorded for TiO_2; this reveals that the combination between RuO_2 and TiO_2 leads to the formation of a new material with interesting electric properties.

The presence of PANI on the surface of RuO_2-TiO_2 has a significant effect on the electrical conductivity of the final nanocomposites. Cao et ***al.*** [55] were the first to obtain PANI films with a high electrical conductivity greater than 10^2 S/cm. The PANI present on the surface of RuO_2-TiO_2 is doped with SO_4^{2-} at 50% and the measured conductivity is 94 S/cm. the results reveal that the conductivity of the nanocomposites obtained increases with the increase of the amount of PANI; it's worth 343 and 384 S/cm for RuO_2-TiO_2/PANI and RuO_2-TiO_2/DPA/PANI respectively.

The conductivity and the resistivity of materials are controlled by the number of free electrons and/or their mobility. As a matter of fact, the mobility of electrons increases with the increase of grain size [56], which is the case in this study.

3.3.2. X-Ray Diffraction

XRD was used to identify the different crystalline phases containing the samples of the heterostructure RuO_2-TiO_2 NPs, RuO_2-TiO_2/DPA, RuO_2-TiO_2/PANI and RuO_2-TiO_2/DPA/PANI nanocomposite. The pattern of RuO_2-TiO_2 NPs (Fig. 4a) obtained in the range $65° \geq 2\theta \geq 20°$ confirms the formation of the mixed oxide and the total conversion of $RuCl_3$ into RuO_2. It exhibits the different peaks expected for TiO_2 in its anatase form: 2θ = 25.4°, 37.1°, 37.79°, 53.8°, 55.2° , 62.9° and 70.06° related to TiO_2 reflections in planes (1 0 1), (1 0 3), (0 0 4), (1 0 5), (2 0 0) (2 0 4) and (2 2 0) respectively, and those of RuO_2 rutile: 2θ = 28.1°, 35°, 40.1°, 40.8°, 45.3, 59.6° and 69.6° corresponding to RuO_2 reflections in planes (1 1 0), (1 0 1), (2 0 0), (1 1 1), (2 1 0), (0 0 2) and (3 0 1), respectively. The intensity of peaks corresponding to RuO_2 is low compared to that recorded for peaks of TiO_2, which means that titanium oxide is predominant. The crystallite size estimated using Scherer's formula for each oxide, calculated from the broadening of their most intense dispersion bands (TiO_2: (1 0 1), RuO_2: (110)) is 6.5 nm for TiO_2 and 8.7 nm for RuO_2.

The diffraction spectra of RuO_2-TiO_2 after modification with diazonium salt and PANI reveal the expected peaks of pristine RuO_2-TiO_2. No new phase was detected, however, the peaks located at 28.12°, 37.79°, 45.31° and 59.6° characteristics of RuO_2-TiO_2 NPs do not appear on the spectra (b), (c) and (d) corresponding to RuO_2-TiO_2/DPA, RuO_2-TiO_2/PANI and RuO_2-TiO_2/DPA/PANI. No other peaks corresponding to the diazonium salt appeared on the spectra, it is noted that the X-ray diffraction does not detect non-crystalline organic matter.

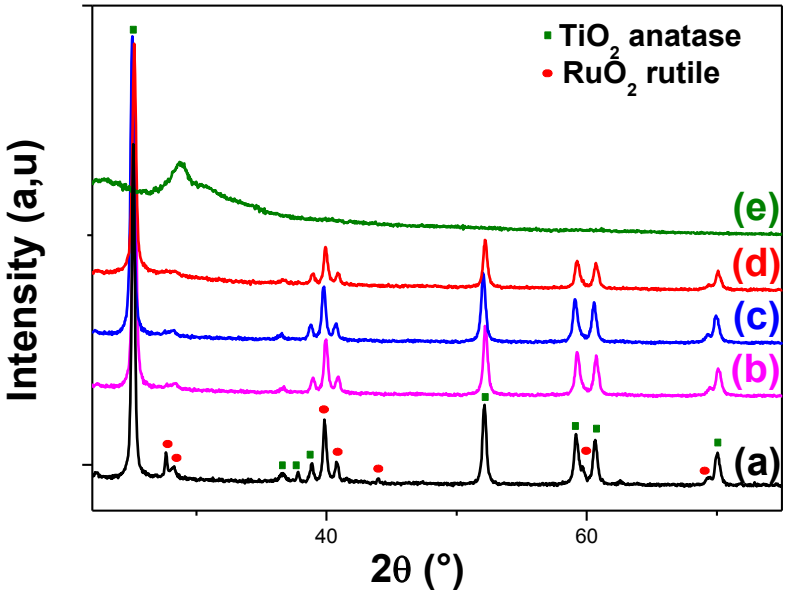

Figure 4. XRD patterns of RuO_2-TiO_2 NPs (a), RuO_2-TiO_2/DPA (b), RuO_2-TiO_2/PANI (c), RuO_2-TiO_2/DPA/PANI (d) and PANI (e).

3.3.3. UV-vis

Figure 5 displays UV-vis spectra of the samples recorded in the wave range 200-800 nm. The spectrum of RuO_2-TiO_2 NPs is marked by the presence of lower intensity TiO_2 absorption bands centred at 200 and 350 nm. Furthermore, there are broad bands between 400 and 600 nm corresponding to RuO_2; these bands are characterized by a high intensity which is due to the strong absorption of RuO_2. The width of these bands is probably due to the charge transfer between oxygen and ruthenium.[57] The absorption of visible light by the mixed oxide RuO_2-TiO_2 can be attributed to the external effect of resonance that is related to the excitation of electron collective oscillations in the RuO_2 nanoparticles by the electric field of the electromagnetic wave [58].

The band gap energy (Eg) of the RuO_2-TiO_2 heterostructure was calculated from the UV-vis spectrum applying the following equation:

$$\alpha(h\upsilon) = A(h\upsilon\text{-}Eg)^n$$

where α: absorption coefficient, υ: light frequency, Eg: band gap energy and A: constant. (n) is determined by the type of optical transition of semiconductor (n=1/2 or n=2 for direct or indirect transition). Therefore, the band gap energy calculated for RuO_2-TiO_2 heterojunction

from the $(\alpha h\upsilon)^n = f(h\upsilon)$ plot was 2.7 eV for indirect transition and 3.19 eV for direct transition.

PANI has high absorption in the UV as well as in the visible light [59]. Compared to RuO_2-TiO_2 NPs, the TiO_2 absorbance in the RuO_2-TiO_2/PANI nanocomposite increased significantly in the visible range while that of the RuO_2 decreased in the UV. This indicates that the presence of PANI even in small amounts has extended the absorption of TiO_2 to the range of visible light [59]. The RuO_2-TiO_2/DPA/PANI nanocomposite has the same optical properties as the PANI; the corresponding spectrum is almost similar to that of the polyaniline represented in the literature [59,60]. The spectrum reveals the increase of the absorbance with the appearance of a small wave between 469 and 510 nm, corresponding to the π-π* transition in the polymeric chain.[61] The increase in the absorption of the two nanocomposites is due to the delocalization of the carrier's n-π* [62].

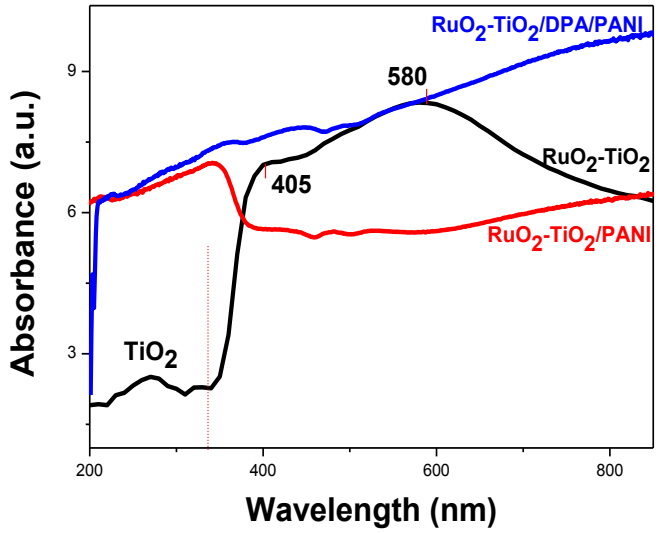

Figure 5. UV-vis spectra of RuO_2-TiO_2 NPs, RuO_2-TiO_2/PANI and RuO_2-TiO_2/DPA/PANI nanocomposite.

3.3.4. Infrared Spectroscopy

Figure 6 displays superimposed spectra of RuO_2-TiO_2/DPA/PANI and related compounds. The spectrum of pristine RuO_2-TiO_2 NPs (Fig. 6a) presents two characteristic bands of titanium dioxide located at 432 and 815 cm^{-1} attributed to Ti=O and Ti-O-Ti stretching vibrations, respectively. The band centred at 690 cm^{-1} accounts for the vibration of Ru-O and deformation of Ru-O-H [63]. Uddin et *al.* [6] did not obtain any band corresponding to RuO_2 in their IR study of RuO_2-TiO_2 mixed oxide and the spectrum they have displayed was similar to that of pure TiO_2. The spectrum of DPA diazonium (Fig. 6b) is marked by bands centered at 1580 cm^{-1} and 1610 cm^{-1} which correspond to the aromatic C=C stretching, a signal has been recorded around 1180 cm^{-1} which is assigned to C-H benzene ring stretching band [64]. The spectrum shows the characteristic bands of diazonium salt at 3340 and 2232 cm^{-1} corresponding to the N-H and N≡N stretching mode of diazonium salt, respectively. Particularly, the characteristic N≡N band does not appear in the spectrum of RuO_2-TiO_2/DPA (Fig. 6c) which confirms the attachment of aryl layer by diazonization of the parent diazonium salt [65]. The spectrum of the RuO_2-TiO_2/PANI nanocomposite (Fig. 6e), is almost similar to that of the pristine mixed oxide except three bands belonging to the PANI vibrational result, a band at 1232 cm^{-1} is ascribed to C-N stretching vibration. That located at 1400 cm^{-1} is relative to C=C aromatic ring stretching of the benzenoid vibration. An intense peak appeared around 1126 cm^{-1} attributed to C-H in-plane deformation [66]. The analysis of the RuO_2-TiO_2/DPA/PANI sample (Fig. 6f) showed the same features as pure PANI (Fig. 6d), all bonds detected belong to the polymer. In addition to the bands present on the RuO_2-TiO_2/PANI nanocomposite spectrum, a band at about 1565 cm^{-1} is lumped with C=C stretching of quinoid vibration.**[67]** This result means that the RuO_2-TiO_2/DPA surface is totally covered by PANI.

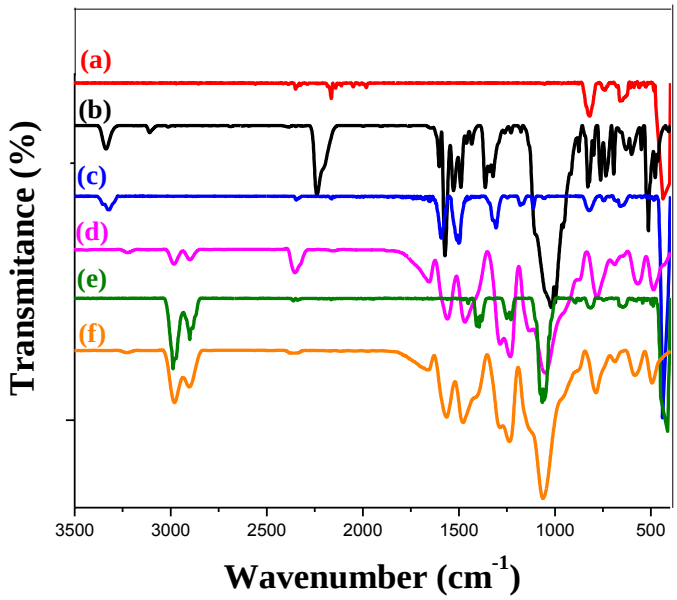

Figure 6. FTIR absorption spectra of (a): RuO_2-TiO_2, (b): DPA, (c): RuO_2-TiO_2/DPA, (d): PANI, (e): RuO_2-TiO_2/PANI and (f): RuO_2-TiO_2/DPA/PANI.

3.3.5. Raman

Ruthenium dioxide in rutile phase has a tetragonal structure with two molecules of RuO_2 per unit cell; it has fifteen modes of optical phonons, three of which are Raman-active in the 400-800 cm^{-1} range with the symmetries E_g corresponding to a doublet as well as A_{1g} and B_{2g} which are singlets [68]. Several studies have already shown that the TiO_2 anatase is usually manifested with Raman-active modes that are E_g (144 cm^{-1}), E_g (197 cm^{-1}), B_{1g} (399 cm^{-1}), A_{1g} (514 cm^{-1}), B_{1g} (514 cm^{-1}) and E_g (639 cm^{-1}) [69]. The RuO_2-TiO_2 heterostructure is a combination of Rutile RuO_2 and TiO_2 anatase which could be distinguished by their Raman-active modes on the same spectrum. Figure 7 displays superimposed Raman spectra of RuO_2-TiO_2 NPs, pure PANI and their reference materials. The spectrum of pristine RuO_2-TiO_2 NPs (Fig. 7a) shows three distinct peaks located at 528, 646 and 716 cm^{-1} assigned to E_g, A_{1g} and B_{2g} phonons vibrations respectively corresponding to ruthenium oxide in the rutile phase, these bands are in agreement with those reported in the literature [70]. The spectrum shows also another band at 197 cm^{-1} attributed to the vibration mode E_g specific to TiO_2 anatase.

The spectrum of DPA-modified RuO_2-TiO_2 NPS shows a very remarkable red shift of RuO_2-TiO_2 characteristic bands, which confirms the grafting of DPA on the surface of the

heterostructure (Fig. 7b). It is noted that the Raman shift is a difference in atomic weight between pure RuO_2-TiO_2 and RuO_2-TiO_2/DPA.

The polymerization of PANI on RuO_2-TiO_2 NPs surface did not lead to the displacement of the Raman bonds of the nanoparticles, but to a slight broadening of the latter and a vibrational response recorded between 1200 and 1800 cm^{-1} which corresponds to the polymer (Fig. 7c). The spectrum of RuO_2-TiO_2/DPA/PANI nanocomposite shows an increase in the baseline comparing with RuO_2-TiO_2 and RuO_2-TiO_2/DPA curves. An increase in the intensity and a considerable broadening of the bands have been registred, in addition to the shift of the characteristic bands of PANI toward lower; this can be explained by the insertion of a large amount of organic matter, *ca.* PANI in the actual case (Fig. 7d).

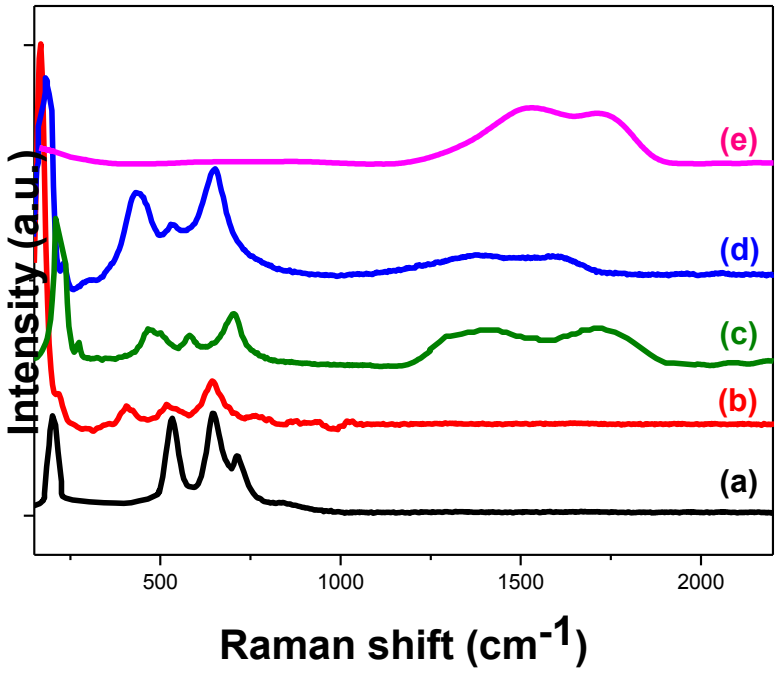

Figure 7. Raman spectra of pristine RuO_2-TiO_2 NPs (a), RuO_2-TiO_2/DPA (b), RuO_2-TiO_2/PANI (c), RuO_2-TiO_2/DPA/PANI (d) and PANI (e).

3.3.6. Thermogravimetric analysis (TGA)

The mass loading of organics attached on the surface of RuO_2-TiO_2 heterostructure NPs was determined using TGA carried under air flow. Pristine RuO_2-TiO_2 mixed oxide and DPA-modified RuO_2-TiO_2 exhibit a thermal stability up to 800 °C (Fig. 8a and 8c). The weight loss is negligible; it is 1% for RuO_2-TiO_2 bare and 1.5% for RuO_2-TiO_2/PANI which could be

caused by the evaporation of H_2O molecules adsorbed on the surface (Fig. 8 a, b). The quantity of organic matter loaded on the surface of RuO_2-TiO_2 heterostructure was determined according to the weight loss, it was 1.52 % of PANI, and 9.8% of DPA. In the case of RuO_2-TiO_2/DPA/PANI, the weight loss is as high as 27.8% for the aryl and PANI layers. These results confirm the role of DPA as a coupling agent for the polymer on the RuO_2-TiO_2 NPs surface. The thermal degradation of RuO_2-TiO_2/PANI and RuO_2-TiO_2/DPA/PANI nanocomposite occurs in two steps: the reduction of the initial mass of the samples in the temperature range between 50 and 230 °C which can be attributed to the removal of H_2O molecules adsorbed on the surface of the particles. The second step between 230 and 800 °C, assigned to the thermal decomposition of the inserted polyaniline chains (Fig. 8 b, d). The total thermal decomposition of the polymer on the unmodified RuO_2-TiO_2 surface occurred at temperatures above 600 °C while for the RuO_2-TiO_2/DPA/PANI nanoocomposite, the total decomposition of PANI occurred at temperatures raised above 800 °C; this is probably due to the diazonium salt, which seems to have a retarding effect on the decomposition of the polymeric chains. The addition of DPA has strengthened the bonds between RuO_2-TiO_2 nanoparticles and PANI and the increase of the interaction between these two elements led to the formation of a highly temperature-resistant composite material.

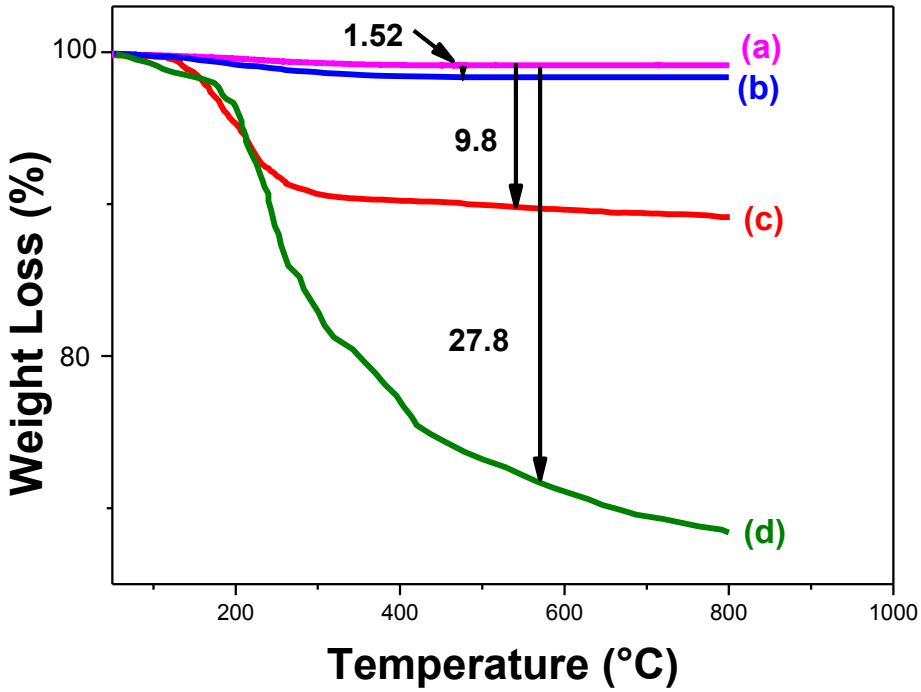

Figure 8. Thermogravimetric analysis (TGA) curves of pristine RuO_2-TiO_2 NPs (a), RuO_2-TiO_2/PANI (b), RuO_2-TiO_2/DPA (c), RuO_2-TiO_2/DPA/PANI (d).

3.3.7. SEM-EDX

Figure 9 depicts SEM images and X-ray emission spectra of the different materials. The images of RuO_2-TiO_2 mixed oxide reveal the presence of spherical and cubic shaped particles. A contrast has been observed on the image which is directly related to the atomic number Z of the elements containing the analyzed sample; a particle with a high Z appears with a clear contrast; so the bright light spots are attributed to the ruthenium oxide because it is the heaviest element in the heterostructure RuO_2-TiO_2 NPs (Fig. 9 a,b). EDS spectrum shows peaks corresponding to Ti and Ru metals as well as a signal attributed to oxygen molecule, confirming the composition of the simple analyzed and the formation RuO_2 and TiO_2 oxides (Fig. 9 c). The SEM images of RuO_2-TiO_2/PANI show that the particles are aggregated and the morphology is similar to that of pristine RuO_2-TiO_2 (Fig. 9 d,e). The corresponding EDS spectrum shows no signal associated to the PANI, which is due to the negligible amount of PANI on the surface of RuO_2-TiO_2 (Fig. 9 f). In the presence of DPA, the nanoparticles are much more scattered. The decrease in the agglomeration is very clear (Fig. 9 g, e). The presence of DPA is testified by the increase in the percentage of carbon on EDS spectrum. It

is noted that is difficult to see the peak of nitrogen when we have a considerable amount of Ti, the latter causes a total masking of the nitrogen signal (Fig. 9 i). The nanocomposite RuO_2-TiO_2/DPA/PANI reveals a porous texture and spherical and highly agglomerated particles, which is due to the presence of PANI on the surface of diazonium-modified RuO_2-TiO_2 (Fig. 9 j, k); this was confirmed by the EDS spectrum which shows an increase of carbon ratio in the nanocomposite and the appearance of nitrogen and sulfur signals with the decrease of the intensity of Ti and the absence of Ru, which confirms the good coverage of RuO_2-TiO_2/DPA by PANI (Fig. 9 l).

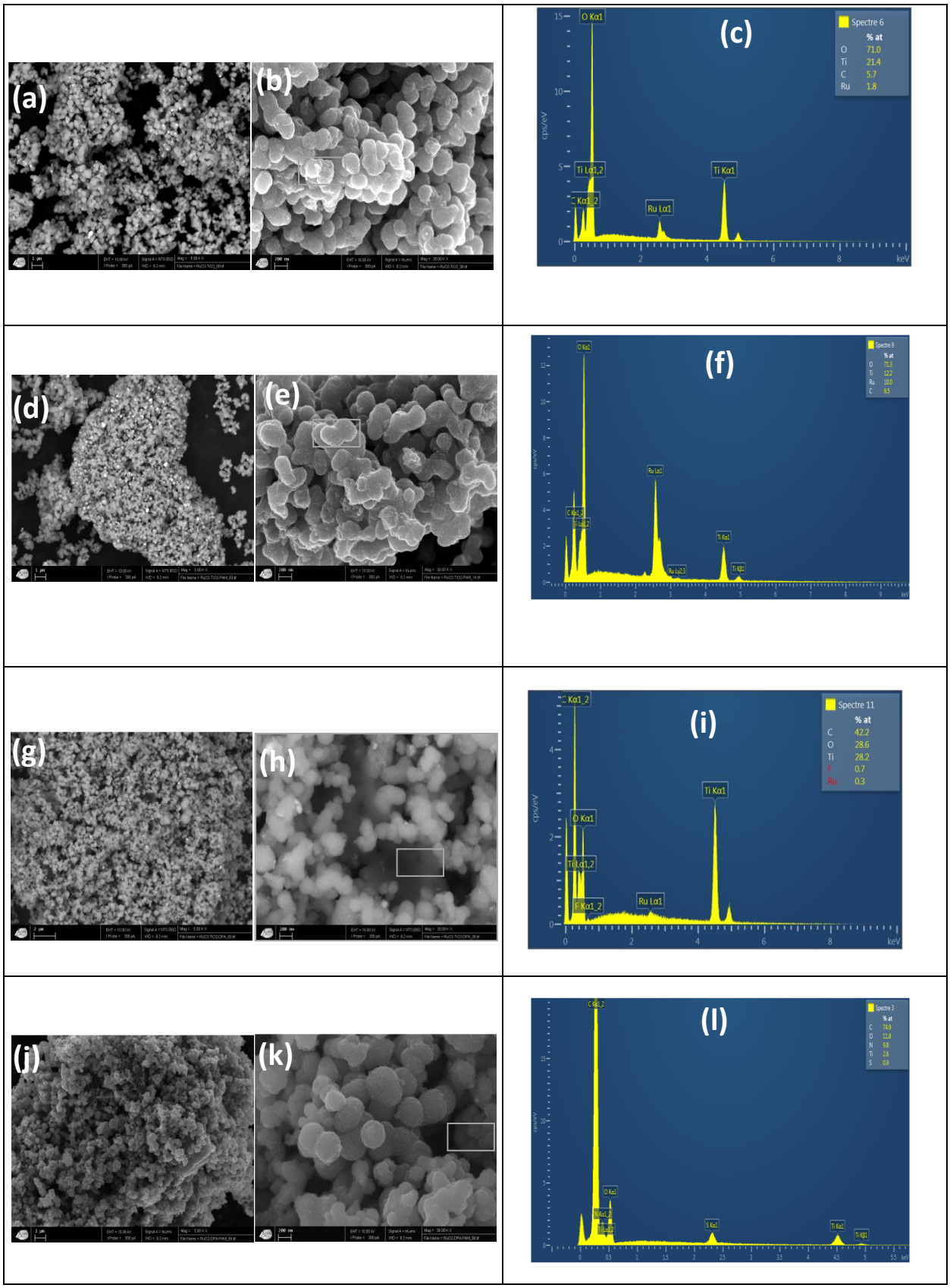

Figure 9. SEM images (a, b, d, e, g, h, j, k) and elementary spectra (c, f, i, l) of RuO_2-TiO_2 NPs (ab, c), RuO_2-TiO_2/PANI (de, f), RuO_2-TiO_2/DPA (gh, i), RuO_2-TiO_2/DPA/PANI (jk, l).

3.3.8. XPS

The samples were examined by XPS to check the stepwise coating of the underlying photocatalyst by RuO_2-TiO_2 by the DPA aryl layer followed by the PANI top layer.

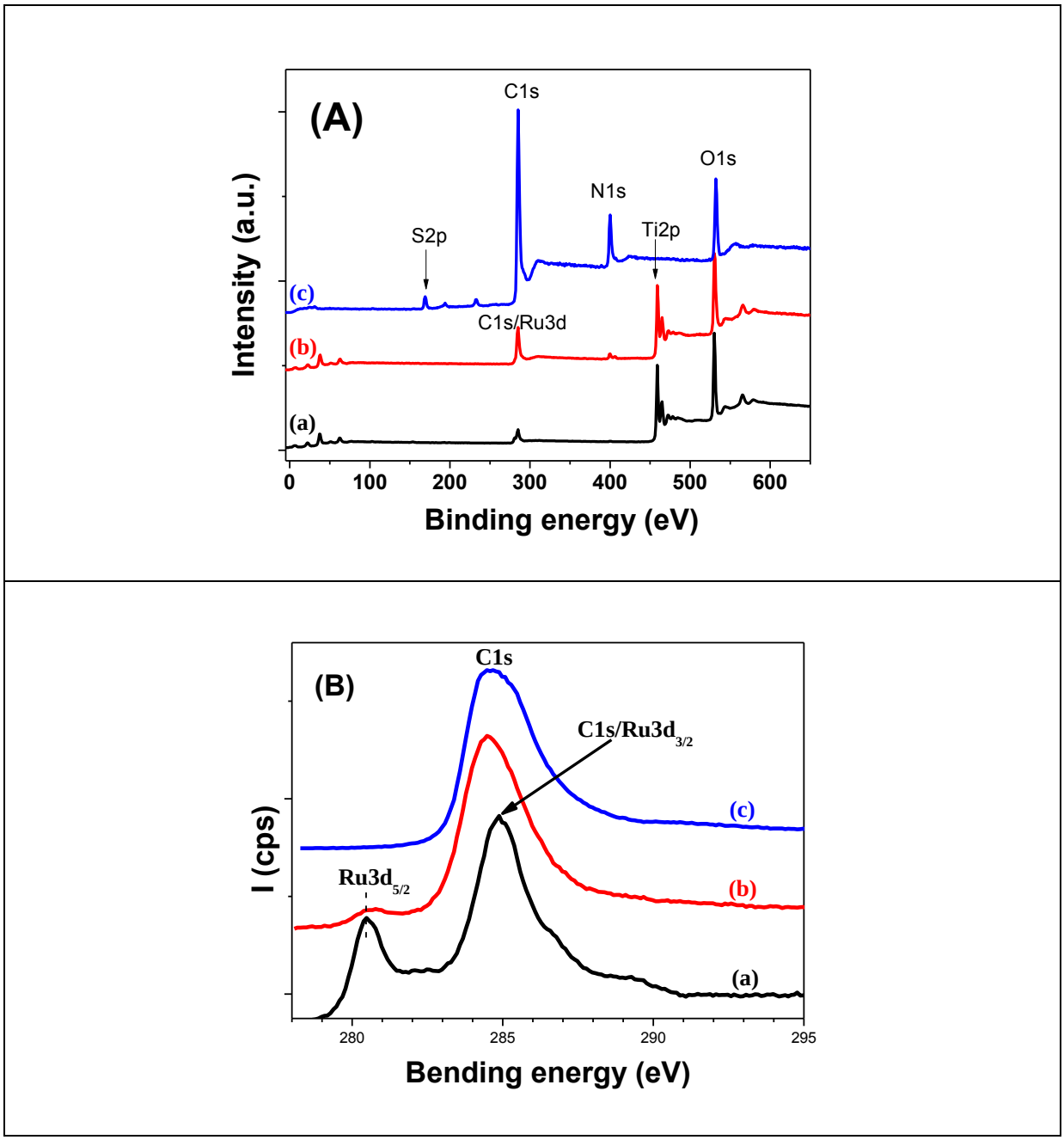

Figure 10. XPS survey scans (A) and high resolution C1s spectra (B) of RuO_2-TiO_2 (a), RuO_2-TiO_2/DPA (b), and RuO_2-TiO_2/DPA/PANI (c).

Figure 10A displays the survey regions of RuO_2-TiO_2 (Fig. 10Aa), RuO_2-TiO_2/DPA (Fig. 10Ab) and RuO_2-TiO_2/DPA/PANI (Fig. 10Ac) which display C1s, N1s, O1s and S2p from PANI as well as the characteristic Ru3d and Ti2p from the photocatalyst (Fig.s 10Aa-b). The

C1s (285 eV) and N1s (400 eV) peaks in Fig. 10Ab exhibit higher relative intensity compared to $Ti2p_{3/2}$ (457 eV). No distinct specific peaks from the RuO_2-TiO_2 photocatalysts are noticed in Fig. 10Ac which testifies for the efficient screening by PANI due to the DPA adhesive layer. Indeed, sharp C1s, N1s and O1s peaks are noted in Fig. 10Ac; they account for PANI. As far as the dopants are concerned, S2p is centred at 169 ev which accounts for sulfates. It is worth to note that for RuO_2-TiO_2/DPA/PANI, S/N atomic ratio = 0.23 which means that the doping level is 46% if we consider the double negative charge of the sulfates. This doping level accounts for the conductivity of PANI. The O/S ratio is ~ 4.3 indicating that oxygen is essentially due to the SO_4^{2-} dopant.

Figure 10B displays the high resolution C1s-Ru3d regions; $Ru3d_{5/2}$ is centred at 280.5 eV and $Ru3d_{3/2}$ is lumped with the main C1s component at ~285 eV. The $Ru3d_{5/2}$ is significantly attenuated by the DPA aryl layer meaning that the aryl layer is homogeneous. After in situ polymerization of aniline, the C1s-Ru3d region reduces to the C1s spectrum of pure PANI [71].

3.4. Adhesion of polyaniline to RuO_2-TiO_2 nanoparticles

The diazonium salt acts as a coupling agent, binding the PANI to the surface of RuO_2-TiO_2 nanoparticles. PANI is soluble in some organic solvents such as N-methyl-2-pyrrolidone **(**NMP), dimethyl sulfoxide (DMSO), tetrahydrofuran (THF) and hexafluoropropan-2-ol (HFIP) [72,73]. It is thus interesting to investigate the effect of diphenyl amine diazonium (DPA) in the stability of the nanocomposite formed by testing the adhesion of polyaniline to the surface of modified and unmodified nanoparticles in organic polar (DMF, NMP, THF, HFIP and DMSO), and non-polar solvents (chloroform, 1,2-dichloroethane, xylene, toluene)**.** The mixtures of the materials (PANI, RuO_2-TiO_2/PANI and RuO_2-TiO_2/DPA/PANI) in organic solvents are shown in Fig. 11. The experiment confirmed the solubility of polyaniline in DMSO, NMP, THF and HFIP, while in DMF and toluene the solubility is medium and very low in 1,2-dichloroethane and Xylene (Fig. 11A).

PANI is not adherent on the surface of unmodified RuO_2-TiO_2 nanoparticles, the solutions are turns to deep green color because of the leaching of PANI from the surface (Fig. 11B). The presence of DPA has improved the stability of the nanocomposite by preventing the solubility of PANI in organic solvents. Indeed, the polymer is insoluble thanks to the role of DPA in strengthening the links between PANI and RuO_2-TiO_2 NPs. It is to note that when DPA is used, the solutions are all transparent exception of a slight staining of DMSO and NMP

solutions, due to the dissolution of polymer chains non-related to RuO_2-TiO_2 surface (Fig. 11C). These results are in agreement with those obtained in the case of TiO_2 NPs [39] which again confirm the interest of the incorporation of the aryl layer in the nanocomposite.

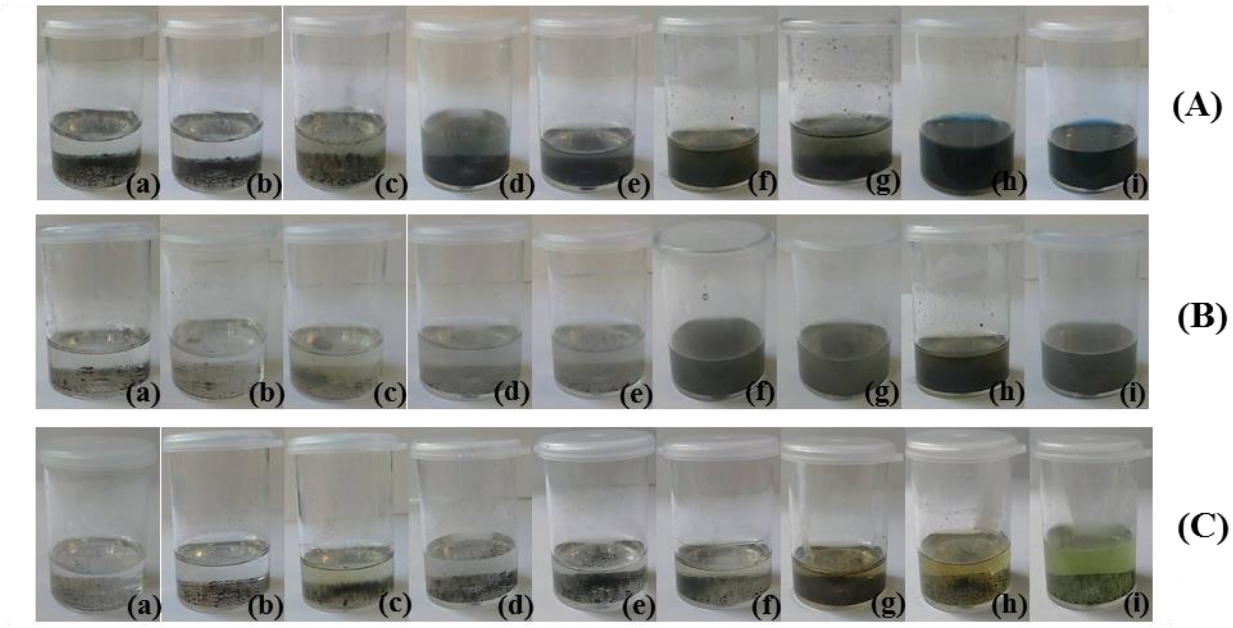

Figure 11. Digital photographs of (**A**): PANI, (**B**): RuO_2-TiO_2-PANI, (**C**): RuO_2-TiO_2-DPA-PANI in : (a) Chloroform, (b)1,2-dichloroethane, (c) Xylene, (d)Toluene, (e) DMF, (f)THF, (g) HFIP , (h)NMP, (i) DMSO.

3.5. Catalytic performances of RuO_2-TiO_2-DPA-PANI

Methyl Orange (MO) dye was taken as a model of organic pollutant in order to evaluate the catalytic and photocatalytic abilities of the materials under test. The experiments were carried out with suspensions of 10 mg of catalysts in 50 mL of aqueous methyl orange solution, at pH of 5.5.

It has been shown that the catalytic activity of materials decreases with increasing pH [74,75]. In acidic medium (pH < 2), MO degradation leads to the formation of quinone as a final product, the latter being much more toxic than the starting molecule [76]. Ammeri *et al.*[75] demonstrated that the photo-degradation of Methyl Orange is favored at pH < pH_{PZC} of the catalyst, because of the strong adsorption of the Methyl Orange on the catalyst surface

positively charged, this is due to the electrostatic attraction of the positive charge of the catalyst surface and the negative charge of the dye.

Before illumination was turned on, the suspensions were stirred magnetically in the dark for 55 minutes (t_1) to reach the adsorption equilibrium. However, it was found that the discoloration of MO started during this time under the catalytic effect of the materials, the solutions containing RuO_2-TiO_2/PANI nanocomposite turned yellow and very light yellow in the presence of RuO_2-TiO_2/PANI and RuO_2-TiO_2/DPA/PANI respectively (Fig. 12A c, d), while unmodified RuO_2-TiO_2 and the solution without any catalyst remained unchanged (Fig. 12Aa, b). The suspensions were kept in the dark for more time. The solution of MO containing RuO_2-TiO_2/DPA/PANI nanocomposite became completely colorless after 75 min (t_2= adsorption time + 20 min) (Fig. 12B d), while that containing the RuO_2-TiO_2/PANI nanocomposite took about 95 min (t_3= adsorption time + 40 min) (Fig. 12C c); this indicates the role of the catalysts in the activation of the MO degradation process in darkness. The solution containing RuO_2-TiO_2 nanoparticles and the one containing no catalyst (Fig. 12, t_2 and t_3: a, b) did not undergo any color change. This means that no degradation has taken place and that the catalyst has no catalytic effect at least in the dark.

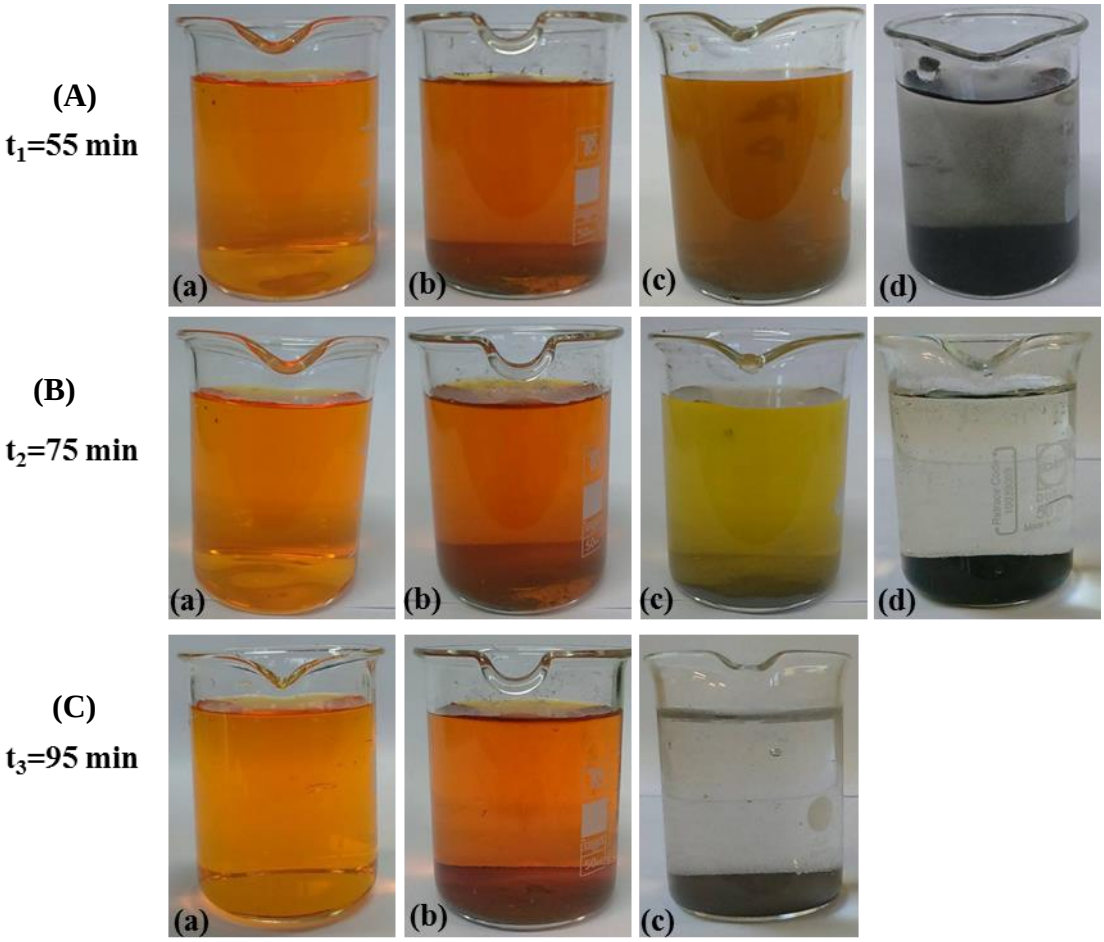

Figure 12. Digital photographs of methyl orange solutions after storage in the dark for (A) after t_1=55 min, (B) after t_2=75 min and (C) after t_3=95 min. (a) Without catalyst, (b) RuO_2-TiO_2 NPs, (c) RuO_2-TiO_2/PANI, (d) RuO_2-TiO_2/DPA/PANI.

2 mL of H_2O_2 were added to non-degraded solutions which were stored in the dark period. The solutions were left again in the dark for 20 min until the organic molecule is absorbed on the surface of RuO_2-TiO_2 NPs. In order to follow the process of MO photo-degradation in the presence and the absence of the catalyst, samples were taken every 5 min for 15 min and followed by UV-vis analysis. The first sample was taken just before exposing the solution to visible light in order to determine the initial concentration (C_0) of the dye. The absorbance of dye solutions before and after irradiation was measured at different degradation time. After 15 min of irradiation, no change in color was recorded in the absence of the catalyst (Fig. 13a). However, the presence of RuO_2-TiO_2 nanoparticles caused total discoloration of the MO (Fig. 13b); this highlighted the spectacular role of mixed oxide nanoparticles during the MO degradation process under visible light.

.

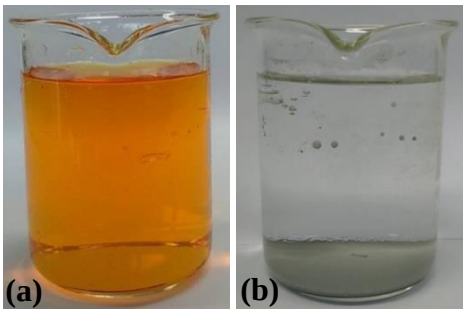

Figure 13. Digital photographs of methyl orange solutions after irradiation for 15 min. (a) Without catalyst, (b) RuO_2-TiO_2 NPs.

3.5.1. Kinetic analysis in darkness

In order to follow the kinetic of MO decomposition in the dark under the catalytic effect of RuO_2-TiO_2/PANI and RuO_2-TiO_2/DPA/PANI nanocomposites, samples were carried out progressively at $\mathbf{t_0}$= before adsorption, $\mathbf{t_1}$= adsorption equilibrium (55 min), $\mathbf{t_2}$=75 min and $\mathbf{t_3}$=95 min, and analyzed with UV-Vis, using a quartz cell and the absorbance measurements were recorded in the range of 200–800 nm.

The UV-vis absorption spectra obtained for the two colorless solutions show the disappearance of the two characteristic bands of methyl orange located between 250-300 nm and 400-500 nm attributed to the phenyl and azo group respectively. This confirms the total decomposition as well as the mineralization of the methyl orange dye solution under the effect of the nanocatalysts (Fig. 14c-d). It is noted that the catalytic effect of RuO_2-TiO_2/DPA/PANI is much greater than that of RuO_2-TiO_2/PANI; this is probably due to the amount of PANI loaded in the nanocomposite.

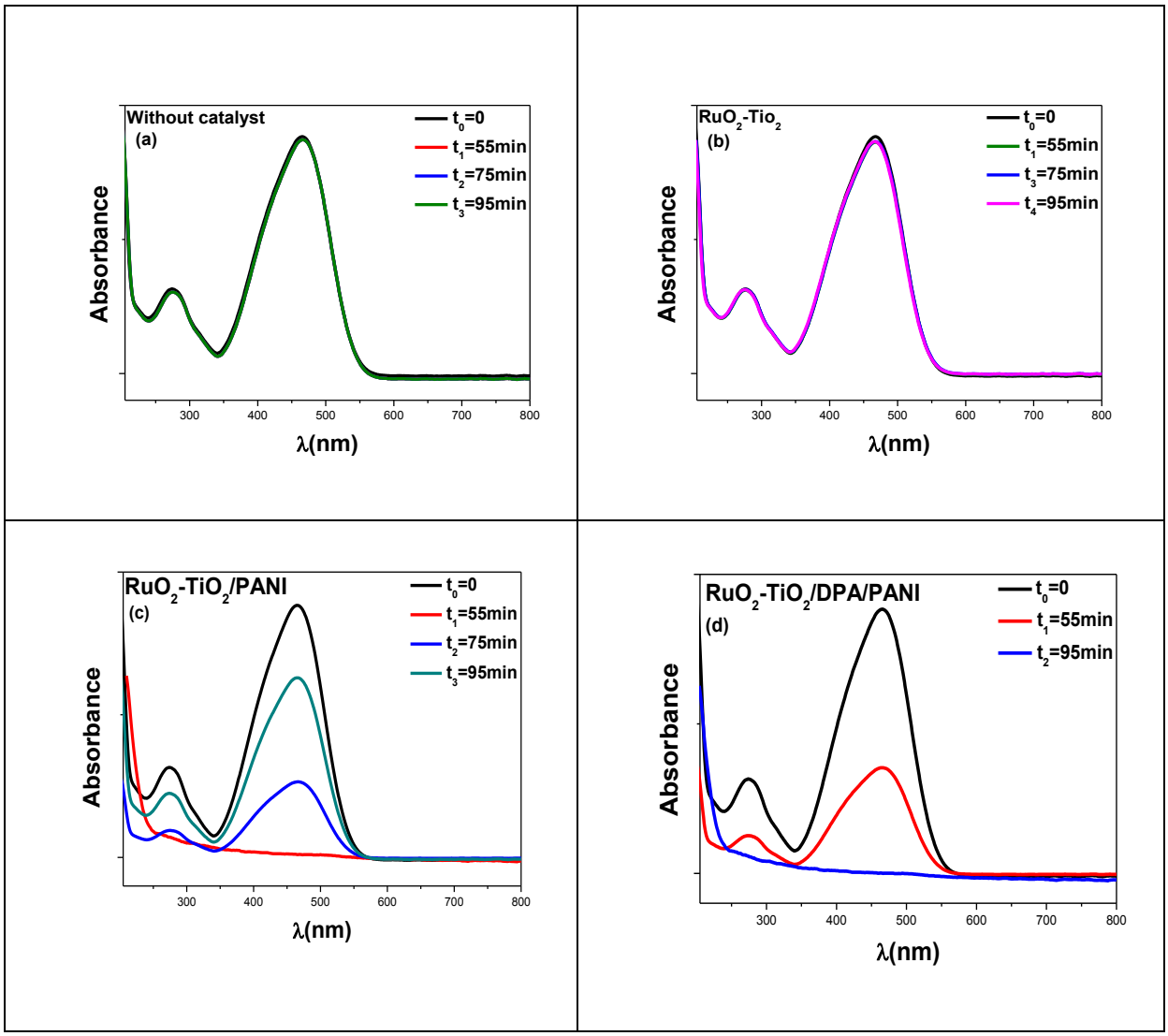

Figure 14. UV-vis absorption spectra of MO solutions before and after storage in darkness. (a) Without catalyst, (b) RuO_2-TiO_2 NPs, (c) RuO_2-TiO_2/PANI, (d) RuO_2-TiO_2/DPA/PANI**.**

The kinetics of MO degradation in the dark in the presence of the RuO_2-TiO_2/PANI and RuO_2-TiO_2/DPA/PANI nanocomposites as a function of the initial concentration of the dye has been reported in Figure 15. The C/C_0 vs. t (min) curves show a negligible degradation rate in the presence of RuO_2-TiO_2 nanoparticles and thus in the absence of catalyst. The dye is completely decomposed under the catalytic effect of the RuO_2-TiO_2/PANI and RuO_2-TiO_2/DPA/PANI nanocomposites, the time required for the removal of the MO varies according to the amount of PANI inserted on the surface of RuO_2-TiO_2 nanoparticles; the degradation rate in the presence of RuO_2-TiO_2/DPA/PANI is much greater than that in the presence of RuO_2-TiO_2/PANI.

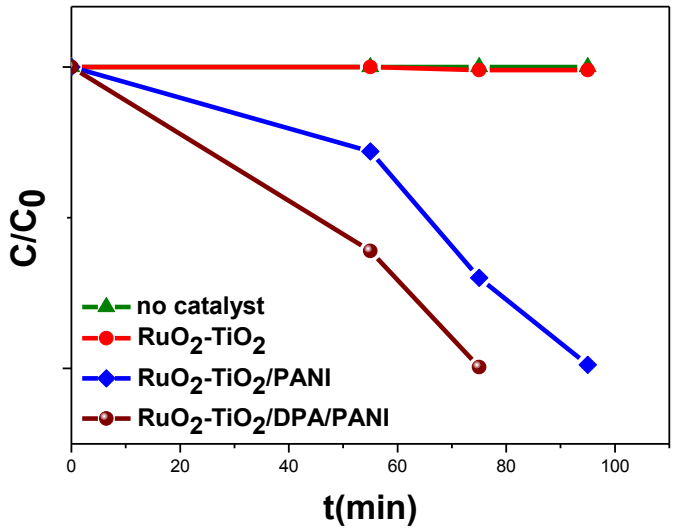

Figure 15. Kinetics of degradation of Methyl Orange solution (C=50mg.L^{-1}) in the dark.

Many studies have shown that Methyl Orange degradation follow a first-order kinetic [77,78]:

$$Ln\ \frac{C}{C_0} = -kt$$

where, C_0 is the initial concentration, k (min^{-1}) is the apparent rate constant and C is the concentration of MO. The Ln C/C_0 vs t(min) plots are linear with correlation coefficients (R) of 0.8573 for RuO_2-TiO_2/PANI and 0.9599 for RuO_2-TiO_2/DAP/PANI nanocatalyst, this shows that the degradation of the MO follows effectively the pseudo-first-order kinetics (Fig. 16). The apparent rate constant (min^{-1}) (k_{app}) determined from this plots are 0.0137 and 0.105 min^{-1} in the presence of RuO_2-TiO_2/PANI and RuO_2-TiO_2/DPA/PANI, respectively. These results account for the conductivity measurements made by Four Point Probe **(***see section* ***3.3.1***).

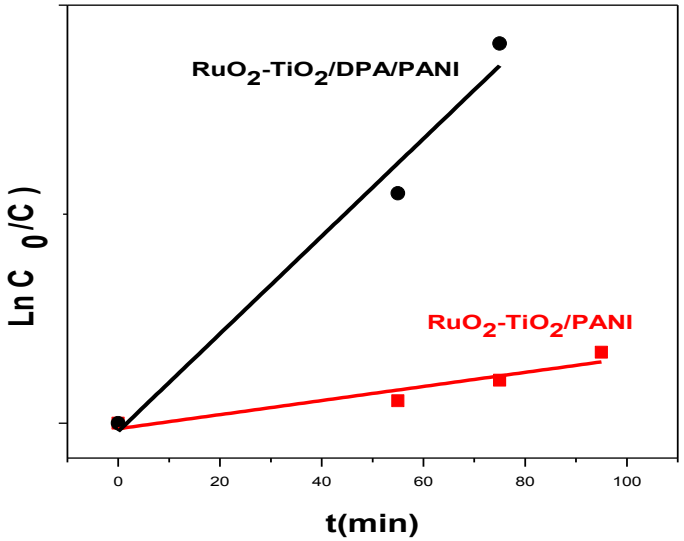

Figure 16. First order linear transforms of the degradation of methyl orange in the dark in the presence of RuO_2-TiO_2/PANI and RuO_2-TiO_2/DPA/PANI nanocomposites.

Catalysis in the dark is an alternative method to photocatalysis, which generally requires a high energy and cannot take place in the absence of light. The oxidative decomposition of organic molecules, in the so-called Fenton reaction, has attracted a lot of attention in recent years, because it is exempt from the need for light and only requires the presence of a source of the active radicals ($OH^{\cdot}$, $O^{\cdot}$ and $O^{2-\cdot}$) during the degradation reaction [79]. In this context, several studies have already been undertaken on the catalytic degradation process of organic molecules in the dark, at ambient conditions, without any irradiation and in the presence of metal catalysts [80,81,82]. Perovskite metal oxides are the most used materials as catalysts in this type of reaction. Liew et *al.*[83] have studied the catalytic power of perovskite $SrFeO_{3-\delta}$ metal oxide during the decomposition reaction of Bisphenol A and Acid Orange 8. The degradation occurred after 30 hours and 60 min respectively in the presence of any reactants generating the formation of radicals. The authors attributed this catalytic effect to the strong adsorption of the organic molecules used on the surface of the catalyst. The same perovskite containing Ba instead of Sr, was used by Sun *et al.*[84] in the degradation of Acid Orange 8 and the degradation time was 5 days. This reveals that the cation used in the perovskite compound plays a major role in the catalytic decomposition of pollutants. Using the same material, the degradation of Methyl Orange (20 mg. L^{-1}) in the dark took 50 hours [85]. Very recently, Chen

and co-workers demonstrated that CuO based metal oxides were very efficient in the degradation of Orange II dye under dark conditions as $CaSrCuO_3$ [79]. Wei et *al.* [85] prepared the nanocomposite Fe_3O_4@SiO_2@TiO_2@MIP in the presence of Methyl Orange and used as catalyst for the degradation of Congo Red in the darkness at room temperature and atmospheric pressure. The authors found a high catalytic activity of this composite which is due to the polymer which brings to the composite a higher binding capacity toward MO in the binding test compared with the ones that do not contain polymer.

Despite the important catalytic activity that these materials represent in the processes of degradation of organic pollutants, the complete decomposition time remains important compared to our results.

According to Sun et *al.* [84], on the one hand, the presence of oxygen vacancy in the catalyst structure favors the degradation of MO in the dark. The dye decomposes by oxidation at the oxygen vacancy location of the surface of catalyst. On the other hand, Nguyen et *al.*[1] associated the catalytic efficiency of the Pt-WO_3/Ti-Au nanocomposite to the interfacial contact between WO_3 and TiO_2 and the Au-induced surface plasmon resonance and the presence of oxygen vacancy in WO_3.

TiO_2 is a photocatalyst that activates only under UV light; it does not contribute to the degradation process of MO in the dark.

PANI is known as an electron donor; in the dark, the electrons that are stored on the LUMO are released and recovered by RuO_2 leaving holes on the HOMO. The electrons and holes are very important in any catalytic process; they promote the formation of $OH^{\bullet}$ radicals and $O_2^{\bullet-}$ anion radicals which are responsible for the decomposition reaction of organic pollutants. Scheme 2 illustrates the possible mechanism proposed to explain the catalytic activity of RuO_2-TiO_2/PANI and RuO_2-TiO_2/DPA/PANI nanocomposites with respect to the degradation reaction of MO dye in the dark.

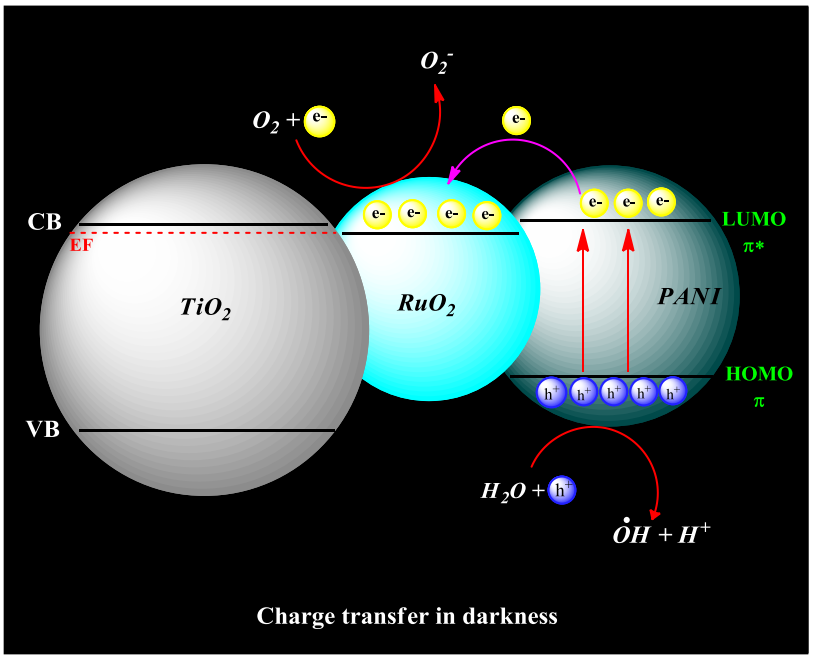

Scheme 2. Charge transfer in RuO_2-TiO_2/DPA/PANI nanocomposite in darkness.

3.5.2. Kinetic analysis under visible light

UV-vis spectra show a decrease in the intensity of the absorption bands of the MO with the degradation time, after 15 min, the bands disappear completely which is due to the degradation and the mineralization of MO under the catalytic effect of RuO_2-TiO_2 nanoparticles (Fig. 17b); this is testified by the C/C_0 plots as a function of the degradation time (Fig. 18). The apparent rate constant (k_{app}) found from the curve Ln C_0/C vs t(min) is 0.106 min^{-1} (Fig. 19).

The photocatalytic activity of RuO_2-TiO_2 mixed oxide under sunlight has already been confirmed by other researchers [21,29, 86], the RuO_2-TiO_2 heterostructure exhibits better catalytic performances than that of pure TiO_2 and RuO_2 [21,6,86]. This is due to the improved separation of the electron-hole pairs and the acceleration of the charge transport at the interface RuO_2//TiO_2 [21,6].

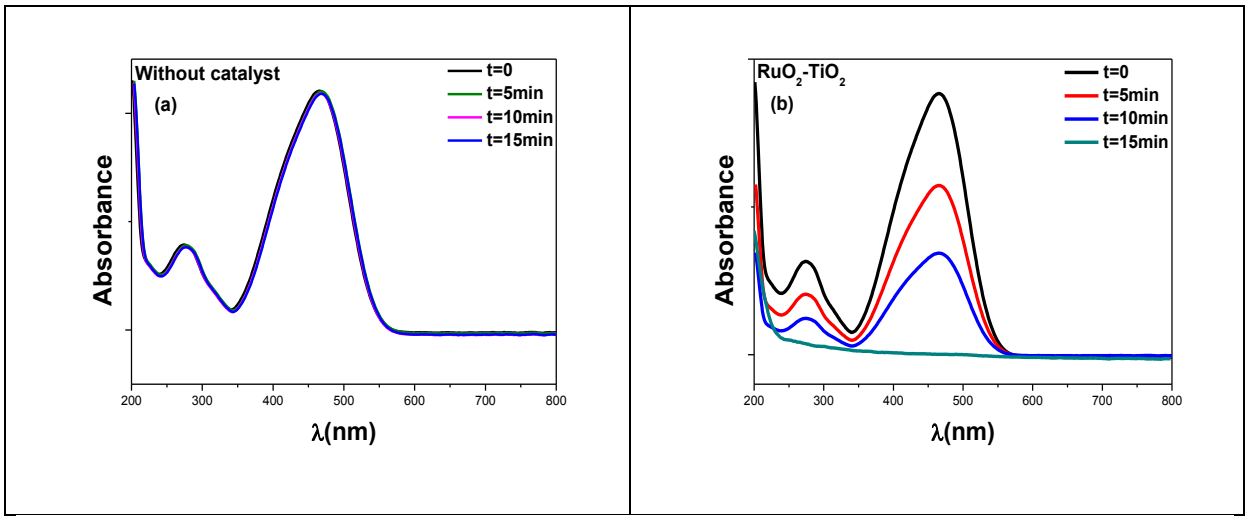

Figure 17. UV-vis absorption spectra of MO solutions before and after irradiation for various periods. (a) without catalyst, (b) RuO_2-TiO_2 NPs.

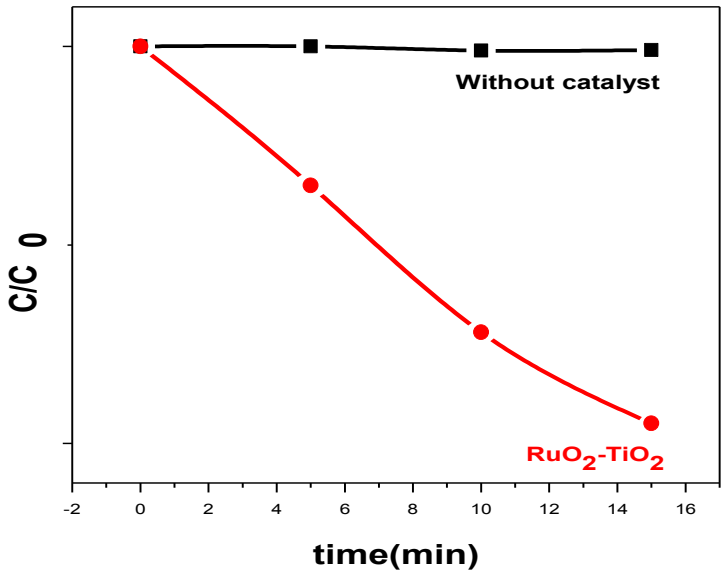

Figure 18. Kinetics of photodegradation of Methyl Orange solution without and in the presence of RuO_2-TiO_2 catalyst under visible light.

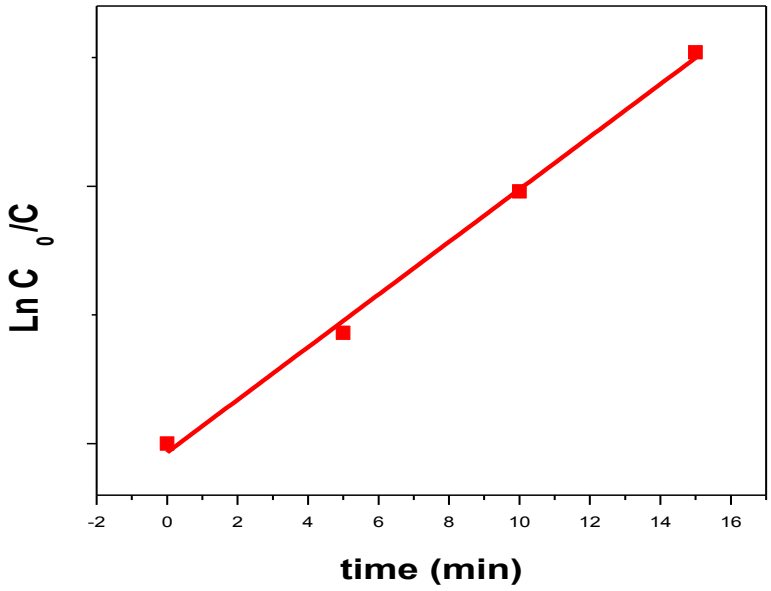

Figure 19. First order linear transforms of the degradation of methyl orange under visible light in the presence of RuO_2-TiO_2 NPs (R= 0.9955).

RuO_2 and TiO_2 have the same Fermi level; this leads to the formation of electron depletion region at Schottky barrier. Under visible light, the electrons of the TiO_2 valence band (VB) are excited and move towards the conduction band (CB), leaving holes in VB. The electron depletion region formed at the Schottky barrier leads to an internal electric field at the TiO_2//RuO_2 interface. This field is responsible on the separation of the photogenerated electron-hole pairs. The holes and the electrons photogenerated are the most important species in the photocatalytic systems. The electrons on the CB of TiO_2 participate in the formation of the $O_2^{\bullet -}$ anion radicals and the holes are responsible for the formation of the $OH^{\bullet}$ radicals from water and hydrogen peroxide. In addition, the photogenerated holes which are transferred to RuO_2 leads to the oxidation of H_2O molecules physisorbed on the surface of the nanoparticles, forming oxidizing hydroxyl species which are strongly active in the photocatalytic degradation processes. The mechanism of electron-hole pair separation and the formation of the active species under visible light are described by Scheme 3 and the equations (1-6).

$RuO_2\text{-}TiO_2 + h\upsilon \longrightarrow h^+(RuO_2) + e^-(TiO_2)$ **(1)**

$H_2O_2 + h^+ \longrightarrow 2\dot{O}H$ **(2)**

$H_2O + h^+ \longrightarrow \dot{O}H + H^+$ **(3)**

$O_2 \longrightarrow O_2^*$ **(4)**

$O_2^* + 1e^- \longrightarrow \dot{O}_2^-$ **(5)**

$\overset{\ominus}{O}\text{—}\dot{O} \longrightarrow H\text{—}O\text{—}\dot{O}$ **(6)**

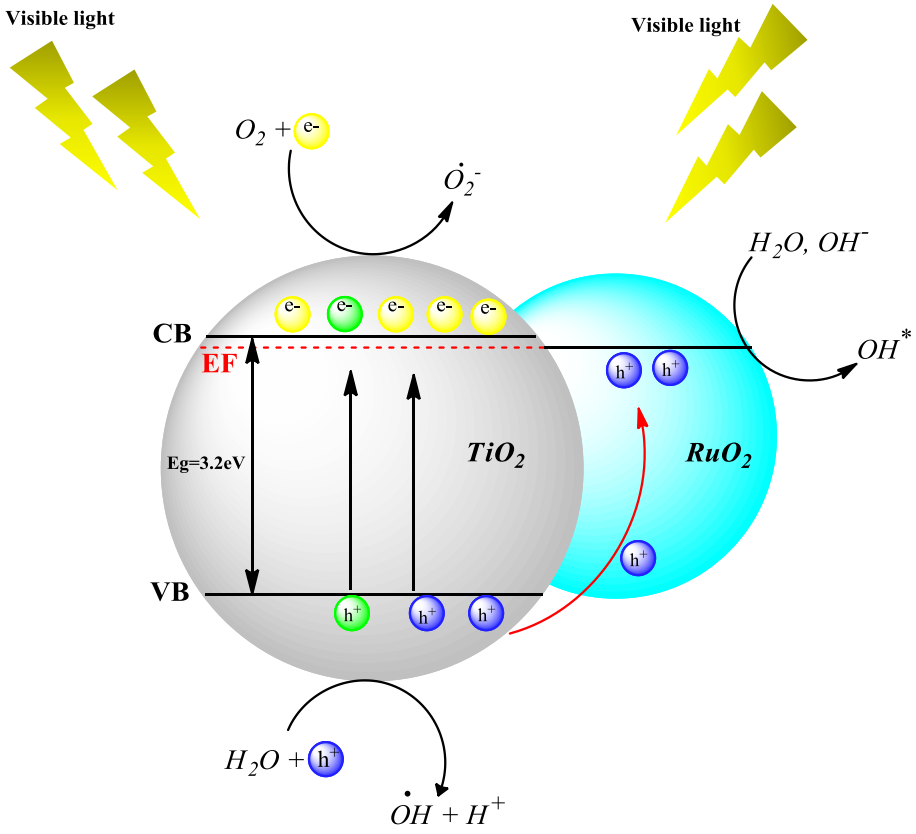

Scheme 3. Charge transfer in $RuO_2\text{-}TiO_2$ nanoparticles under visible light.

3.5.3. Degradation extent (%) of Methyl Orange

The percentage of the degradation of the dye was calculated for various degradation times from the following equation [78]:

$$\% = \frac{C_0 - C}{C_0} * 100$$

Where C_0 is the initial concentration of dye and C is the concentration of MO at time t.

The results are summarized in Table 2.

Table 2. Degradation extent (%) of Methyl Orange without and with different catalysts under visible light and darkness.

	Darkness				**Visible light**		
Time (min) / **Catalysts**	**0**	**55**	**75**	**95**	**5**	**10**	**15**
without	0	0	0	0	0	0	0
RuO_2-TiO_2	0	0	0	0.1	36	62	98
RuO_2-TiO_2/PANI	0	57	74	98.7	_	_	_
RuO_2-TiO_2/DPA/PANI	0	67	99.4	_	_	_	_

The photocatalytic effect of RuO_2-TiO_2 under visible light is known, the degradation extent of Methyl Orange increases with the time of the photocatalytic reaction until total decomposition of the dye. The presence of the polyaniline brings benefits not only to the degradation rate and extent of Methyl Orange, but also allows a gain of energy, the addition of PANI to the nanoparticles of RuO_2-TiO_2 mixed oxide makes it a first-class catalyst operating without any irradiation. The degradation percentage of Methyl Orange is higher with RuO_2-TiO_2/DPA/PANI compared to that obtained with RuO_2-TiO_2/PANI nanoparticles in darkness; this depends on the electron exchange between TiO_2 and RuO_2 on the one hand and between RuO_2-TiO_2 and PANI which is known as an electron donor, on the other hand. This again highlights the spectacular role of the diazonium salt as a coupling agent for attaching the PANI to RuO_2-TiO_2 nanoparticles surface.

3.5.4. Degradation products: mineralization

MO solution before and after the degradation process was analyzed by infrared spectroscopy in order to identify and to determine the nature of the final products formed with and without irradiation, under the catalytic effect of the various catalysts (RuO_2-TiO_2 under light visible), RuO_2-TiO_2/PANI and RuO_2-TiO_2/DPA/PANI in the dark). Figure 20 illustrates the spectra obtained between 4000 and 400 cm^{-1}.

The spectrum of the initial MO solution (Fig. 20a) exhibits a peak around 3429 cm^{-1}, attributed to the N-H stretching vibration. The bands at 2905 and 2854 cm^{-1} are assigned to the C-H stretching vibration of -CH_3. The peaks at 1610 and 1540 cm^{-1} are due to the single bond C-C vibration in the aromatic core. At 1426 cm^{-1} is located the N=N vibration band [87,88]. The band centred at 1380 cm^{-1} is corresponding to the vibration -S=O. Two peaks are located at 1225 and 1170 cm^{-1} and are attributed to C-N vibration. The C-H stretching vibrations of the benzene ring are observed at 1030, 847, 816 and 697 cm^{-1} [88]. The bands 624 and 570 cm^{-1} are due to the -C-S stretching vibration.[89]

The IR spectra of the degradation products of MO in the presence of RuO_2-TiO_2 under visible light (Fig. 20b), RuO_2-TiO_2/PANI (Fig. 20c) and RuO_2-TiO_2/DPA/PANI (Fig. 20d) in the darkness shows the disappearance of most of the characteristic MO vibration bands, with the appearance of a large and intense peak around 3300 cm^{-1}, corresponding to the vibration of H_2O molecules [90]. We also recorded another band at 1637 cm^{-1}, which is due to HCO_3^- from CO_2 dissolved in water [91]. These results confirm the decomposition as well as the total mineralization of Methyl Orange and highlight the outstanding catalytic effect of the catalysts used.

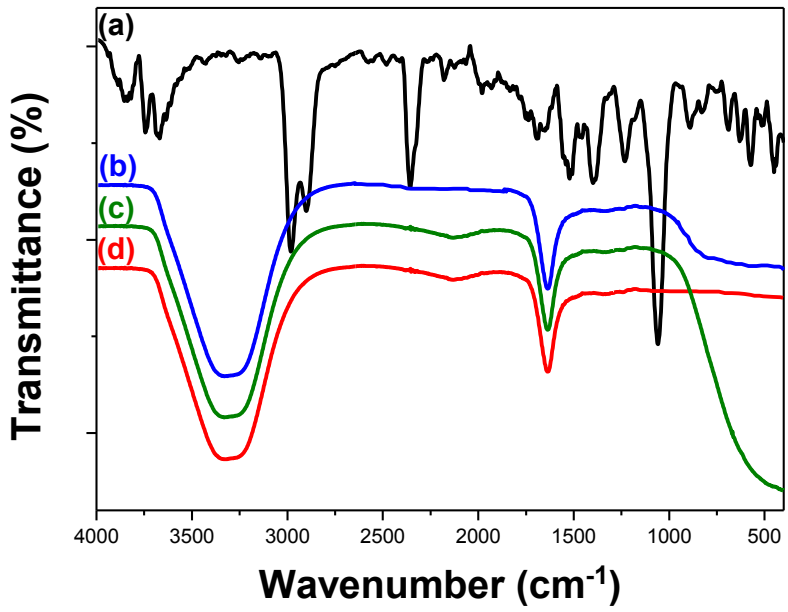

Figure 20. FTIR spectra of Methyl Orange solutions before (a), and after degradation using RuO_2-TiO_2 NPS under visible light (b), RuO_2-TiO_2/PANI (c) and RuO_2-TiO_2/DPA/PANI (d) in the dark.

3.5.5. Stability of the catalysts

The long term use of a catalyst rests on its stability [75]. This property is very important for the evaluation of catalysts and their application [92]. The catalysts already used in the degradation of the MO under and without irradiation were separated, washed several times with the di-ionized water and ethanol and dried at room temperature overnight before reusing them again in the degradation of a new solution of MO. The experiment was carried out under the same conditions as described above (concentration of the solutions, pH, mass of the catalysts, degradation time, hυ, dark).

It was found that all the catalysts present a high stability even after several successive catalytic runs. The results show no decrease in MO degradation rate until the 6th, 8th and 10th test in the presence of RuO_2-TiO_2, RuO_2-TiO_2/PANI and RuO_2-TiO_2/DPA/PANI, respectively, making these catalysts promising for several applications, especially in industry (Fig. 21).

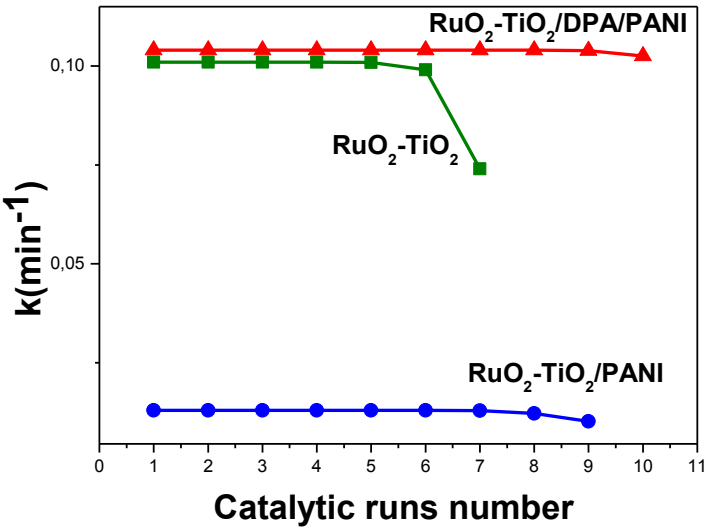

Figure 21. Plot of kinetic constants vs photocatacatalyzed test number in the presence of RuO_2-TiO_2, RuO_2-TiO_2/PANI and RuO_2-TiO_2/DPA/PANI.

4. Conclusion

A novel catalytic support based on RuO_2-TiO_2 mixed oxide NPs coated PANI was prepared by in situ oxidative polymerization of aniline on diazonium-modified RuO_2-TiO_2 heterostructure. We have demonstrated through this study that this new association combining different materials of type metal-semiconductor n heterostructure and conductive polymer offers spectacular properties to the final materials. The nanocomposites show enhanced catalytic activity in the decomposition of MO in darkness; this activity depends on the presence of PANI on the one hand, and its amount in the final nanocomposite on the other hand, namely. Indeed, the RuO_2-TiO_2 mixed oxide is an excellent photocatalyst under visible light, while the nanocomposite RuO_2-TiO_2/DPA/PANI exhibits significantly improved catalytic performance in the dark compared to RuO_2-TiO_2/PANI nanocomposite. This stresses the role of the diazonium salt as coupling agent for PANI; it gives the nanocomposite a better thermal and chemical stability, and harnesses adhesion of PANI on the surface of RuO_2-TiO_2 NPs. The enhancement in catalytic activity of designed materials is associated with a synergistic effect between PANI and RuO_2 metal and RuO_2-TiO_2 interfacial contacts which result in the separation of electron-hole pairs and the reduction of its recombination rate. Therefore, RuO_2-TiO_2/DPA/PANI catalyst is highly stable and reusable up to 9 times without any loss in catalytic activity, which shows a promising potential for practical applications.

In a serendipitous way, while our primary goal was to test the ability of polyaniline to improve the visible light photoactivity of RuO_2-TiO_2 mixed oxide NPs, we have designed in a unique way, unprecedented and highly efficient catalysts for the degradation of pollutants in the darkness. The new catalyst design process is scalable which opens new windows for the general degradation of organic pollutants.

Acknowledgements

FM would like to thank Campus France for the provision of PROFAS B+ fellowship No 880797C. All authors are indebted to NATO for financial support through the SfP program (CATALTEX project No 984842).

Conflicts of interest

There are no conflicts to declare

References

[1] C. C. Nguyen, N. N. Vu, T. O. Do, *J. Mater. Chem. A* **2016**, 4, 4413-4419
[2] L. Wu, D. Bresser, D. Buchholz, G. A. Giffin, C. R. Castro, A. Ochel and S. Passerini, *Adv. Energy. Mater.* **2015**, *5*, 2.
[3] M. Tahir and N. S. Amin, *Appl. Catal. B: Environ* **2015**, *162*, 98-109.
[4] F. Mushtaq, A. Asani, M. Hoop, X. Z. Chen, D. Ahmed, B. J. Nelson, S. Pané. *Adv. Funct. Mater* **2016**, *26*(38), 6995-7002.
[5] W. Zhou, Z. Yin, Y. Du, X. Huang, Z. Zeng, Z. Fan, H. Liu, J. Wang and H. Zhang, *Small* **2013**, *9*(1), 140-147.
[6] M. T. Uddin, Y. Nicolas, C. Olivier, T. Toupance, M. M. Müller, H. J. Kleebe, K. Rachut, J. Ziegler, A. Klein and W. Jaegermann, *J. Phys. Chem C* **2013**, 117(42), 22098-22110.
[7] B. Cao, G. Li and H. Li, *App.Catal. B: Environ.* **2016**, *194*, 42-49.
[8] A. K. Chakraborty, M. E. Hossain, M. M. Rhaman and K. M. A. Sobahan, *J. Environ. Sci* **2014**, 26(2), 458-465.
[9] P. Kongsong, L. Sikong, M. Masae, W. Singsang, S. Niyomwas and V. Rachpech, *Songklanakarin J. Sci. Technol* **2018**, *40*(3).
[10] L. Zhang, W. Yu, C. Han, J. Guo, Q. Zhang, H. Xie, Q. Shao, Z. Sun and Z. Guo, J. Electrochem. Soc **2017**, 164, H651–H656.
[11] A. V. Rudakova, A. V. Emeline and D. W. Bahnemann, *J. Phys. Chem C.* **2019**.
[12] D. P. Wang, H. C. Zeng, *Chem. Mater **2009**, 21*(20), 4811-4823.

[13] P. Eskandari, M. Farhadian, A. R. Solaimany Nazar and B. H. Jeon, *Ind. Eng. Chem. Res* **2019**, 58, 2099−2112.
[14] L. Yao, W. Wang, L. Wang, Y. Liang, J. Fu and H. Shi, *Inter. J. Hydrogen Energy* **2018**, *43*(33), 15907-15917.
[15] Z. Chen, Y. Gao, Q. Zhang, L. Li, P. Ma, B. Xing and Z. Zhang, *J. Alloys. Compd* **2019**, *774*, 873-878.
[16] J. Saavedra, C. J. Pursell and B. D. Chandler, *J. Am. Chem. Soc* **2018**, *140*(10), 3712-3723.
[17] C. Zhang, Y. Zhou, Y. Zhang, S. Zhao, J. Fang, X. Sheng, *Appl. Organomet. Chem* **2018**, 32(3), e4160.
[18] F. Wang, R. J. Wong, J. H. Ho, Y. Jiang, R. Amal, *ACS appl. Mater. Inter **2017**, 9*(36), 30575-30582.
[19] J. Tian, Z. Zhao, A. Kumar, R. I. Boughton and H. Liu, *Chem. Soc. Rev* **2014**, *43*(20), 6920-6937.
[20] V. Panić, A. Dekanski, G. Wang, M. Fedoroff, S. Milonjić and B. Nikolić, *J. Colloid. Interface Sci* **2003**, *263*(1), 68-73.
[21] J. Tian, X. Hu, N. Wei, Y. Zhou, X. Xu, H. Cui and H. Liu, *Sol. Energy Mater. Sol. Cells* **2016**, *151*, 7-13.
[22] L.A. Näslund, C. M. Sánchez-Sánchez, A. S. Ingason, J. Bäckström, E. Herrero, J. Rosen and S. Holmin, *J. Phys. Chem C* **2013**, *117*(12), 6126-6135.
[23] T. Mitsuhashi and A. Watanabe, *J. Therm. Anal. Calorim.* **2000**, *60*(2), 683-689.
[24] J. Riga, C. Tenret-Noel, J. J. Pireaux, R. Caudano, J. J. Verbist and Y. Gobillon, *Phys. Scr* **1977**, *16*(5-6), 351.
[25] A. A. Ismail, D. W. Bahnemann and S. A. Al-Sayari, *App. Catal A: Gen* **2012**, *431*, 62-68.
[26] L. M. Silva, R. P. dos Santos, C. C. Morais, C. L. Vasconcelos, C. A. Martínez-Huitle and S. S. Castro, *J. Electrochim. Soc* **2017**, *164*(13), E489-E495.
[27] Y. Jiao, H. Jiang and F. Chen, *Acs. Catal* **2014**, *4*(7), 2249-2257.
[28] K. Kuramasu, S. Saito, K. Okano and Y. Takahashi, *J. Ceram. Soc. Jpn* **1996**, *104*(1213), 844-849.
[29] A. A. Ismail, L. Robben and D. W. Bahnemann, *Chem.Phys.Chem* **2011**, *12*(5), 982-991.
[30] V. Houšková, V. Štengl, S. Bakardjieva, N. Murafa and V. Tyrpekl, *Appl. Catal. B: Environ* **2009**, *89*(3-4), 613-619.
[31] P. B. Amama, K. Itoh and M. Murabayashi, *J. mater.Sci.* **2004**, *39*(13), 4349-4351.
[32] M. Košević, S. Stopic, V. Cvetković, M. Schroeder, J. Stevanović, V. Panić, and B. Friedrich, *Appl. Surf. Sci* **2019**, *464*, 1-9.
[33] V. Panić, A. Dekanski, S. Milonjić, R. Atanasoski and B. Nikolić, *Electrochim. Acta* **2000**, *46*(2-3), 415-421.
[34] D. Mitrovic, V. Panic, A. L. E. K. S. A. N. D. A. R. Dekanski, S.Milonjic, R. A. D. O. S. L. A. V. Atanasoski and B. Nikolic, *J.Serb. Chem. Soc* **2001**, *66*(11/12), 847-858.
[35] J.S. C. Buenviaje, K. A. S. Usman and J. L. M.Payawan, In *AIP Conference Proceedings* (Vol. 1958, No. 1, p. 020015).2018, AIP Publishing.
[36] L. Gnanasekaran, R. Hemamalini and M. Naushad, *Desalination. Water Treat* **2018**, *108*, 322-328.
[37] Z. Zhao, Y. Zhou, W. Wan, F. Wang, Q. Zhang and Y. Lin, *Mater. Lett* **2014**, *130*, 150-153.
[38] J. Li, Q. Xiao, L. Li, J. Shen, D. Hu, *Appl. Surf. Sci* **2015**, 331, 108–114.
[39] F. Mousli, A. Chaouchi, S. Hocine, A. Lamouri, M.R. Vilar, A. Kadri and M. M. Chehimi, *App. Surf. Sci* **2019**, 465, 1078–1095.

[40] M. M. Chehimi (Ed.). Aryl diazonium salts: new coupling agents in polymer and surface science. John Wiley & Sons **2012**.
[41] A. A. Mohamed, Z. Salmi, S. A. Dahoumane, A. Mekki, B. Carbonnier and M. M. Chehimi, *Adv. Colloid. Interface sci* **2015**, *225*, 16-36.
[42] F. Mirkhalaf and J. E. Graves, *Chem. Pap.* **2012**, 66, 472-483.
[43] Z. Salmi, S. Gam-Derouich, S. Mahouche-Chergui, M. Turmine and M. M. Chehimi, *Chem. Pap* **2012**, *66*, 369-391.
[44] M. Lo, R. Pires, K. Diaw, D. Gningue-Sall, M. A. Oturan, J. J. Aaron and M. M. Chehimi, *Surfaces* **2018**, *1*, 43–58.
[45] F. C. Marques, M. C. Canela and A. M. Stumbo, *Top. Catal* **2017**, *60*(15-16), 1196-1209.
[46] Y. Li, Z. Qin, H. Guo, H. Yang, G. Zhang, S. Ji and T. Zeng, *PloS one* **2014**, *9*(12), e114638.
[47] S. O. N. G. Mianxince, B. Liang, Z. Tianliang and Z. H. A. O. Xiaoyong, *J. Rare Earths* **2008**, *26*(5), 693-699.
[48] T. Uchikoshi, T. S. Suzuki, S. Iimura, F. Tang and Y. Sakka, *J. Eur. Ceram. Soc* **2006**, 26(4-5), 559-563.
[49] P. Gogoi, T.S. Kumar, P. Sharma and D. Pamu, *J. Alloys Comp* **2015**,619, 527-537.
[50] A. Tabib, N. Sdiri, H. Elhouichet and M. Férid, *J. Alloys Compd* **2015**, *622*, 687-694.
[51] A. M. Badr, H. A. Elshaikh and I. M. Ashraf, *J. Mod. Phys* **2011**, *2*(01), 12.
[52] K. Fröhlich, V. Cambel, D. Machajdík, P. K. Baumann, J. Lindner, M. Schumacher and H. Juergensen, *Mater. Sci. Semicond. Proc* **2002**, *5*(2-3), 173-177.
[53] E. V. Jelenkovic, K. Y. Tong, W. Y. Cheung and S. P. Wong, *Microelectron. Eng* **2004**, *71*(3-4), 237-241.
[54] J. H. Huang and J. S. Chen, *Thin Solid Films* **2001**, *382*(1-2), 139-145.
[55] Y. Cao, P. Smith and A. J. Heeger, *Synth. Met* **1992**, 48, 91.
[56] N. H. Salah. PhD Thesis, Université de Grenoble. **2012**. https://tel.archives-ouvertes.fr/tel-00781668/ . Last accessed 28 mars 2019.
[57] L. B. Gao, S. H. Liu, L. Y. Zhang, L. X. Shi and Z. N. Chen, *Organomet* **2006**, *25*(2), 506-512.
[58] M. T. Uddin. PhD Thesis, Université Sciences et Technologies-Bordeaux I. **2013**. https://tel.archives-ouvertes.fr/tel-00879226/. Last accessed 01 April 2019.
[59] X. Li, D. Wang, G. Cheng, Q. Luo, J. An and Y. Wang, *Appl. Catal B: Environ* **2008**, 81(3-4), 267-273.
[60] S. Wahyuni, E. S. Kunarti, R.T. Swasono and I. Kartini, Indones. *J. Chem.* **2018**, 18, 321-330.
[61] S. Masid, R. Tayade and N. N. Rao, *Int. J. Photocatal. Photon* **2015**, 119, 190-203.
[62] S. Min.; F. Wang and Y. Han, J. Mater. Sci **2007**, 42, 9966-9972.
[63] S. Musić, S. Popović, M. Maljković, K. Furić and A. Gajović, *Mater. Lett* **2002**, *56*(5), 806-811.
[64] Y. R. Leroux, H. Fei, J. M. Noël, C. Roux and P. Hapiot, *J. Am. Chem. Soc* **2010**, *132*(40), 14039-14041.
[65] S. A. Orefuwa, M. Ravanbakhsh, S. N. Neal, J. B. King and A. A. Mohamed, *Organomet* **2013**, *33*(2), 439-442.
[66] M. Tanzifi, S. H. Hosseini, A. D. Kiadehi, M. Olazar, K. Karimipour, R. Rezaiemehr and I. Ali, *J. Mol. Liquids* **2017**, *244*, 189-200.
[67] M. Baibarac, I. Baltog, S. Frunza, A. Magrez, D. Schur and S. Y. Zaginaichenko, *Diamond. Relat. Mater* **2013**, *32*, 72-82.
[68] Y. M. Chen, A. Korotcov, H. P. Hsu, Y. S. Huang and D. S. Tsai, *New. J. Phys* **2007**, *9*(5), 130.

[69] M. C. Ceballos-Chuc, C. M. Ramos-Castillo, J. J. Alvarado-Gil, G. Oskam and G. Rodríguez-Gattorno, *J. Phys. Chem C* **2018**, *122*(34), 19921-19930.
[70] S. Y. Mar, C. S. Chen, Y. S. Huang and K. K. Tiong, *Appl. Surf. Sci* **1995**, *90*(4), 497-504.
[71] C. Barthet, S. P. Armes, M. M. Chehimi, C. Bilem and M. Omastova, *Langmuir* **1998**, *14*, 5032-5038.
[72] N. Bıçak, B. F. Şenkal and E. Sezer, *Synth. Met* **2005**, *155*(1), 105-109.
[73] Y. Wang, H. Zheng, L. Jia, H. Li, T. Li, K. Chen and Y. Gu, *J. Macromol. Sci. Part A* **2014**, *51*(7), 577-581.
[74] Z. Wang, L. Shen, S. Zhu, *Int. J. Photoenergy. **2012***. Article ID 202519, 6 page. https://doi.org/10.1155/2012/202519.
[75] A. Ammuri, S. Hejiouej, K. Ziat and M. Saidi, *Mater. Environ. Sci. **2014**, 5*, 2066-2072.
75 P. Niu, *Asian. J. Chem **2014**, 5*, 2066-2072.
[76] L. C. Chen, F. R. Tsai and C. M. Huang, *J. Photochem. Photobiol A: Chem* **2005**, *170*(1), 7-14.
[77] M. T. Islam, H. Jing, T. Yang, E. Zubia, A. G. Goos, R. A. Bernal, C. E. Botez, M. Narayan, C. K. Candace and J. C. Noveron, *J. Environ. Chem. Eng* **2018**, 6, 3827–3836.
[78] T. A. Saleh and V. K. Gupta, *J. Colloid. Interface. Sci* **2012**, 371(1), 101-106.
[79] H. Chen, J. Motuzas, W. Martens and J. C. D. da Costa, *Appl. Catal B: Environ* **2018**, 221, 691-700.
[80] N. A. Zubir, C. Yacou, J. Motuzas, X. Zhang, X. S. Zhao and J. C. D. da Costa, *Chem. Commun* **2015**, 51(45), 9291-9293.
[81] J. Zheng, Z. Gao, H. He, S. Yang and C. Sun, *Chemosphere* **2016**, 150, 40-48.
[82] X. Liang, Y. Zhong, S. Zhu, J. Zhu, P. Yuan, H. He and J. Zhang, *J. hazard. Mater* **2010**, 181(1-3), 112-120.
[83] M. Y. Leiw, G. H. Guai, X. Wang, M. S. Tse, C. M. Ng, O. K. Tan, *J. Hazard. Mater* **2013,** 260, 1-8.
[84] M. Sun, Y. Jiang, F. Li, M. Xia, B. Xue, D. Liu, *Mater. Trans.* **2010**, 51(11), 1981-1989.
[85] S. Wei, X. Hu, H. Liu, Q. Wang, C. He, *J. Hazard. Mater* **2015**, *294*, 168-176.
[86] M. T. Uddin, O. Babot, L. Thomas, C. Olivier, M. Redaelli, M. D'Arienzo, T. Toupance, *J. Phys. Chem C* **2015**, *119*(13), 7006-7015.
[87] P. Li, Y. Song, S. Wang, Z. Tao, S. Yu, and Y. Liu, *Ultrason. Sonochem* **2014**, *22*, 132-138.
[88] T. Shen, C. Jiang, C. Wang, J. Sun, X. Wang, X. Li, *RSC. Adv* **2015**, *5*(72), 58704-58712.
[89] G. K. Parshetti, A. A. Telke, D. C. Kalyani, S. P. Govindwar, *J. Hazard. Mater* **2010**, *176*(1-3), 503-509.
[90] M. S. Babushkina, L. P. Nikitina, A. G. Goncharov, N. I. Ponomareva, *Geol. Ore Deposits* **2009**, *51*(8), 712-722.
[91] E. Garand, T. Wende, D. J. Goebbert, R. Bergmann, G. Meijer, D. M. Neumark, K. R. Asmis, *J. Am. Chem. Soc* **2009**, *132*(2), 849-856.
[92] L. Ge, C. Han, J. Liu, *Appl. Catal B: Environ **2011**, 108*, 100-107.

Chapter 4: Design and catalytic properties mixed oxide-modified woven cotton fabrics for the visible light degradation of hazardous organic pollutants

Mixed oxide-polyaniline composite-coated woven cotton fabrics for the visible light catalyzed degradation of hazardous organic pollutants

Fatima Mousli*, Ahmed M. Khalil, François Maurel Abdelaziz Kadri, Mohamed M. Chehimi

Paper submitted to Cellulose on 08 October 2019

Graphical abstract

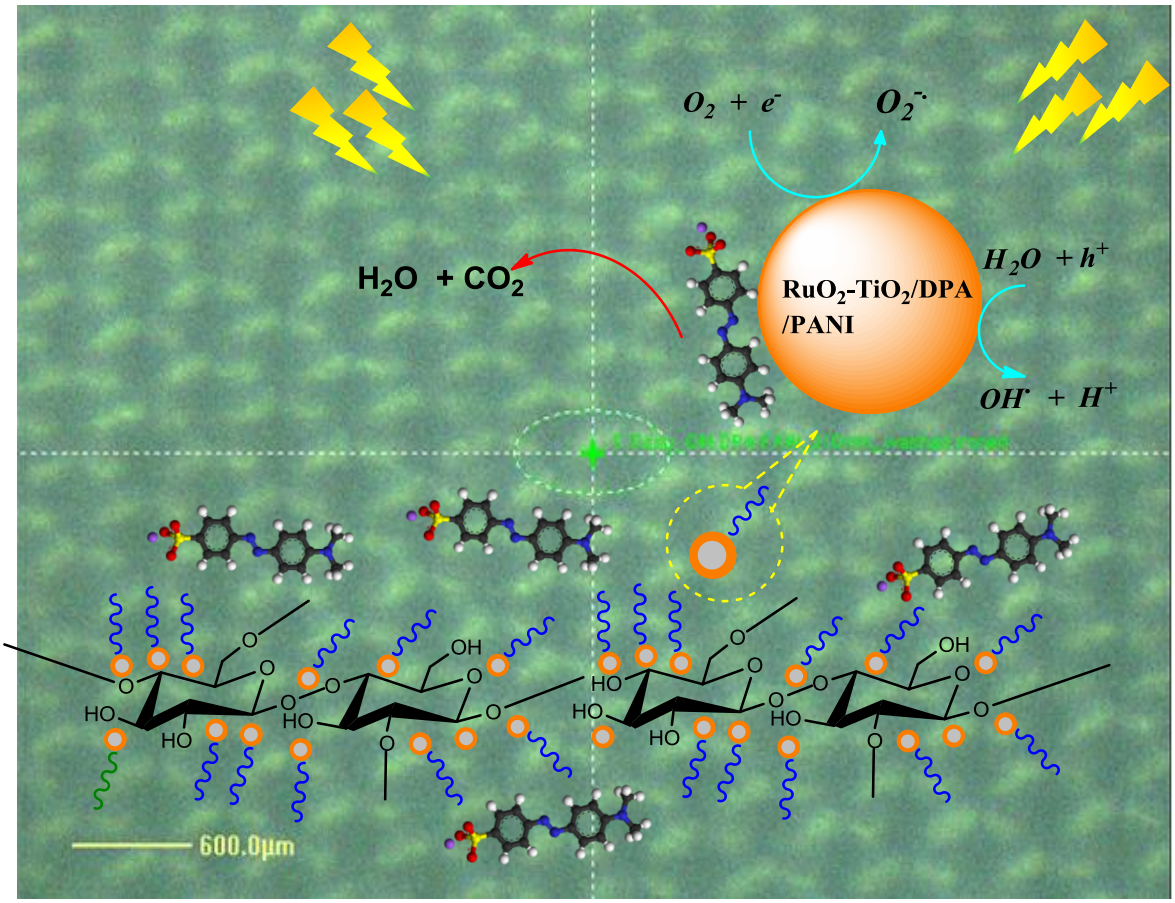

Objectives

The objective of this part is the conception of new efficient, stable and recyclable catalytic hybrid materials by combining the physico-chemical and the catalytic performances of RuO_2-TiO_2-based nanocomposites and the flexibility of cellulose, and this by a very easy and

effective process of soft chemistry. We have questioned the efficiency of the textile photocatalysts in the degradation of organic pollutants, and its recovery after several stresses such as color fastness, sonication, machine washing and ironing.

Method

This section of the thesis deals with the design of functional cotton fabrics coated with RuO_2-TiO_2-based photocatalysts. The modified woven fabrics were obtained by a dip-coating process in a mixed oxide suspension and at neutral pH. A layer of PANI was prepared by in situ oxidative polymerization of the aniline monomer on 4-diphenylamine-diazonium salt modified RuO_2-TiO_2 nanoparticles coated cotton fabric. The fabrics loaded with the nanocatalysts were characterized by XRD, SEM-EDS, FTIR, Raman and XPS then used in the photodegradation of methyl orange dye under visible light.

Significance

This work paves the way to the scalable design of robust textile catalysts based on cotton impregnated with diazonium-modified RuO_2-TiO_2 nanoparticles and top coated with PANI.

Results

- Successful design of cotton fabric coated with RuO_2-TiO_2-based hybrid photocatalyst nanocomposite.
- The catalyst-coated cotton fabrics have been characterized by IR, Raman, XRD, SEM-EDS and XPS.
- The diphenylamine adhesive layer served as a coupling agent for the in situ prepared polyaniline film thus imparting strong adhesion of the latter to RuO_2-TiO_2 nanoparticles and cotton fabric surface.
- The cotton fabric hybrid materials exhibit excellent photocatalytic activity and led to the complete mineralization of Methyl Orange dye under visible light. This activity depends strongly on the amount of PANI in the nanocomposite photocatalyst.
- The cotton fabric/RuO_2-TiO_2/DPA@polyaniline obtained by in situ polymerization on RuO_2-TiO_2/DPA coated cotton fabric is more stable resistant to durability tests (insolation, washing, and washing followed by ironing) than other nanocomposites thanks to the polyaniline which constitutes a protective layer.

Mixed oxide-polyaniline composite-coated woven cotton fabrics for the visible light catalyzed degradation of hazardous organic pollutants

Fatima Mousli[1,2]*, Ahmed M. Khalil[3], François Maurel[2]
Abdelaziz Kadri[1], Mohamed M. Chehimi[4,]*
[1] Laboratoire de Physique et Chimie des Matériaux (LPCM), Faculté des Sciences,
Université Mouloud Mammeri, Tizi-Ouzou 15000, Algeria.
[2] Sorbonne Paris Cité, Université Paris Diderot, CNRS, ITODYS (UMR 7086), 75013 Paris, France
[3] Photochemistry Department, National Research Centre, 33 El-Buhouth Street, Dokki, Giza 12622, Egypt
[4] Université Paris Est, CNRS, ICMPE (UMR 7182), 94320 Thiais, France

Abstract

Clean water and sea free of organic pollutants are among the 17 United Nation Sustainable Development Goals (SDGs). In this global concern, the design of efficient, stable and recyclable catalytic materials remains challenging. In this context, we designed a series of mixed oxide-modified cotton fabrics and their related composites and interrogated their propensity to catalyze the degradation of methyl orange (MO) (a model pollutant). More specifically, functional cotton fabrics (CF) coated with RuO_2-TiO_2 based-photocatalysts were obtained by dip-coating method at neutral pH. A layer of Polyaniline (PANI) was prepared by in situ oxidative polymerization of the aniline monomer on 4-diphenylamine diazonium salt (DPA) modified-RuO_2-TiO_2 nanoparticles (NPs) coated-CF. The modified CFs catalyzed photodegradation and mineralization of MO under visible light, which depended on polyaniline mass loading. The CF/RuO_2-TiO_2/DPA@PANI obtained by in situ polymerization was the best catalyst due to DPA adhesive layer for polyaniline to RuO_2-TiO_2, and the strong attraction force between cellulose OH groups and anilinium during polymerization. The photodegradation rate constant was 0.101, 0.0532, 0.0775 and 0.0828 min^{-1} for RuO_2-TiO_2/DPA@PANI, RuO_2-TiO_2, RuO_2-TiO_2/PANI and RuO_2-TiO_2/DPA/PANI coated-CFs, respectively. The catalytic activity is favored by the photoactive species ($OH^{\bullet}$,$O_2^{-\bullet}$) which are formed by the excitation of electrons under visible light but also by the electronic exchanges at the RuO_2//TiO_2, RuO_2-TiO_2//PANI and RuO_2-TiO_2/PANI//CF interfaces.
CF/RuO_2-TiO_2/DPA/PANI photocatalyst was stable under simulated sunlight and reusable three times. A mechanism is proposed to account for the efficient CF catalytic properties.

Keywords:
Cotton fabric, RuO_2-TiO_2, diazonium salt, polyaniline, photocatalysis**.**

Corresponding authors
F. Mousli : fatima.mousli@yahoo.fr ; M. M. Chehimi : chehimi@icmpe.cnrs.fr

1. Introduction

There is an ever growing demand for specialty textile with one specific or multiple functions. Indeed, much has been achieved recently in this domain, namely textiles with odour elimination property (Wang, Lu, Wang & Wang, 2019); Zhu et al., 2019), textiles for tissue engineering (Augustine et al., 2017) and wound healing (Kim, Cha & Gong, 2018), specialty textiles for military applications (Revaiah, Kotresh & Kandasubramanian, 2019), textiles for wearable electronics (Zhou et al., 2019), or catalytic applications (Fujii & Nakamura, 2013). Either woven or non-woven, cotton fibers remain the most used for clothing or specialty textiles due to the biodegradability, strong absorption capacity and porosity of these cellulosic fibers. (Ahmad, Kan & Yao, 2019)

One of the most common modifications of textile surfaces is dyeing. The process has been known for over 2000 years. It is based on textile surface chemistry in which the dye molecules react with a functional group of the textile surface (Mayer-Gall, Lee, Opwis, List & Gutmann, 2016).

Various strategies have been developed not only for the dyeing but also to give the fabric other functionalities namely the antibacterial activity, UV protection, self-cleaning, antifouling (Uddin et al., 2008; Wu, Ma, Pan, Chen, Sun., 2016; Avila Ramirez, Suriano, Cerrutti & Foresti, 2014; Hassan, 2017) and new properties such as better electrical conductivity, (Xu et al., 2016) hydro/oleo-phobia and ease of ironing (Zhou et al., 2019) The strong growing demand for functional textiles necessitates the development of inexpensive synthetic methods based on sustainable raw materials (cotton) while preserving the environment and the ecosystem. The easiest and most direct method for the development of functional cotton fabrics is the dip-coating method, which consists of incorporating the nanoparticles on the surface by direct emersion, leading to the formation of a fibrous surface loaded with NPs.

(Yang et al., 2013) have prepared a functional textile by assembling several positively charged NPs of Au on the surface of cotton fabric, by electrostatic interactions between the metal NPs and the surface of the textile. It has been found in the same study that the prepared materials exhibit excellent catalytic properties.

In situ synthesis was also described by (Xi et al., 2016) who developed catalytic cotton fabric loaded with palladium NPs composite material in the presence of polydopamine, acting as a reducing agent for the formation and the growth of palladium NPs on the textile surface.

Recently, another method has been developed and seems to be adopted in the preparation of functional textile surfaces; it is the photo-grafting approach, which generates superficial

radicals by exposing the textile surface to ultraviolet light. The radicals thus generated are able to fixing different types of organic molecules on the textile surface. .(Mayer-Gall, Lee, Opwis, List & Gutmann, 2016).

TiO_2 nanoparticles are widely used in the coating of fabric surfaces, designed for photocatalytic applications, thanks to these spectacular catalytic properties and its ability to increase the hydrophilic character of the fibrous surface. (Mishra & Butola, 2019) studied the degradation of rhodamine B under UV light using cotton fabric coated with TiO_2 NPs prepared via in situ solvothermal method.

The catalytic efficiency of the TiO_2-coated fabric is negligible under visible light, due to the low protonation of TiO_2 under visible radiation (Nosrati, Olad & Najjari, 2017).

Various components such as metal/non-metal, organic complexes and conductive polymers essentially polypyrrole and PANI have been used as sensitizers of TiO_2 impregnated on the textile surface, under visible light.

(Wang et al., 2019) have developed fabric-based materials loaded with TiO_2/g-C_3N_4 powder, with a simple layer-by-layer self-assembly strategy. They found that the materials are very photo-active in the degradation process of Rhodamine B and toluene under visible light, unlike TiO_2-laden tissue pieces.

Ag-doped TiO_2 coated cotton fabric was the subject of the study conducted by Mishra et al. (Mishra & Butola, 2019) the silver was added as TiO_2 dopant after depositing the latter in situ by sol gel on the textile surface. Their study highlights the interest of the addition of Ag by studying the degradation of Rhodamine B, it significantly improves the catalytic performance of the material under the UV light and visible.

The modification of the cotton fibers with TiO_2 and conducting polymer-based nanocomposite catalysts imparts new properties to the material, ensuring other applications to the cotton fabric support. However, despite the interest raised by the numerous strategies of making specialty catalytic textiles we found they are time consuming to be designed, employ expensive chemicals, require high temperature, and harsh conditions or aggressive chemicals that destroy the surface of the fabric. For these reasons, some authors classify the methods of modifying the fabric surface in two groups: chemical modification which has an impact on the composition of the fibers, and physical methods which rather alter the structure of the fibers (Shahidi, Wiener & Ghoranneviss, 2013). In the light of the advantages and limitations of the previously reported methods, we were motivated to design new catalytic textiles while maintaining the chemical composition as well as the starting structure of the fabric. This is

possible provided one operates under mild chemistry conditions, ensuring efficiency, robustness and high catalytic performances of materials.

In this work, we report a detailed study on the development of a functional cotton fabric modified with a nanocomposite catalysts based on RuO_2-TiO_2 NPs functionalized by diazonium salt and coated with polyaniline, active in darkness, and the evaluation of the degradation kinetics of Methyl Orange dye in an aqueous medium under visible light at multiple catalyst interfaces.

2. Experimental

2.1. Materials

RuO_2-TiO_2 nanoparticles (NPs), RuO_2-TiO_2/diphenylamine diazonium salt (DPA), RuO_2-TiO_2/polyaniline (PANI) and RuO_2-TiO_2/DPA/PANI nanocomposites were prepared as described in our previous paper (Mousli et al., 2019), H_2O_2 (14%), ethanol (Sigma-Aldrich, 99.9%), ammonium persulfate (APS, Aldrich, 98% purity), nitric acid (Carlo Erba, 60% purity), aniline (Aldrich, 99.5% pure), Methanol (Sigma-Aldrich, 95%), Methyl Orange (Sigma-Aldrich). Woven, bleached, and scoured cotton fabric (CF), Deionized water was used in the preparation of all solutions and samples.

2.2. Fabrication process

Several hybrid materials based on textiles have been prepared. To start, pieces of cotton fabric (2×2 cm) were simply soaked for 2h in suspensions of RuO_2-TiO_2 nanoparticle prepared by sol-gel, RuO_2-TiO_2/DPA, RuO_2-TiO_2/PANI and RuO_2-TiO_2/DPA/PANI nanocomposites in an equivalent mixture of di-ionized water and ethanol. The mass/volume ratio is 3g/l. These suspensions were ultrasonicated for 10 min before dipping the textile in order to well disperse the nanomaterials and reduce their aggregation in solution. This process was carried out at room temperature. The cotton fabrics samples were then extracted from the solution, rinsed several times with distilled water, sonicated for 5 min to remove any nanoparticles that were not impregnated between the fibers of the fabric, rinsed one last time with water and finally dried at room temperature for 12h. The obtained samples were denoted as CF/RuO_2-TiO_2, CF/RuO_2-TiO_2/DPA, CF/RuO_2-TiO_2/PANI and CF/RuO_2-TiO_2/DPA/PANI.

The CF/RuO_2-TiO_2/DPA sample was used for the preparation of an hybrid material denoted CF/RuO_2-TiO_2/DPA@PANI by the in situ oxidative polymerization of the aniline monomer on the surface of the fabric impregnated with RuO_2-TiO_2 mixed oxide already functionalized with diphenylamine diazonium. A solution containing 0.15g (1.61 mmol) of aniline monomer

and 0.05g (0.75 mmol) of nitric acid is stirred for 60 min to form the anilinium cation. The CF/RuO_2-TiO_2/DPA sample was then emerged into the mixture and kept under stirring for 60 min in order to have the anilinium cation on the surface of the modified fabric and to form the polymer on the surface. 0.2 g (0.87 mmol) of APS dissolved in 5 ml of distilled water were added dropwise to the solution, the mixture is stirred for 2h. Once the polymer began to form (appearance of a dark green color) on the surface of the modified fabric, we waited 15 min before stopping the reaction of the polymerization by separating the sample from the solution containing the monomer. The sample is then rinsed several times with methanol and water to remove the un-reacted monomer and dried at room temperature for 24h.

2.3. Characterization methods

Infrared spectra of pristine and printed cotton fabrics were investigated using a Bruker apparatus in the scan range of 4000-400 cm^{-1}, the analysis was to determine all the functional groups that are on the surface of the textile.

The Raman spectra were recorded on a Nicolet Raman 960 spectrometer operating at 633 nm.

The surface and the composition of the cotton modified with the different nanomaterials were performed with Merlin Carl Zeiss scanning electron microscope (SEM) fitted with an energy dispersive X-ray (EDX) analyzer.

X-ray photoelectron (XPS) measurements were carried out on K Alpha apparatus (Thermo Fisher Scientific, Al X-ray source hυ = 1486.6 eV; spot size = 400 µm). Charge compensation was achieved using a flood gun. The composition was determined using the manufacturer's sensitivity factors.

2.4. Photocatalytic activity

To study the catalytic behavior of the various hybrid materials obtained (CF/RuO_2-TiO_2, CF/RuO_2-TiO_2/PANI and CF/RuO_2-TiO_2/DPA/PANI and CF/RuO_2-TiO_2/DPA@PANI, we have studied the photo-degradation reaction of Methyl Orange (MO) under visible light. The study was conducted in the presence of pristine textile and functional RuO_2-TiO_2 based catalysts coated-cotton fabrics pieces (1×2 cm). In a typical experiment, each sample was tramped in flasks containing 10 ml of MO aqueous solution (50 mg/l) and shaken in the solutions before being stored in the dark for 1h to reach the equilibrate adsorption. After this time and before visible light was turned on, 3 drops of H_2O_2 (14%) were added to each flask enhance the reaction rate by the formation of cation radicals in the solutions under irradiation

during the degradation reaction. The pH of MO solutions is 6.5 and the tests were carried out at room temperature under visible light generated by UV CUBE (Honle UV technology).

2.5. Durability test

2.5.1. Washing, Washing/ironing and sunstroke test

The durability test of the modified cotton fabric is very important; it allows to study the effect of cleaning, ironing and exposure to sunlight on the reuse of the modified fabrics.

i). Cleaning: the test was carried out on two samples of cotton fabric with a same size, modified with RuO_2-TiO_2/DPA/PANI nanocomposite. The test was realized in a standard washing machine in the presence of a detergent.

The samples were washed at 40°C for 2h. After that, the samples were dried in ambient air.

ii). Ironing: one of the two samples already cleaned was ironed, making 10 passes on both sides at T = 200 °C.

The RuO_2-TiO_2/DPA/PANI nanocomposite content in the washed/washed and ironed cotton fabric was measured to determine the loss of the catalyst during washing and also after ironing.

iii). Sunstroke: this test is to study the effect of visible light rays on the catalytic activity of a sample modified with RuO_2-TiO_2/DPA/PANI nanocomposite.

The test consists of leaving the cotton fabric under irradiation for 1h before subsequently using it in the decomposition of MO solution (50mg/l). The distance between the lamp and the sample is 26 cm. The kinetics of the degradation reaction was determined and compared to that of a similar non-irradiated sample.

3. Results and discussion

3.1. Design and physicochemical characterization of catalyst-loaded cotton fabrics

Figure 1 presents a schematic summary of the protocol adopted for the preparation of modified cotton fabric with the various nanomaterials already synthesized.

The scheme highlighted the simplicity and efficiency of the strategy for making functional catalysts cotton fabrics. The different hybrid materials were prepared by dipping pieces of fabric into the suspensions containing the catalyst. This method leads to the formation of modified textiles with a fairly large amount of nanomaterials on the surface; Washing with distilled water and ethanol allowed to lose the excess powder not fixed between the fabric fibers and also to have a homogeneous surface.

The CF/RuO_2-TiO_2/DPA/PANI hybrid material can be prepared by dipping (Fig 1B) and by in situ oxidative polymerization of the aniline monomer, on the surface of the textile impregnated with diazonium modified-RuO_2-TiO_2 NPs (Fig 1C). The diazonium salt is used as a coupling agent; it serves to improve the adhesion of the PANI on the surface of the RuO_2-TiO_2 mixed oxide, hence the formation of a thick layer of PANI on the fabric surface. In addition, the strong combination force between OH groups located on the cotton fibers surface and the anilinium cation was leading to coat the DPA-modified RuO_2-TiO_2 NPs easily on the fabric. The thickness of the polymeric layer must be controlled; a large thickness blocks the catalytic effect of RuO_2-TiO_2 NPs (Fig 1C). The acidity of the media during the in situ polymerization of aniline has a detrimental effect on the resistance of the fabric (Onar et al., 2009); this type of synthesis is therefore not recommended if the sample will be used as functional conductive textiles.

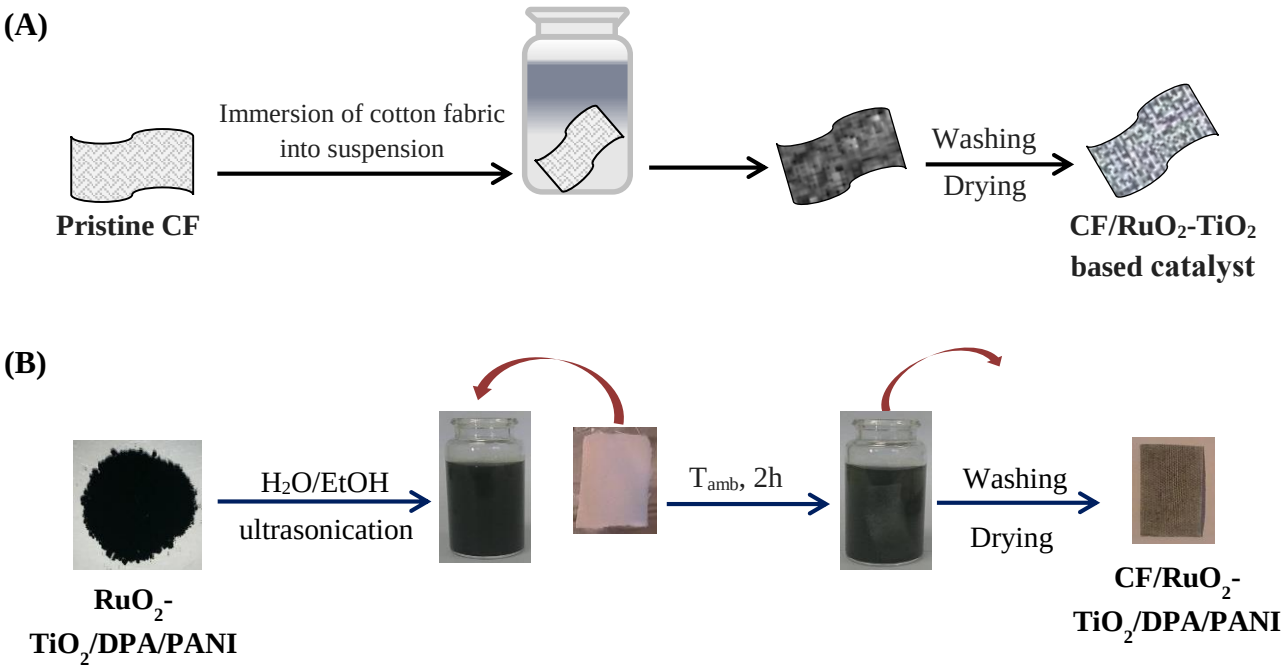

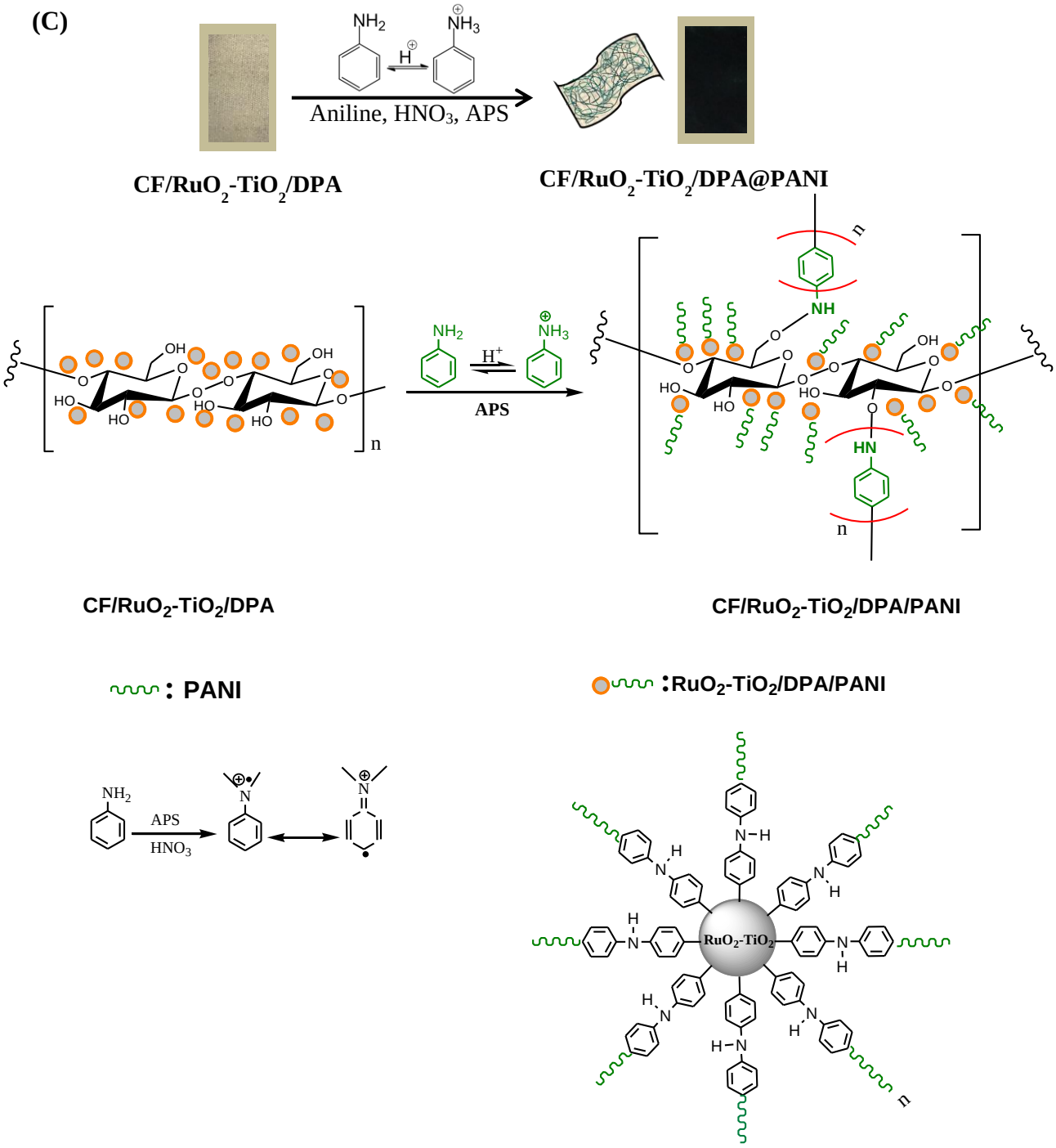

Fig. 1. Schematic view of preparation process of RuO_2-TiO_2 based catalysts functional cotton fabrics: **(A)** general, **(B)** in the presence of RuO_2-TiO_2/DPA/PANI nanocomposite and **(C)** in situ polymerization of aniline onto CF/RuO_2-TiO_2/DPA.

Figure 2 provides digital photographs of the cotton fabric modified with RuO_2-TiO_2 NPs, RuO_2-TiO_2/DPA, RuO_2-TiO_2/PANI and RuO_2-TiO_2/DPA/PANI nanocomposites.

The images display a color change of the fabric comparing to the pristine cotton fabric. The color of the samples depends of the color of the catalysts which is in suspension. After impregnation of the nanomaterials, the fabric turn from its original white color to gray in the presence of RuO_2-TiO_2 NPs (Fig 2b) but also in the presence of RuO_2-TiO_2/PANI nanocomposite (Fig 2c) because the negligible amount of PANI inserted on the RuO_2-TiO_2 surface. In the presence of RuO_2-TiO_2/DPA/PANI (Fig 2e), the color is rather black because of the color of the nanocomposite and the amount of polyaniline attached to RuO_2-TiO_2 NPs, thanks to the diazonium salt used as a coupling agent. The cotton fabric is brown in the presence of RuO_2-TiO_2 functionalized with diphenylamine diazonium salt (Fig 2d), this same sample passes to very dark green color, obtained by in situ polymerization of aniline; this last sample is completely covered with PANI layer in both sides (Fig 2f).

The catalytic powders are well impregnated between the fibers of the fabric. After washing and drying, the distribution of the nanoparticles on the surface appears to be homogeneous. The color of the CF/RuO_2-TiO_2/DPA@PANI (Fig 2f) depends of the polymerization time; the color becomes darker with the increase of the reaction time.

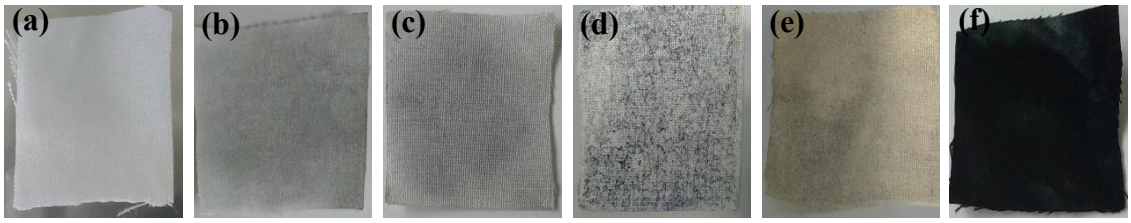

Fig. 2. Digital photographs of functional cotton fabric obtained by dipping: pristine cotton fabric (a), CF/RuO_2-TiO_2 (b), CF/RuO_2-TiO_2/PANI (c), CF/RuO_2-TiO_2/DPA (d), CF/RuO_2-TiO_2/DPA/PANI (e) and CF/RuO_2-TiO_2/DPA@PANI (f).

3.2. Morphology analysis of modified-cotton fabrics

The morphology as well as the chemical composition of the cotton fabric before and after modification were studied. Figure 3 shows SEM images and EDS spectra of pristine and RuO_2-TiO_2 based-catalysts cotton fabric. The control sample (Fig. 3 ab) exhibits a spun yarn with fiber sizes between 5 and 10 μm, this fibers are more in less organized in a compact woven texture. After modification, the images show the presence of small particles agglomerated on the fibers of the fabric (Fig. 3 cd,ef,gh). The color of the RuO_2-TiO_2 NPs

and the RuO_2-TiO_2/PANI nanocomposite attached on textile surface (Fig. 3 cd, ef) is light gray, while that of the RuO_2-TiO_2/DPA/PANI nanocomposite is dark, which is due to the dark green color of PANI which coats the RuO_2-TiO_2/DPA (Fig. 3gh).

During the preparation process, the samples did not undergo any thermal or chemical treatment which resulted in oxidation of the cellulose; this oxidation leads to the destruction of the fibers constituting the fabric and thus modifying the crystalline structure of the cellulose (Shahidi, Wiener & Ghoranneviss, 2013; Faruk & Ain, 2013).

The immersion of a surface in a solution containing the aniline monomer leads to the total coverage of the surface with the PANI. The thickness of the polymeric layer strongly depends on the contact angle of the substrate with the solution containing the monomer as well as the polymerization conditions. SEM images of CF/RuO_2-TiO_2/DPA coated PANI obtained by in situ polymerization of aniline in an acidic medium (Fig. 3 j), indicates the formation of a porous and very adherent coating on the surface, covering all RuO_2-TiO_2/DPA NPs and all the fibers. The coating consists of porous clusters as well as tubular shapes of nonmetric diameter that are randomly oriented on the fabric fibers (Fig. 3 j').

PANI nanofibers deposited by in situ polymerization on cotton fabric were obtained by (Tissera, Wijesena, Rathnayake, de Silva, de Silva, 2018), they demonstrated that the nanofibrous forms are obtained only in acidic medium (pH = 2) and that these nanofibers shows a slight fusing behavior once in higher pH.

EDS analysis confirms the elementary composition of the samples after modification. The fibers of the fabric contain more oxygen than carbon. The RuO_2-TiO_2 nanoparticles present on the surface of the fabric are manifested by the appearance of Ti and oxygen on the spectrum with a significant percentage in the case of the RuO_2-TiO_2 and RuO_2-TiO_2/PANI coating fabric (Fig. 3 b', c'). The Ru has a very weak and even negligible signal compared to that of Ti, which means that the analyzed zone is crippled in Ru (Fig. 3 b', c').

The modified textile with RuO_2-TiO_2/DPA/PANI nanocomposite shows no Ti and Ru signal; they are replaced by the carbon and nitrogen of PANI, which covers the entire surface of RuO_2-TiO_2 mixed oxide (Fig 3 d').

The coverage of RuO_2-TiO_2/DPA NPs by the PANI obtained by in situ polymerization is confirmed by the corresponding EDS spectrum (Fig 3 e'). The coating consists of a large amount of carbon, oxygen, nitrogen and sulfur, which is a precursor of the SO_4^{2-} doping anion; these elements make the composition of PANI film and cellulose. The spectrum indicates also the presence of a small percentage of Al corresponding to the fluorescence of the sample holder during the analysis.

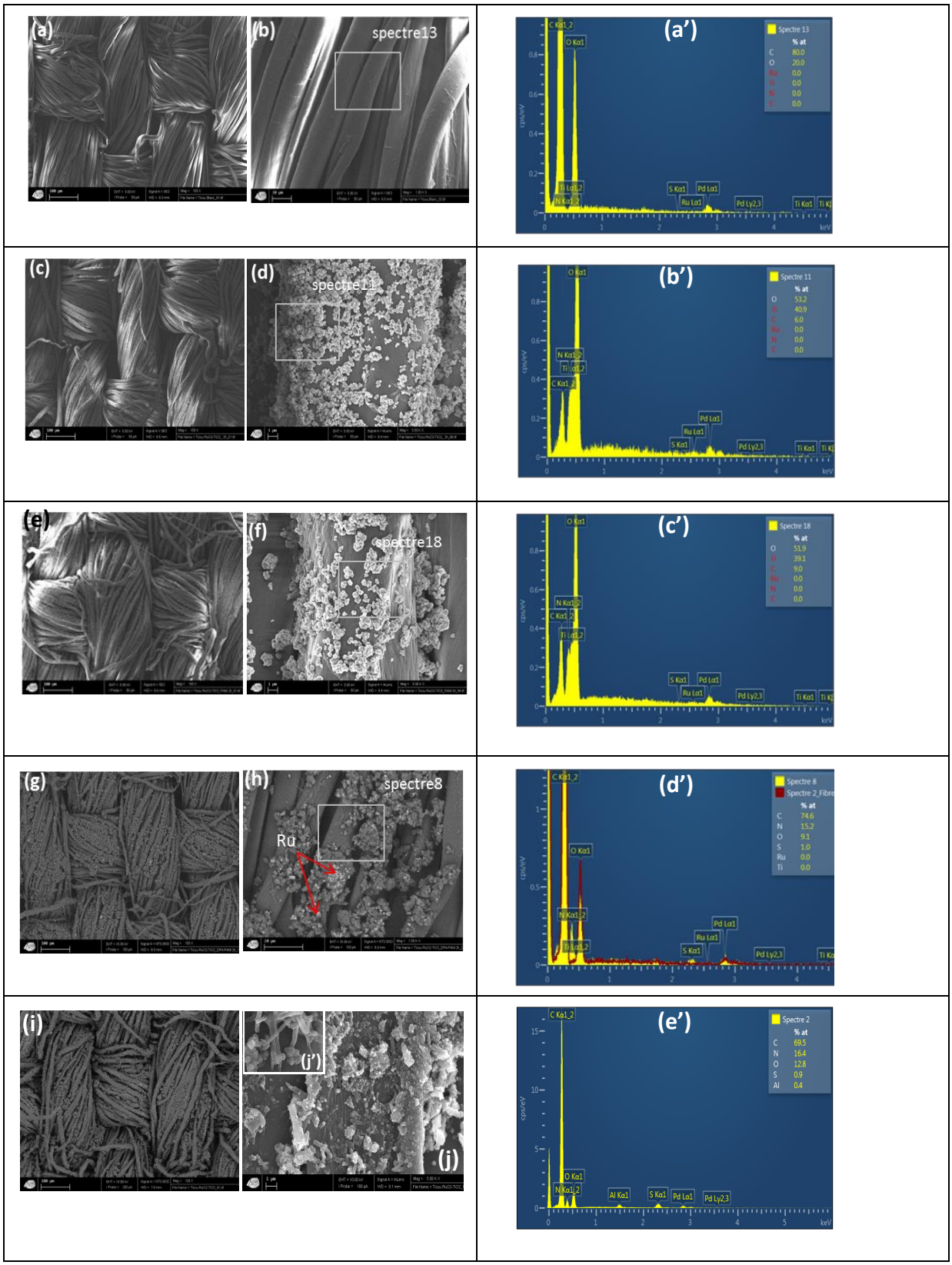

Fig.3. SEM images and elemental spectra of pristine cotton fabric (a, b, a'), CF/RuO_2-TiO_2 (c, d, b'), CF/RuO_2-TiO_2/PANI (e, f, c'), CF/RuO_2-TiO_2/DPA/PANI (g, h, d') and CF/RuO_2-TiO_2/DPA@PANI (I, j, j', e').

3.3. XRD

Figure 4 illustrates the XRD patterns of the control cotton fabric and the coated cotton RuO_2-TiO_2/PANI hybrid. The diffractogram of cellulose has peaks at 14.9°, 16.7° and 22.9° corresponding to the Miller indices (100), (010) and (110), respectively (Fig 4 a) (Daoud & Xin, 2004; Zhou., 2019). The presence of RuO_2-TiO_2 on the surface results in the appearance of the characteristic peaks of TiO_2 anatase at 25.45°, 36.9° and 48.07° and a peak at of 37.84° corresponding to RuO_2 rutile (Fig 4 b, c, d). The presence of PANI in the RuO_2-TiO_2/DPA/PANI powdery nanocomposite and in the hybrid material CF/RuO_2-TiO_2/DPA@PANI caused the attenuation of RuO_2-TiO_2 peaks (Fig 4 e, f). The peaks of the cellulose in the treated cotton fabric are slightly shifted towards the lower values of 2θ, indicating the diffusion of RuO_2-TiO_2/PANI, RuO_2-TiO_2/DPA/PANI and RuO_2-TiO_2/DPA@PANI nanocomposites and RuO_2-TiO_2 NPs into the amorphous and para-crystalline regions of cellulose, without affecting the its crystallinity (Savitha & Gurumallesh Prabu, 2013). This results are similar to that reported by (Savitha & Gurumallesh Prabu, 2013) in the case of coated cotton, insight polyaniline–TiO_2 hybrid (Bhat, Seshadri & Radhakrishnan, 2004) and (Muthukumar & Thilagavathi, 2012) in the case of polyaniline coated cotton fabric.

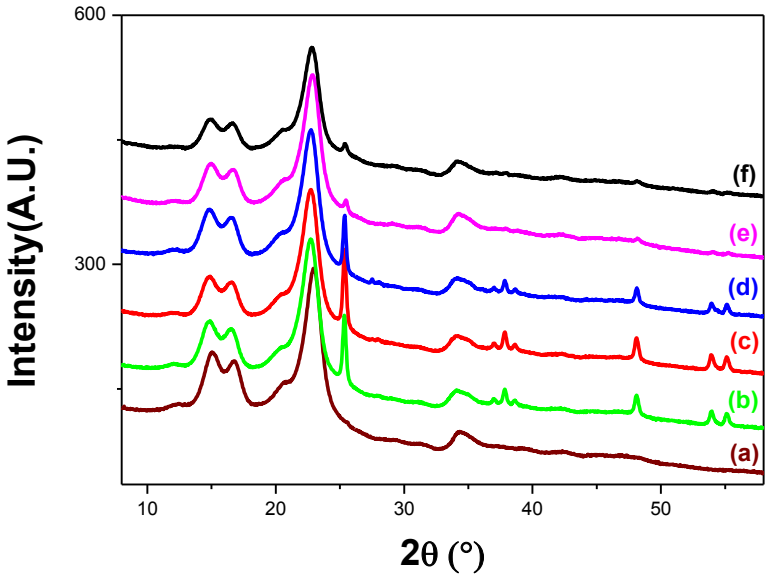

Fig. 4. XRD patterns of uncoated cotton fabric (a), CF/RuO_2-TiO_2 (b), CF/RuO_2-TiO_2/DPA (c), CF/RuO_2-TiO_2 /PANI (d), CF/RuO_2-TiO_2/DPA/PANI (e) and CF/RuO_2-TiO_2/DPA@PANI (f).

3.4. FTIR

Figure 5 depicts the IR spectra obtained for all different nanocomposite materials. The spectrum (a) corresponding to pristine cotton fabric has several peak characteristics of pure cellulose., the vibration band located at 898 cm^{-1} is attributed to the asymmetric out-of-phase ring stretch C–O–C. (Chen & Jakes, 2002; Gilbert, Kokot & Meyer., 1993; Tao et al, 2018; Carrillo, Colom, Sunol & Saurina, 2004; Zahran, Ahmed & El-Rafie, 2014; Chung, Lee & Choe, 2004). At 1030 cm^{-1} is situated the C-O stretching vibration. The bands at 1114 and 1169 cm^{-1} are assigned to asymmetric bridge C-O-C. The band located at 1318 cm^{-1} is due to C-H wagging. The pic appeared at 1372 cm^{-1} is attributed to C-H bending (deformation stretch) and that at 1435 cm^{-1} is corresponding to C-H in plane bending. The spectrum displays a band at 1642 cm^{-1} relative to the adsorbed water molecules. The peak appearing at 2913 cm^{-1} is assigned to C-H stretching band. The spectrum exhibits a broad band between 3100 and 3650 cm^{-1} which is due to O-H stretch. In addition to the characteristic bands of cotton fabric, some new bands attributed to the nanomaterials inserted on the tissue fibers appear after treatment (Fig 5: b, c, d, e and f).

The modification of the cotton fabric with RuO_2-TiO_2 mixed oxide (Fig 5 b) is manifested by the appearance of a vibration band situated at 690 cm^{-1} which corresponds to Ru-O and deformation of Ru-O-H (Musić, Popović, Maljković, Furić & Gajović, 2002). It should be noted that the bands of cellulose are stored because of the amount of RuO_2-TiO_2 NPs on the surface. The CF/RuO_2-TiO_2/PANI spectrum (Fig 5 d) shows no significant difference from that of CF/RuO_2-TiO_2 (Fig 5 b). The spectrum shows only the peaks of cellulose and those of RuO_2-TiO_2. The small amount of PANI polymerized on the surface of RuO_2-TiO_2 NPs results in the absence of its signals under IR. The presence of the functionalized nanoparticles on the fabric is manifested by the appearance of certain peaks on the spectrum of CF/RuO_2-TiO_2/DPA (Fig 5 c), include those located at 1580 and 1160 cm^{-1}, which are attributed to the aromatic C=C stretching and C-H benzene ring stretching band, respectively (Leroux, Fei, Noël, Roux & Hapiot, 2010). These bands are associated with other apparent on the spectrum and which are attributed to the cellulose and RuO_2-TiO_2 mixed oxide. The spectrum of CF/RuO_2-TiO_2/DPA@PANI (Fig 5 f) exhibits only PANI bands, they are located at 792, 1026, 1154, 1493, 1574, 3251 and 3488 cm^{-1} wish correspond to C-N^+ stretching vibration, plane bending of C-H, C-H benzene ring stretching band, N-N stretching vibration. C=N stretching of quinoid vibrations (Yuzhen, Yuan, Liangzhuan Wu & Jinfang, 2013), N-H stretching (Zhang, Liu & Su, 2006) and adsorbed H_2O molecules (Bishop, Pieters & Edwards, 1994) respectively. The absence of the cellulose signs is due to the fact that the thickness of

PANI coating is greater than the effective penetration depth of IR radiation as well as the high absorption of polyaniline (Bajgar et al., 2016).

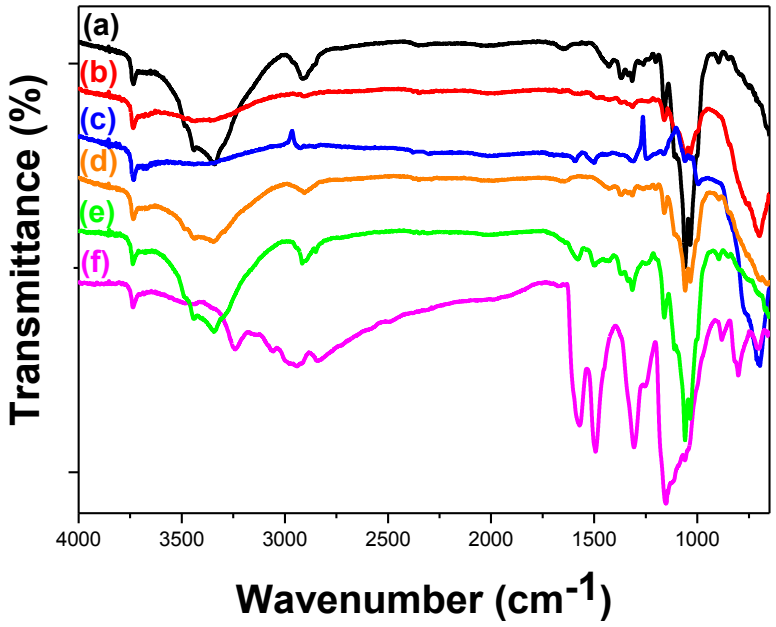

Fig.5. FTIR spectra of pristine cotton fabric (a), CF/RuO_2-TiO_2 (b), CF/RuO_2-TiO_2/DPA (c), CF/RuO_2-TiO_2 /PANI (d), CF/RuO_2-TiO_2/DPA/PANI (e) and CF/RuO_2-TiO_2/DPA@PANI (f).

3.5. Raman

Generally, the mixed metal oxides are manifested with Raman active modes corresponding to each oxide constituting the mixed material. this has already been demonstrated in our previous study conducted on RuO_2-TiO_2 mixed oxide (Mousli et al., 2019)]; the latter, under the Raman laser gives signals that are attributed to each of the two oxide namely the TiO_2 anatase that occurs with seven modes of Raman actives vibration that are E_g (144 cm^{-1}), E_g (197 cm^{-1}), B_{1g} (399 cm^{-1}), A_{1g} (514 cm^{-1}), B_{1g} (514 cm^{-1}) and E_g (639 cm^{-1}) (Arsov, Kormann & Plieth., 1991) [1]], and the rutile RuO_2 which absorbs between 400 and 800 cm^{-1} with the symmetries E_g corresponding to a doublet and A_{1g} and B_{2g} phonons vibrations corresponding to the singlet (Chen, Korotcov, Hsu, Huang & Tsai., 2007) [2]], they are they are usually located at 528, 645 and 716 cm^{-1} respectively (Mar, Chen, Huang and Tiong, 1995). On the CF/RuO_2-TiO_2 spectrum, no signal is attributed to RuO_2. All the peaks are assigned to the anatase, this is due to the analyzed area which is possibly disabled in ruthenium (Fig 5 b). Ditto for the fabric impregnated with RuO_2-TiO_2/PANI, the spectrum is almost the same to that of CF/RuO_2-TiO_2. The negligible amount of PANI inserted on the surface of RuO_2-TiO_2 is not

sufficient to be detected in Raman, hence the absence of its peaks on the spectrum (Fig 5 c). A slight red shift and a widening of the peaks are recorded for RuO_2-TiO_2 NPs already functionalized with diphenylamine diazonium modified cotton fabric samples (Fig 5 d). In the presence of PANI, the bands of RuO_2-TiO_2 mixed oxide are attenuated (Fig 5 e) even masked (Fig 6 f) by PANI which completely covers RuO_2-TiO_2-DPA materials; all the bands appearing on the spectra are corresponding to the PANI, they are located at 1168, 1250, 1335, , 1510, and 1595 cm^{-1}; they are assigned to C–H bending of the quinoid and benzenoid ring, C-N^+ stretching vibration, , C=C stretching of the benzenoid ring, and C=C stretching of the quinoid rings (Jlassi et al., 2014); Jin, 2018). It is noted that the Raman response of the cellulose is hidden by TiO_2 which absorbs strongly in the same zone as cellulose.

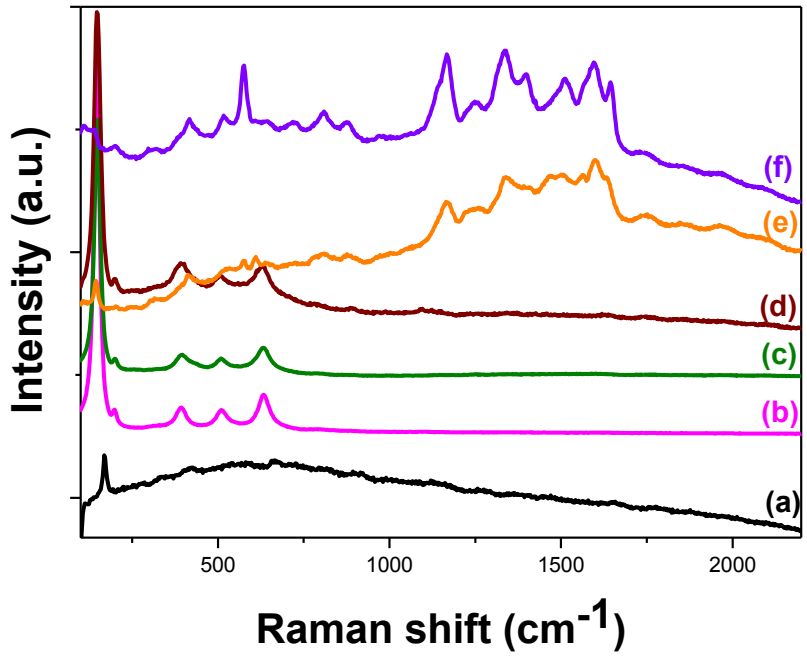

Fig.6. Raman spectra of pristine cotton fabric (a), CF/RuO_2-TiO_2 (b), CF/RuO_2-TiO_2 /PANI (c), CF/RuO_2-TiO_2/DPA (d), CF/RuO_2-TiO_2 /DPA/PANI (e) and CF/RuO_2-TiO_2/DPA@PANI (f).

3.6. XPS

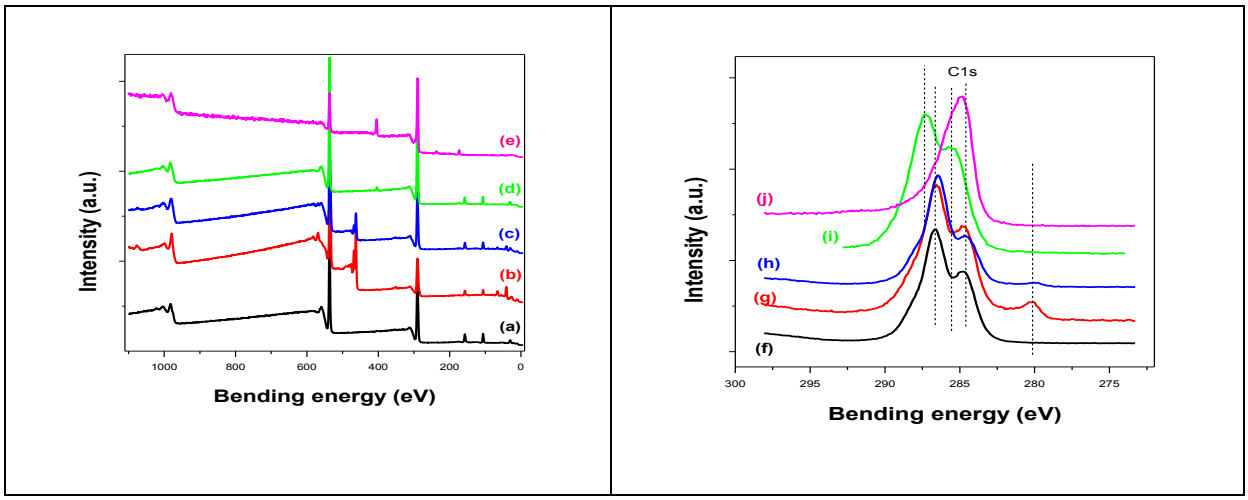

Fig.7 XPS survey scans (a-e) and C1s narrow regions (f-j) of pristine cotton (a,f), CF/RuO_2-TiO_2 (b,g), CF/RuO_2-TiO_2/PANI (c,h), CF/RuO_2-TiO_2 /DPA/PANI (d,i) and CF/RuO_2-TiO_2/DPA@PANI (e,j).

XPS was used to monitor the stepwise modification of cotton woven fabric by the catalytic materials. Figure 7 displays survey and high resolution C1s spectra from cotton before any surface modification (Figures 7a,f) and after dip coating in aqueous suspensions of RuO_2-TiO_2 (Figures 7b,g), RuO_2-TiO_2/PANi (Figures 7c,h) and RuO_2-TiO_2/DPA/PANI (Figures 7d,i). Figures 7e,j display the survey spectrum and narrow C1s region of cotton fabric dip coated first in RuO_2-TiO_2/DPA suspension and then top coated with PANI prepared in situ by oxidative polymerization.

The survey regions exhibit the main peaks S2p, C1s, N1s, Ti2p and O1s centred at 168, 285, 400, 458 and 532 eV, respectively. Ru3d is too weak to be visible on the survey regions as it is located at the onset of the C1s peak. Ti2p is readily visible after immobilization of the RuO_2-TiO_2 nanocatalyst (Figure 7b) compared to pristine cotton (Figure 7a), but the Ti2p/C1s peak intensity ration decreases for CF/RuO_2-TiO_2/PANI compared to CF/RuO_2-TiO_2 since the nanocatalyst RuO_2-TiO_2 was first modified with PANI prior to attachment to the cotton fabric by dip coating (Figure 7c). One can note in Figure 7d a total absence of Ti2p due to the modification of the cotton fabric by RuO_2-TiO_2/DPA/PANI. Indeed, we have demonstrated recently (Mousli et al., 2019) that the modification of RuO_2-TiO_2 by the DPA diazonium coupling agent permits to achieve much higher PANI mass loading that resulted in the total screening of the RuO_2-TiO_2 nanocatalysts. As a matter of fact, the C1s narrow region displayed in Figure 7i does not exhibit any Ru3d at ~280-282 eV. For CF/RuO_2-TiO_2/DPA@PANI, Figure 7e shows a relatively intense N1s peak at 400 eV due to the in situ

synthesis of PANI at the surface of CF/RuO_2-TiO_2/DPA. This coating is deep green (quasi looking as black, see digital photograph in Figure 1C, upper panel) and in line with the detection of an intense N1s peak. Interestingly, and compared to RuO_2-TiO_2/DPA/PANI dip coated on cotton (Figure 7d), one can now see S2p (168 eV) and S2s from the PANI doping. Another interesting feature of the survey region displayed in Figure 7e is the shape of the inelastic background. After the O1s peak at 532 eV and towards the apparent high binding energy (in reality at low kinetic energy side), the survey spectrum in Figure 7e exhibits ever increasing intensity of the inelastic background which is due to inelastically emitted electrons from the buried surface underneath PANI (cotton and RuO_2-TiO_2/DPA). In contrast, the inelastic background between the C1s and O1s peaks is horizontal or slightly decreasing, which is characteristic of a top layer, herein PANI. These aspects contrast markedly with the situation of noted in Figure 7d for CF/RuO_2-TiO_2/DPA/PANI. Indeed, dip coating RuO_2-TiO_2/DPA/PANI on the cotton fabric does not screen the cellulosic substrate, and for this reason one can note the decreasing intensity of the background at higher binding energy side of the C1s and O1s peaks which mainly due to cotton.

For the narrow C1s regions, Figure 7f displays a main peak at 286.5 eV due to C-O and a shoulder at 288 eV due to hemiacetal group O-C-O. Possible COOR groups are present on the cotton as judged from the small shoulder at ~289 eV. After modification with RuO_2-TiO_2, the cotton fabric exhibits Ru3d doublet at ~280-282 eV (Figure 7g) the intensity of which decreases relatively compared C1s in the case of CF/RuO_2-TiO_2/PANI (Figure 7h) since the nanocatalyst RuO_2-TiO_2/PANI does not have much surface immobilized PANI (Mousli et al., 2019). For CF/RuO_2-TiO_2/DPA/PANI (Figure 7i) there is no Ru3d doublet, but the C1s peak looks like that of pristine cotton except it is slightly broad due certainly due to contribution from PANI. Finally, Figure 7j exhibits distinct C1s spectrum (recorded for CF/RuO_2-TiO_2/DPA@PANI) compared to that shown in Figure 7i and underlines the essential difference between CF/RuO_2-TiO_2/DPA/PANI and CF/RuO_2-TiO_2/DPA@PANI. In the former case, RuO_2-TiO_2/DPA/PANI nanocatalyst is immobilized by dip coating and remains between the cotton fibers, whereas for the latter, PANI is synthesized in situ on cotton that has been pre-dip coated with RuO_2-TiO_2/DPA nanoparticles. Polymerization occurs on the bare cotton C-OH sites but also on the DPA groups from the immobilized nanocatalyst. This important difference in the processes induces significant differences in the surface compositions as judged from XPS.

For the final, PANI-rich surface CF/RuO_2-TiO_2/DPA@PANI, the C/N atomic ratio is 7.4 higher than the theoretical value of 6 for PANI and that reported by (Barthet, Armes, Chehimi,

Bilem & Omastova, 1998) for PANI surface, due to possible contribution of the cotton fabric and presumably some adventitious hydrocarbon contamination. The doping level is given by:

$$D\% = \frac{S \times 2}{N} \times 100\% = 49.4\%$$

where *S* and *N* are the atomic percents of sulfur and nitrogen. The factor 2 stands for double charge born by the $SO_4^{=}$ dopant. This D% is matching 50%, the doping level for conductive PANI.

3.7. Stability of catalytic textiles.

3.7.1. SEM monitoring of the morphology of washed and washed/ironed-cotton fabrics

After washing, the RuO_2-TiO_2/DPA/PANI nanocomposite deposit on the fabric surface has become much more homogeneous. All the powder agglomerated on the surface is gone during the washing, remains only the particles that are impregnated between the fibers and that are well attached to the surface (Fig 8 a, b).

The SEM images show that the washing has disordered the fibrous structure of the samples and the surface contains very few nanoparticles comparing to the unwashed sample (Fig 8 cd, fg). The presence of the nanoparticles on the fabric and the complete composition of the surface have been confirmed by EDS. It is noted that the surface analyzed is crippled in Ru (Fig 8 e, h).

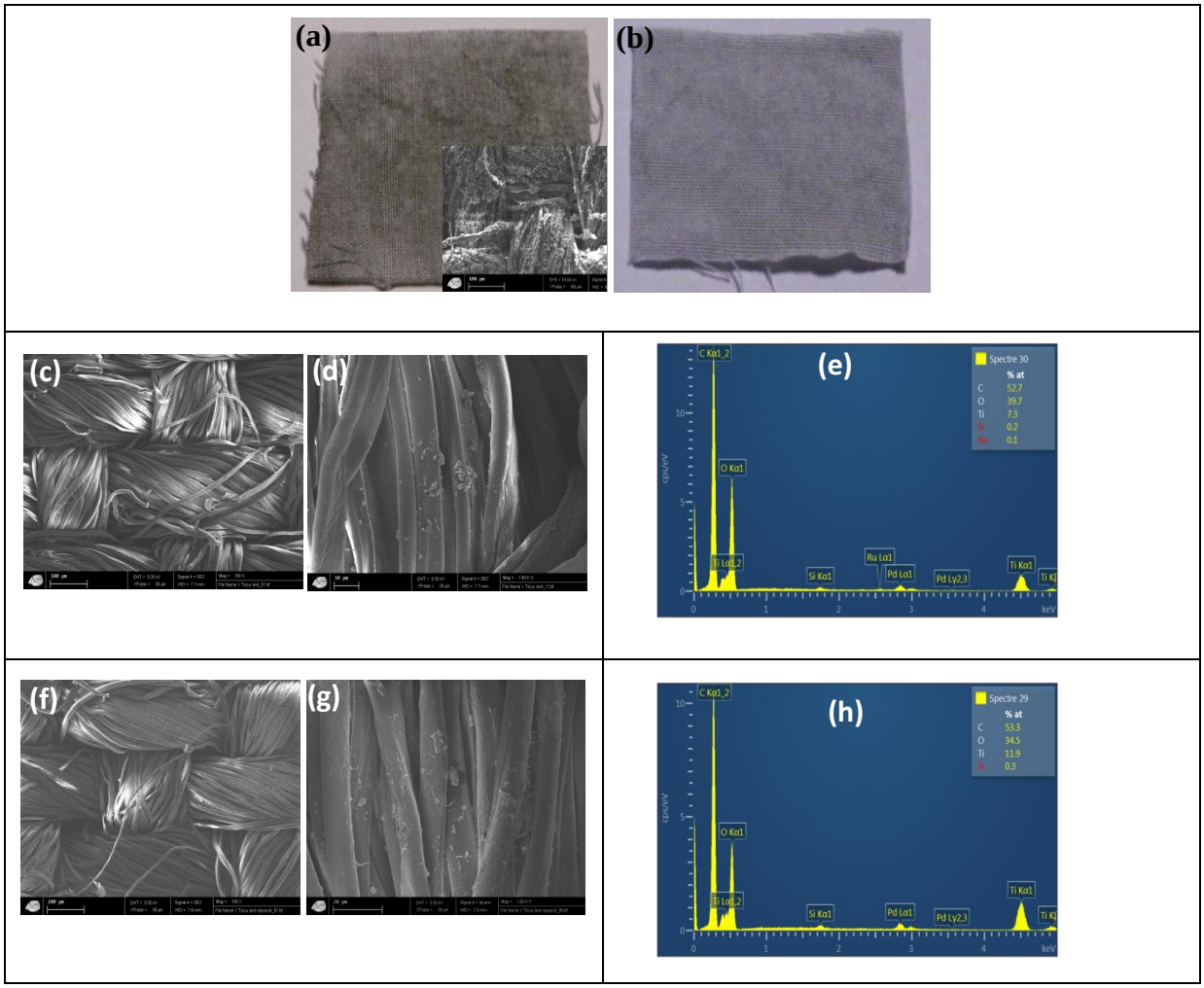

Fig.8. Digital photographs of CF/RuO_2-TiO_2/DPA/PANI as prepared with SEM image in inset (a) and after washing (b) SEM images and elemental spectra of CF/RuO_2-TiO_2/DPA/PANI after washing (c-e) and cleaning and iron (f-h).

3.7.2. XPS after washing/ washing and ironing

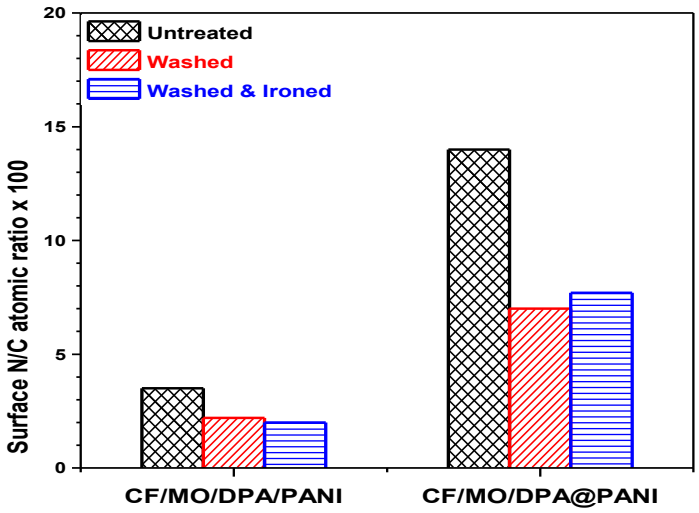

Fig. 9. XPS-determined N/C atomic ratios for untreated, machine washed, and washed/ironed samples of CF/RuO_2-TiO_2/DPA/PANI and CF/RuO_2-TiO_2/DPA@PANI. For the sake of clarity, RuO_2-TiO_2 is noted MO for mixed oxide in the labels.

The cotton textile catalysts CF/RuO_2-TiO_2/DPA/PANI and CF/RuO_2-TiO_2/DPA@PANI were also examined by the surface sensitive XPS in order to check any subtle change in the surface composition as a result of fastness tests conducted by machine washing using industrial detergents at standard dose (75 ml for 5 kg clothes, T°=40 °C, cotton program). We have selected herein the most efficient catalytic textiles prepared using diazonium compounds. PANI was loaded on the diazonium modified catalyst prior to dip coating or prepared in situ as mentioned above in the presence of CF/RuO_2-TiO_2/DPA.

Despite the presence of DPA and covalent bonding of PANI in either cases, we have noted decrease of the surface N/C atomic ratios for both catalytic textile. However, ironing the washed textile does not induce any additional change.

It follows that XPS can provide deep insight in the surface composition particularly for CF/RuO_2-TiO_2/DPA@PANI textile which remains very dark even machine washing. In contrast, for CF/RuO_2-TiO_2/DPA/PANI, one could note leaching of the catalyst even with the naked eye as the nanocatalyst has been removed partially after washing, and the result is confirmed by XPS.

The essential difference between the surfaces comes from the N/C ratio which is even higher for washed CF/RuO_2-TiO_2/DPA@PANI compared to the untreated CF/RuO_2-

TiO_2/DPA/PANI. Obviously, in situ polymerization of aniline is important in providing a continuous PANI top layer that withstands machine washing.
These surface composition aspects will be correlated to the catalytic activity of the textiles.

4. Photocatalytic activity

The catalytic efficiency of RuO_2-TiO_2 NPs, RuO_2-TiO_2/PANI and RuO_2-TiO_2/DPA/PANI powdery nanocomposites with respect to the MO degradation reaction under the same conditions as the present work ([MO]=50 mg/l, pH=6.5, $T=T_{amb}$) was reported in a previous study(Mousli et al., 2019). It is noted that the RuO_2-TiO_2/PANI and RuO_2-TiO_2/DPA/PANI nanocomposites are effective catalysts in the darkness (Mousli et al., 2019), the amount of the catalysts coated on cotton fibers is very small compared to the volume of the volume of MO solution and its concentration, hence the choice to use visible light to activate the nanocatalysts and to accelerate the degradation reaction of the MO.

The study found that the presence of PANI improves the catalytic properties of RuO_2-TiO_2 mixed oxide, namely: the catalysts containing PANI are very active in the dark, while pristine RuO_2-TiO_2 is an effective catalyst under visible light; in addition, the catalytic effect of the catalyst increases with increasing the amount of PANI in the nanocomposite.
Despite the fact that they are the same powders that are impregnated on the surface of the fabric and used in MO degradation process, the materials are not catalytically active in the dark because of the small amount of catalyst inserted on the surface and between the fabric fibers (0.4 mg). The solutions are therefore exposed to visible light for 45 min. The decomposition of the dye is controlled by the transition from its orange color to the colorless followed by the absorption spectra measured at regular time intervals.
Under visible light, the MO solution containing RuO_2-TiO_2, RuO_2-TiO_2/PANI, RuO_2-TiO_2/DPA/PANI and RuO_2-TiO_2/DPA@PANI nanocatalyst-modified cotton fabrics became completely colorless after 45 min as compared with the solution containing the pristine sample. This is strong supporting evidence for the effect nanocatalysts loaded on the fabric surface (Fig 10).

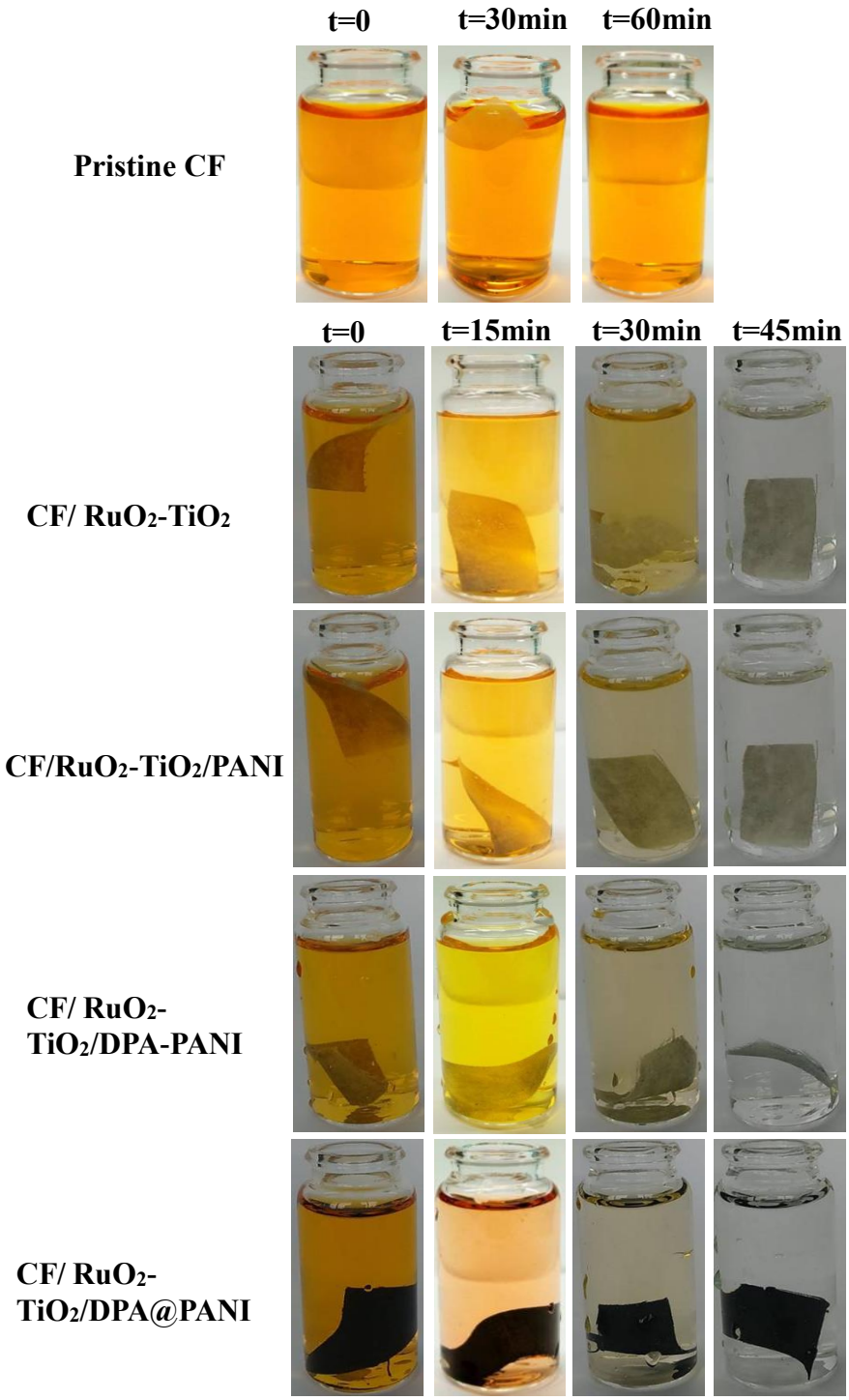

Fig. 10. Digital photographs of Methyl Orange under visible light.

The photo-activity of the different materials (pristine CF, CF/RuO_2-TiO_2, CF/RuO_2-TiO_2/PANI, CF/RuO_2-TiO_2/DPA/PANI and CF/RuO_2-TiO_2/DPA@PANI) was evaluated and compared by measuring the concentration of the dye in solution by UV-Vis at different time intervals. Figure 11 shows the recorded spectra.

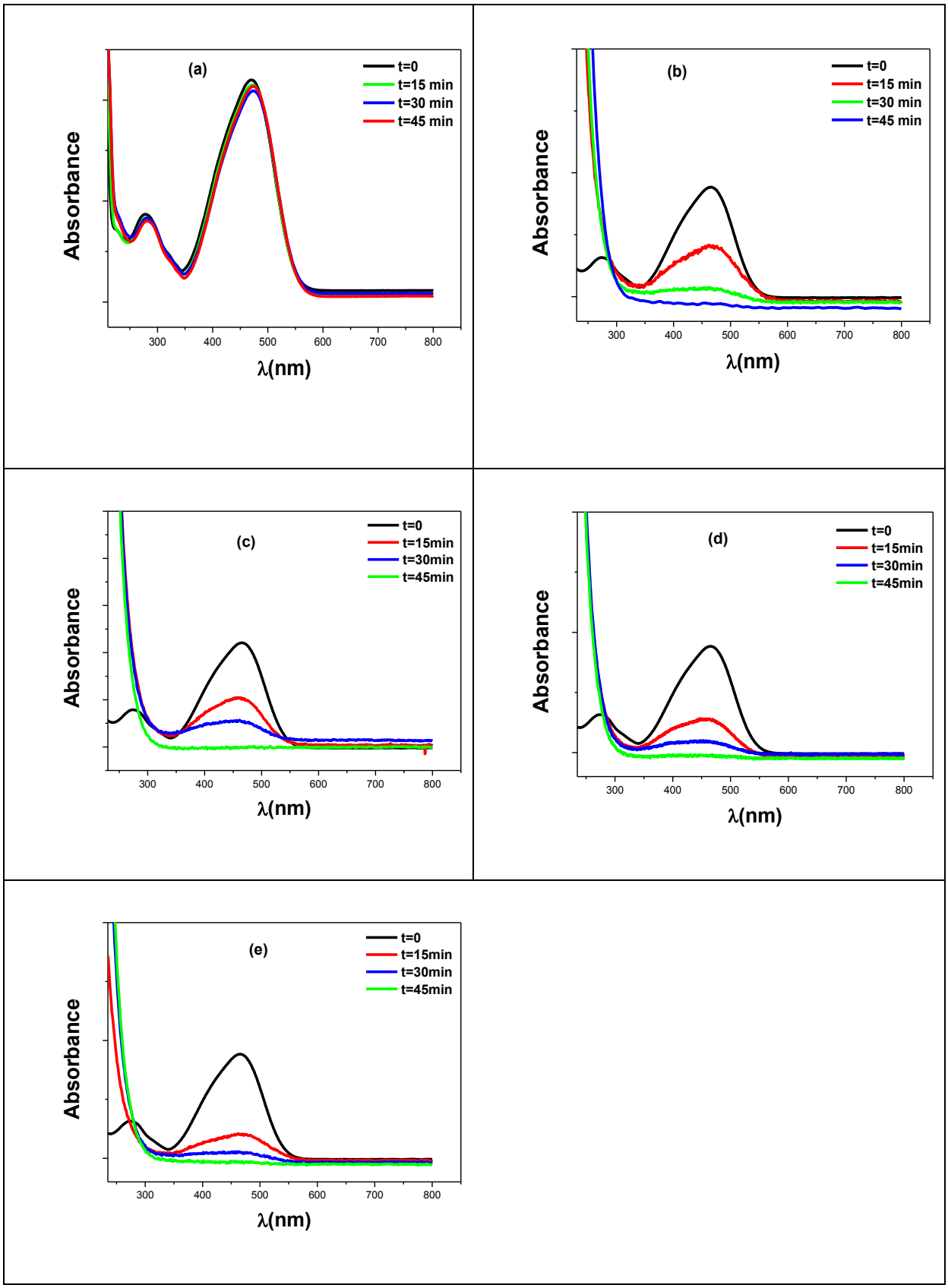

Fig.11. UV-vis absorption spectra of Methyl Orange solutions (50 mg/l) for various periods: pristine cotton fabric (a), CF/RuO_2-TiO_2 (b), CF/RuO_2-TiO_2/PANI (c), CF/RuO_2-TiO_2/DPA/PANI (d) and CF/RuO_2-TiO_2/DPA@PANI (e).

The MO is characterized by a band in the visible region attributed to the azo form and located between 400-500 nm and which monitors the effect of the photocatalysis on the degradation of MO; and another band situated between 250-300 nm which is due to the phenyl group in the dye.

Under visible light and in the presence of H_2O_2 as oxidant and composite materials (CF/RuO_2-TiO_2, CF/RuO_2-TiO_2/PANI, CF/RuO_2-TiO_2/DPA/PANI and CF/RuO_2-TiO_2/DPA@PANI), the band at 250 nm disappears completely after 15 min, only the band located at 500 nm which remains but decreases with time until its complete disappearance after 45 min indicating the total decomposition and mineralization of MO (Fig 11 b,c, d, e).

In the presence of pristine cotton fabric, the characteristic bands of MO have retained their intensity throughout the irradiation period, which means that the unmodified textile has no role in the photocatalytic degradation process of MO and that the decomposition of the latter is necessarily due to the catalyst inserted on the fabric surface and their interaction with it (Fig 11a).

The concentration of MO in the solution at different degradation times depends on the catalytic efficiency of each material. The degradation extent (%) is calculated by the following relationship:

$$\% = \frac{\boldsymbol{C^\circ - C}}{\boldsymbol{C^\circ}} * \mathbf{100}$$

Figure 12 shows the percentage of dye degradation as a function of treatment time for all photocatalytic materials. It is found that the effectiveness of the photocatalysis in the presence of the different cotton fabric samples differs markedly.

The decomposition of the dye in the presence of RuO_2-TiO_2-modified fabric already coated with PANI appears to be active compared to pristine RuO_2-TiO_2; this is due to the presence of the polymer and the electronic transfer between the different materials constituting the nanocomposites (PANI, RuO_2-TiO_2 and cellulose).

We have demonstrated in the previous studies that the elimination of MO is better in the presence of PANI and that the catalytic activity of the nanocomposites containing the polymer is directly related to the amount of the conductive polymer in the composite (Mousli et al., 2019 a; b, 2019). In this study, the CF/RuO_2-TiO_2/DPA@PANI sample contains a rather thick layer of PANI compared to the other ones. For this reason, its activity is better, and likely due to the porosity of the cotton fabric and the strong interaction of aniline and OH group of cellulose but also to the presence of the diazonium salt on the surface of RuO_2-TiO_2 mixed

oxide NPs, which acts as a coupling agent and which served for the insertion and adhesion of PANI to the surface of the mixed oxide on the one hand, and on the fabric surface on the other hand.

PANI is an excellent photosensitizer; it acts both as an efficient electron donor and as good hole transporter. The presence of PANI in the heterojunction based-photocatalysts improves the catalytic efficiency as well as the kinetics of the degradation reaction of pollutants, due to the incorporated nanostructure and the synergistic effect between the species **(**Tanwar & Mandal., 2019) **[3]**. This makes PANI an attractive element used in the design and development of novel catalytic hybrid materials to progress in the field of heterogeneous catalysis under irradiation and even in the dark (Mousli et al., 2019).

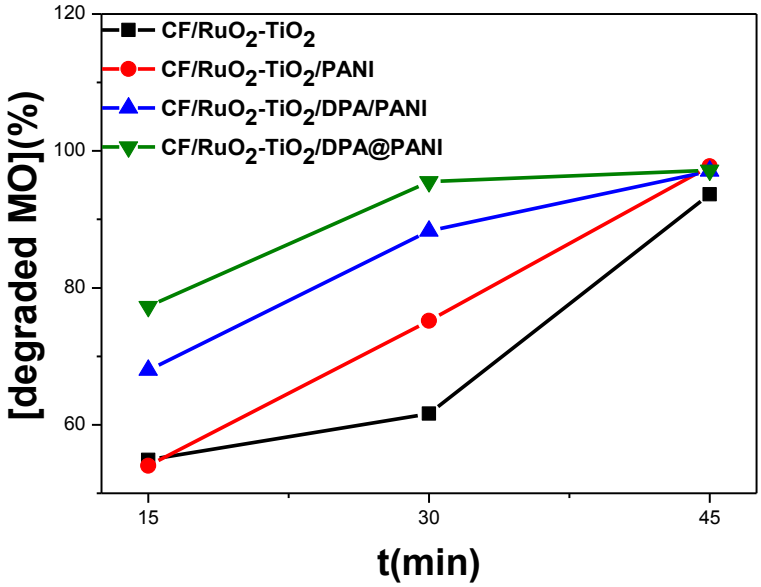

Fig. 12. Variation of the percentage of degraded MO as a function of the time in the presence of different catalysts

The studies carried out on the photodegradation of MO indicate that the reaction follows kinetics of order 1 whose integration of the reaction rate is given as follows:

$$Ln\ \frac{C}{Co} = -Kt$$

where, C_0 is the initial concentration of the pollutant, K (min^{-1}) is the apparent rate constant and C is the concentration of pollutant at t.

Figure 13 shows the kinetics treatment for an apparent first order for the decomposition of MO under the catalytic effect of the different catalytic materials.

A good linear correlations of ln (C/C_0) against time ($0.99< R^2 <1$) were acquired, suggesting that the catalytic reaction obey pseudo-first-order kinetics. These plots allowed also calculating the rate constant of the MO degradation reaction; they are 0.0532, 0.0775, 0.0828 and 0.101 min^{-1} for the reaction catalyzed by CF/RuO_2-TiO_2, CF/RuO_2-TiO_2/PANI, CF/RuO_2-TiO_2/DPA/PANI and CF/RuO_2-TiO_2/DPA@PANI (Fig 13).

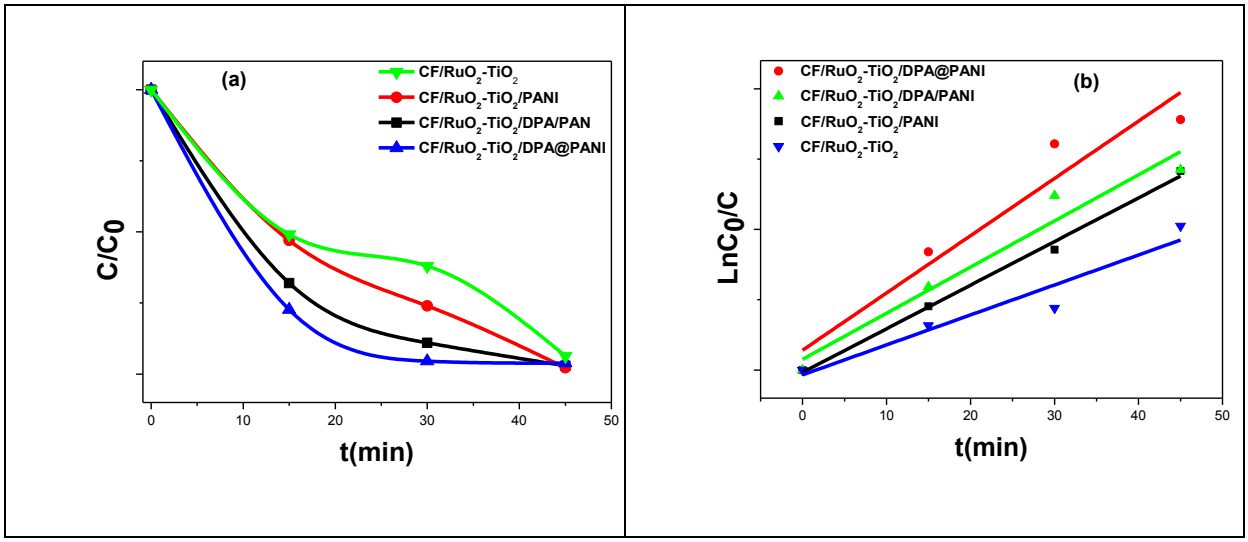

Fig. 13. Kinetics of degradation (a) and first order linear transforms of the decomposition of Methyl Orange solution (50 mg/l) under visible light.

4.1. Degradation product

Figure 14 shows the original IR spectrum of MO and that after decomposition in the presence of CF/RuO_2-TiO_2/DPA/PANI and CF/RuO_2-TiO_2/DPA@PANI under visible light. The original spectrum (Fig 14 a) exhibits a peak at 3430 cm^{-1} for N-H stretching vibration. The C-H stretching vibration of $–CH_3$ are located at 2905 and 2854 cm^{-1}. At 1610 and 1540 cm^{-1} are located C-C vibrations of benzene skeleton, and the band 1426 cm^{-1} is attributed to N=N (Shen, 2015). The pic at 1380 cm^{-1} is assigned to –S=O vibration. The band C-N is observed at 1225 cm^{-1} and C-H stretching vibrations of benzene ring were pointed at 1030, 847 and 697

cm^{-1} (Tanwar & Mandal, 2019). Stretching vibration –C-S is manifested by an IR signal at 624 cm^{-1}. The spectra of the degraded products in the presence of both CF/RuO_2-TiO_2/DPA/PANI (Fig 14 b) and CF/RuO_2-TiO_2/DPA@PANI (Fig 14 b) are similar; they illustrate only two bands which were not observed in the original spectrum of the dye. they include a large band at 3300 cm^{-1} due the H_2O molecules and a peak centred at 1634 cm^{-1} which is attributed to HCO_3^- derived from CO_2 dissolved in water **(**Babushkina, Nikitina, Goncharov & Ponomareva, 2009; Garand et al., 2009)**.** These spectra reflect the total mineralization of MO under visible light.

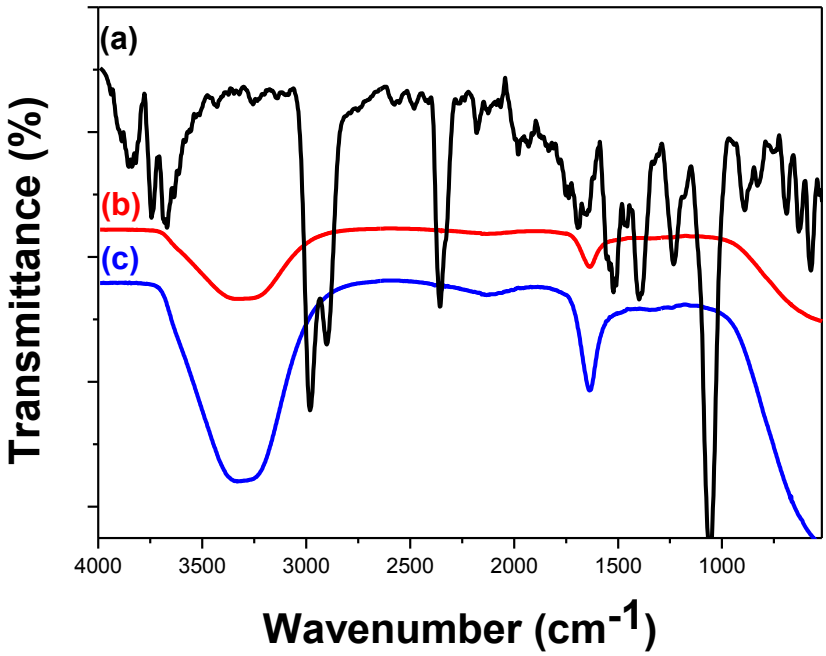

Fig.14. IR spectra of Methyl Orange before (a) and after degradation in the presence of CF/RuO_2-TiO_2/DPA/PANI (b) and CF/RuO_2-TiO_2/DPA@PANI (c) under visible light.

The illumination of the RuO_2-TiO_2-coated cotton fabric leads to the excitation of electron positioned on the valence band (VB) of TiO_2 and move towards the conductance band (CB) leaving holes on the VB; the latter migrate to RuO_2 and participate in the formation of $OH^{\bullet}$ radicals on the surface of the nanocomposite. In addition, the excited electrons diffuse on the surface and react with oxygen to generate $O_2^{-\bullet}$ anion radicals. These radical species ($OH^{\bullet}$,$O_2^{-\bullet}$)

are very powerful oxidants and can destroy several organic molecules. The role of the generated photoactive species is explained by the proposed mechanism shown in Fig 15.

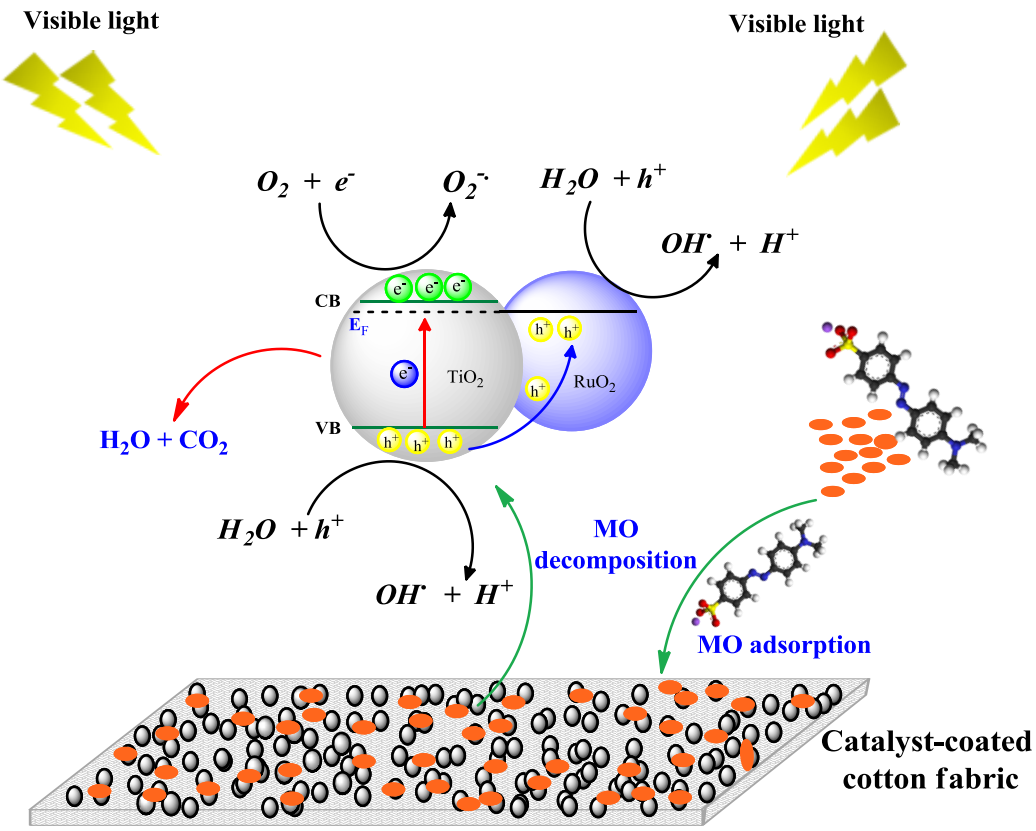

Fig. 15. mechanism of Methyl Orange degradation on RuO_2-TiO_2-coated cotton fabric surface.

The modified-fabric has been widely used in heterogeneous catalysis either for degradation of organic pollutants or to enhance antibacterial activity. For an antibacterial application, (Krishnamoorthy, Navaneethaiyer, Mohan, Lee & Kim, 2012) have modified the cotton fabric using graphene oxide (GO) nanostructure by dip coating method for the bacterial quantitative reduction of both Gram-negative and Gram-positive bacteria. In 2019, **(**Ahmad, Kan & Yao, 2019) evaluated the catalytic performance of cotton fabric impregnated with TiO_2 nanoparticles coupled with phthalocyanine based reactive dye, Reactive Blue-25 used as a visible light absorber for degradation of Rhodamine under visible light. The same experimental process was adopted by (Zhu et al., 2017), who made ZnO nanoparticle substitute with Methylene Blue (MB) dye and coated cotton fabric by dip-pad-dry method for self-cleaning textile application.

The materials that are cotton fabric-based used in photocatalysis often bear TiO_2 nanoparticles which are known as an excellent catalyst under UV light (Stan et al., 2018; Mishra & Butola, 2018; Nosrati, Olad & Najjari, 2017). ZnO nanaostructure has also been widely used in the same field of application; it represents an alternative thanks to its wide gap (3.37 eV), exciton binding energy (60 meV) and its low price (Zhu et al., 2017). Nanocomposites such as TiO_2-PANI-based cotton fabric have also been used in photocatalysis, the materials exhibits better photocatalytic activity thanks to the synergistic effect at the TiO_2//PANI interface . (**Nosrati, Olad & Najjari, 2017;** Kumar & Pandey, 2018).

4.2. Durability test

In this part and among the cotton fabrics modified with the powdery catalyst (CF/RuO_2-TiO_2, CF/RuO_2-TiO_2/PANI and CF/RuO_2-TiO_2/DPA/PANI), we have chosen the sample CF/RuO_2-TiO_2/DPA@PANI and CF/RuO_2-TiO_2/DPA/PANI which catalyzes better the reaction of the decomposition of MO to study the effect of the adhesion tests (washing and insolation) on the catalytic activity of the catalyst (RuO_2-TiO_2/DPA/PANI nanocomposite). Adhesion tests were performed as described above. The samples were used as catalysts in the degradation of MO under the same conditions as previously ([MO], pH=6.5, T_{amb}, CF size, volume of MO and the source of visible light).

Figure 16 and 17 illustrate the digital photographs of the MO solutions at different irradiation times in the presence of CF/RuO_2-TiO_2/DPA/PANI and CF/RuO_2-TiO_2/DPA@PANI insolated during 1h (Fig 16/17 A), washed (Fig 16/17 B) and washed and ironed (Fig 16/17 C).

Under irradiation, the behavior of MO solutions containing both samples exposed to sunlight is the same as those of the non-irradiated same samples. The MO solution lost completely its orange color after 45 min, which is the case even before sunlight exposure; so the samples are very stable under the visible light rays and the irradiation does not affect its catalytic properties (Fig 16/17A).

Washing and ironing led to a weight loss of 8% and 6.4% of the mass of washed CF/RuO_2-TiO_2/DPA/PANI and washed and ironed CF/RuO_2-TiO_2/DPA/PANI respectively, this loss decreased the catalytic capacities of the samples and the discoloration of MO solution take place after 200 min in the presence of the washed sample and 250 min in the presence of the washed and ironed sample (Fig 16 B, C). However, CF/RuO_2-TiO_2/DPA@PANI seems to be

very stable and washing and washing followed by ironing have no effect on the catalytic power of the nanocomposite (Fig 17 B, C). The PANI layer deposited on the surface constitutes a protective layer of the RuO_2-TiO_2/DPA powders nanocatalyst, hens its stability during the catalytic process.

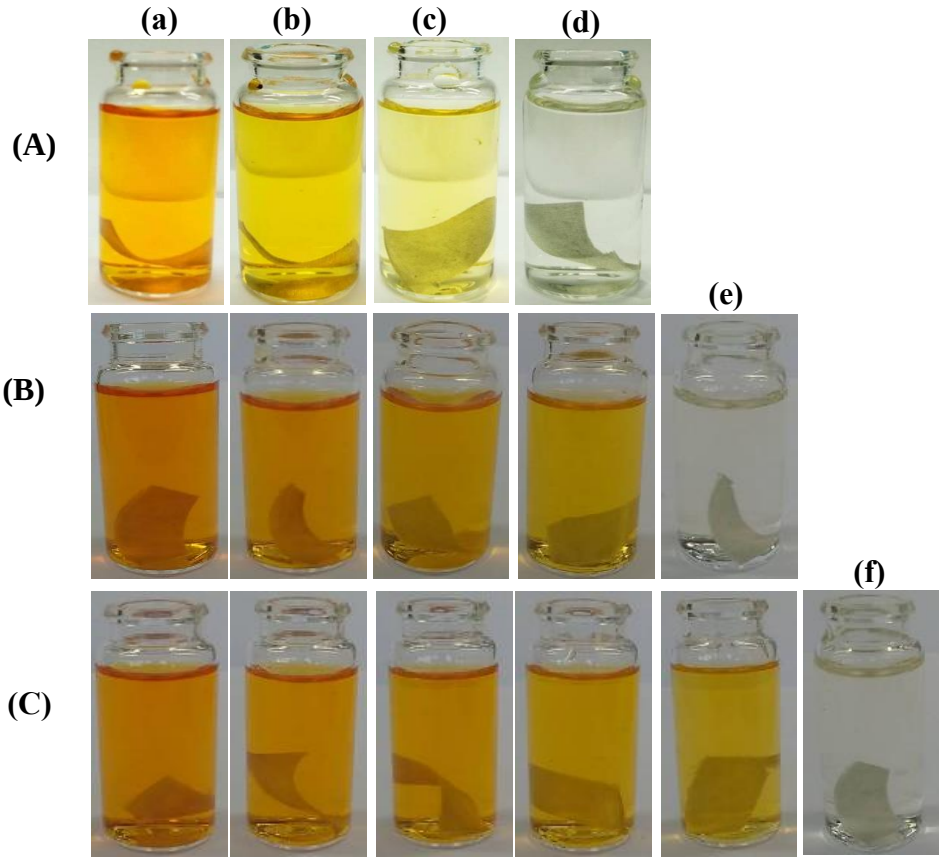

Fig. 16. Digital photographs of MO solutions under visible light in the presence of CF/RuO_2-TiO_2/DPA/PANI insolated (A), washed (A), washed and ironed (C). a, b, c, d, e and f correspond to the sampling times 0, 15, 30, 45, 100, 150, 200 min respectively.

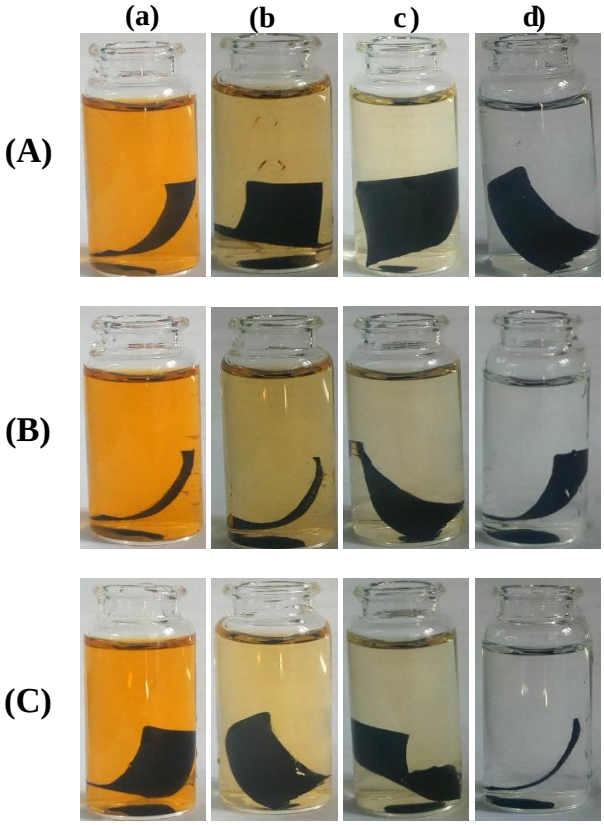

Fig. 17. Digital photographs of MO solutions under visible light in the presence of CF/RuO_2-TiO_2/DPA@PANI insolated (A), washed (A), washed and ironed (C). a, b, c, d correspond to the sampling times 0, 15, 30, 45 min respectively.

Although the mass loss of the washed/ironed sample is lower than that of the washed one, which means that ironing has an effect on the catalytic properties of the catalytic materials. The CF exposed to sunlight gives better degradation of MO under visible light. The mineralization took place after 15 min of irradiation. The rate constant of the dye degradation reaction is calculated to be 0.0959, 0.0155 and 0.01302 min^{-1} in the presence of CF/RuO_2-TiO_2/DPA/PANI fabric exposed to sunlight, washed and washed/ironed samples, respectively (Fig 18).

The degradation rate of MO in the presence of CF/RuO_2-TiO_2/DPA@PANI is constant even after the three tests (insolation, washing, washing and ironing), which confirms that the washing and the heat of the iron do not have any impact on the catalytic properties of RuO_2-TiO_2 and this thanks to the layer of PANI deposited on the surface (Figure 18).

The rate constant is 0. 994 min^{-1} for the washed sample and 0.1 min^{-1} for the insolated and the washed and ironed sample while it is 0.101 min^{-1} before the durability test.

.

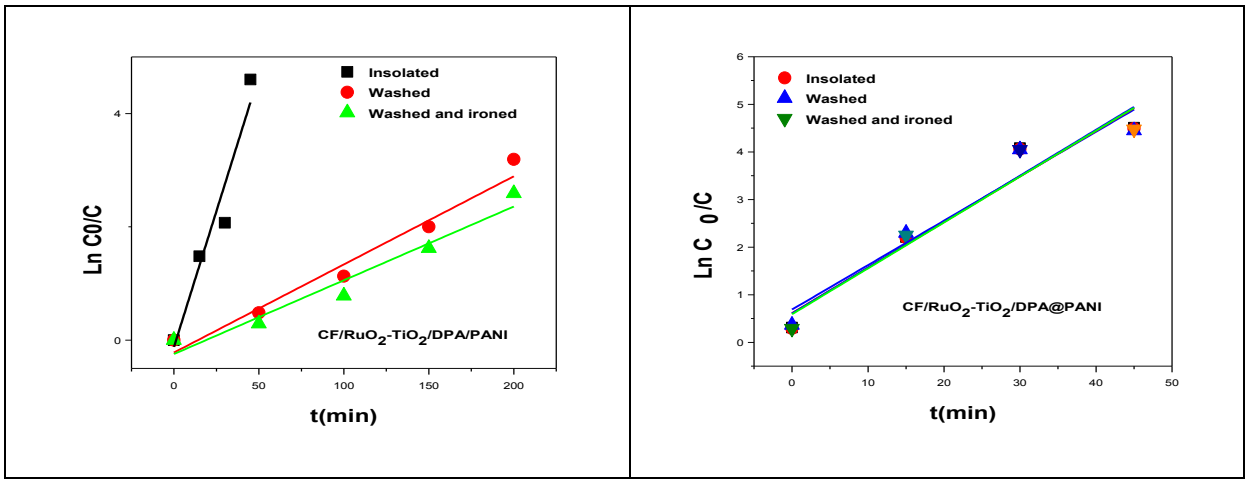

Fig.18. First order linear transforms of degradation of MO solutions (50 mg/l) in the presence of CF/RuO_2-TiO_2/PANI and CF/RuO_2-TiO_2/DPA@PANI: sonicated for 1h, washed, washed and ironed

5. Conclusions

The present work sets a pathway for designing cotton fabric coated with hybrid photocatalysts operating under visible light.

The nanostructure coated-CFs have a significant catalytic activity in the photodegradation and the mineralization of MO dye under visible light. This catalytic activity depends on the PANI amount in the nanocomposite. Indeed, the cotton fabric based on in situ synthesis of PANI exhibits better catalytic performance as compared to other catalysts coated-CFs. The PANI film was uniformly deposited over the entire surface of the fabric and on both sides, trapping a large amount of RuO_2-TiO_2 on the fibrous surface, thanks to the diphenyl amino group from diazonium salt which served as a coupling agent for attaching the PANI to RuO_2-TiO_2 surface but also to the strong interaction between PANI and fabric forming O-N covalent band. The improvement of the degradation kinetics and the catalytic performances could be credited to the strong interfacial interactions between the nanocomposite components that maximizes the interfacial contact between RuO_2-TiO_2 and PANI and the synergistic effect as well as charge transfer at different interfaces of CF/RuO_2-TiO_2/DPA@PANI. It turned out that the washing of the cotton fabrics as well as the washing followed by the ironing affect the performances of the materials but they keep their retain substantial photocatalytic activity under simulated sunlight but do not block the catalytic effect of CF/RuO_2-TiO_2/DPA@PANI hybrid material. In the case of exposure to simulated sunlight, but without any washing, the catalytic textiles remain very stable and catalytically active. This feature makes them suitable for the design of

textile-based structured solar cells, anti-pesticide clothes and for other industrial and outdoor environmental applications.

Acknowledgements

FM would like to thank Campus France for the provision of PROFAS B+ fellowship. All authors are indebted to NATO for financial support through the SfP program (CATALTEX project No 984842)

References

Ahmad, I., Kan, C. W., & Yao, Z. (2019). Reactive Blue-25 dye/TiO_2 coated cotton fabrics with self-cleaning and UV blocking properties. *Cellulose*, *26*(4), 2821-2832.

Arsov, L. D., Kormann, C; Plieth, W. Electrochemical synthesis and in situ Raman spectroscopy of thin films of titanium dioxide. *Journal of Raman spectroscopy*. 1991, *22*(10), 573-575.

Augustine, R., Dan, P., Sosnik, A., Kalarikkal, N., Tran, N., Vincent et al. (2017). Electrospun poly (vinylidene fluoride-trifluoroethylene)/zinc oxide nanocomposite tissue engineering scaffolds with enhanced cell adhesion and blood vessel formation. Nano Research, 10(10), 3358-3376.

Babushkina, M. S., Nikitina, L. P., Goncharov, A. G., & Ponomareva, N. I. (2009). Water in the structure of minerals from mantle peridotites as controlled bythermal and redox conditions in the upper mantle. *Geology of Ore Deposits*, *51*(8), 712-722.

Bajgar, V., Penhaker, M., Martinková, L., Pavlovič, A., Bober, P., Trchová, M., & Stejskal, J. (2016). Cotton fabric coated with conducting polymers and its application in monitoring of carnivorous plant response. *Sensors*, *16*(4), 498.

Barthet, C., Armes, S. P., Chehimi, M. M., Bilem, C., & Omastova, M. (1998). Surface characterization of polyaniline-coated polystyrene latexes. *Langmuir*, *14*(18), 5032-5038.

Bhat, N. V., Seshadri, D. T., & Radhakrishnan, S. (2004). Preparation, characterization, and performance of conductive fabrics: Cotton+ PANi. *Textile research journal*, *74*(2), 155-166.

Bishop, J. L., Pieters, C. M., & Edwards, J. O. (1994). Infrared spectroscopic analyses on the nature of water in montmorillonite. *Clays and clay minerals*, *42*(6), 702-716.

Chen, R., & Jakes, K. A. (2002). Effect of pressing on the infrared spectra of single cotton fibers. *Applied spectroscopy*, *56*(5), 646-650.

Chen, Y. M., Korotcov, A., Hsu, H. P., Huang, Y. S., & Tsai, D. S. (2007). Raman scattering characterization of well-aligned RuO_2 nanocrystals grown on sapphire substrates. *New Journal of Physics*, *9*(5), 130.

Chung, C., Lee, M., & Choe, E. K. (2004). Characterization of cotton fabric scouring by FT-IR ATR spectroscopy. *Carbohydrate Polymers*, *58*(4), 417-420.

Daoud, W. A., & Xin, J. H. (2004). Nucleation and growth of anatase crystallites on cotton fabrics at low temperatures. *Journal of the American Ceramic Society*, *87*(5), 953-955.

Faruk, O., & Ain, M. S. (2013). Biofiber reinforced polymer composites for structural applications. In *Developments in Fiber-Reinforced Polymer (FRP) Composites for Civil Engineering* (pp. 18-53). Woodhead Publishing.

Fujii, S., & Nakamura, Y. (2013). Surface coating of soft materials with conducting polymer-metal nanocomposite. *Applied Surface Chemistry of Nanomaterials*, 303-318.

Garand, E., Wende, T., Goebbert, D. J., Bergmann, R., Meijer, G., Neumark, D. M., & Asmis, K. R. (2009). Infrared spectroscopy of hydrated bicarbonate anion clusters: $HCO_3^-(H_2O)$ 1− 10. *Journal of the American Chemical Society*, *132*(2), 849-856.

Gilbert, C., Kokot, S., & Meyer, U. (1993). Application of DRIFT spectroscopy and chemometrics for the comparison of cotton fabrics. *Applied spectroscopy*, *47*(6), 741-748.

Hassan, M. M., & Leighs, S. J. (2017). Effect of surface treatments on physicomechanical, stain-resist, and UV protection properties of wool fabrics. *Applied Surface Science*, *419*, 348-356.

Jin, L., Jiang, Y., Zhang, M., Li, H., Xiao, L., Li, M., & Ao, Y. (2018). Oriented polyaniline nanowire arrays grown on dendrimer (PAMAM) functionalized multiwalled carbon nanotubes as supercapacitor electrode materials. *Scientific reports*, *8*(1), 6268.

Jlassi, K., Mekki, A., Benna-Zayani, M., Singh, A., Aswal, D. K., & Chehimi, M. M. (2014). Exfoliated clay/polyaniline nanocomposites through tandem diazonium cation exchange reactions and in situ oxidative polymerization of aniline. *RSC Advances*, *4*(110), 65213-65222.

Kim, T. S., Cha, J. R., & Gong, M. S. (2018). Investigation of the antimicrobial and wound healing properties of silver nanoparticle-loaded cotton prepared using silver carbamate. Textile Research Journal, 88(7), 766-776.

Krishnamoorthy, K., Navaneethaiyer, U., Mohan, R., Lee, J., & Kim, S. J. (2012). Graphene oxide nanostructures modified multifunctional cotton fabrics. *Applied Nanoscience*, *2*(2), 119-126.

Kumar, A., & Pandey, G. Comparative Photocatalytic Degradation of Rose Bengal Dye under Visible Light by TiO_2, TiO_2/PAni and TiO_2/PANI/GO Nanocomposites.

Leroux, Y. R., Fei, H., Noël, J. M., Roux, C., & Hapiot, P. (2010). Efficient covalent modification of a carbon surface: use of a silyl protecting group to form an active monolayer. *Journal of the American Chemical Society*, *132*(40), 14039-14041.

Li, Y., Yu, Y., Wu, L., & Zhi, J. (2013). Processable polyaniline/titania nanocomposites with good photocatalytic and conductivity properties prepared via peroxo-titanium complex catalyzed emulsion polymerization approach. *Applied surface science*, *273*, 135-143.

Lv, J., Zhou, P., Zhang, L., Zhong, Y., Sui, X., Wang, B et al. (2019). High-performance textile electrodes for wearable electronics obtained by an improved in situ polymerization method. *Chemical Engineering Journal*, *361*, 897-907.

Mar, S. Y., Chen, C. S., Huang, Y. S., & Tiong, K. K. (1995). Characterization of RuO_2 thin films by Raman spectroscopy. *Applied surface science*, *90*(4), 497-504.

Mayer-Gall, T., Lee, J. W., Opwis, K., List, B., & Gutmann, J. S. (2016). Textile Catalysts—An unconventional approach towards heterogeneous catalysis. *ChemCatChem*, *8*(8), 1428-1436.

Mishra, A., & Butola, B. S. (2018). Development of Cotton Fabrics with Durable UV Protective and Self-cleaning Property by Deposition of Low TiO_2 Levels through Sol–gel Process. *Photochemistry and photobiology*, *94*(3), 503-511.

Mishra, A., & Butola, B. S. (2019). Photocatalytic Decolorization of Rhodamine B Dye Solution Using TiO_2 Coated Cotton Fabric. In Functional Textiles and Clothing (pp. 139-150). Springer, Singapore.

Mishra, A., & Butola, B. S. (2019). Silver-Doped TiO_2-Coated Cotton Fabric as an Effective Photocatalytic System for Dye Decolorization in UV and Visible Light. *Photochemistry and photobiology*, *95*(2), 522-531.

Mousli, F., Chaouchi, A., Hocine, S., Lamouri, A., Vilar, M. R., Kadri, A., & Chehimi, M. M. (2019). Diazonium-modified TiO_2/polyaniline core/shell nanoparticles. Structural characterization, interfacial aspects and photocatalytic performances. *Applied Surface Science*, *465*, 1078-1095.

Mousli, F., Chaouchi, A., Jouini, M., Maurel, F., Kadri, A., & Chehimi, M. M. (2019). Polyaniline-Grafted RuO2-TiO2 Heterostructure for the Catalysed Degradation of Methyl Orange in Darkness. *Catalysts*, *9*(7), 578.

Musić, S., Popović, S., Maljković, M., Furić, K., & Gajović, A. (2002). Influence of synthesis procedure on the formation of RuO_2. *Materials letters*, *56*(5), 806-811.

Muthukumar, N., & Thilagavathi, G. (2012). Development and characterization of electrically conductive polyaniline coated fabrics.

Nosrati, R., Olad, A., & Najjari, H. (2017). Study of the effect of TiO_2/polyaniline nanocomposite on the self-cleaning property of polyacrylic latex coating. *Surface and Coatings Technology*, *316*, 199-209.

Onar, N., Akşit, A. C., Ebeoglugil, M. F., Birlik, I., Celik, E., & Ozdemir, I. (2009). Structural, electrical, and electromagnetic properties of cotton fabrics coated with polyaniline and polypyrrole. *Journal of applied polymer science*, *114*(4), 2003-2010.

Ramírez, J. A. Á., Suriano, C. J., Cerrutti, P., & Foresti, M. L. (2014). Surface esterification of cellulose nanofibers by a simple organocatalytic methodology. *Carbohydrate polymers*, *114*, 416-423.

Revaiah, R. G., Kotresh, T. M., & Kandasubramanian, B. (2019). Technical textiles for military applications. *The journal of the textile institute*, 1-36.

Savitha, K. U., & Prabu, H. G. (2013). Polyaniline–TiO_2 hybrid-coated cotton fabric for durable electrical conductivity. *Journal of Applied Polymer Science*, *127*(4), 3147-3151.

Shahidi, S., Wiener, J., & Ghoranneviss, M. (2013). Surface modification methods for improving the dyeability of textile fabrics. *Eco-Friendly Textile Dyeing and Finishing*, 34-50.

Shen, T., Jiang, C., Wang, C., Sun, J., Wang, X., & Li, X. (2015). A TiO_2 modified abiotic–biotic process for the degradation of the azo dye methyl orange. *RSC Advances*, *5*(72), 58704-58712.

Stan, M. S., Nica, I. C., Popa, M., Chifiriuc, M. C., Iordache, O., Dumitrescu et al. (2018). Reduced graphene oxide/TiO_2 nanocomposites coating of cotton fabrics with antibacterial and self-cleaning properties. *Journal of Industrial Textiles*, 1528083718779447.

Tanwar, R., & Mandal, U. K. (2019). Photocatalytic activity of $Ni_{0.5}Zn_{0.5}Fe_2O_4$@ polyaniline decorated BiOCl for azo dye degradation under visible light–integrated role and degradation kinetics interpretation. *RSC Advances*, *9*(16), 8977-8993.

Tao, J., Tang, B., Li, P., He, D., Liao, L., Peng, Z., & Wang, X. (2018). Natural rubber particle modified fabrics with catalytic activity and hydrophobicity. *Composites Science and Technology*, *162*, 123-130.

Tao, J., Tang, B., Li, P., He, D., Liao, L., Peng, Z., & Wang, X. (2018). Natural rubber particle modified fabrics with catalytic activity and hydrophobicity. *Composites Science and Technology*, *162*, 123-130.

Tissera, N. D., Wijesena, R. N., Rathnayake, S., de Silva, R. M., & de Silva, K. N. (2018). Heterogeneous in situ polymerization of polyaniline (PANI) nanofibers on cotton textiles: improved electrical conductivity, electrical switching, and tuning properties. *Carbohydrate polymers*, *186*, 35-44.

Uddin, M. J., Cesano, F., Scarano, D., Bonino, F., Agostini, G., Spoto et al. (2008). Cotton textile fibres coated by Au/TiO_2 films: Synthesis, characterization and self cleaning properties. *Journal of Photochemistry and Photobiology A: Chemistry*, *199*(1), 64-72.

Uddin, M. J., Cesano, F., Scarano, D., Bonino, F., Agostini, G., Spoto, G et al. (2008). Cotton textile fibres coated by Au/TiO_2 films: Synthesis, characterization and self cleaning properties. *Journal of Photochemistry and Photobiology A: Chemistry*, *199*(1), 64-72.

Wang, J., Lu, X., Wang, J., & Wang, X. (2019). Quantitative and sensory evaluation of odor retention on polyester/wool blends. *Textile Research Journal*, *89*(13), 2729-2738.

Wang, Y., Ding, X., Zhang, P., Wang, Q., Zheng, K., Chen, L et al. (2019). Convenient and Recyclable TiO_2/g-C3N4 Photocatalytic Coating: Layer-by-Layer Self-assembly Construction on Cotton Fabrics Leading to Improved Catalytic Activity under Visible Light. *Industrial & Engineering Chemistry Research*, *58*(10), 3978-3987.

Xi, J., Xiao, J., Xiao, F., Jin, Y., Dong, Y., Jing, F., & Wang,. (2016). Mus-inspired functionalization of cotton for nano-catalyst support and its application in a fixed-bed system with high performance. *Scientific reports*, *6*, 21904.

Xu, Q., Li, M., Yan, P., Wei, C., Fang, L., Wei, W et al. (2016). Polypyrrole-coated cotton fabrics prepared by electrochemical polymerization as textile counter electrode for dye-sensitized solar cells. *Organic Electronics*, *29*, 107-113.

Yang, B., Zhao, C., Xiao, M., Wang, F., Li, C., Wang, J., & Yu, J. C. (2013). Loading metal nanostructures on cotton fabrics as recyclable catalysts. *Small*, *9*(7), 1003-1007.

Zahran, M. K., Ahmed, H. B., & El-Rafie, M. H. (2014). Surface modification of cotton fabrics for antibacterial application by coating with AgNPs–alginate composite. *Carbohydrate polymers*, *108*, 145-152.

Zhang, L., Liu, P., & Su, Z. (2006). Preparation of PANI–TiO_2 nanocomposites and their solid-phase photocatalytic degradation. *Polymer degradation and stability*, *91*(9), 2213-2219.

Zhou, P., Lv, J., Xu, H., Wang, X., Sui, X., Zhong, Y et al. (2019). Functionalization of cotton fabric with bismuth oxyiodide nanosheets: applications for photodegrading organic pollutants, UV shielding and self-cleaning. *Cellulose*, *26*(4), 2873-2884.

Zhou, P., Lv, J., Xu, H., Wang, X., Sui, X., Zhong, Y et al. (2019). Functionalization of cotton fabric with bismuth oxyiodide nanosheets: applications for photodegrading organic pollutants, UV shielding and self-cleaning. *Cellulose*, *26*(4), 2873-2884.

Zhu, C., Shi, J., Xu, S., Ishimori, M., Sui, J., & Morikawa, H. (2017). Design and characterization of self-cleaning cotton fabrics exploiting zinc oxide nanoparticle-triggered photocatalytic degradation. *Cellulose*, *24*(6), 2657-2667.

Zhu, L., Liu, Y., Ding, X., Wu, X., Sand, W., & Zhou, H. (2019). A novel method for textile odor removal using engineered water nanostructures. RSC Advances, 9(31), 17726-17736.

General conclusion

General conclusion

This research has been dedicated to the development of new TiO_2/TiO_2-based heterostructure/conductive polymer nanocomposite materials for heterogeneous catalysis. We have taken advantage of diazonium coupling agent to tightly attach conductive polyaniline (PANI) to TiO_2 and RuO_2-TiO_2 to drastically shift and enhance the photocatalytic activity of TiO_2-based catalysts to the visible light. Surprisingly, as summarized below, the combination of TiO_2, RuO_2 dopant and diazonium coupling agent for the attachment of PANI, synergetic effects permitted to catalyze degradation of dyes in darkness. Our strategy is novel and unique, it permitted to efficiently contribute to the general domain of heterogeneous catalysis on the one hand, and the surface/interface chemistry in composite materials, on the other hand.

The Thesis is constructed with a General Introduction, 4 Chapters and this General Conclusion. In the Chapter 1, we have summarized the fundamentals of heterogeneous catalysis by semiconductors, with emphasis on TiO_2. This was followed by the discussion of the basic principles of solid state photocatalysis and thermodynamics which governs the photocatalytic performances of the material. Then we directed the lighting on essentials which was achieved in the catalysis in the presence of TiO_2-based heterostructure associated with a conductive polymer, particularly PANI. This has been presented in the form of a review paper which gathers the essential works reported in the last decade.

In the second Chapter, we investigated the role of grafted diazonium salts on the surface of TiO_2 nanoparticles in the design of novel TiO_2/polyaniline photocatalysts by in situ oxidation polymerization of aniline for mineralization of model organic pollutant.

Physico-chemical characterization permitted to confirm the modification of TiO_2 by diazonium salts and more importantly, to highlight the effect of such a surface modification on the loading and covalent attachment of PANI. XPS study brought strong supporting evidence for the core/shell structure.

The nanocomposites exhibited excellent catalytic performances under UV light, which depend on the amount of PANI. The results obtained underline the spectacular role of diphenylamine tetrafluoroborate diazonium salt in the coating of high quantity of PANI and in the stability of the formed photocatalysts. The synergistic effect at the interface of the n-p (TiO_2-PANI) heterojunction formed by this association leads to the separation of the electron-hole pairs

which is the origin of the improvement of the catalytic properties of TiO_2 NPs in the degradation of methyl Orange.

The next part (Chapter 3) is a continuation of the work done in the second Chapter; it consists of the design of the heterostructure photocatalyst system based on TiO_2 and RuO_2 which was revisited with a particular focus on the strategies to improve the photocatalytic activity. The modification of TiO_2 photocatalyst by RuO_2 metal particles showed a strong effect on the electrical, thermodynamic, optical and photocatalytic performances of the system. The range of the photocatalytic activity of TiO_2 shifts from the UV to the visible by doping it with the RuO_2 metal.

Diazonium salt-based aryl coating of RuO_2-TiO_2 made it possible to deposit a rather thick layer of PANI on the surface. Conductive polymer adhesion was found to be strong not only in aqueous solution but also in several polar and apolar organic solvents. The PANI layer has the power to improve significantly the physical and chemical properties of the system with high chemical and thermal stability. In terms of the electrical conductivity, it goes from 317 S/cm for RuO_2-TiO_2 to 343 and 384 S/cm for RuO_2-TiO_2/PANI and RuO_2-TiO_2/DPA/PANI, which is translated by a strong transfer of electrons into the various interfaces of the nanocomposite material. This electronic exchange is at the origin of the strong catalytic activity of the nanocomposite, even in darkness. This activity depends on the presence of PANI on the surface and its amount in the final nanocomposite catalyst, which stresses again the vital role of the diazonium salt as coupling agent for PANI on the nanoparticles surface. This was also demonstrated in the last part of this thesis when designing nanocomposite based on cotton fabric. The layer of PANI is a good electron donor but also constitutes in all the studied cases a protective layer of the nanoparticles or nanoparticle impregnated in the fibrous surface, and this resulting in the reuse of the different catalysts during the methyl orange degradation reaction. The new catalyst design process is scalable which opens new windows for the general degradation of organic pollutants. However, a systematic study of the effect of various parameters such as specific surface area, porosity and energy band alignment in such systems is still largely unexplored.

This Thesis resulted in excellent achievements published or under submission to be reported in international journals. It offers chemists with new tools to design innovative materials while opening up, particularly, new perspectives in the chemistry of diazonium salts and heterogeneous catalysis.

Abstract

The considerable development of industrial and agricultural activities has led to the formation of several organic and inorganic pollutants that are resistant to conventional treatment processes. New treatment techniques have been developed to efficiently remove and/or degrade these pollutants. In this respect, heterogeneous photocatalysis emerged as one of the most extensively studied techniques in the past two decades. In the framework of this global concern, nanocomposite catalysts based on TiO_2 and RuO_2-TiO_2 mixed oxide nanoparticles (NPs) were prepared by sol gel route and functionalized with 4-diphenylamine diazonium (DPA) prior to in situ polymerization of aniline. The resulting nanocomposites catalyzed the degradation and the mineralization of Methyl Orange (MO), a model organic pollutant. The analysis of these materials revealed a strong adhesion of PANI on NPs surface thanks to the diazonium salt which is unique coupling agent of the polymer at the surface. The thus prepared materials exhibit superior catalytic performances in MO degradation under visible light and even in darkness. The combination of the metal-semiconductor n heterojunction and the conductive polymer has resulted in outstanding catalytic properties in darkness. Such activity is due to the high PANI mass deposited on the surface of the catalysts. Electronic displacements at the metal/semiconductor interface under visible light and the synergistic effects between PANI/TiO_2 and PANI/RuO_2 result in the separation and reduction of the electron-hole pair recombination rate as well as significant catalytic activity under UV and in darkness, respectively.

RuO_2-TiO_2 based nanocatalysts were used to design functional hybrid materials based on cotton fabrics by dip-coating process at neutral pH process. A layer of PANI was prepared by oxidative in situ polymerization of aniline on DPA-grafted RuO_2-TiO_2-coated fabric.

The catalytic activity of the catalysts impregnated between the fibers of the textile was studied by measuring the decomposition rate of MO under visible light. The materials lead to complete removal and mineralization of the dye. This catalytic activity is excellent in the presence of PANI and strongly depends on its amount in the nanocatalysts, namely, the nanocomposite obtained by in situ polymerization of aniline has high catalytic properties thanks to the DPA layer which was used for attaching PANI onto RuO_2-TiO_2 surface, on the one hand, and the high attraction force between the OH groups of cellulose and anilinium cation during the polymerization reaction, on the other hand.

Keywords: *Diazonium salt, TiO_2, RuO_2-TiO_2, heterojunction, polyaniline, conductive polymer, heterogeneous catalysis, grafting, nanocomposite, colorant, organic pollutant, mineralization.*

Résumé

Le développement considérable des activités industrielles et agricoles a conduit à la formation de nombreux polluants organiques et inorganiques résistants aux procédés de traitement conventionnels. De nouvelles techniques de traitement ont été développées pour éliminer et/ou dégrader efficacement ces polluants. À cet égard, la photocatalyse hétérogène est l'une des techniques les plus étudiées de manière approfondie depuis deux décennies. Dans ce contexte, et dans le cadre de cette Thèse, Des catalyseurs nanocomposites à base de nanoparticules (NPs) de TiO_2 et d'oxyde mixte RuO_2-TiO_2 préparées par sol gel et fonctionnalisées avec le 4-diphenylamine diazonium (DPA) pour la polymérisation in situ du monomère aniline ont été élaborés par voie chimique pour la dégradation et la minéralisation de polluant organique modèle. L'analyse de ces matériaux a révélé une forte adhésion de PANI sur la surface des NPs, et ce grâce au sel de diazonium qui est un agent de couplage du polymère à la surface. Les matériaux ainsi préparés présentent des performances catalytiques supérieures dans le processus de dégradation de Méthyl Orange (MO) sous éclairage UV ou dans l'obscurité. La combinaison entre l'hétérojonction métal-semi-conducteur (n) et le polymère conducteur a engendré des propriétés catalytiques uniques dans l'obscurité. Une telle activité est due à la masse de PANI élevée déposée sur la surface des catalyseurs. Les déplacements électroniques à l'interface métal/semi-conducteur sous la lumière visible et les effets synergiques entre PANI/TiO_2 et PANI/RuO_2 entraînent la séparation et la réduction du taux de recombinaison des paires électron-trou ainsi qu'une activité catalytique significative sous la lumière UV, visible et dans l'obscurité, respectivement. Les nanocatalyseurs à base de RuO_2-TiO_2 ont servi à la conception des matériaux hybride fonctionnels à base de tissus de coton par un procédé de revêtement (immersion) à pH neutre. Une couche de PANI a été préparée par polymérisation in situ oxydative de l'aniline sur un tissu-enduit de nanoparticules de RuO_2-TiO_2 greffées de DPA.

L'activité catalytique des catalyseurs imprégnés entre les fibres du textile a été étudiée en mesurant la vitesse de décomposition du MO sous lumière visible. Les matériaux conduisent à l'élimination complète et à la minéralisation du colorant. Cette activité catalytique est excellente en présence de PANI et dépend fortement de sa quantité dans les nano-catalyseurs, à savoir, le nanocomposite obtenu par polymérisation in situ de l'aniline présente des propriétés catalytiques élevées grâce à la couche de DPA qui a servi à la fixation du PANI sur la surface de RuO_2-TiO_2 d'une part et à la force d'attraction élevée entre les groupements OH de cellulose et de cation anilinium lors de la réaction de polymérisation, d'autre part.

Mots clés : *Sel de diazonium, TiO_2, RuO_2-TiO_2, Polyaniline, polymère conducteur, catalyse hétérogène, greffage, nanocomposite, hétérojonction, polluant organique, colorant, minéralisation.*